NOTTINGHAM TRENT UNIVERSITY

NEURONAL DYNAMICS AND CONNECTIVITY ANALYSIS OF NEURONAL CULTURES ON MULTI ELECTRODE ARRAYS

Nikesh Lama
N0687666

A thesis submitted in partial fulfilment of the requirements of Nottingham Trent University for the degree of *Doctor of Philosophy*

October 2020

This thesis is dedicated to my parents with great gratitude.
Undoubtedly, without their prayers and support this thesis would
have been impossible.

Acknowledgements

I would like, first and foremost, to thank my Director of Studies, Prof Martin McGinnity, for giving me the rare opportunity to get involved in this interesting and challenging project that spans many disciplines. His constant support, encouragement and kindness have always helped me get through difficult times over the last few years. I would also like to thank my supervisory team, Dr Alan Hargreaves and Prof Bob Stevens, for their invaluable advice and support. I will forever be grateful to Dr Alan Hargreaves for teaching me invaluable bioscience techniques, that proved crucial to complete this work. I would also like to thank the Vice Chancellor's scholarship for funding my PhD studentship.

A heartfelt word of thanks to all of my friends and colleagues here at the university, especially Pedro Machado, Yuan Shen and David Adama for always being there to take my mind off things. Special thanks to my colleagues from bioscience group who have always been extremely supportive and helpful all throughout my PhD.

A very big thank you to my extended family and my cousins (Abhishek, Sarina didi, Suman dai and Sera vauju) for their endless support and love. Their constant support and encouragement have made my PhD journey that much enjoyable. My utmost sincere gratitude to my aunt and uncle, without whom, it would have been impossible to embark on this journey. I must thank my very close friends - Girwan Karki, Alin Shrestha, Kishan Tamrakar and Hywin Francis for always being supportive and helpful. I would also like to thank my very good friend, Bindu Gurung, for all the support and engaging me in intellectually stimulating and fun conversations during stressful times.

It goes without saying, my parents and my siblings (Nisha and Nilam) have always been my source of inspiration and motivation in life.

Nikesh Lama
2020

Abstract

Despite a number of attempts over the past two decades, research into reliable, controlled induction of long term evoked responses, mimicking low level learning and memory in dissociated cell cultures remains challenging. In addition, a full understanding of the stimulus-response relationships that underlie synaptic plasticity has not yet been achieved, and many of the underlying principles remain largely unknown. Plasticity studies have been predominantly limited to low density Multi/Micro Electrode Arrays (MEAs). With the advent of complementary metal-oxide-semiconductor (CMOS) based High-Density (HD) MEAs, unprecedented spatial and temporal resolution is now possible. In this thesis, an attempt to bridge the gap between studies of neural plasticity and the use of CMOS based HD-MEAs with thousands of electrodes, is reported. Additionally, since such HD-MEAs generate a large volume of data and require advanced analytics to efficiently process and analyse recordings, computational tools and novel algorithms to infer connectivity during plasticity have been developed.

The study showed that the responsiveness, stability and initial firing rate of neuronal cultures are the deciding factors to reliably induce evoked responses. With multi-site stimulation, sustained long term potentiation was achieved, which was validated both by evoked response plots and overall firing rates measured at five different time points - before and after repeated stimulation, and at a three day time points. In contrast, while depression responses were observed, it was found that the effects were not sustained over many days. The findings of the study suggest that appropriate selection of neuronal cultures is crucial for inducing desired evoked responses and criteria for this have been developed. Furthermore, it is concluded that the initial responses to test stimuli can be used to determine whether potentiated or depressed responses are to be expected.

To analyse the recordings, pipeline of computational tools was developed. Firstly, neuronal synchrony metrics were adapted for the first

time for large HD-MEA recordings and shown to correspond effectively to the firing dynamics. To analyse functional connectivity, an information theoretic approach, Transfer Entropy(TE), was utilised. The method showed accurate estimation of functional connectivity with mid 80^{th} percentile accuracy on simulated data. A superimposition method was proposed to enhance confidence in the connectivity estimation. To statistically evaluate connectivity estimation, a new surrogate method, based on ISI distribution approach, was proposed and validated with a simulated Izhikevich network. The method achieved improved accuracy, compared to the existing ISI shuffling method. This newly developed method was later utilised to infer connectivity and refine connections during the learning process of real neuronal cultures over many days of stimulation. The connectivity inference corresponded accurately to both the spontaneous and stimulated networks during evoked responses and the proposed method permitted observation of the evolution of connections for the potentiated network.

Publications

The following papers have been published as a direct result of this thesis:

Refereed Conference Papers

N. Lama, A. Hargreaves, B. Stevens and T. M. McGinnity, "Transfer Entropy Based Connectivity Estimation of Spontaneously Firing Hippocampal Cultures on Multi Electrode Arrays," 2019 International Joint Conference on Neural Networks (IJCNN), Budapest, Hungary, 2019, pp. 1-8, doi: 10.1109/IJCNN.2019.8851864. [accepted]

N. Lama, A. Hargreaves, B. Stevens and T. M. McGinnity, "Spike Train Synchrony Analysis of Neuronal Cultures," 2018 International Joint Conference on Neural Networks (IJCNN), Rio de Janeiro, 2018, pp. 1-8, doi: 10.1109/IJCNN.2018.8489728. [accepted]

The following journal papers are currently under review or under preparation for submission

N. Lama and T. M. McGinnity, "ISI Distribution Based Surrogate Method for Spiking Neural Network Connectivity Analysis" (2020) IEEE Transactions on Neural Networks and Learning Systems. [Submitted - Under Review]

N. Lama and T. M. McGinnity, "Multi channel stimulation for induction of long term plasticity" [Draft paper]

Contents

List of Figures

List of Tables

List of Abbreviations

AMPA	α amino-3-hydroxy-5-methyl-4-isoxazolepropionic
APS	Active Pixel Sensor
AUC	Area Under the Curve
CC	Cross-Correlation
CDF	Cumulative Distribution Function
CMOS	Complementary Metal-Oxide-Semiconductor
CSV	Comma Separated Values
DAPI	4',6-diamidino-2-phenylindole
DDW	Double Distilled Water
DIV	Days In-vitro
ECDF	Empirical Cumulative Distribution Function
EEG	Electroencephalography
EPSP	Excitatory Post-Synaptic Potential
FET	Field-Effect Transistor
FN	False Negative

FP	False Positive
FPR	False Positive Rate
GABA	γ-aminobutyric acid
HDF5	Hierarchical Data Format
ISI	Interspike Interval
JE	Joint Entropy
LDH	Lactate Dehydrogenase
LTD	Long Term Depression
LTP	Long Term Potentiation
MAP2	Microtubue Associated Protein 2
MBR	Mearn Bursting Rate
MEA	Multi/micro Electrode Arrays
MEG	Magnetoencephalography
MI	Mutual Information
NMDA	N-methyl-D-aspartate
OD	Optical Density
PBS	Phosphate Buffer Saline
PDF	Probability Density Function
PDL	Poly-D-lysine
PEI	Polyethylene-immine
PSTH	Peri/post Stimulus Time Histogram
RMSE	Root Mean Squared Error

RMSE	Root Mean Squared Error
ROC	Receiver Operating Characteristic
SDW	Sterilised Distilled Water
SNR	Signal-to-Noise Ratio
STDP	Spike Timing Dependent Plasticity
TBS	Tri Buffered Saline
TE	Transfer Entropy
TN	True Negative
TP	True Positive
TPR	True Positive Rate
fMRI	Functional Magnetic Resonance Imaging

Chapter 1

Introduction

1.1 Introduction

The human brain is an intricate and highly interconnected network of neurons. Higher level brain functions, such as learning and memory, are emergent behavioral concepts, dependent on the development and modification of neural interconnections during life experiences.

The ability of the nervous system to adapt and change to a new functional and structural state in response to intrinsic or extrinsic factors can be broadly defined as '*Neural Plasticity*'. The physiological mechanisms underlying synaptogenesis and neural plasticity involved in learning and memory are often studied in *in-vitro* neuronal cultures. Coupled with Multi Electrode Array(MEA) , these have been established as very useful experimental paradigms [1]. Such models offer unique ability to simultaneously stimulate and record extracellular activity in a non-invasive way [2, 3]. With the advent of technological advancements, thousands of sensing electrodes are now possible in MEAs, allowing an unprecedented spatial and temporal resolution. In particular, long term plasticity studies have benefited immensely from the ability to stimulate neuronal networks whilst recording simultaneously and keeping the culture healthy and functioning for a prolonged period of time.

Over the last two decades of studies in neural plasticity in neuronal cultures coupled with MEAs, different researchers have tried different protocols and have

successfully induced plasticity to some degree [4–11]. A protocol that can reliably induce plasticity in multiple different scenarios currently doesn't exist. It is still unclear what would be the nature of an underlying common protocol that could consistently lead to a guaranteed induction of plasticity in a controlled manner. The problem is exacerbated due to the occurrence of network bursts where the network activity is concentrated, which could cancel out transient plasticity, making it much harder to induce long term plasticity.

In a neural circuit, the activity of a neuron is not only due to its intrinsic properties but also due to direct or indirect interactions with other neurons. Accurate connectivity characterisation of such direct and indirect interactions in neuronal circuits is very useful in understanding neuronal dynamics, neural pathways and neural information processing. During neural plasticity, new functional connections are formed and modified, as a direct result of external input to the neuronal network. Inferring and understanding the neural wiring that underlies high level representation in the brain is crucial in explaining how such representations are produced and developed [12, 13]. The ability to infer neural connectivity during the learning process characterised by synaptic plasticity, provides invaluable insights into development of neural pathways. However, accurate inference of neural connectivity from HD-MEA electrophysiological recordings is a challenging problem in computational neuroscience.

Neuronal cultures are complex, non-stationary systems which makes the modeling of such dynamical systems difficult for connectivity inference. Hence, a model-free approach, Transfer Entropy(TE) , has gained much popularity [14–17]. The TE method has outperformed many other popular methods such as cross-correlation(CC) [18], joint entropy(JE) [19], mutual information(MI) [14, 15] to identify connectivity from simulated networks. However, the problem of how to differentiate true connections from spurious connections, from real experimental data, where ground truth information is not present, still persists. Due to the dynamical and non-stationary nature of neuronal cultures, trial based statistical testing is not feasible as cultures may attain a different dynamical state at each trial, especially for stimulated experiments to induce plasticity. To mitigate this problem, a surrogate method is a commonly chosen approach where surrogate trial data are generated under some null hypothesis that is to be tested.

Surprisingly, there are only a handful of methods that are applicable to discrete neuronal spiking events from MEAs. Improving such surrogate methods to generate a richer set of surrogates is an important step that supplements TE or any connectivity estimation. Also, as more HD-MEA data are available, developments in the analysis of such big data recordings becomes more important than ever in utilising such information to reveal many neurological processes.

1.2 Objectives of the thesis

The limitations briefly presented in Section 1.1 highlighted the challenges in plasticity studies when attempting to induce long lasting network responses and in the inference of connectivity from experimental recordings in the absence of ground truth information. The research presented in this thesis seeks to continue to progress in these aspects. In particular, it aims to utilise state-of-the-art complementary metal-oxide-semiconductor (CMOS) based MEAs, focused on controlled induction of plasticity and the study of network connectivity, to enhance the understanding of neuronal dynamics. To achieve this goal, several objectives are established.

- Development of methods to successfully grow and maintain dissociated neuronal cultures, grown on the state-of-the-art high density CMOS based MEAs, for a prolonged period of time(up to 4 weeks at least).
- Characterisation of electrophysiological properties of spontaneous activity and design criteria to select cultures that are responsive to stimulation and could potentially exhibit plasticity.
- Development of stimulation protocols to demonstrate a long term network response change, symptomatic of network plasticity, and study network dynamics before and after the stimulation.
- Quantification of network connectivity using an information theoretic approach and the development of a novel non-parametric surrogate test to identify statistically significant connections from the experimental recordings.

1.3 Thesis contribution and outline

The work presented in this thesis encompasses a substantial body of work in multi disciplinary research across bioscience, computing and electronics, to study neural plasticity on neuronal cultures grown on HD-MEAs and to develop computational tools to analyse HD-MEA recordings. Specifically, the development of experimental protocols and a systematic approach to induce long term network responses in dissociated neuronal cultures grown on the state-of-the-art CMOS based MEAs, are presented. Furthermore, HD-MEAs produce huge datasets even for short recordings, necessitating developments of analytics techniques to gain an understanding of the neuronal dynamics. Hence, the development of computational tools and techniques to facilitate the analysis of neuronal dynamics is also presented.

The main contributions of this thesis can be summarised briefly into two categories.

Computational contribution

1. Adaptation of neuronal synchrony metrics (ISI distance and SPIKE-distance) for large HD-MEA recordings and demonstration of effective identification of synchronous patterns.

2. Development of a new firing density superimposition method as an alternative to ground truth information for better confidence in the TE based connectivity inference.

3. Development of a new ISI distribution based surrogate method to compensate lack of ground truth information and provide statistical classification of inferred connections.

Experimental contribution

1. Development and optimisation of methods for cell culture growth on sensitive CMOS based MEAs, so as to successfully grow and maintain dissociated neuronal cultures for prolonged periods (up to 4 weeks).

2. Establishment of neuronal cultures for plasticity studies and design of criteria to select potential cultures for plasticity based on responsiveness, stability and firing rate.

3. Stimulation protocol selection to induce wide range of evoked network responses.

4. Application of developed ISI distribution surrogate data to study neural connectivity during long term responses.

The contributions are discussed in detail in chapters 5, 6 and 7. A brief outline of the thesis structure is presented below.

Chapter 2: This chapter introduces essential terminologies and concepts that lay the foundational background knowledge covering bioscience, computing and electronics for the review of the related works and the research presented in this thesis.

Chapter 3: This chapter focuses on an extensive literature review of related research and describes the rationale behind the work presented in this thesis, discussing current limitations. The aims and objectives of the thesis are further elaborated at the end of this chapter so as to set context for upcoming chapters.

Chapter 4: In this chapter, the materials and methodology undertaken throughout the research are described. Details of cleaning of MEAs, cell culture on MEAs, experimental setup and basic data analytics used are presented.

Chapter 5: This chapter presents the first computational contribution of adapting synchrony metrics for HD-MEA recordings. Two mathematical metrics to quantify neuronal synchrony, namely - ISI-distance and SPIKE-distance, are adapted and validated with synthetic data before applying on experimental HD-MEA data.

Chapter 6: Transfer entropy based connectivity inference is utilised in this chapter. The chapter is divided into two sections, each discussing a contribution. The first section proposes superimposition method as an alternative to ground truth information and the second section takes this further by introducing new ISI distribution based surrogate method.

Chapter 7: This chapter discusses the effects of repeated stimulation on neuronal cultures on HD-MEAs, reflecting on long term network responses, germane to neural plasticity, connectivity and development during plasticity. The later half of the chapter applies the connectivity estimation tools previously developed in chapter 6.

Chapter 8: This chapter summarises the overall research contribution ,and discusses the potential for further research and future directions.

Chapter 2

Scientific Background

2.1 Introduction

This chapter aims to introduce essential terminologies and concepts that lay foundational background for the review of the related works and the research of this thesis.

In this chapter, some basic background on neurons, their dynamics and how they communicate with each other (Section 2.2) are presented. Different types of *in vitro* neuronal preparations (Section 2.3) are also reported briefly. Furthermore, an overview on electrophysiological techniques for *in vitro* settings (Section 2.4) is discussed. Finally, a brief discussion on the history on Micro Electrode Arrays(MEAs) from the early MEAs to the current state-of-the-art MEAs with thousands of electrodes along with MEAs application in neuroscience studies (Section 2.5) is presented. The data data analysis challenges for such high volume recordings are also considered.

2.2 Neurons and synapses

The brain is composed of a large number of highly specialised information processing cells, namely, neurons - that constitute the building blocks of the central nervous system. Neurons communicate among each other via short burst of electrical pulses called *action potentials* or *spikes*. Cell-cell interactions among single neurons or a group of related neurons form the basis of neurological processes. The capability of nervous system to produce a range of responses to many complex sensory inputs depend on the way neurons are interconnected with each other; rather than the dynamics of individual neurons [20, 21].

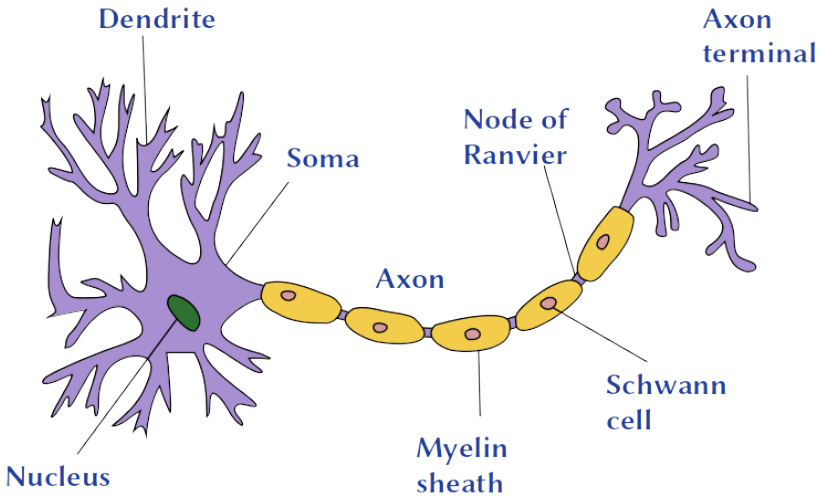

Figure 2.1: Illustration of a neuron [22]

Even though there are thousands of different types of neurons, they all share the same common morphology. A neuron is composed of four main distinct morphological parts - soma, axon, dendrites and presynaptic terminals or axon terminals as shown in the Figure 2.1. The soma is the main cell body which contains the nucleus and the cytoplasmic organelles. Dendrites are branch like projections which emanate and ramify from the cell body, forming the main signal receiving structures from other nerve cells and function as an input unit. The axon is the main outgoing signal conducting structure that extends away from

the neuron, in most cases, much farther away from the soma, and acts as an output unit of the neuron. In vertebrates, most axons are coated with a layer of fatty insulating material, namely, myelin sheath which promotes rapid signal conduction [23]. Neuronal physiology is supported by cells known as *neuroglia* or *glial* cells that maintain homeostasis and protection to neuronal cells [24] .

The membrane potential results from the difference in ionic content between the inside and outside of the membrane of neurons and neuronal processes [1]. The difference in the distribution of ions, specifically Na^+ and K^+, on either side of the membrane due to the permeability of the membrane, primarily contributes to the change in membrane potential. At resting state, K^+ is concentrated inside the cell and Na^+ outside the cell, giving rise to a steady resting membrane potential, which in a typical neuron is -70mV relative to that of the surrounding environment. The opening of faster Na^+ channels allows for the rapid flow of Na^+ into the cell increasing the membrane potential and this phenomenon is called *Depolarisation*. Depolarisation is followed by a slower inactivation of Na^+ channels and activation of K^+ channels resulting in the flow of K^+ out of the cell which decreases the membrane potential, a phenomenon called *Repolarisation*. Input current from a presynaptic cell invokes a voltage response in the cell membrane and if the input current crosses a threshold voltage, a positive feedback is initiated causing the membrane potential to depolarise suddenly giving rise to a short burst of electrical signal called an action potential or a spike. The membrane potential decays rapidly after the action potential generation due to the activation of the faster K^+ channels. The membrane potential hyperpolarises below the resting potential before coming back to the original equilibrium resting potential. During this decay period, additional input won't have any effect on the membrane potential to evoke another action potential - this period is called a *refractory period* and can last up to tens of milliseconds after the spike. Figure 2.2 illustrates the action potential generation.

The key insight into the mechanism of action potential generation came from Hodgkin and Katz in 1949, [25]. They discovered the role of Na^+ and K^+ ions in the generation of action potentials. The presence of voltage-gated ion channels in the cell membrane which can modify its membrane permeability to specific ions

[1] Any projections from the neuronal cell body, also termed as *neurites*

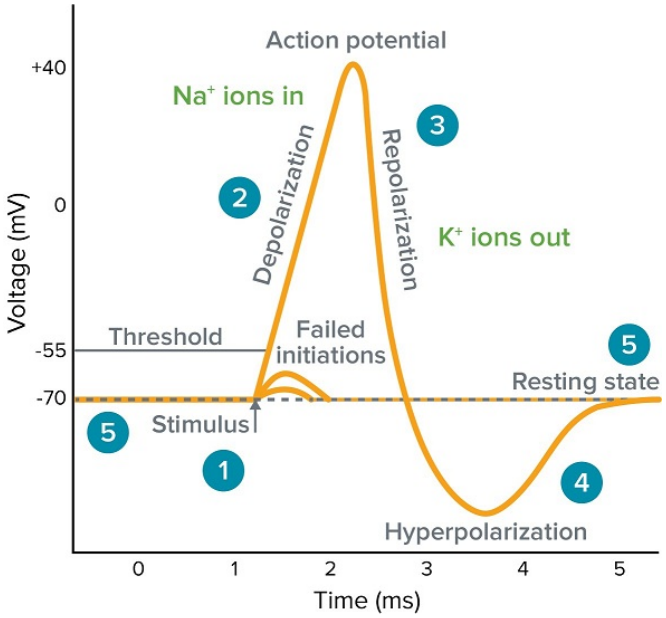

Figure 2.2: Illustration of an action potential generation

results in the generation of the spike. Evoked spikes are then propagated along the axon and transmitted to connected neurites at the axon terminals. Since the spikes can propagate over large distances, such signals are particularly of great importance.

Neurons transmit information among each other via a specialised location called a *synapse*, and synaptic transmission of signals among a network of neurons is fundamental in neural functionality and high level cognitive behaviours such as perception, learning, memory etc. [26]. There are two different types of synapses - chemical and electrical. Electrical synapses are synapses where voltage gated ion channels in the presynaptic membrane depolarises the postsynaptic membrane potential directly. Gap junctions are electrical synapses. In chemical synapses, presynaptic action potential releases neurotransmitters at the synaptic junctions which in turn open or close postsynaptic voltage gated ion channels resulting in membrane potential change. Synaptic transmission via action potential through the axon is a chemical synapse.

Presynaptic terminals are terminal structures of an axon where electrical signals (i.e. action potentials) travelling down the axon from the cell body are converted into chemical signals (i.e. neurotransmitters). Neurotransmitters re-

leased from the presynaptic neuron are bonded with the specific postsynaptic receptors present in dendrites of the postsynaptic neuron. This causes the ion channels in the postsynaptic neuron to open or close allowing for the flow of ions. This ionic flow through the membrane results in a change in membrane potential depending on the type of neurotransmitter i.e. excitatory(depolarising eg. L-glutamate) or inhibitory(hyperpolarizing eg. γ-aminobutyric acid(GABA) - thus completing the synaptic transmission [27]. A detailed illustration of the synaptic transmission at a chemical synapse is shown in Figure 2.3.

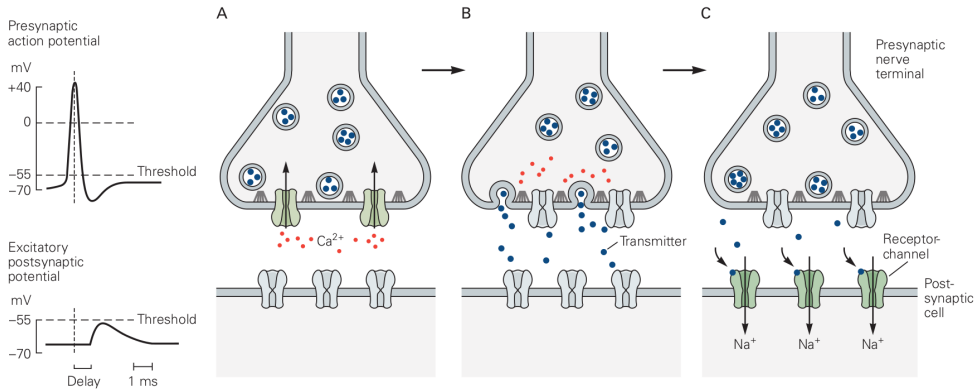

Figure 2.3: Synaptic transmission at chemical synapse [28]. **A.** An Action potential arriving at the presynaptic terminal causes the voltage-gated Ca^{++} to open. **B.** The Ca^{++} channel opening causes the vesicles containing neurotransmitter shown in blue dots, to fuse with the membrane and release their contents into the synaptic cleft. **C.** The released neurotransmitter molecules then diffuse across the synaptic cleft and binds with the corresponding receptors at the postsynaptic membrane. These receptors cause ion channels to open and close, thus changing the membrane potential of the postsynaptic neuron.

2.3 *In-Vitro* neuronal culture

In-vitro research refers to studies conducted using some components of the living organism, but outside the organism and in a controlled environment. The capability of *in-vitro* neuronal culture has been fundamental in the advancement of understanding of brain functions. *In vivo* on the other hand refers to studies performed on whole living organisms. The landmark work by [29,30] demonstrated -

for the first time - the successful growth of nerve fibres of embryonic tissue outside the body. His studies not only answered fundamental questions about the growth and development of nerve cells to nerve fibres, but transformed biological science to a new direction in development studies in neuroscience.

Over the past century, a diverse plethora of techniques have been developed for *in-vitro* neuronal culture. Figure 2.4 shows the emergence timeline over the last 100+ years of different neuronal culture techniques. A detailed review of different techniques is reported in [31].

Fundamentally, there are two main approaches for an *in-vitro* neuronal culture - *Acute or Organotypic Slice* [32] and *Dissociated* culture. The dissociated culture method has been a preferred method to study individual neurons or group of neurons for decades due to the ease of dissociating neurons and maintaining the culture. Even though all the experiments for the work in this thesis utilise the dissociated culture technique, a brief overview of slice culture is presented for completeness.

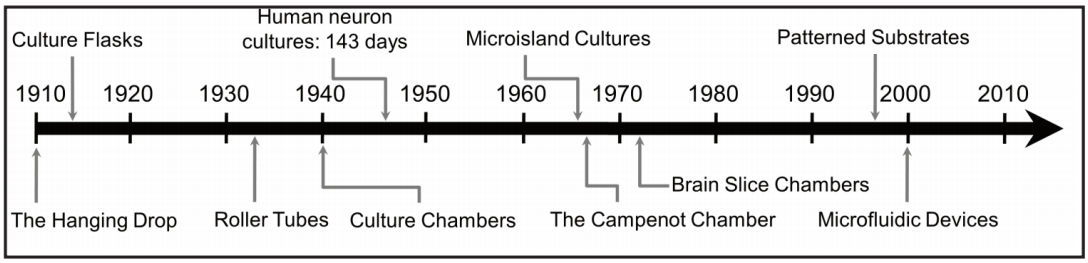

Figure 2.4: Emergence of cell culture methods. The timeline shows introduction of new neuronal culture methods over the past century. [31]

2.3.1 Brain slice culture

Slice culture utilises thinly sliced ($100 - 500\mu$m thick) sections of the brain in a controlled *in-vivo* like environment. The complex neural circuitry and the spatial distribution of the neurons established during the development stage are relatively undisturbed along with tissue functions in a tissue slice under favourable *in vitro* conditions [33]. The main advantage of such brain slices is the partial preservation of functional and structural properties of the original intact brain.

Such brain slices are used for a diverse range of studies - from intrinsic developmental studies, network dynamics to synaptic plasticity. In many cases, brain slices are the preferred choice for many neuroscientists due to the structural and functional integrity of the slice culture. With the development of Micro(also referred as Multi) Electrode Arrays(MEAs), brain slices may be coupled with MEAs to record electrophysiological activities [34, 35]. It is straightforward to record data from slices when coupled with MEAs, in comparison to the dissociated cultured networks which can take many weeks for the culture to mature to start measurements. An example of a rat brain (hippocampus) slice coupled with CMOS based MEAs is shown in Figure 2.5.

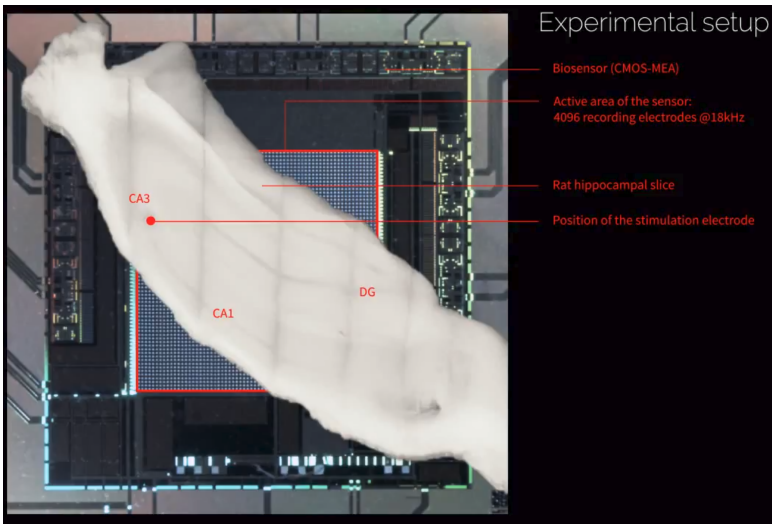

Figure 2.5: Rat hippocampal slice recorded by high density Multi Electrode Arrays(4096 electrodes). Screenshot from [36]

Although the main advantage of the slice culture is its partial morphological and functional integrity, the same feature becomes undesirable when the study focuses on the dynamical evolution of the neuronal network from an unstructured initial condition under some external stimulation. Slice cultures are not ideal in studies that focus on inducing specific network response or how the network connectivity evolves with time when started from a random unstructured distribution of neuronal cells. Dissociated cultures on the other hand provides the desired flexibility and control to study a plethora of research topics.

2.3.2 Dissociated culture

Demonstration of growth and maturation of tissues not just inside the organism (*in-vivo*) but also outside of the body (*in-vitro*) has opened new and innovative opportunities for neuroscientists [37] to study nervous system and neuronal dynamics that underlie the foundation of higher level behaviours such as cognition, memory, learning and more.

Among neuroscientists, the dissociated neuronal culture is a common method to study neurobiology due to the relative ease with which the brain tissues can be dissociated to isolate neurons, maintain and measure physiological phenomenon. Such dissociated cultures can be kept healthy for a long period (up to months) making them an ideal experimental setup to study a variety of brain functions. Dissociated neuronal cultures grown on planar MEAs provide non invasive extracellular electrophysiological recordings (further discussed in Section 2.4) of the neurons at different time points under different desired pharmacological or electrical stimulation conditions.

Neurons grown in dissociated cultures form seemingly random synaptic interconnections without maintaining the *in-vivo* like network. However, neurons tend to retain the morphological and physiological properties that correspond closely to the *in-vivo* properties [38]. Hence, such dissociated cultures can be seen as a reasonably simplified biological model of areas of the brain. Such a model is an appealing experimental setup to study a wide range of brain functions due to the fact that despite its simplicity, such a simple model exhibits rich neuronal dynamics [39].

Cultured neurons provide a "close to ideal" substrate to study brain functions since the cultured neurons can be grown healthily for months. This allows for a controlled experimental setup to start a biological network without any preconfigured interconnections, and investigate and alter these connections to study overall network dynamics in response to different stages in network change or controlled external perturbations. Neuronal mechanisms such as long-term potentiation (LTP) or long-term depression (LTD) are particularly interesting to study because these mechanisms are synaptically analogous to learning. Neuronal culture models to study network dynamics will be discussed further in the

next chapter.

2.4 Electrophysiology

Electrophysiology is the study of the electrical properties of living neurons or tissues and investigates the underlying cellular processes that control such signaling. It is a "gold standard" technique to study neural signals. Since the discovery of the intrinsic relationship between the nervous system and its electrical properties by Galvani more than 200 years ago, an immense technological advancement in the instrumentation has resulted in highly sensitive electrophysiological tools with high temporal resolution. Electrical recording of neuronal activity has been commonly used to analyse a wide range of dynamics of single cell to network level neuronal systems [7, 40–46].

With different electrophysiological techniques it is possible to measure and evoke electrophysiological activities at different spatial scales. Intracellular methods allow for membrane potential measurement from across the cell membrane by physically probing the cell. This requires two electrodes - one inside the membrane and one outside the membrane. The patch-clamp technique has been a gold standard technique for intracellular electrophysiology [47](and the references within). Though this technique provides an accurate measurement of the electrical activity, the technique is invasive and the viability of patched neurons lasts only up to a few hours. In addition, intracellular techniques require intricate skills to perform and it becomes impractical to analyse network wide activity. These limitations make the patch-clamp technique unscalable to study large network of neurons [48].

In contrast to intracellular recording techniques, extracellular recordings are performed by placing an electrode close to the cell membrane and a reference electrode placed far away in extracellular fluid. Due to the non-invasive nature of the technique, it has been widely used to study population wide activity for a prolonged period of time. When there is an action potential or a spike, both intracellular and extracellular ionic contents are changed due to opening and closing of ionic channels on the membrane as described in Section 2.2. This change in ionic concentration is registered by the extracellular electrode placed near the

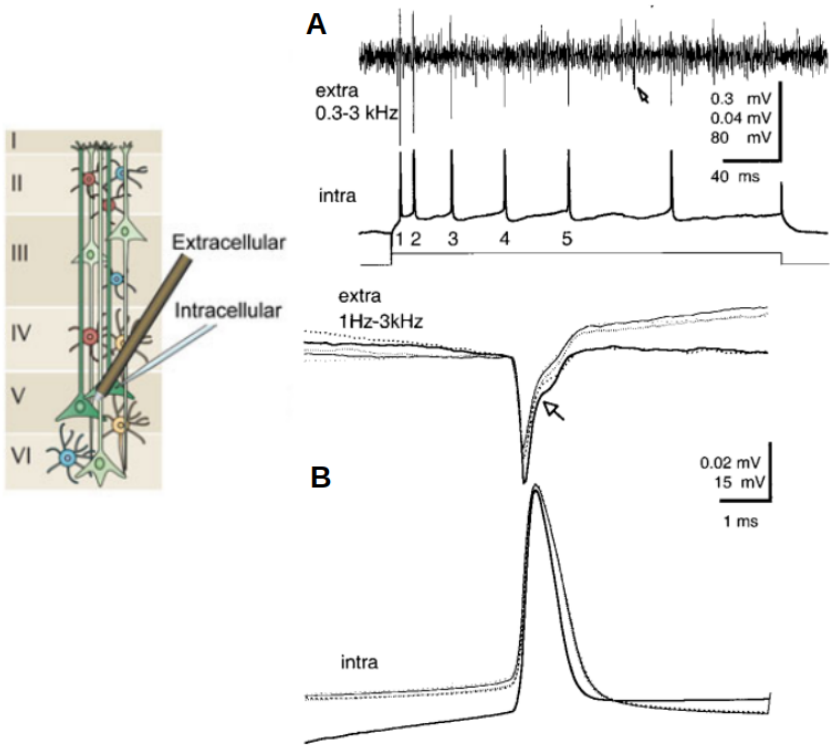

Figure 2.6: Band-pass filtered extracellular and intracellular recordings. **Left:** Illustration of cells across cortical layers with extracellular and patch clamp electrophysiology. **Right: A.** Simultaneous extracellular recording and intracellular whole cell patch clamp recordings. **B.** Averaged extracellular and intracellular waveforms from the same neuron. [49]

membrane as a drop in resistance between the recording and reference electrode. Figure 2.6 shows an illustration of extracellular and intracellular recordings and simultaneous intra and extracellular spike waveforms.

The intracellular and extracellular recordings are different not just in the range of amplitude - the extracellular signals' magnitude are lower than intracellular, but also in the shape of the waveform as shown in the Figure 2.6(B). Extracellular recording is not a direct measurement, but a measurement of the corresponding changes on the extracellular fluid near the cell. Hence, the extracellular spike waveform shape is a complementary, negative spike, to the direct intracellular spike. Intracellular recording records the voltage difference between the inside

and outside of the cell membrane. Extracellular recording records relative voltage change outside of the membrane which corresponds to the true voltage changes inside the cell membrane. So, it is conventional in extracellular data analysis to use the complementary inverted signals as shown in 2.6(A).

To map high resolution network-wide neuronal activity, a tightly spaced array of electrodes can be utilised. In an *in vivo* setting, an array of electrodes such as tetrodes can be placed on the brain region of interest to record extracellular activity. For an *in vitro* neuronal culture setting - which is the setting used for this thesis work, substrate based MEAs have become a standard electrophysiological device to study various neuronal properties.

2.5 MEA technology

Over the years the term "MEAs" has become an umbrella term that encompasses a wide variety of different forms of recording device. These may be differentiated based on the type of transducers (multi-transistor array, capacitive-coupled array, micro-electrode array), substrates (active array, passive array, silicon array, CMOS array), shape of the device (tetrodes, needle, polytrodes) or the application (*in vivo* - implantable, *in vitro* - non implantable). Hence, it is important to briefly set the context for the terminologies used with regards to MEAs in this chapter and the whole thesis in general.

The generic term MEA covers both implantable neural probes (see Figure 2.7) and electrode-integrated planar substrates (see Figure 2.8). Implantable neural probes can be placed directly on the region of interest in a living organism to record extracellular neural activity. Electrode-integrated substrate MEAs are not implantable and generally used for *in vitro* neuronal cultures. Such MEAs have a cell culture dish or a chamber to hold the culture medium (see Figure 2.8). The term *array* refers to the spatial layout of the array of electrodes, though the MEAs refers to the whole device. For the context of this thesis work, MEAs refers to substrate based MEAs and not the implantable neural probes.

The work of [51] describing a planar Micro-Electrode Arrays (MEA), also referred as Multi-Electrode Arrays - and a successful demonstration of recording and stimulation of network of neuronal culture by [52], were important milestones

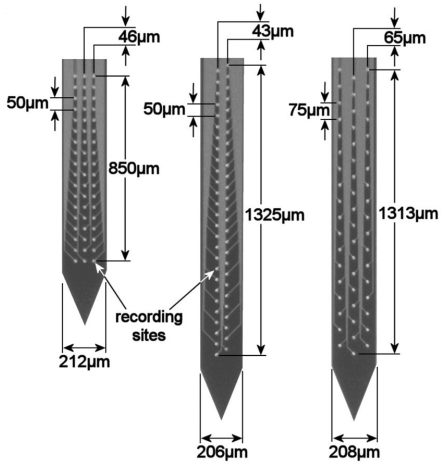

Figure 2.7: Fifty-four site polytrodes. The polytrodes have electrodes or recording sites in 2 or 3 columns spaced at $43 - 75\mu$m [50]

in *in-vitro* electrophysiology. These landmark works opened up new avenues in the area of *in-vitro* electrophysiology to study a wide variety of neural functions. MEAs are essentially an array of multiple low impedance electrodes laid out on a planar substrate which are sensitive enough to detect slight changes in the membrane potential of contacted cells.

In the early 1990s, Fromhertz et al [53] mounted a cell on the surface of a Field-Effect Transistor(FET) on Silicon(Si) allowing for direct coupling of neurons and Si without the use of interfering metal electrodes. Since then with the development in CMOS (Complementary Metal Oxide Semiconductor) technology, it is possible to record and stimulate simultaneously from an integrated circuit packed with thousands of electrodes which is especially beneficial to study neural plasticity and neural dynamics.

In the current technology, with the few exception of high density MEAs, MEAs are usually composed of a few hundred electrodes with an electrode pitch of 100-500 μm embedded on a glass substrate as shown in Figure 2.8. The electrodes are typically made of Gold (Au), Indium-tin Oxide (ITO), Titanium Nitride (TiN) or platinum(Pt) which are bio-compatible and have low impedance (less than 500Ω at 1kHz).

The limited number of electrodes and large electrode pitch distance pose a

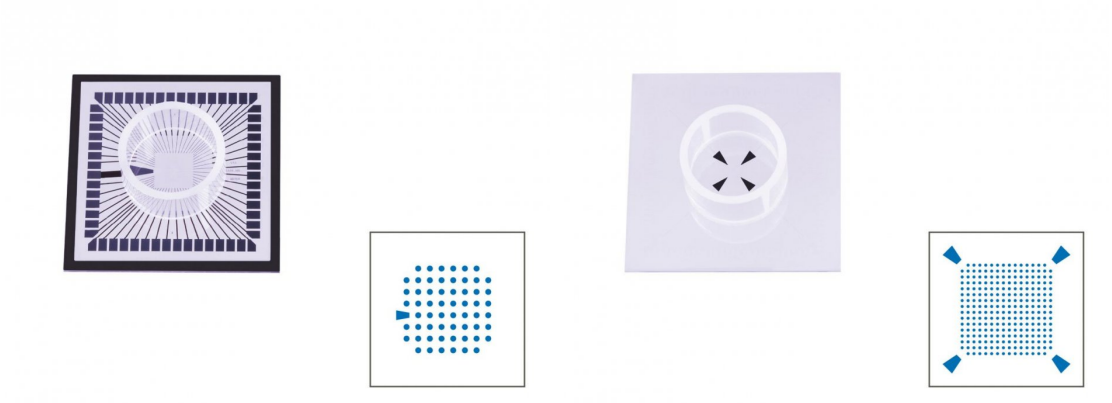

(a) 60 electrodes MEA with electrode layout (b) 256 electrodes MEA with electrode layout

Figure 2.8: MEA devices with electrode layout

limitation in terms of substantial spatial under-sampling of the neuronal network. This is not enough to unlock the full capability of MEAs; specifically studying electrophysiological activity to study correlation/synchrony at both cellular and network level. MEA electrodes with size and distance approximating that of neuronal cells dimensions can provide a much better spatial resolution and help provide a much better insight into the neuronal activity [54].

Active pixel sensor (APS) CMOS based MEAs allow for a higher density of electrodes with reduced electrode size and electrode pitch distance. APS devices consider each electrode as a pixel which can register changes in electrophysiological activity.

The experimental setup for this work is based on a CMOS MEA (3Brain AG, Switzerland). This MEA has 4096 electrodes laid out in a 64 x 64 grid. The dimension and spatial layout is designed to capture as much detail as possible from the neuronal culture. The system comes with a recording device, BioCam, with BrainWaveX software to visualise, record and do preliminary data analysis. The device can record at up to 18kHz sampling frequency. Figure 2.9**(A)** shows a CMOS based MEAs (3Brain AG) with a zoomed in section of the active area **(B)** where 4096 electrodes are laid out in a 64 x 64 grid, along with neuronal responses recorded with the BrainWaveX software **(C)**.

Each pixel of the biochip embeds on-chip amplification and filter stages di-

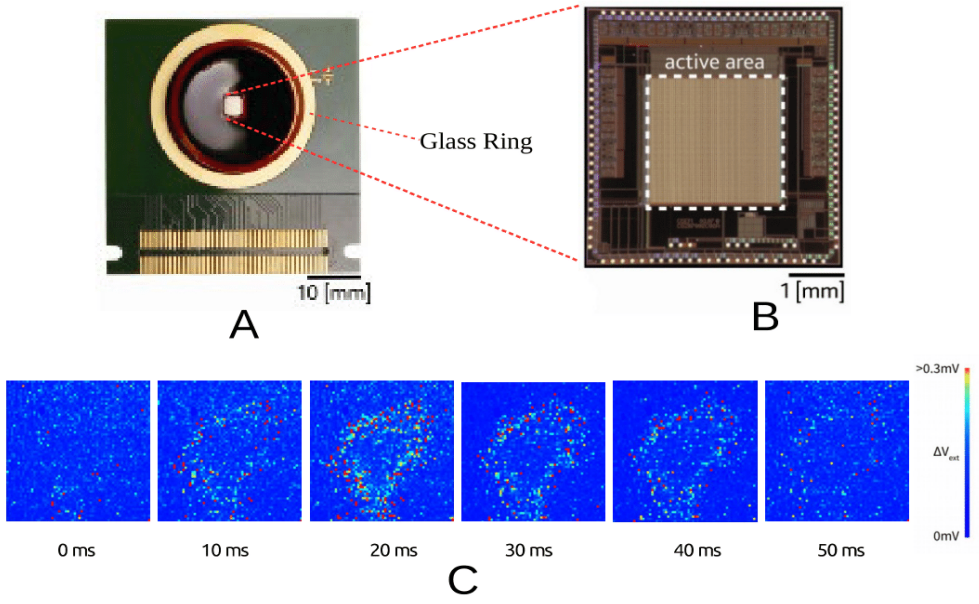

Figure 2.9: **A.** High density CMOS-based MEA **B.** Zoomed in section of the active area of the MEA chip **C.** Electrical activity recorded by 4096 electrodes of the APS device.

rectly at the point where the biological signals are measured. Due to multiplexing, multiple channels can be read from a single wire which results in minimisation of the number of physical wires and an increase in the density of the electrodes.

The MEAs used are of three different types with different area size and electrode layout.

- HD-MEA Prime: Prime is an electrode array of 4096 electrodes laid out in an area of 2.67 mmx 2.67 mm Figure 2.10(A). The electrode size 21µmx21µm with pitch distance of 42µm.
- HD-MEA Arena: Arena has the same recording array as the Prime, but it offers a larger surrounding flat area(6mmx6mm) Figure 2.10(B). This can be useful for placing a larger tissue slice on the chip for optimum coupling.
- HD-MEA Stimulo: The Stimulo, as the name suggests, incorporates in addition stimulating electrodes laid out in a 4x4 uniform grid. The Stimulo

has a large sensing area of 5.12mmx5.12mm with electrode pitch distance of 81µm Figure 2.10(C).

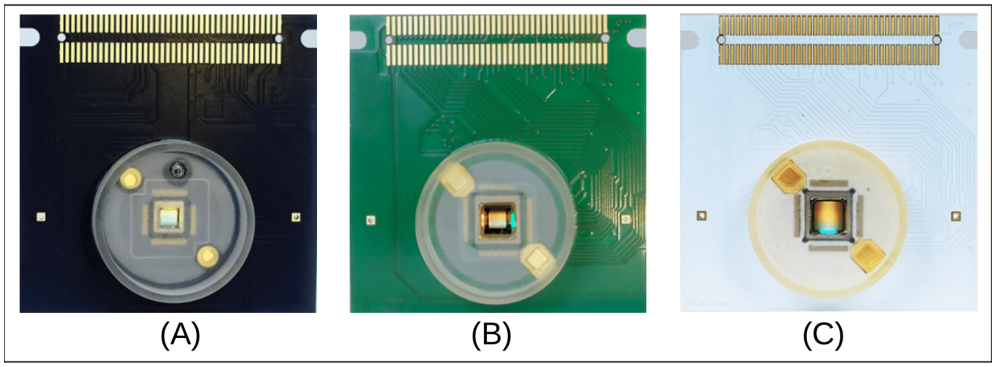

Figure 2.10: **(A).** HD-MEA Prime **(B).** HD-MEA Arena. **(C).** HD-MEA Stimulo

2.6 Spike detection and sorting

As discussed earlier, recent progress in CMOS technology has provided the technological capability to simultaneously record from increasing neuron density at a high sampling frequency. Typically, raw voltage extracellular recordings from HD-MEAs are very large in volume, which complicates the processing of raw voltage recordings into discernible *spikes*. The problem is exacerbated by closely spaced electrodes which results in recording from multiple neuronal sources as a composite signal. Hence, processing raw voltage signals to a series of *spike trains* becomes crucial since further analysis depends on this stage. *Spike trains* are representation of neural activity obtained by detecting extracellular action potentials or spikes, but only preserving the time of the event [55, 56]. Keeping only the time of the event, provides an abstraction of the neurophysiological recordings in the form of a simple sequence of ordered spike trains.

Earlier studies assumed that information is encoded in the rate of the spikes [57–59], a process also known as rate coding. However, it later became evident that rate coding cannot explain encoded information for complex behaviours and timing of the spikes plays a key role in encoding information [60–62].

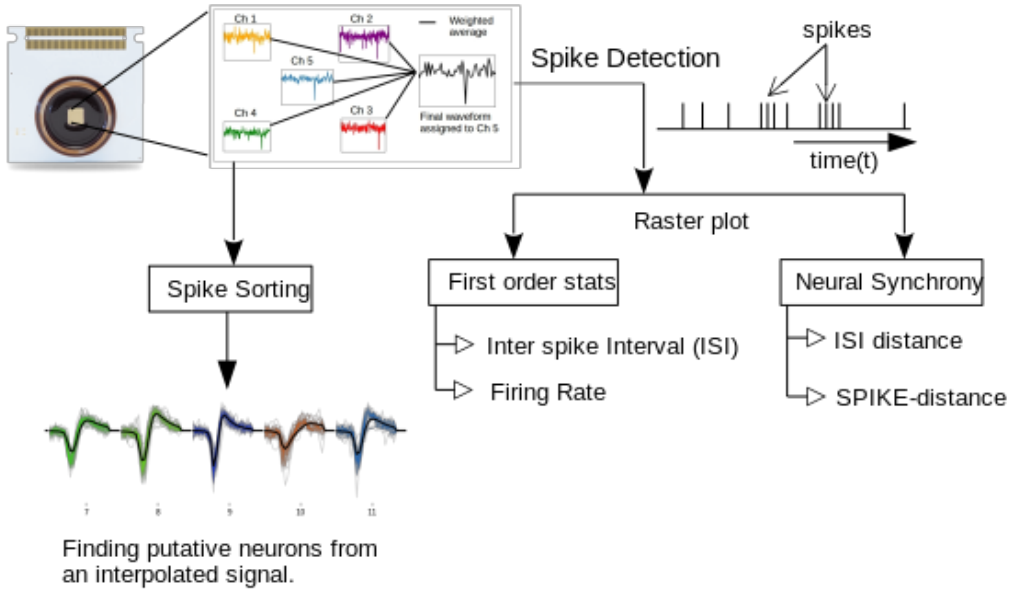

Figure 2.11: Processing of raw voltage traces into different statistical and spike sorting analysis

HD-MEA recordings generate a large volume of data, mainly due to ever increasing number of electrodes and the recording sampling frequency. For instance, a 3Brain BioChip with 4096 electrodes generates uncompressed data at approximately 7 GB/min when recorded at 18 kHz sampling frequency. This poses a number of challenges.

- Processing speed
- Noise interference
- Accurate detection of spiking events
- Feature extraction for spike sorting

Figure 2.11 shows a simplified illustration of the process flow from raw voltage traces into putative signals from each electrode or spike train analysis after spike detection on the channel signals.

The neuronal response signals recorded are subject to noise and interference from neighbouring electrodes. Recorded signals need to be accurately associated with spiking events to reduce the voltage readings into point process (spike trains). These spike trains are prerequisites for spike train analysis. Due to the typical large volume of data, a spike detection algorithm has to be highly efficient and fast to process and detect true spiking events successfully [63].

In HD-MEA recordings, the signals are most likely to be recorded by multiple channels due to closely spaced electrodes which causes signal overlapping and waveform assignment problems. However, this redundancy can be exploited to improve the signal to noise (SNR) ratio and hence spike detection [64, 65].

Conventional thresholding-based event detection on high density recording does not provide sufficient information to reliably detect true spikes. An interpolation spike detection method optimised for HD-MEA data, to detect events from closely electrodes successfully discarding most of the background noise and false activities, which was developed by Muthmann et al [63] is implemented for spike detection in this work.

The interpolation method uses voltage traces from five neighboring channels which are weighted with a relatively stronger weight for the central channel than the four surrounding channels. These weights are then averaged and assigned to the central channel as a new signal as shown in Figure 2.11. Threshold value for spike detection can be adjusted to capture most of the possible events and reduce probability of false negatives.

Though many works have been done to bring together many different spike detection and sorting algorithms, there seems to be a significant disagreement between different methods. Without the availability of ground truth information about where each neuron is located with respect to the electrodes, spike sorting becomes particularly difficult for HD-MEA recordings.

2.7 Conclusions

This chapter introduced the relevant topics and terminologies necessary to set the context for the review of the related literature and state of the art which will be presented in the next chapter and for the overall research presented in

this thesis. The chapter has covered a basic background introduction to neurons, their dynamics, and a summary of approaches to study the neuronal properties. Electrophysiological studies are also discussed along with different technological advancements in MEAs. The chapter also covers the choice of MEAs for the thesis work. Finally, the challenges of data analysis are discussed.

Chapter 3

Literature Review

3.1 Introduction

In the last chapter, generic concepts in neuroscience/computational neuroscience were introduced to set the context for the reader. This chapter focuses on a review of related research and describes the rationale behind the work presented in this thesis, discussing current limitations in the research literature.

In this chapter, the concept of synaptic plasticity and Hebbian based learning and how it evolved as a convincing phenomenon in the study of higher level cognitive tasks such as learning and memory (see Section 3.2) is presented. Following that, early developmental studies into neuronal dynamics and synaptic plasticity in *in vitro* dissociated neuronal cultures and the advantages of such models (see Section 3.3) are discussed. The past 20 years of plasticity studies in MEAs based neuronal cultures are outlined, highlighting the landmark studies and new findings that helped shape this area of research (see Section 3.3.3). A critical analysis of the difficulties and limitations of an *in vitro* experimental model for plasticity studies is presented. Finally, the concept that high density MEAs with thousands of electrodes for extensive plasticity study may help to provide a better understanding of such neural plasticity phenomena and neuronal dynamics in general, is also discussed, justifying the use of HD-MEAs as the chosen electrophysiology approach for the study. Following that, different types of network connectivity and methods to infer connectivity are presented (see Section 3.4). Finally, prob-

lems in network connectivity are highlighted together with a summary of the current knowledge gap in connectivity inference methods (see Section 3.5.3).

3.2 Activity-dependent synaptic plasticity

The ability of the nervous system to adapt and change to a new functional and structural state in response to intrinsic or extrinsic factors can be broadly defined as *'Neural Plasticity'*. Neural plasticity is manifested from the micro scale at the level of neurons and synaptic modifications to a macroscale as changes in spatiotemporal patterns at different brain regions. The concept of neural plasticity is not a new idea. The early conceptualisation of neural plasticity can be traced back to 1913 to Ramon y Cajal, who put forward the idea that changes in synaptic connections could be the foundation for memory [66].

Activity-dependent plasticity is a form of neural plasticity, both functional and structural, as a result of personal experiences and cognitive functions [67] and is believed to constitute the cellular basis of learning and memory [68]. Activity dependent modifications of neural connections provide a powerful mechanism to describe development and shaping of neural responses to neural inputs. Coordinated development and shaping of neural responses at network level can give arise to interesting stimulus-specific responses, which at a higher level may be manifested as higher level cognitive activity such as learning and memory.

The seminal idea on neural plasticity, proposed by Donald Hebb [69], which later was became known as Hebb's rule, attempted to relate neural activity with synaptic plasticity. Hebb boldly postulated:

"When an axon of cell A is near enough to excite a cell B and repeatedly or persistently takes part in firing it, some growth process or metabolic change takes place in one or both cells such that A's efficiency, as one of the cells firing B, is increased"(p.62) [69]

Essentially Hebb proposed that repetitive correlated activation of pre- and postsynaptic neural activity gives rise to longer lasting changes in or between these neurons involved, which can be simplified as, *"when one neuron drives another neuron to fire repeatedly, the connection between the two is potentiated'* or *'Neurons that fire together wire together'* [69]. Although Hebb's formulation wasn't well received when first formulated, subsequent advances in neurophysiological technology allowed for accumulating neurophysiological data that confirms Hebb's postulate. The instances of Hebb's synapse was later reported in

an induced long term potentiation experiment by Bliss and Tomo in 1973, which showed evidence of synaptic change based on pre- and post-synaptic neuron's activity [70], and kindling [71]. Theoretical studies have indicated that along with Hebbian like potentiation, depression between two neurons that are not active, is also equally necessary [72, 73]. Depression is necessary to prevent saturation of all the synapses to maximum output which affects the stimulus selectivity properties, and to prevent a runway positive feedback loop between network activity and synaptic weights [74].

In 1973, a study of the neural pathway in rabbit hippocampus by Bliss and Tomo [70] discovered that rapidly and repeatedly activating the synapses resulted in a long lasting increment in the synaptic strength, which is defined as long term potentiation; a reverse phenomenon, first observed in rabbit cerebellar cortex in 1982 [75], also exists in which the synaptic strengths weaken with repeated activation of synapses. This is called, long term depression. Long-term potentiation (LTP) and long-term depression(LTD) are important phenomenon in the study of neural plasticity. Both LTP and LTD have long been regarded as potential mechanisms for memory and learning. Induction of LTP includes depolarisation of the postsynaptic neuron and activation of N-methyl-D-aspartate (NMDA) receptors by release of glutamate, which causes an increase in intracellular Ca^{++}, which in turn increases the amount of functional α amino-3-hydroxy-5-methyl-4-isoxazolepropionic acid (AMPA) receptors in the membrane, increasing the excitability of the postsynaptic cell [20].

3.2.1 From Hebbian rule to spike-timing dependent plasticity

The Hebbian learning framework has been refined into a temporally asymmetric learning rule induced by temporal correlation between spikes of pre- and post-synaptic neurons. One such form of Hebbian learning is called Spike-timing Dependent Plasticity (STDP) , and is relevant to neuronal network dynamics. STDP can be considered as a spike-based adaptation of the Hebbian learning rule where repeated arrival of a presynaptic spike just a few milliseconds before the postsynaptic spike leads to strongly potentiated synaptic weights (LTP) and

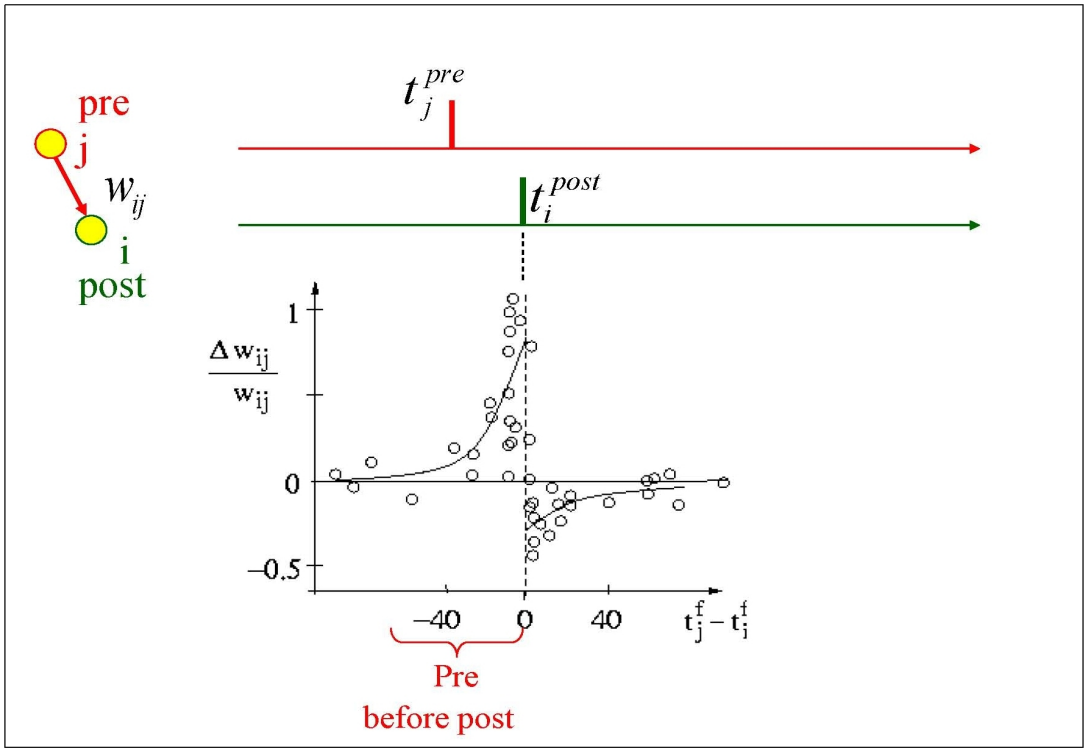

Figure 3.1: STDP function schematic that shows the change of synaptic weight change as a function of the relative timing of pre- and post-synaptic spikes. [76]

arrival of a presynaptic spike a few milliseconds after the postsynaptic spike lead to strongly depressed synaptic weights (LTD). The repeated controlled firing of pre- and post-synaptic neurons induces a change in the amplitude of a single excitatory post-synaptic potential (EPSP) . Figure 3.1 shows synaptic potentiation and depression plotted against the spike time difference $\Delta t = t_{post} - t_{pre}$. The degree of synaptic change to the relative timing of spikes suggests that information transfer may be encoded as temporal coding in the range of milliseconds.

The early experiments with precisely timed pre- and post-synaptic spikes at milliseconds resolution was conducted by [77, 78]. Even earlier investigations can be traced back to 1983 by Levy and Stuart, although Levy and Stuart's experiments used lower temporal resolution and bursts of spike rather than single spikes [79]. Further works by [80–82], paved a path as a precursor for model STDP investigations. Bi and Poo [82] demonstrated that in cultures of rat hip-

pocampal neurons, correlated spiking of pre- and postsynaptic neurons induces persistent potentiation and depression of glutamatergic synapses. The strength of potentiation and depression was dependent on the timing of postsynaptic spike before or after presynaptic firing, demonstrating dependence on spike timing. Mathematically, a basic STDP model can be expressed with a small number of simple expressions as follows.

Consider two neurons, a presynaptic neuron j and postsynaptic neuron i. The synaptic weight change Δw_{ij} from presynaptic neuron j is dependent on the relative spike timing between presynaptic spike arrival and the postsynaptic spike generated. Let's describe the presynaptic spike arrival times at synapse j by t_j^f where $f = 1, 2, 3, ...$, which is the spike count. Similarly, t_i^n with $n = 1, 2, 3, ...$ indicates the firing times of the postsynaptic neuron. According to [83], the total synaptic weight change induced by stimulation can be expressed as,

$$\Delta w_{ij} = \sum_{f=1}^{N} \sum_{n=1}^{N} W(t_i^n - t_j^f) \tag{3.1}$$

where $W(x)$ denotes the learning window function illustrated in Figure 3.1 which can be further expressed as,

$$W(x) = A_+ \exp(-x/\tau_+) \qquad for \quad x > 0 \tag{3.2}$$

$$W(x) = -A_- \exp(x/\tau_-) \qquad for \quad x < 0 \tag{3.3}$$

The parameters A_+ and A_- may depend on the current values of the synaptic weight w_{ij}; τ_+ and τ_- are time constants which are of the order of $10ms$. $x > 0$ indicates postsynaptic spike after presynaptic spike, leading to potentiation and $x < 0$ indicates postsynaptic spiking before presynaptic spiking, leading to depression. These STDP models have been used to fit experimental data [81] and also on simulation models [84].

3.3 Dynamics and plasticity in neuronal networks

To study the general characteristics of long-term network dynamics, independent of cell type, it is useful and important to have **(1)** a generic model without any predefined anatomical structures, **(2)** a stable system that allows for long-term neuronal activity and **(3)** a highly controllable system.

In this section, a brief overview of a neuronal culture model is presented, highlighting the advantages of such models interfaced with MEAs to study long term network dynamics. Furthermore, critical reviews on the previous works on induced plasticity with electrical stimulation on neuronal cultures coupled with MEAs are discussed. The aims of this section are to provide a critical review of related research, and set a context for the thesis work. It also discusses the challenges in reliably inducing network connectivity changes.

3.3.1 Neuronal culture model to study network dynamics

As described in Chapter 2.3.2, neuronal cultures are simple, yet effective biological models and have long been considered a more suitable experimental setup than the native tissue to study neuronal dynamics [85,86], biochemistry, pharmacological properties, molecular biology and neuroimaging. This idea of extracting brain cells and culturing them in the lab in a controlled environment started as early as half a century ago in 1950s [87].

As with any type of adherent cells, neuronal culture preparation requires a plating surface to undergo some form of treatment to promote cell attachment. Pre-coating the surface with a thin layer of Extra Cellular Matrix(ECM) polymers such as collagen has been proven to be an effective treatment [88]. Similarly, simple polymers such as poly-L-lysine(PLL) with positively charged amino residues, are reported to be just as effective for cell adherence and cell growth promotion [89]. Due to the simplicity of the coating procedure, PLL coating has now become a standard in neuronal culture. The procedure constitutes incubating the plating surface with coating factors for several hours before proceeding with seeding the cells on the plates. Similarly, there are other coating factors such as

polyethylene-immine(PEI) , Laminin, poly-d-lysine (PDL) etc which work just as well.

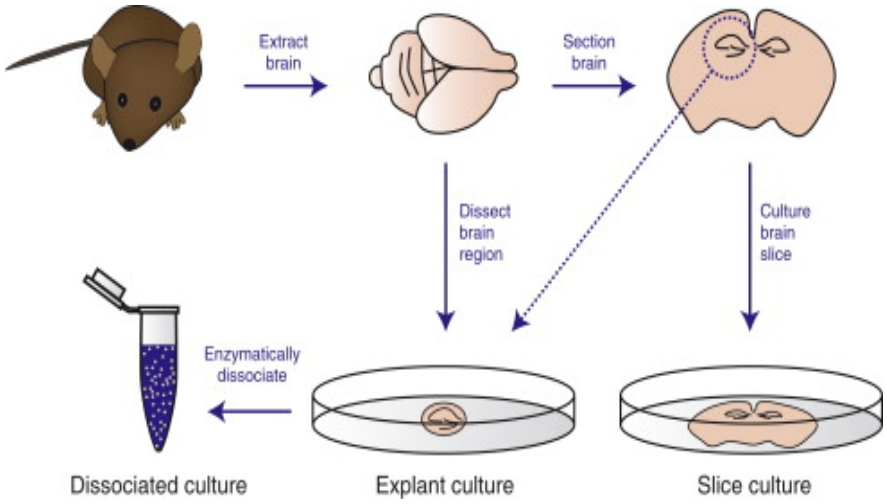

Figure 3.2: Primary cell cultures procedure; dissociated and slice [90]. After extracting specific brain tissue, the tissue can be cultured as fully intact slices or enzymatically and mechanically dissociated into single cells (neurons, glial cells) to obtain a dissociated culture.

To study long-term neural dynamics and neural processes in a controlled environment, it is important that the experimental system satisfies optimum growth conditions(usually an incubation at $37°C$, 5% CO_2 and 65% humidity), that are crucial to study different phenomenon.

3.3.1.1 Generic model

Dissociated neuronal cultures are usually prepared from brain tissues at an embryonic stage. For rat and mice, brain tissue from a 15-18 day embryonic stage are usually used for successful preparation. At this stage, the cells are at a very early stage without a defined network morphology and appear to be undifferentiated - differentiated neuronal cells are neuronal cells which already exhibit morphological structures of a neuron and differentiated cells do not yet exhibit neuronal structures; though neurons from different brain regions maintain initial inherent morphological, molecular and physiological properties. This allows for tweaking initial culture conditions to drive the cell culture to produce different cellular

compositions i.e. neurons to astrocytes combinations [91]. Hence, sometimes the cells from such cultures are referred to as progenitor cells [92].

As illustrated in Figure 3.2, after extracting specific brain tissue, the tissue can be cultured as fully intact slices or enzymatically and mechanically dissociated into single cells (neurons, glial cells) to obtain a dissociated culture. The dissociated primary culture contains both excitatory and inhibitory neurons as observed in fully formed intact tissues - the ratio being $\approx 10\%$ inhibitory [93]. Studies conducted to compare the distributions of types of neurons(by immunohistochemistry) between an *in vivo* and *in vitro* networks show a similar distribution. Similar to an *in vivo* network, the majority of the neurons have been found to be glutamatergic excitatory neurons with 10-25% GABAergic inhibitory neurons [94, 95]. Such cultures also show demonstrate classical excitability properties with typical voltage gated membrane currents and synaptic connections(eg.AMPA, NMDA, glutamate gated channels) [88, 96], along with general physiological processes. Cultured networks also exhibit rich spontaneous activity dynamics [1, 8] characterised by synchronised network bursts followed by low firing phases.

In addition to the developmental changes, homogeneously distributed neurons self assemble into many clusters of neurons interconnected by fasciculated neurites [97, 98] . The availability of many different such processes has made the culture model an appealing choice to study connectivity relationship between structural and functional properties during neuronal development [99, 100]. Whether sporadic or synchronised bursts, the network activity is correlated with the development of synaptic connections. Studies have shown that an increase in the network bursts may be correlated with the number of synapses [101, 102]. Due to the flexibility of culture models with similar network properties and dynamics to the *in vivo* counterpart, such models are generic models that can be easily adapted for many different types of experiments to study a wide range of neuronal dynamics. The main advantages of such neuronal cultures are *flexibility* and *adaptability*; ability to respond to a wide range of novel stimuli and adapt to changing external stimuli.

Long term stability: It is crucial to maintain the stability of the neuronal network system especially if one wishes to study long-term response dynamics. Evoked electrophysiological responses of a network after electrical stimulation can

be obtained by culturing neuronal cells on substrates integrated with hundreds to thousands of micro electrodes in multi electrode arrays (MEAs). The electrodes measure the extracellular potential in a non-invasive manner, which makes it possible to do measurements over a long period of time. Neuronal activity characterisation is further discussed in the Section 3.3.2. Recent studies have shown that it is possible to maintain such dissociated cultures coupled with high density MEAs for up to 3 months with successful stimulation and recording [103].

Controllability: Reliable maintenance of a steady, consistent environment to support neuronal culture development can be achieved by ensuring control of the temperature, CO_2, oxygen level, humidity and timely exchange of the culture medium [99,100,104]. Pharmacological treatments can be applied to block specific synaptic receptors or channel types. Network activity can be manipulated by pharmacological or mechanical intervention by having patterned structures on the substrate upon which neurons grow [100]. Depending on the type of experiment and study under consideration, the environment can be easily manipulated to mimic different environments to study neurophysiological properties.

3.3.2 Spiking activity characterisation in neuronal culture

Early recordings of electrical activities in neuronal cultures relied mostly on the insertion of electrodes directly into the cell membrane to measure the intracellular potentials. Though such techniques provide a direct measurement with relatively higher signal-to-noise ratio(SNR) compared to extracellular recordings (with voltage in the mV range), this is a physically invasive process that requires manual intervention with a significant limitation in the number of simultaneous multi-site recordings, making this impractical for monitoring multiple cells for long term experiments.

In 1957, Hubel [105] reported detection of sharp potential fluctuations in extracellular space in synchrony with action potentials from nearby cells when he inserted thin metallic wires in cat's spinal cord. Such extracellular potential fluctuations were later termed as *'spikes'*. The process of spike generation is commonly referred as *firing*. These extracellular(EC) spikes are thought to be produced due to transient ionic flow in the extracellular vicinity during intracel-

lular potentiation. Hence, the shape of the extracellular spike is complementary to intracellular spikes as already discussed in Chapter 2.4. Since these extracellular currents are free to propagate, the amplitude scales with the inverse of the distance r between the source and the recording site [106]. Due to this, to measure EC spikes, the electrode has to be placed in close proximity to neurons and the spikes generally have much lower amplitude, usually in the µV range, as compared to intracellular spikes which are in the mV range. Despite these shortcomings, the EC potential allows for non-invasive recording, making it possible for multi-site long term recordings to study neurodynamics, plasticity and many other neurophysiological properties.

In the case of a dissociated neuronal culture, electrodes are embedded into a planar culture substrate. Neurons are dissociated and seeded on these MEA surfaces where neurons attach, grow and interface with the electrodes [3, 8, 39, 52, 53]. Since the neurons are seeded directly on top of the electrodes, the electrodes are in close proximity to the neurons to detect EC voltage fluctuations without any invasive contact with the actual cells.

Many of the *in vitro* neuronal culture studies with MEAs require characterisation of the spiking activity of the culture at some stage. In fact, a significant amount of work has been dedicated to the study and characterisation of spiking activity for many different objectives - neurodynamics [107,108], plasticity [4,109], learning in-vitro [7, 104], pharmacological testing [40] etc.

Neuronal cultures self-organise into highly interconnected networks that promote the generation of spontaneous, correlated neural activity even after a few days in *in vitro* [8, 110, 111]. The culture typically reaches maturity at about 3 weeks *in vitro* exhibiting high firing density and plateaus after that [8, 112], eventually declining in health after about 5 weeks *in vitro*. The network activity change is representative of the development time course of excitatory synapses [113]. Inhibitory synapses appear at a later stage with more prevalent GABAergic synaptic structures after 3-4 weeks [114]. This delayed prevalence of inhibitory synapses is manifested in the network activity of neuronal cultures after 3-4 weeks, where the network bursting activity becomes shorter in duration [115].

The network activity is typically organised into spontaneous network bursts that last for 100-200ms. *Bursting* can be defined as periods of high-frequency fir-

ing of a neuron followed by a period of silence. Bursting events can be studied for both synchronised network wide activity or single cell bursts. Both are common for MEA recordings from a cultures of dissociated neurons [8, 116]. At single cell level, the bursting consists of brief periods of high frequency firing separated by a quiescence period, as shown in Figure 3.3.

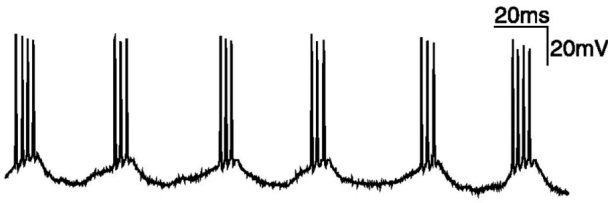

Figure 3.3: Intracellular voltage trace from a rhythmically bursting neuron, recorded from cat visual cortex *in vivo* [117]

Although bursting events are believed to play an important role in transfer of information in the brain, the precise mechanism of the burst generation and their purpose are only partially understood [118]. Neural synapses have been shown to display low probabilities of neurotransmitter release in response to a single presynaptic spike, making the transfer of information through single spikes unreliable and ineffective [119, 120]. The rapid bursts of spikes can cause build-up of intracellular Ca^{++}, due to not enough time between the spikes to allow a return back to the baseline level. This increased level of Ca^{++} in turn increases the probability of neurotransmitter release and the generation of post synaptic potential with each burst [121, 122], increasing the reliability of information transfer at the synapses. Bursting mechanisms have also been involved in LTP and LTD. Experimentally, in the hippocampus, temporally spaced postsynaptic bursting at relevant intervals have been shown to be sufficient to cause long term synaptic changes [123, 124] and also induced LTP and LTD implicated by bursting has been observed in other brain regions [125].

3.3.3 Plasticity studies in MEA based neuronal cultures

After the discovery of LTP in rabbit hippocampus in 1973 [70] and the subsequent discovery of LTD observed in the cerebellar cortex in 1982 [75], several long

term plasticity studies have been conducted over recent decades. In particular, the processes of synaptic plasticity have long been studied in simple nervous system of invertebrates interfaced with MEA. Invertebrate neurons have a large cell body which promotes better neuron to transducer interfaces, allowing for electrophysiological measurements with higher Signal-to-Noise Ratio (SNR) [126]. Neural plasticity processes observed in simple nervous systems such as *Aplysia* [127, 128], *Drosophila* [44], *Helix* [129, 130], *Lymnaea* [131], and *Helisoma* [132, 133] are also common and observed in mammalian nervous systems along with many molecular mechanism underlying simple to complex forms of learning and memory.

A dissociated neuronal culture grown on MEAs is an appealing experimental setup as a biological model to study a wide range of brain functions and neuronal network dynamics due to the fact that despite its simplicity, such a simple model exhibits rich dynamics similar to *in-vivo* conditions [2, 3]. There have been vast amount of research done over the past few decades with MEA based neuronal cultures, and it has become a gold standard method in neuroscience investigations. Such experimental setup has been utilised to characterise and study dynamics from several biological preparations; from invertebrates to different mammalian brain regions such as cortex [116] and hippocampus [134], by studying network development and applying electrical [11, 41, 46, 135] and chemical stimulation [42, 136] to induce synaptic plasticity at the network level.

However, the MEA method has also been the subject of criticism related to the fidelity of comparable neural activity, gene expression, morphology etc., in comparison to the *in vivo* scenarios, mostly due to brain being a 3D structure and planar MEAs being a 2D substrate. It is difficult to assess the degree of compromise presented by such *in vitro* cultures since the principles of neural computation in the real brain are not yet fully understood. Furthermore, the criticism may be viewed not so much a comment on the MEA approach but rather a criticism of all investigations on 2D substrates such as well plates. In terms of practicality and ethical perspectives, such *in vitro* cultures are the most relevant to investigate fundamental properties in a controlled setting over a prolonged period of time.

In the following section, a critical review of landmark research performed over

the past 20 years, to induce synaptic plasticity with electrical stimulation on neuronal cultures coupled with MEAs is presented. A discussion on the fundamental challenges with such models in reliably inducing plasticity, primarily due to variability in such dynamical systems, is also presented.

3.3.3.1 Searching for controlled plasticity through stimulation

Randomness is only a measure of our ignorance of the different causes involved in the production of events [137]

Mammalian neuronal cultures exhibit spontaneous activity, mainly characterised by mixture of discrete spiking events and network wide bursts. Such dynamics evolve with the development stages of the cultures. Though rich spontaneous and *in vivo* like physiological properties have been reported for *in vitro* neuronal cultures, *in vitro* neuronal systems are also very much subject to unexplained variability under similar conditions. Such variability have been observed at all levels of brain-behaviour organisations from spontaneous activity to trial-to-trial network responses with the application of repeated identical stimulus [138].

Several attempts to understand and modulate such variability in network dynamics by application of electrical and/or chemical stimulation can be found in the literature. Studies have shown that in general, low-frequency stimulation locks the phase of periodic bursts to the applied stimuli [107, 126]. Higher amplitude and frequency of electrical stimulation have been shown to induce a transition from synchronised bursting to more sparse spiking activity, similar to the dynamics of awake cortex *in vivo* [41]. Tailored electrical stimulation patterns can be applied to induce modifications of the network dynamics in terms of firing rates and bursting rate. During tetanic stimulation process, the strongest connections relative to other synaptic connections get stronger. Such mechanisms show selectivity properties by preserving connections that are more informative and relevant in the network dynamics under the stimulation.

Plasticity studies on neuronal cultures coupled with MEAs started in the 1990s and in particular this area of neuroscience was pioneered by Maeda and his team in 1998, by demonstrating functional plasticity in cultured mammalian networks on MEAs [4, 107]. They studied the effect of tetanic slow, periodic site focus

Table 3.1: Summary of the electrical stimulation protocols used in mammalian neuronal cultures - layout taken from [8, 126]

Reference	Year	Plasticity Protocol
Maeda et al., 1998 [4]	1998	20 bursts at 0.2 Hz, each with 11 pulses at an intraburst frequency of 20 Hz delivered from 5 electrodes
Jimbo et al., 1998 [5]	1998	11 bursts at 0.2 Hz, each with 11 pulses at an intraburst frequency of 20 Hz
Tateno and Jimbo,1999 [6]	1999	10 bursts at 0.2Hz, each with 11 pulses to to the tetanised electrodes
Shahaf and Marom, 2001 [7]	2001	Repeated stimulation at low frequency (0.3-1Hz) until a desired responses
Ruaro et al., 2005 [139]	2005	L shape simultaneous stimulation to several electrodes. Bursts of 100 pulses delivered at 250Hz
Wagenaar et al., 2006 [8]	2006	Bursts completely suppressed by 50Hz background stimulation distributed over 20-40 electrodes, except during tetanisation
Chiappalone et al., 2008 [9]	2008	Jimbo protocol with additional trains of pulses at 0.2Hz falling in the middle of the tetanic burst
Brewer et al., 2009 [134]	2009	Chronic stimulation for either 0,1 or 3h/day between 7 and 22 days
Le Feber et al., 2010 [10]	2010	Biphasic stimulation at low frequency(0.2-0.33Hz)
Pimashkin et al., 2016 [46]	2016	Biphasic pulses of 400-8–mV with 600 μs Multi site stimulation.
Nieus et al., 2018 [11]	2018	Biphasic pulses (600μs in duration, amplitude tuned between $200 - 600\mu A$)delivered at 0.2Hz from 8 spatially distributed sites in randomised sequences

stimulation on neuronal cultures. They reported that tetanic stimulation on one or more electrodes was able to evoke bursting responses that were time-locked to the stimuli [107] and their work reported that spontaneous bursting was modified after strong tetanic stimulation [4]. Soon after, Jimbo et al. reported a modified rate of spontaneous activity after application of tetanic stimulation [5]. These experimental results paired with technological advancement in MEAs promoted

several attempts to determine features/parameters of the electrical stimulation such as frequency, number of electrodes, amplitude and duration of the stimulation that contributes maximally to induce synaptic changes and long term changes in dynamics. Table 3.1 summarises the most significant plasticity studies and protocols so far since the pioneering work by Maeda et al.

Crucially despite many attempts over the past two decades, it is still unclear and not yet established whether neuronal cultures can be trained to learn specific stimulus-response relationships reliably. This is primarily due to the fact that neural information processing is still an active area of research, and that basic principles are not yet fully established. In addition, the main difficulties can be divided into two aspects:

- **Experimental design and consistency**: Designing a network stimulation protocol to induce desired network responses reliably is a difficult task; partly due to the non stationary nature of such a dynamical system. Each neuronal culture is different in terms of structural configuration and variations during the development stage, leading to difficulties in reliable repetition of results, making this problem even more difficult due to the inevitable variability.

- **Electrophysiological endpoint**: There is a lack of "electrophysiological endpoint" that reliably correlates with the induced plasticity [126]. [140] proposed the hypothesis that in long-term plasticity experiments, not only synaptic potentials but also overall change in firing patterns should be taken into account to better understand the effects of plasticity.

In 2006, Wagenaar et al [8] published an interesting negative result where they discussed the difficulty in inducing plasticity in neuronal cultures on high density MEAs. They did rigorous experiments over many cultures to reproduce previously reported plasticity effects but failed to reproduce the results reliably. Earlier they hypothesised [41] that spontaneous bursts interfere with plasticity. Following this hypothesis, they applied distributed electrical stimulation to silence spontaneous bursting and then applied stimulation from paired electrodes in tandem with an inter-stimulus gap of 10ms. This resulted in successful induced

plasticity in terms of significant changes in network activity. They concluded that controlling burst interference is crucial in inducing plasticity. The successful outcome of plasticity with such a protocol could be attractive in confirming that the effect is due to STDP, since the protocol applies tandem stimulations which, in theory, can control pre- and post-neuron firings. From the failed experiments they concluded that plasticity induction by extracellular stimulation of dense dissociated neuronal cultures on MEAs is not a straightforward process and just delivering stimulation in presence of the spontaneous burstings cannot induce plasticity significantly and reliably. In contrast, further works from different groups determined that the complete suppression of the spontaneous bursting is not a prerequisite for inducing plasticity [9, 10, 126].

One of the key conditions that needs to be addressed for plasticity induction experiments is the stability and responsiveness of the system. Both cortical and hippocampal dissociated cultures have a degree of variability in the spontaneous activity from culture to culture. To address this issue, Chiappalone et al [9], developed a procedure to quantify and evaluate variability in the spontaneous activity and responsiveness in terms of evoked responses to stimulus. They selected the potential cultures based on the initial activity(pre-stimulation) and how they respond to low frequency stimulation and set out a very systematic way of assessing the quality of a culture for plasticity studies so that all the cultures for the study passed certain initial requirements for consistency. Firstly, they checked for a stable firing rate before the stimulation and that the firing rate is above a threshold. For stimulus-evoked responses, they only selected the electrodes that could evoke a global response in at least 50% of the recording electrodes. Based on these factors, they set a threshold and only selected cultures that met these requirements (as shown in Figure 3.4) as potential cultures for plasticity studies. The mean firing rates(MFR) measured before and after the stimulation were plotted on a logarithmic scale. The blue squares in the Figure 3.4 represents cultures that fall into the sub-threshold region and are discarded. The red circles represents cultures that exhibit strong enough network activity and responsiveness to stimulus, so these are considered for plasticity studies. This approach was utilised in the research reported in Chapter 7 of this thesis.

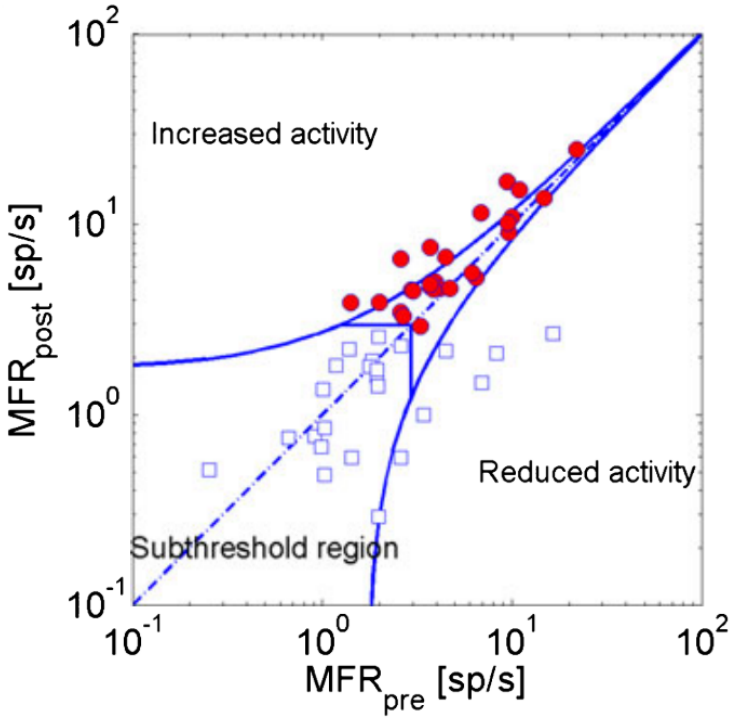

Figure 3.4: Bilogarithmic plot of the mean spontaneous firing at the beginning(MFR_{pre}) and after the test stimulus session(MFR_{post}). Curved line denote confidence intervals. Red circles represents the potential cultures for plasticity studies, blue square are the cultures with not enough responsiveness to the test stimulus, hence not suitable for plasticity studies. [9]

3.3.3.2 Stimulation protocols

The stimulation protocols to induce plasticity can be broadly classified into slow and fast stimulation. Although high frequency stimulation (20-100Hz) patterns are extremely efficient in inducing network response changes, both in *in vitro* and *in vivo*, such stimulation patterns are not common in nature [141], and often such stronger stimulation quite drastically affects the natural spontaneous dynamics. Earlier plasticity studies made use of high frequency tetanic[1] stimulation in cortical networks coupled with MEAs [4, 5] which resulted in induced plasticity

[1]High frequency (eg.20Hz) electrical stimulation used to induce functional plasticity

characterised by increased evoked and spontaneous activity. Experiments by [5] discovered similar results with a weaker tetanic stimulation. [109] later reported that repeatedly applying stimulus to one electrode resulted in response changes on other electrodes when the stimulus is applied to those electrodes. More recently, there have been attempts to study plasticity in dissociated cultured networks by analysing spontaneous activity pre- and post-tetanic stimulation and by investigating plasticity properties of the network in terms of evoked responses [8, 142].

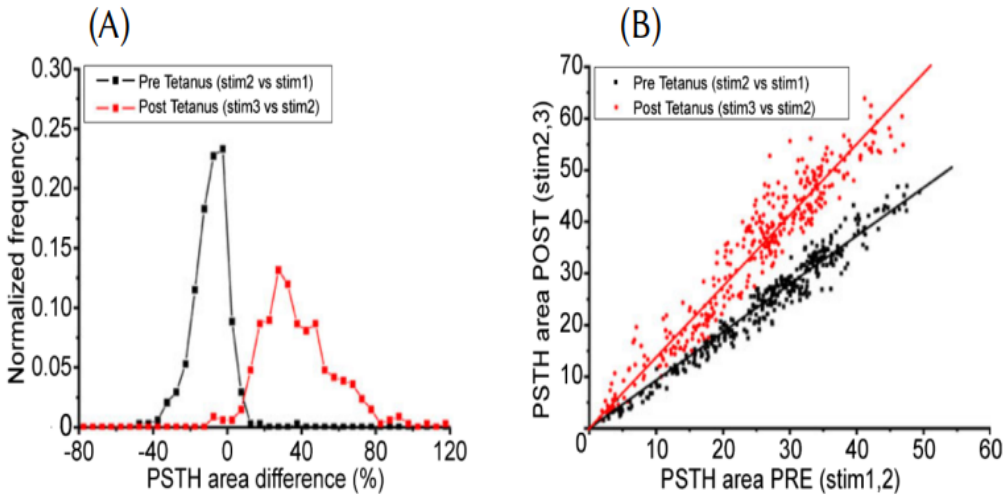

Figure 3.5: Network response pre- and post-tetanic stimulation paired with 0.2Hz slow stimuli. This associative protocol produces a larger ,distributed and more reliable potentiation.(A) Histogram of PSTH area difference (B) Scatter plot of the PSTH area pre- and post-tetanus, linear fitting of the two clusters [9]

Chiappalone et al., 2008 [9] conducted a systematic study of the effects of combining fast and slow stimulation on *in vitro* cortical networks based on previous works [143, 144]. They developed a set of experimental protocols by pairing fast tetanic bursts (20 Hz) with low-frequency stimuli ($\leq$ 1Hz) delivered through two separate channels(i.e. associative tetanic stimulation). The results demonstrated induction of long term potentiation was greatly increased, up to twenty-four hours after tetanisation when the tetanic stimulation was paired with slow stimulation; though only tetanic stimulation can also induce changes in network response as shown in other studies as listed in Table 3.1. The authors summarised their

findings into three main takeaway points; (i) low-frequency stimuli produce no discernible changes to the network responses, (ii) associative tetanic stimulation is able to induce plasticity demonstrated by measurements of evoked responses and (iii) the degree of change is dependent on the stimulation features. The essence of the work of [9] is that the single tetanic stimulation is not effective in inducing reliable responses; pairing such tetanic stimulation with a slow stimuli can greatly increase the degree of network responses as indicated in Figure 3.5 which shows comparison between pre- and post-stimulation network responses when the pairing method is used.

Le Feber et al., 2010 [10] conducted experiments with slow stimulation only. The stimulation used was a biphasic pulse at frequency between 0.2-0.33Hz. They made use of functional connectivity modifications induced by stimulation and hypothesised that low frequency stimulation is not necessarily less effective or intense than tetanic stimulation. They concluded that, for effective plasticity induction, the stimulation has to trigger network bursts regardless of the stimulation frequency. If the stimulation can excite the network to burst, which could be different stimulation frequencies for different culture model or site of the stimulation, then the stimulation could potentially induce plasticity. They used adaptive stimulation protocols where they first randomly stimulated all electrodes and evaluated the responses to select only the most response-inducing electrodes. The stimulation process itself was adaptive in automatically stopping the stimulation when a certain threshold response was reached. The authors made the assumption that the adaptive stimulation may force the network to a new balance leading to large connectivity change. The authors finally state, *"We hypothesise that networks develop an equilibrium between connectivity and activity. Induced connectivity changes depend on the combination of applied stimulus and initial connectivity. Plain stimuli may drive networks to the nearest equilibrium that accommodates this input, whereas adaptive stimulation may direct the space for exploration and force networks to a new balance, at a larger distance from the initial state."* [10]

In contrast to [10] and [9], there are groups who are also working with more "classical" tetanic based stimulation protocols to induce plasticity *in vitro*. A more recent study by [46], used biphasic pulses with 600 µs duration such that

the inter-stimulus interval for each dissociated hippocampal culture was set to match the mean inter-burst interval to maximise the probability of evoking a burst response. The stimulation site was chosen casewise so that the site evokes population bursts 80% of the time the stimuli is delivered. The study itself was focused on selectivity properties of the stimulus induced responses. They found that the response properties of the network bursts can be used to retrieve information about the source location of the stimulus.

In conclusion, different researchers have tried different protocols and have successfully induced plasticity with different protocols. However, to date there is no common agreement on a protocol that can reliably induce plasticity under different conditions for different cultures or enable prediction of the response and no systematic, reliable protocol that will guarantee specific and measurable plasticity changes. It is still unclear what are the underlying factors that encourage or hinder reliable plasticity induction in a controlled manner.

3.3.3.3 Closed-loop systems

So far only stimulation protocols in an open loop setting have been discussed. Another interesting approach for inducing changes in a neuronal culture is the idea of training the culture with some sort of reward signal by closing the loop between the output and input signals. In traditional stimulation experiments, the stimulation is delivered without adapting input signals based on the output during or shortly after the stimulation stage. A closed-loop system takes the output signals into consideration to alter the input signals at the next timestamp; essentially the input signal at time t is a function of an output signal at time $t-1$. Closed-loop experiments in *in vitro* neuronal cultures started as an investigation on whether the culture can perform some sort of learning task characterised by a desired output signal.

In 2001, Shahaf and Marom [7] conducted a relatively simple activity-dependent stimulation protocol such that the stimulation was stopped once the network activity reached a predefined threshold. With such an adaptive stimulation protocol, the neuronal culture can be trained to respond in a specific manner to test pulses after the training, by repeated stimulation until a desired response is

achieved. During the training, reduction of the driving stimulus constitutes the reward which strengthens specific stimulus-response association and prevents new associations from forming. The general stimulus regulation based on the output forms the basis for such experimental approaches.

More recently, [10] and [145] also reported similar closed-loop experiments by analysing the strength of connectivity between any pair of electrodes in real time to modulate and drive the input stimulation adaptively. The advantage of such a setup is the fact that a closed-loop setting may be useful to induce specific or desired network changes without much *a priori* knowledge of network architecture. Utilising such concepts, studies have been conducted to interface such a closed-loop system with an artificial animal or a robot, which are completely controlled by responses from the neuronal cultures. Potter's lab in 2008 [146] reported experiments where they were able to demonstrate training of neuronal cultures to provoke a change in the "*animat's*" (i.e. an artificial animal) behaviour. They highlighted that the stimulation patterns that induced plasticity in a closed-loop setting did not cause plasticity in an open-loop setting. Since then many hybrid neurorobotic systems have been introduced [64, 147–149]. Such closed-loop systems in the neurorobotic domain aim to mimic the physiological sensory-motor loop where the sensory information from the robot sensor are encoded as electrical stimuli and the network responses are decoded and used to drive the robot safely.

3.4 Network connectivity

High dimensional neural data from a network of neurons (or neural circuit) allows us to infer representational information in the brain based on correlated activity between sensory and motor signals. Inferring and understanding the neural wiring that underlies such representations in the brain is crucial in explaining how such representations are produced, and how the network would behave in a novel situation [12, 13]. In a neural circuit, activity of a neuron is not only due to its intrinsic properties but also due to direct or indirect interactions with other neurons. Characterisation of the connectivity of such direct and indirect interactions in neuronal circuits is essential in understanding neuronal dynamics,

neural connectivity and neural information processing. A network of neural circuits can be analysed at different spatial scales - macro, meso and microscopic scales [150]. At the macroscopic scale, large sections of the brain with more than a hundred anatomical regions and connectivity across those areas provide an overall understanding of the brain information processing. Mesoscopic scale includes interconnections among a population of neurons at a localised area, to understand mechanisms of neural information processing. The connectivity study of network of dissociated neuronal cultures is an example of a mesoscopic level. Microscopic scale incorporates study of a single (or very small number of) neuron and its axonal and dendritic arbours, to understand fundamental operational mechanism of a single neuron. The network connectivity in this thesis refers to connectivity at a mesoscopic level from a culture of neurons grown on MEAs.

The network connectivity used to describe the neuronal interactions in a population of neurons can be furthermore categorised as: structural, functional and effective [151].

3.4.1 Structural connectivity

Structural connectivity refers to the physical (anatomical) interaction due to electrical or chemical synapses between neural units (neurons) in a network at a given time [13]. The structural connections are morphological direct interactions among neural units and can be observed at both microscale at local microcircuit and long-range interaction among different sub-networks. Fluorescence imaging techniques can be applied, which can further be analysed to identify structural connectivity. However, for a large highly interconnected networks, it may not always be effective to correctly identify all the structural interconnections.

3.4.2 Functional connectivity

Functional connection corresponds to a correlated interaction between two neural units. It measures the statistical dependence between two neural units or *spike trains (in this context)* without any implication of causal effects. Such connections are time-dependent and "model-free". Model-free connectivity refers to connections where no assumptions on the underlying mechanisms are made. Functional

connections may or may not mean a presence of a physical connection. So, two neural units can be functionally linked even though there is no physical link. For an example, neuron A might be connected to neuron B which in turn is connected to neuron C. Even though there is no physical connection between neuron A and neuron C directly, neuron A is functionally linked with neuron C.

3.4.3 Effective connectivity

Effective connectivity refers to the relationship between two neural units where the activity of one unit directly affects the activity of another unit, indicating a causal relationship [15]. Due to the causal nature, effective connectivity is directional, meaning, connectivity from neuron A to neuron B in a network is not the same as connectivity from neuron B to neuron A at the given time.

3.5 Connectivity inference methods

Mathematically, connectivity analysis can be described as model-based or model-free. Model-based approaches are approaches where the connectivity is estimated by explicitly modeling the data generation process. Neuronal cultures are complex and non-stationary systems which makes the modeling of such dynamical systems difficult. Hence, model-free approaches are usually used to infer the functional and effective connectivity. Some of the most popular model-free connectivity inference methods applied to *in vitro* neuronal cultures coupled with MEAs, can further be divided as: *descriptive statistics* and *information theoretic methods*.

3.5.1 Descriptive statistics

This method utilises statistical features to infer connectivity between two neurons from a population of neurons. Some of the most commonly used descriptive statistics methods are described below.

3.5.1.1 Cross-correlation(CC)

Cross-correlation measures the correlation between two point processes (such as a spike train). It indicates the degree of delayed linear relationship between two processes, one "target" and one "reference", and measures the frequency at which the "target" cell fires in relation to the "reference" process [18]. Mathematically, CC has been described by [152] as *"the probability of observing a spike in one train x_j at time $t + \tau$ given there is a spike at time t in a second train x_i"*. τ is the time lag or time shift. The strength of the connection is evaluated based on the peak value of the CC function. Despite extensive literature, there is no standard definition of CC, but many different variations depending on the scenarios. Regardless, based on the peak value of the CC function, an nxn connectivity matrix can be defined for n number of neurons. This connectivity matrix can then be used to plot a connectivity map showing neural interconnections.CC is also a causal indicator meaning information of the direction of connection can be inferred.

3.5.1.2 Cross-covariance(CCov)

The cross-covariance (CCov) method shares all the properties described for CC. Unlike CC, CCov is applied to time series data. The CCov can be defined as the probability of observing a spike in X at time s and a spike in Y at the same time. Due to the fact that CCov is applied to time series data, the method can be applied not only to data from an *in vitro* model but also to other brain signals such as electroencephalography (EEG) , magnetoencephalography (MEG) , and functional magnetic resonance imaging (fMRI) [153]. For extracellular recordings from *in vitro* neuronal cultures, the data are pre-processed into discrete "spikes", hence CCov is not an appropriate method since discrete spikes are not continuous time series.

3.5.2 Information theoretic methods

Information theory is a branch of mathematics founded by Claude Shannon to formalise the fundamental limits on signal processing covering the topics of quan-

tification of information, information transmission and compression [154]. Information theory has since found its application in various other areas such as neuroscience [155], statistics [156], thermal physics [157], quantum computing [158] etc. In neuroscience, information theory has been used to quantify the flow of information in neural circuits. Some of the most popular information theoretic approaches are briefly described for such scenarios.

3.5.2.1 Mutual information(MI)

Given two stochastic processes, mutual information(MI) measures the statistical dependencies between these two. MI quantifies the "amount of information" in one random process given the observation on another random process. Mathematically, the MI of two activities of two neurons x_i and x_j can be defined as:

$$MI_{i,j} = \sum_{ij} P(x_i, x_j) \log \frac{P(x_i, x_j)}{P(x_i)P(x_j)} \tag{3.4}$$

MI is symmetric; hence this approach cannot identify directionality information. In comparative studies performed by Garofalo et.al [14], it was found that MI was less effective in identifying connections in comparison to Joint Entropy and Transfer Entropy.

3.5.2.2 Joint entropy(JI)

Joint entropy(JE) is a bi-variate causal measurement between two spike trains; more specifically, it is an entropic measure of the cross inter spike interval(cISI) [14, 159]. Given two spike trains x_i and x_j corresponding to neurons i and j respectively, the cISI is computed as cISI = t_{x_i} - t_{x_j}, where t_{x_i} and t_{x_j} are the time of successive spikes of neuron i and j, respectively. Mathematically, JE is defined as:

$$JE_{i \to j} = -\sum_{k} P(cISI_k) \log_2 P(cISI_k) \tag{3.5}$$

where $P(cISI_k)$ is the probability of cISI of size k bins. For high JE values, there is a high probability that one spike train is firing as a consequence of firing

from another spike train.

3.5.2.3 Transfer entropy(TE)

Transfer entropy(TE) is an information theoretic based non-parametric measure of the flow of directed information between two random processes - proposed by Schreiber [160]. Transfer entropy is based on transitional probabilities of spiking events, is asymmetric and incorporates both directionality and dynamic information. TE has gained popularity in computational neuroscience [14–17] as it may be used to infer a causal relationship between two neurons based on the spike timings.

The original expression for TE [160] between two random processes, I and J (neurons in this scenario) is given as,

$$T_{J\to I} = \sum p(i_{t+1}, i_t^{(k)}, j_t^{(l)}) \log_2 \frac{p(i_{t+1}|i_t^{(k)}, j_t^{(l)})}{p(j_{t+1}|i_t^{(l)})} \tag{3.6}$$

where i_t and j_t are status of the neurons I and J at time t respectively, which could be 1 or 0 for spike or no spike. i_{t+1} is the status of the neuron I at time, $t+1$. p is the probability of the status denoted in the parenthesis. The parameters k and l denote the order of the TE, the number of time bins to include from the past. The logarithm with base 2 is used so that the units are bits.

Due to axonal delays and physical separation, the causal effect of one neuron may not be apparent in another neuron in the next time step, but might take multiple time steps. Considering this limitation with the traditional TE method, Ito et al [15] extended the single delayed TE method with multiple delays to account for these delayed causal interactions, which leads to a modified TE expression as.

$$T_{J\to I} = \sum p(i_{t+1}, i_t^{(k)}, j_{t+1-d}^{(l)}) \log_2 \frac{p(i_{t+1}|i_t^{(k)}, j_{t+1-d}^{(l)})}{p(j_{t+1}|i_t^{(l)})} \tag{3.7}$$

where d is the delay or number of previous time steps to include. The rest of the parameters remain as described in equation 3.6.

In a recent survey paper [14], the author concluded that the TE method has outperformed many other popular methods such as cross-correlation(CC),joint entropy, mutual information [14, 15, 161] to identify connectivity from simulated

networks.

3.5.3 Network connectivity challenges in neuronal cultures

Several previous studies on the inference on functional connectivity in neuronal cultures [162,163] have been conducted. However, the methods used have suffered from temporal resolution. The temporal pattern of neural interaction is of fundamental importance in understanding communication in mesoscopic neuronal networks [164]. Neuronal communication is known to take place at chemical and electrical synapses, which could have delays in milliseconds and sub-milliseconds due to signal propagation over space. To accurately infer the connectivity, these delays need to be taken into account. At macroscopic level, the system is better understood via synchronised brain rhythms over large temporal scales. For mesoscopic system such as *in vitro* neuronal cultures, the temporal scale is critical. Ito et.al. [15] showed an improved performance in recognising the true connections with the delayed TE method which performed better than the general TE method and other popular methods. Shimono and Beggs, 2015 [165] further improved the reconstruction performance by identifying the delay parameter. These methods were validated with a realistic simulated model encompassing axonal delay and biologically plausible STDP rules. Real neuronal networks, however, are complex dynamical systems with unexplained variability and assessing the performance of the inferred connectivity is still a challenging problem.

One of the main challenges in connectivity estimation from a biological neuronal culture is the fact that extracellular recordings do not provide direct evidence of how neurons are synaptically or electrically connected. Thus there are no 'ground truth' connections against which the connectivity methods can be evaluated. The problem is further exacerbated due to the dynamical and non-stationary nature of the neuronal cultures. Due to these characteristics, there are no multiple trials which can be used to extract statistical features for each neuron or channel to measure the significance of the connections inferred. Additionally, during inference between two processes, statistical noises, biases and coincidental firings may imply a positive causal relationship even though there is none. To statistically determine the degree of potential causal relationship that should be

large enough to have significance, the inferred value must be compared against the values which could be expected under some null hypothesis(hypothesis that there is no causal relationship). Upon exceeding the value, the alternative hypothesis that there exists a causal relationship, can then be accepted. To address this issue, it is possible to use a surrogate method as a thresholding parameter, to determine whether the inferred connection is plausible, given the statistical significance of the connection.

The surrogate method has been an effective method of generating statistically relevant surrogate data to measure statistical significance of parallel spike trains [166]. The idea is to generate surrogate data such a way that all the statistical features of the original data are retained, except the temporal information because the timing of spikes is thought to be a key contributing factor for network interaction. The rationale is to generate surrogates that only differs in the temporal pattern, since connectivity is essentially dependent on causal firing patterns. There exists a few popular methods such as jittering [167], trial shuffling [168] and shuffling or inter-spike-interval(ISIs) [169]. These methods are used for recordings from a small number of electrodes. For recordings from HD-MEAs with thousands of electrodes, it is even more important to retain as many statistical features as possible for surrogate data due to the fact that statistical errors in the estimator are exacerbated with large dense recordings. The performance of the connectivity inference heavily relies on the method of surrogate data generation. However, the existing small number of methods rely on direct manipulation of the spike times. There exists a knowledge gap between the advancements made in connectivity inference, which are tested against simulated data, and the surrogate methods for single trial neuronal recordings. One objective of the thesis is to use and extend these methods on real experimental data - both on spontaneous network responses and connectivity changes during plasticity. For example, utilising the ISI distribution information of the network could allow for efficient and more relevant surrogate data.

3.6 Conclusions and PhD objectives

The ability of MEAs to non-invasively record from multiple sites simultaneously has opened new research avenues in the area of neuroscience. Developments in MEA technology and high electrode densities have introduced new perspectives and investigative platforms in the study of neuronal dynamics and analysis of neuronal networks, both at single cell and network level at an unprecedented spatial and temporal resolution. In particular, plasticity studies have benefited immensely from the ability to stimulate neuronal networks whilst recording simultaneously and keeping the culture healthy and functioning for a prolonged period of time.

Over the last two decades of studies in neural plasticity in neuronal cultures coupled with MEAs, different researchers have tried different protocols and have successfully induced plasticity to some degree. It is evident from the literature that inducing plasticity in a neuronal culture by extracellular stimulation is not as straightforward as in brain slices [170]. A protocol that can reliably induce plasticity in multiple different scenarios currently doesn't exist. Almost all the studies conducted to induce long term plasticity have different protocols designed specifically for that particular scenario. It is still unclear what would be the nature of an underlying common protocol that could consistently lead to a guaranteed induction of plasticity in a controlled manner. The problem is exacerbated due to the occurrence of network bursts where the network activity is concentrated, which could cancel out transient plasticity, making it much harder to induce long term plasticity.

An initial challenge lies in the successful growth of primary neuronal cultures coupled with CMOS based MEAs. Primary neurons are very sensitive to even slight changes in the growth conditions, and the fact that these cultures need to be kept for at least 2-3 weeks and under healthy conditions before any experimental work can occur makes the process even more challenging. CMOS based MEAs are not glass based substrates and require very careful treatment of the surface to facilitate cell attachment and equally careful maintenance henceforth. Secondly, to date, plasticity studies have been performed with low density MEAs with only a few hundred channels. The availability of high-density MEAs with

thousands of electrodes can provide a high spatial and temporal resolution, enabling deeper observational ability during plasticity. Clearly, this is still an active area of research and there is a knowledge gap between the plasticity studies of neural dynamics and the use of HD-MEAs. Due to the high spatial and temporal resolution ability of such HD-MEAs, pre-processing and analysis of the recording is a major challenge. Closely spaced electrodes on HD-MEAs introduce over-lapping signals and the same signal may be detected from multiple electrodes. The challenge lies in pre-processing such raw voltage trace recordings into reliable spiking events for further analysis, for example analysis that underpins plasticity, network synchrony and connectivity. Hence, it is critical that the data are processed correctly to avoid misleading results down the data analysis pipeline. Thirdly, accurate inference of network connectivity of an evolving neuronal culture enables visualisation of the evolution of network interaction during controlled plasticity studies. The connectivity inference of a dynamical system such as a dissociated neuronal culture has to rely on surrogate methods due to the ever changing nature of such a system, where multiple trials are not always possible. A small number of surrogate methods exist for generating statistically relevant data that could enable accurate measurement of statistical significance of the inferred connectivity.

The work presented in this thesis aims to utilise state-of-the-art CMOS based MEAs to study neuronal dynamics, focused on plasticity and network connectivity. To achieve the goal, several objectives are established.

- Development of methods to successfully maintain dissociated neuronal cultures, grown on the state-of-the-art CMOS based MEAs, for a prolonged period of time(upto 4 weeks at least).
- Characterisation of electrophysiological properties of spontaneous activity and design criteria to select cultures that are responsive to stimulation that could potentially induce plasticity.
- Development of stimulation protocols to demonstrate a long term network response change, symptomatic of network plasticity, and study network dynamics before and after the stimulation.

- Quantification of network connectivity using an information theoretic approach and the development of a novel non-parametric surrogate test to identify statistically significant connections from the experimental recordings.

Chapter 4

Materials and Methods

4.1 Introduction

In this chapter, details of the cell culture methods on MEAs from cell dissociation to cell culture maintenance, along with a thorough discussion on preparation of the MEA chips for cell culture, are presented(see Section 4.2). Details on the equipment used and reagents required are listed as well. The experimental setup for electrophysiological measurements and electrical stimulation parameters to evoke network responses are also presented (see Section 4.3.1). The later half of the chapter discusses basic computational tools used to process the raw electrophysiological recordings into discernible spike trains. New tools and algorithms developed during the thesis period are covered in subsequent chapters.

4.2 Cell culture

4.2.1 Cell preparation

Cell cultures were prepared following the methods based on [171]. Hippocampal tissues were obtained from BrainBits UK (now BrainBits USA), from rat embryos at 18 days of gestation(E18) from Sprague Dawley rat. BrainBits dissected the rat brain to extract a pair of intact hippocampal tissues which were delivered within 1-2 days at 4°C. The tissues were delivered in 2 ml of Hibernate EB(HEB; Hibernate E/B27/GlutaMAX; BrainBits HEB 500 ml).

After receiving the tissues, they were dissociated in a cell dissociation solution. The cell dissociation solution was prepared by dissolving 6 mg of sterile papain (BrainBits PAP 6mg) in 3 ml of Hibernate E-Ca(HE-Ca) without B27 for a final working concentration of 2 mg/ml papain. The solution was incubated for 10 minutes in a 30°C water bath to dissolve and mix completely. The solution was then cooled down for 10 mins in an ice bath. A fire polished 9" silanised pasteur pipette with an opening of ≈0.5 mm was used to disperse the tissues. With a pasteur pipette, the tissues were transferred with minimal HEB into the cell dissociation solution vial. The solution was then incubated for 10 min at 30°C. The vial was gently swirled halfway through the incubation period to allow for thorough cell dissociation. The tissues were again transferred back to the HEB medium with the pasteur pipette from the cell dissociation solution. After this, the tissues were triturated with a silanised pasteur pipette for about 1 min (90% tissue dispersal) avoiding air bubbles. The remaining undispersed tissue pieces were left to settle for about 1 min. The supernatant containing dispersed cells were transferred to a 15 ml tube leaving ≈ 50 µl of HEB solution containing debris. The dispersed cell solution was then spun at 1100 rpm(200xG) for 1 min. During centrifugation, cells are pushed to the bottom of the tube forming a pellet of cells. The supernatant was discarded leaving the pellet with ≈ 50 µl of the solution. The pellet was dispersed with a flick at the bottom of the tube and re-suspended in 1 ml growth medium. To measure the cell concentration, the cells were counted using an automated haemocytometer which calculates cells/ml. For counting cells, 20 µl of cell solution was mixed with 20 µl of Trypan Blue. From a

pair of hippocampal tissues the cell extracted were within the range of 1-2 million cells per ml. The cells were diluted to the desired concentration for seeding on different substrates. All steps were performed inside a sterile laminar flow hood.

4.2.2 Cleaning of MEAs

3Brain MEAs, also referred to as BioChips, are not glass substrates but CMOS based substrates. In order to preserve the functionality and integrity of the BioChips, it is paramount that the MEAs are cleaned thoroughly in a manner that does not damage either the electrodes or underlying circuitry. Intensive care is practiced while handling the chips because the MEA area can be very easily damaged. Touching the active area of the BioChips with a finger or any object such as metal can easily damage the electrodes. Latex gloves were worn at all times while handling the chips. To mechanically clean debris from the electrodes, a soft paintbrush was used to gently wash the chip with sterile water. The BioChip has different sections which require different procedures to clean and sterilise. The cleaning procedure of the MEA chips is summarised below:

- Firstly, the chip area needs to be in a pristine condition without any debris or damage before sterilising and coating. The active area of the chip can be inspected with an upright microscope before proceeding with sterilisation. Chips that were stored in dry conditions for a long time were re-hydrated for 1-2 hours by filling the chambers with Double Distilled Water (DDW) .

- After re-hydration and after making sure the chip area was in pristine condition, sterilisation was done. Autoclaving and UV-lights sterilisation were not recommended as these steps could cause the glue in the chips to deteriorate, decreasing the lifetime of the chip. Ethanol sterilisation was performed by completely filling the well chamber of the chips with 70% ethanol for 20 minutes. A longer or higher concentration of ethanol was avoided as these could affect the functionality of the chips. To ensure a higher level of sterilisation, the outside of the chamber well was wiped with tissue soaked in pure ethanol. After 20 minutes, the chamber was abundantly rinsed with sterile DDW and dried under laminar flow hood in a sterile petri dish. Coating was performed after the well had dried completely.

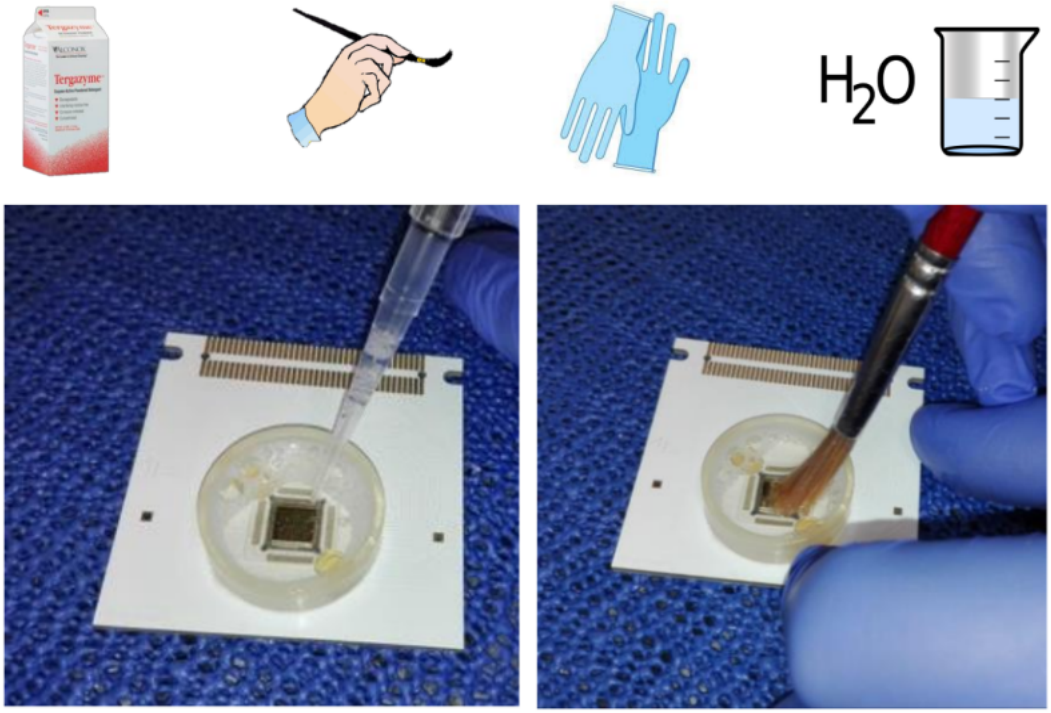

Figure 4.1: General cleaning steps of 3Brain MEAs. The active area of the chip can be cleaned with a soft paint brush and rinsed with DDW.

- After the experiments, it is very important to clean the chips immediately since the cell debris can harden and become difficult to get rid of, or worse, damage the chips. The chips can be rinsed with DDW to get rid of most of the cell debris. For strongly attached debris, the chamber was filled with strongly diluted enzyme active powered detergent, Alconox Tergazyme, for 2 minutes. The solution was then rinsed with DDW. The chips were visually inspected to check for debris. For mechanical cleaning of further debris, the active area of the chip was gently cleaned with a soft brush and rinsed abundantly with DDW. The process was repeated as necessary until the chip area was pristine. The chips were then dried under the laminar hood and stored in a sealed package in dry conditions. The general steps of the cleaning process are illustrated in Figure 4.1.

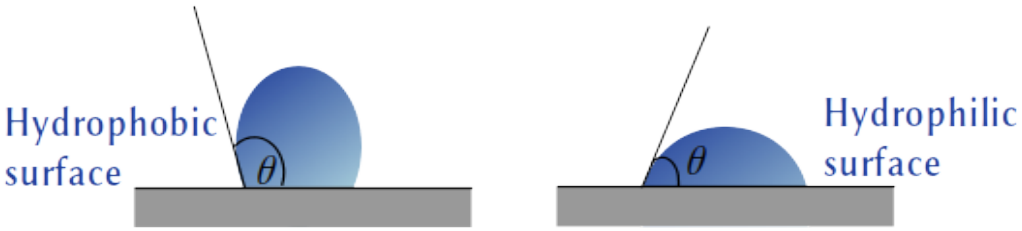

Figure 4.2: Hydrophobicity and hydrophilicity effect on cell culture substrate. Hydrophobic surface has high contact angle(θ) resulting in poor wettability,adhesiveness and cell viability. Hydrophilic surface on the other hand has better wettability, adhesiveness and cell viability

4.2.3 MEA surface coating

Before proceeding with the coating factors, the chip's chamber was filled with sterile growth medium, NbActive 4 (BrainBits), which is composed of Neurobasal/B27 along with additional supplements - creatine, estrogen and cholesterol, used to grow the neurons and incubated for 48 hours. On the following day, the medium was aspirated and dried completely without any rinsing with sterile DDW. Incubating the medium on the chips before coating has been shown to increase hydrophilicity of the MEAs and hence better wettability, cell adhesion and better cell viability. Also, medium incubation preconditions the chip for cell culture. As shown in Figure 4.2, a droplet covers more substrate area on a hydrophilic surface and better wettability allows for cells to adhere better on these surfaces in comparison to a hydrophobic surface.

Two different types of coating factors were used as recommended by 3Brain - a single layer of poly-d-lysine(PDL) and double layer coating with PDL and laminin. For a single layer of PDL, the active area of the MEA chip was coated with a drop($\approx$ 100µl) of poly-d-lysine (Sigma P-6407) at 0.1 mg/ml dissolved in sterile DDW and incubated (37°C,65% humidity,5%CO_2) overnight. For double layered coating, the active area of the chip was coated with a drop($\approx$ 100µl) of laminin (Sigma L-2020) at 0.1 mg/ml dissolved in sterile DDW for 3-5 hours. The drop was then removed without rinsing and the surface was coated again a drop of PDL and incubated overnight.

On the following day, regardless of the coating used, the active area was gently rinsed three times with sterile DDW and dried under a sterile laminar flow hood. Once dry, the cells were seeded immediately on the treated surface.

4.2.4 Seeding and maintenance of neuronal cultures

After the cells were dissociated following the steps in Section 4.2.1, the cell concentration was diluted to about 1000 cells/µl. 80,000 cells were seeded onto the 3Brain Stimulo MEA chip which was precoated with coating factors, with an 80µl droplet. This was left to settle for 1-2 hours in the incubator. The chips were placed inside a sterile petridish. Due to fast evaporation rate and the small volume of the medium, the pH level of the medium may change quite drastically and quickly. It is important that the excess evaporation is brought under control so that the initial seeding can have enough time for the cells to settle and attach on the surface without dying. A custom made humidity chamber (see section 4.2.5) was used for the petridish. This allowed for the culture to settle down well without a drastic change in pH level due to evaporation. After 1-2 hours of initial settling, 1.5 ml of complete growth media(NbActive4) was added gently without disturbing the cells. 25 µM glutamate was added to the medium for the first 4 days to promote cell survival after the seeding and was omitted after that. The culture was incubated at 37°C, 5% CO_2 and 65% humidity. Half of the medium was changed every 4 days. The humidity chamber was used all throughout the culture period to maintain a steady pH level and controlled evaporation. After 2-3 weeks, the culture becomes mature enough to exhibit electrophysiological activities. The electrophysiological activities were recorded from day 21 onward. Similarly, the cells were also seeded onto 24 well plates for comparison and monitoring.

4.2.5 Custom humidity chamber

A custom made additional humidity chamber was used to control excess evaporation. It was found that the cultures were not stable without the humidity chamber and were at risk of excess evaporation and subsequent low cell viability. After using the humidity chamber, the evaporation rate was consistent and

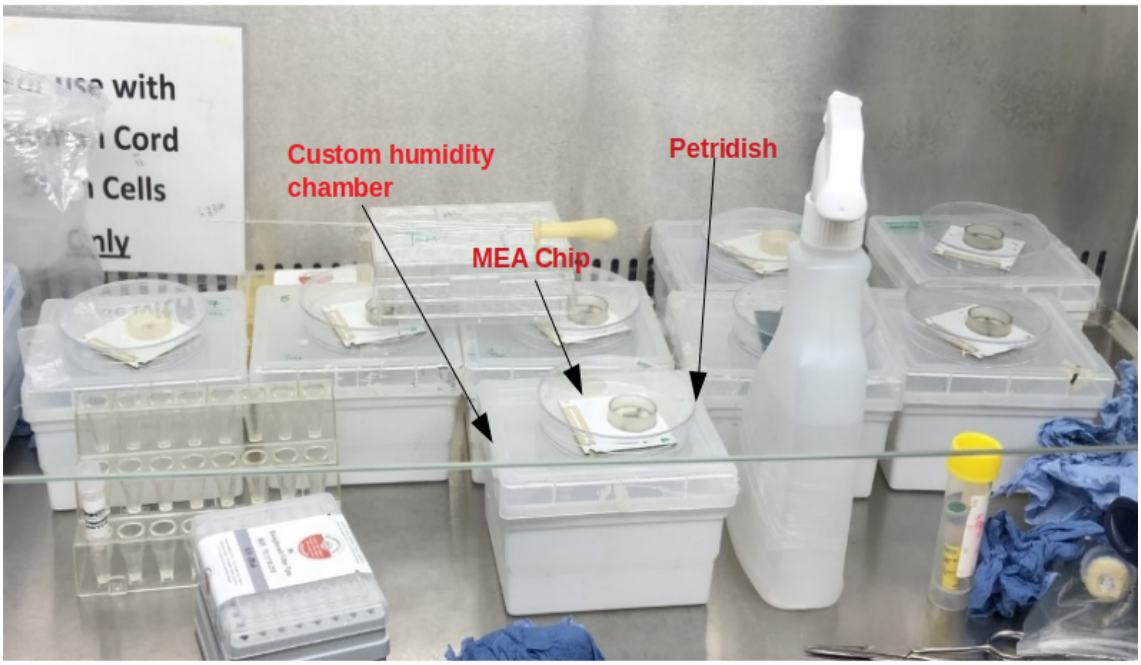

Figure 4.3: Custom made humidity chamber for cell cultures on MEAs.

resulted in more stable cultures without unexplained overnight cell deaths.

A 1ml pipette tip box was used as a humidity chamber. The box was first emptied and sterilised in the autoclave. During autoclaving, the box was placed inside a sealable bag to avoid contamination after sterilisation. After autoclaving, the box was taken from the sealed bag inside the sterile hood and wiped throughout with pure ethanol. 5ml of 70% ethanol was filled inside the box and left for 20 minutes for further sterilisation. The humidity chamber was then rinsed with sterile DDW for 3-5 times and left to dry. The chamber was then filled with 5ml of sterile DDW with 5% $CuSO_4$ to avoid fungal contamination. Figure 4.3 shows MEA chips in the petridish which then goes into the humidity chamber for incubation. The lid of the humidity chamber is not airtight which allows for the flow of gases necessary for the neuronal culture. The humidity box serves as a humidity chamber inside the incubator which also has controlled humidity to avoid any chances of excess evaporation. During early seeding of the cells before adding complete growth medium, evaporation rate was found to be critical as any slight changes in pH was enough to kill cells.

4.2.6 Cell viability assay

Lactate dehydrogenase (LDH) is a cytosolic enzyme that is released into the cell culture medium upon cell damage to the plasma membrane. LDH release assay is a cell cytotoxicity assay to asses the level of cell damage in culture. The cell deaths are directly manifested as increased level of LDH release. Since culture supernatant is used to take measurements, the assay allows to measure cytotoxicity at various time points without affecting the culture .

The LDH assay was performed at required time points (every2-4 days) according to manufacturer's protocols (Thermofisher Scientific). 50µl of culture supernatant was transferred to a 96 well plate. 50µl of LDH reaction mix was added to 50µl aliquots and incubated for 30 minutes. 50µl of blocking solution was then added to stop the reaction. After that, BMG Labtech Clariostar plate reader at 490nm was used to measure absorbance.

Biochips, on average, showed higher cell deaths but due to the unfavourable growth surface on MEAs in comparison to treated plastic well plates, slightly higher cell deaths was anticipated. Since two thirds of growth medium was replaced with fresh growth medium at every medium change, the LDH release in the supernatant was brought down at every medium change due to removal of old medium. Figure 4.4 shows absorbance values displayed as Optical Density(OD) [1]) for three biochips and well plates along with a control culture without any cells. The biochips and the well plates showed similar cell deaths trackable over days.

Cultures with significantly higher cell deaths during this stage were visually inspected and monitored. If the cell deaths kept increasing, the samples were discarded due to unexpected cell deaths and hence the reliability issues. After 2 weeks, neurite extensions start to mature and start to become visible under the microscope with an external light. After week 2-3, electrical characterisations was performed as the culture matured to exhibit strong enough electrical signals.

[1] In spectroscopy, OD is the measure of absorbance, defined as the ratio of light intensity falling on a material and the intensity transmitted.

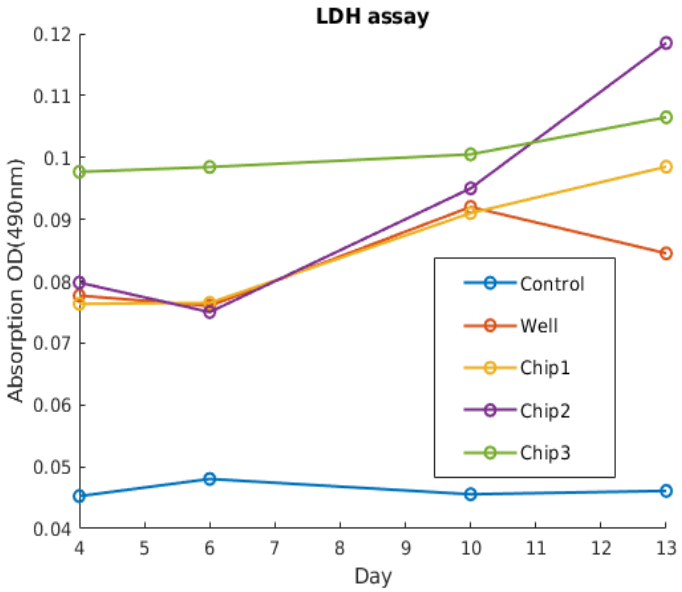

Figure 4.4: LDH release from different samples measured as absorption at 490nm expressed in OD(optical density)

4.2.7 Immunofluorescence staining and imaging

For glass based transparent substrate MEAs, imaging is no different than imaging a well plate or a tissue culture flask. However, the 3Brain MEAs are CMOS based and opaque in nature which makes it much more challenging to image the cultures. Only upright microscopes with a light source coming from the top are able to image the growth on such MEAs. An Olympus BX51 was used to image the fluorescence images of neuronal cultures on MEAs as shown in Figure 4.5. For neuronal cultures on well plates, brightfield images were taken via an inverted microscope and the fluorescence images were taken with a Leica TCS SP5 confocal microscope.

Immunofluorescence staining of neuronal cultures for both MEA cultures and well plates were performed in a similar manner. The staining process was done at the end point of the experiment because the process itself requires killing and fixing the cells before staining. The immunofluorescence staining of the cultures was performed following the protocol listed below:

1. Fixing

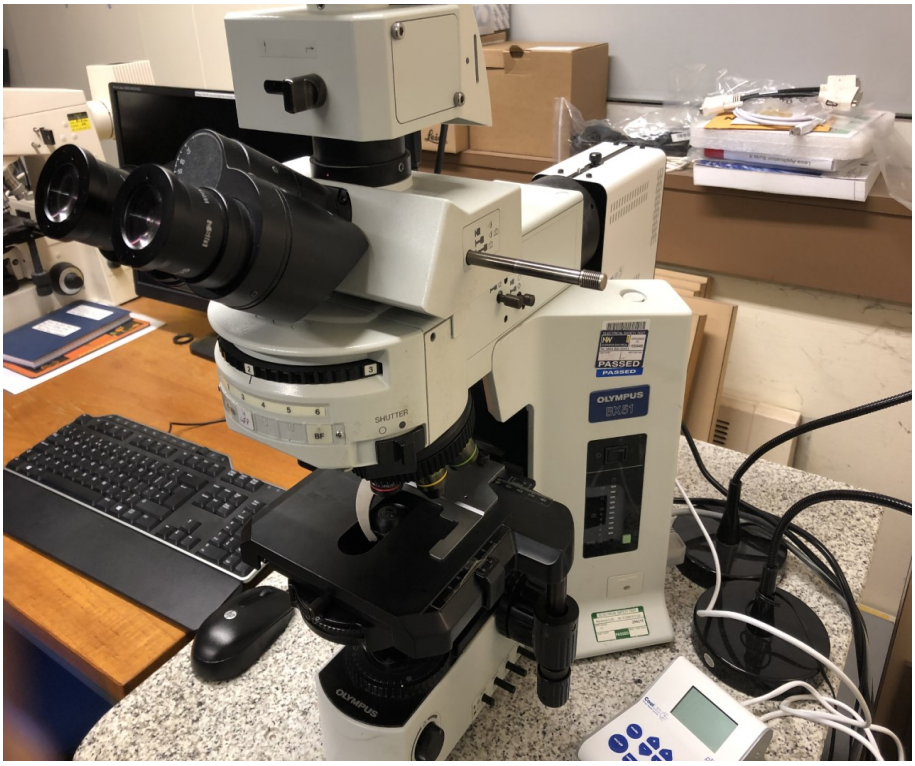

Figure 4.5: Upright Olympus BX51 fluorescent microscope used for imaging neuronal cultures grown on 3Brain MEAs.

After the culture was ready for imaging, a cell monolayer was fixed for 10 min at room temperature in formalin (4% w/v paraformaldehyde in phosphate buffer saline(PBS))

After this, the fixative was removed and the monolayer was rinsed 3 times for 2 mins with Tris buffered saline(TBS) or PBS at room temp.

2. Staining

   (a) Remaining lipids from the cells were extracted by incubating the wells (both well plates and MEAs) in 2ml Tween-20/TBS (0.05%v/v) for 10 min.

   (b) Non-specific binding sites were blocked by incubating the monolayer with 2ml of 3%(w/v) BSA in TBS for 1hr at room temperature.

   (c) Fixed cell monolayer was incubated in primary antibody (anti-MAP2)

. 0.5 ml of primary antibody(1:100) diluted in 3%(w/v) BSA in TBS was added into the well and incubated overnight at 4°C.

(d) The following day the well was washed 3 times for 2 min in TBS.
(for null primary, primary antibody was skipped by skipping the previous step. Also the blocking solution need not be washed with PBS)

(e) The monolayer was incubated in 1 ml fluorescently labelled secondary antibody (eg. Alexa Fluor Plus 488 anti Goat Ig) for 1.5-2 h at room temp in dark.

(f) The well was washed 3 times for 2 mins in TBS.

(g) To avoid fading of the fluorescent dyes, the well was covered with a drop of antifade mountant with DAPI (4',6-diamidino-2-phenylindole) which stains the nucleus of the cells.

3. Imaging

The stained samples were then imaged by either upright fluorescence microscope (MEA chips) or confocal microscope (well plates). For MEA chips, appropriate fluorescence light was selected from the microscope to shine on the samples, and reflected light from the stained neurite structures was imaged to obtain a fluorescence image. Due to the opaque nature of the samples, reflected light signals are rather weak. Further image processing was performed in ImageJ.

Figure 4.6(A)(B) shows a brightfield image of a neuronal culture on a plastic well plate 3 hours after seeding and at day 7 respectively. Within a week, the culture has self assembled into a highly interconnected network. Figure 4.6(C) shows a fluorescence image of the neuronal culture on 3Brain MEAs stained with antibody to MAP2. MAP2 isoforms are expressed only in neuronal cells, especially in cell body and neuronal dendrites. The branch like structures are dendrites - indicating an evenly distributed and highly interconnected network. The black squares in the background are the actual recording electrodes of the MEAs.

The cell culture reagents/chemicals used for the experiments are listed in Table 4.1.

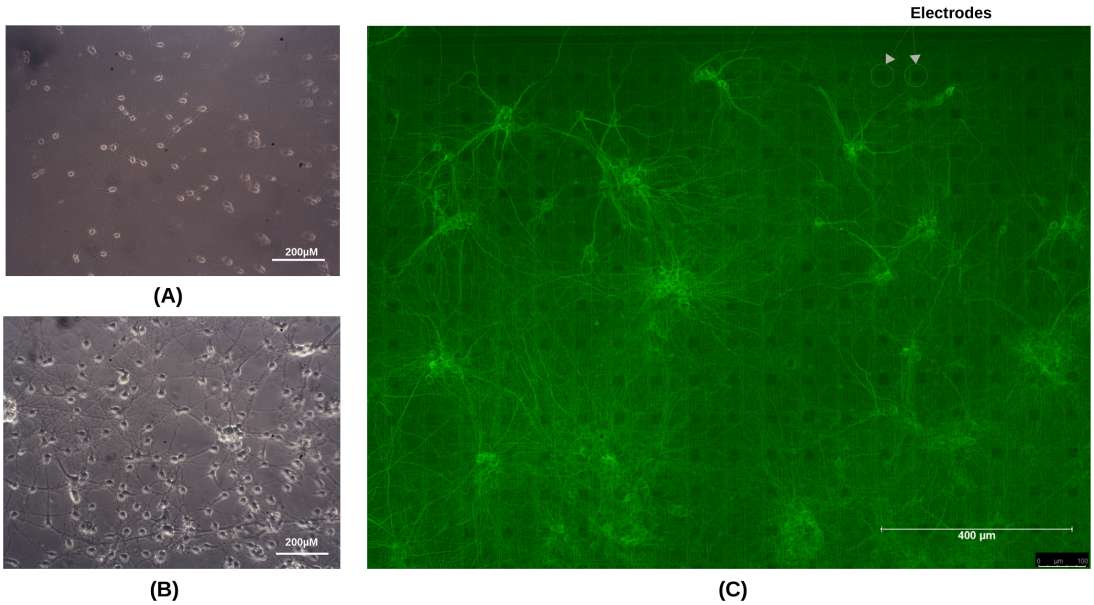

Figure 4.6: (A) Brightfield image of hippocampal culture on a well plate after 3 hours of seeding. (B) Brightfield image of hippocampal culture on well plate at day 7 showing highly interconnected network. (C) MAP2 (Microtubule-associated protein 2) stained fluorescence image of hippocampal culture on CMOS MEAs at day 25. The black squares in the background are the recording electrodes of the MEAs.

4.3 Electrophysiology

It is particularly difficult to find exact stimulation parameters that guarantee specific network responses in neuronal cultures, since, as well as being a dynamical system, each culture is different and always evolving. Experiments were conducted with different stimulation frequencies and repetition that is strong enough to induce some network responses but not too strong to cause network saturation and excitotoxicity - a pathological process by which neurons are damaged due to overactivations of the receptors for the excitatory neurotransmitters.

After 2-3 weeks, the culture becomes mature enough to exhibit discernible electrical signals. Hence, recordings were done after week 3. Since it is typical of a hippocampal culture to exhibit spontaneously firing behaviour, spontaneous firing was firstly recorded as a base recording before evaluating changes arising from stimulation. All the recordings were done inside a sterile laminar hood.

Table 4.1: List of cell culture materials

Materials	Company	Catalog number
NbActive4	BrainBits LLC	Nb4-500
Laminin	Sigma	L2020-1MG
Poly-d-lysine	Sigma	P6407 5MG
Peirce LDH kit	Life Technologies	88953
Boric Acid	Sigma	B6768-500G
Sodium Tetraborate	Sigma	221732-100G
Trypsin	Fisher Scientific	25050-014
Glultamax-I	Fisher Scientific	35050038
Terg-A-Zyme	Sigma	Z273287-1EA
HBSS	Fisher Scientific	15266355
PBS	Sigma	D8537-1L
3Brain MEAs	3Brain AG	-
BioCam acquisition system	3Brain AG	-

The 3Brain BioCamX device was sterilised by wiping with tissue soaked in 70% ethanol before proceeding with the recording. The reference electrode was wiped with pure ethanol and let to dry. The MEA chips were closed with a 3D printed chip cover to avoid interference from light in the activity of the neurons. Figure 4.7 illustrates the setup of the electrophysiological recording where the whole BioCamX device is placed inside the laminar hood for sterility. The chips are outside the incubator so a prolonged duration of recording is damaging to the culture. Hence, the recordings were only performed for 5 minutes at each time.

4.3.1 Electrical stimulation

As a starting point, stimulation parameters described by [11] were selected. This is a biphasic stimulation - 600µs in duration, amplitude tuned between $200 - 600$ µA. Afterwards, for the experimental culture stimulation parameters were fine tuned as a biphasic signal with 500µs in duration, amplitude of 500µA with interphase delay of 100µS, as shown in Figure 4.8.

The other parameters of importance are the stimulation frequency and repetition. The spontaneous firing of the culture is recorded at different time points

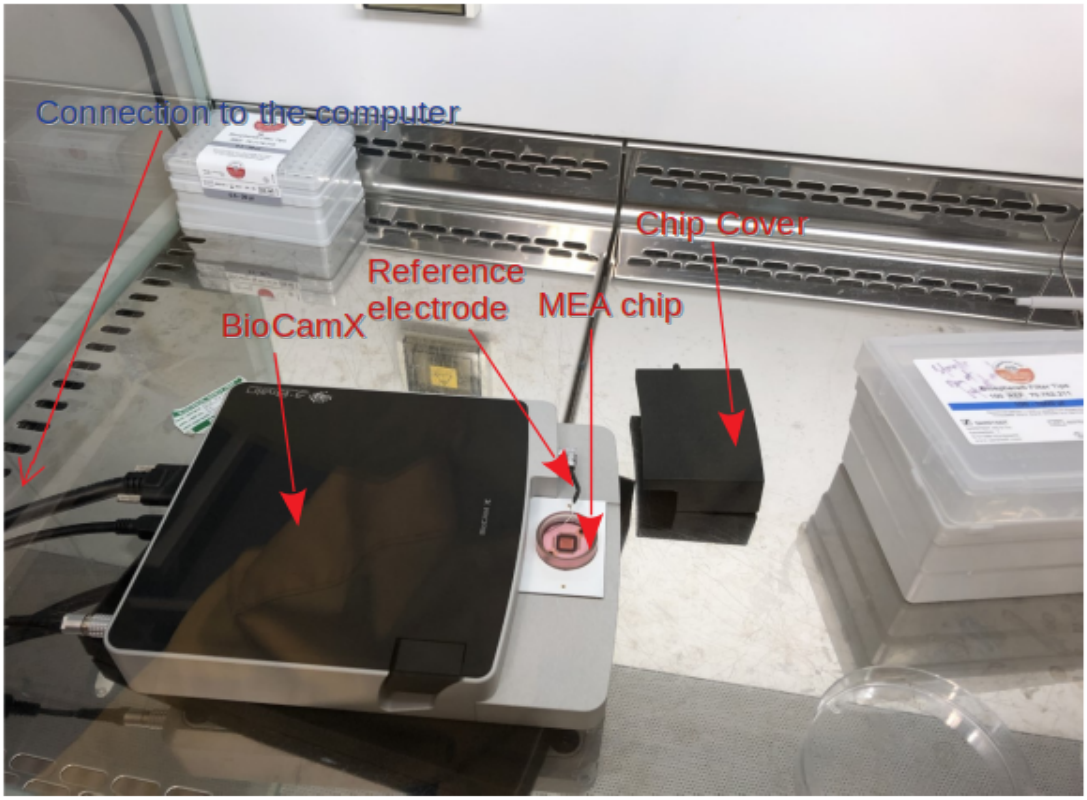

Figure 4.7: Electrophysiological setup with 3Brain MEA.

- before and after applying stimulation, as shown in Table 4.2.

The general idea was to record spontaneous firing before any stimulation, and then apply repeated stimulation to the culture and record post stimulation spontaneous firing at different time points as shown in Table 4.2, i.e. immediately after stimulation, after 30mins of stimulation, after 1hr/2hr/3hrs of stimulation consequently. The process was repeated again the next day as well. This enabled observation of network dynamics immediately after stimulation and how it changes with time. The stimulation methodology is further discussed in detail in Chapter 7.4

After recording at different time points, spikes were detected from raw voltage traces and burst detection was conducted to identify bursting events. Bursting are defined as period of high frequency firing of a neuron separated by silent periods. Bursting behaviour has been associated with a range of neuronal processes, such

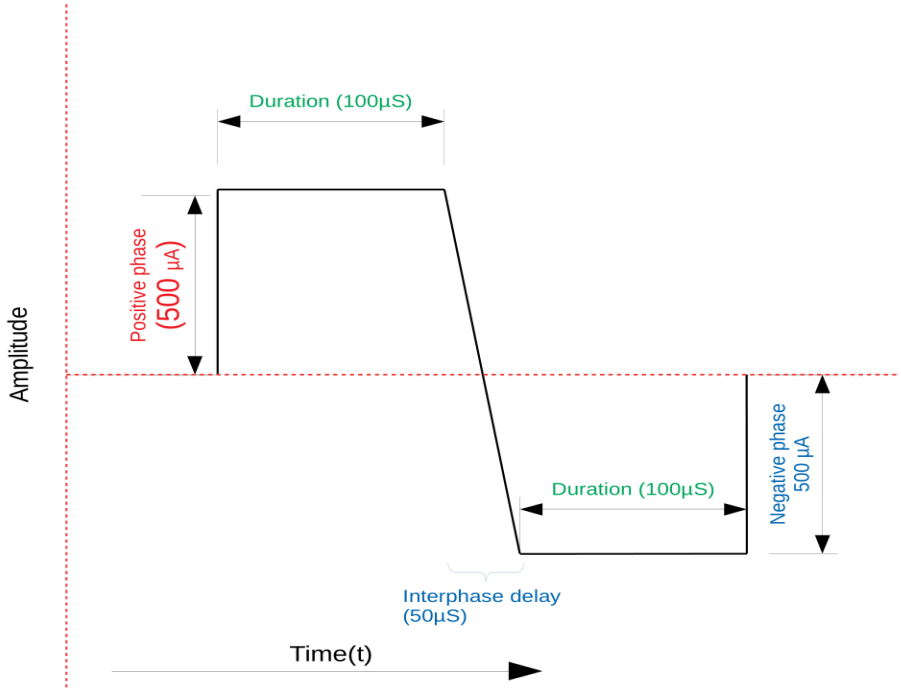

Figure 4.8: Biphasic stimulation with interphase delay

as efficient information processing and formation of functional networks [172]. Hence, the bursting rate was also considered rather than just the mean firing rate.

4.4 Data analytics

Earlier studies assumed that information is encoded in the rate of the spikes [57–59], a process also known as rate coding. However, it later became evident that rate coding cannot explain encoded information for complex behaviours and timing of the spikes plays a key role in encoding information [60–62]. Hence, temporal analysis of the spike train is a valuable process that helps to provide

Table 4.2: Stimulation and recording protocols.

Stimulation experiments and recording time points			
Spontaneous	Stimulation	Post stimulation	Poststim after 30mins/1hr/2hr/3hr
5 minutes	2Hz/5Hz, 10 repetition every 10/20 secs for 5 mins / single or multi channel stimulation	5 minutes spont	5 minutes spont

greater insight into the neural code and allows for improved understanding of brain information processing.

Figure 4.9 shows a simplified illustration of the pipeline from raw voltage traces from MEA chips into single spike signals from each electrode after spike detection on the channel signals.

4.4.1 Spike detection

Neuronal responses are recorded by electrodes placed on the region of interest for both in vivo and in vitro experiments as a time series of voltage fluctuations. The recorded signals are subject to noise and interference from neighboring electrodes. Recorded signals need to be accurately identified with spiking events to reduce the voltage readings into appropriately sequenced point processes which are essentially spike trains. These spike trains are prerequisites for further analysis and inference. Due to the typical large volume of data, a spike detection algorithm has to be highly efficient and fast to process such large datasets and detect true spiking events successfully [63].

In HD-MEA recordings, the signals are most likely to be recorded by multiple channels due to the closely spaced electrodes which causes signal overlapping and waveform assignment problems. However, this redundancy can be exploited to improve the signal to noise (SNR) ratio and hence spike detection [64, 65].

Conventional thresholding-based event detection on high density recording does not provide sufficient information to reliably detect true spikes; furthermore

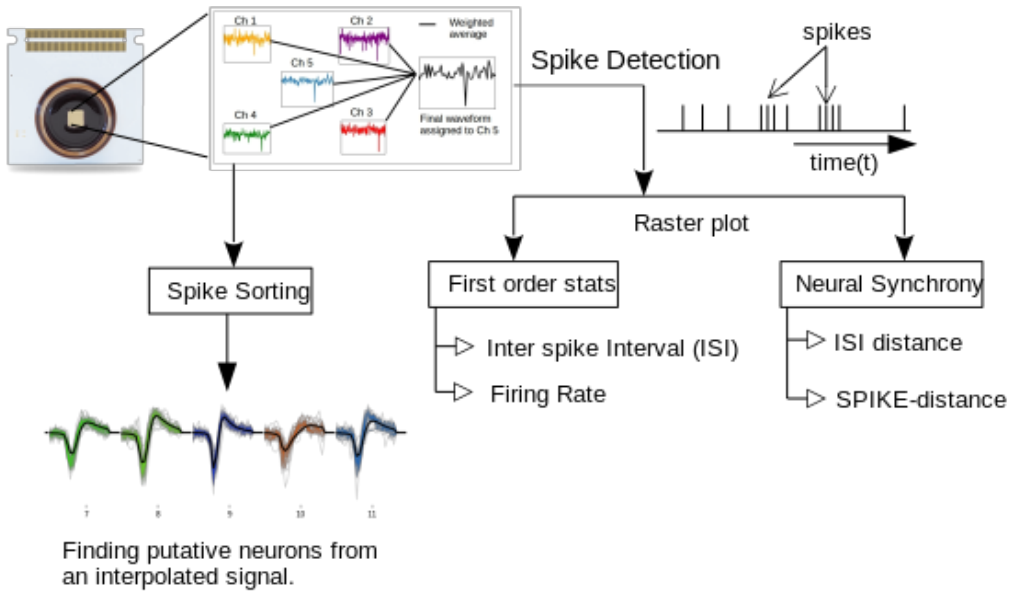

Figure 4.9: Processing of raw voltage traces into different statistical and spike sorting analysis

single unit identification and isolation is not possible for dense recordings. Accordingly, an interpolation spike detection method optimised for HD-MEA data to detect events in close electrodes successfully discarding most of the background noise and false activities, which was developed by Muthmann et al [63] was implemented for spike detection in this thesis.

The interpolation method uses voltage traces from five neighboring channels which are weighted with a relatively stronger weight for the central channel than the four surrounding channels. These weighted signals were then averaged and assigned to the central channel as a new signal, as shown in Figure 4.10. A lower threshold was employed to capture all the possible events and reduce the probability of false negatives. Upon successful spike detection, the spike times were stored for each channel which were then processed using custom scripts written in Python3 to generate spike trains and conduct further analysis.

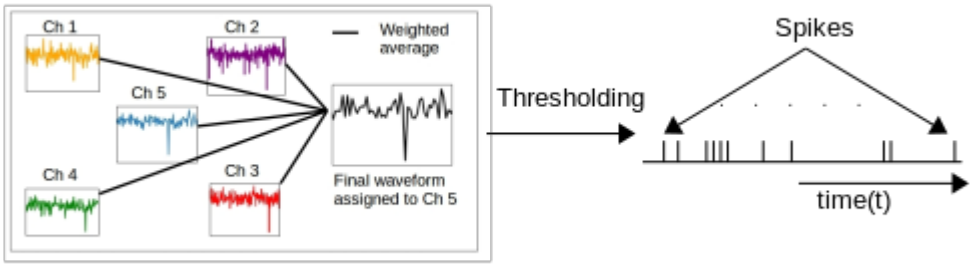

Figure 4.10: Five channel interpolation illustration adapted from [63]

4.4.2 Raster plot

A raster plot is the simplest analysis which basically shows all the spiking activity from selected channels against time. Each dot in a raster plot is a spiking event and the Y-axis shows channels (Figure 4.11).

Custom Python scripts were written to process spike trains generated after the spike detection. The spike trains were recorded into a *.txt file with only the spike times, as shown in Figure 4.12 where each number is a timestamp in milliseconds. The time represents spiking events at that point in time.

The raster plot itself provides a good visual indication into how the population of neurons are firing over time. For example, the general overview may indicate pulsating behaviour of the neuronal population. However, upon closer inspection into a smaller time window, for this example, as shown in Fig. 4.11(B)(C), the firing is more sparse in nature without clear intuitive or numerically quantified indications of the extent of the synchronisation. This is the extent of neural information one can infer from the raster plot. Hence, quantifiable and mathematically sound metrics are required to further analyse the spike data such as neural synchrony metrics and quantifiable causal interactions, which will be discussed in the coming chapters.

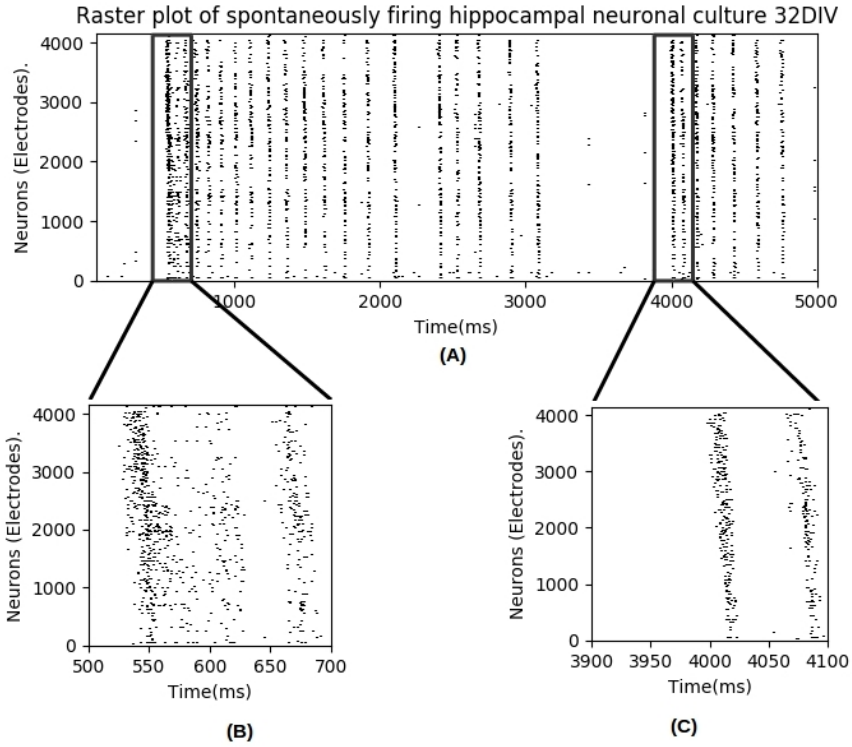

Figure 4.11: Spontaneous synchronous bursting of dissociated neuronal hippocampal culture at 32 DIV. (A) Raster plot of all 4096 electrodes/channels over a 5 second period (B) Zoomed section from $500 - 700$ ms (C) Zoomed section from $3900 - 4100$ ms

```
43 551 555 748 1242 1362 1489 1490 1761 2111 21
44 748 913 1243 1490 1621 1762 2418 2689 2905 3
45 550 554 617 618 746 913 1362 1621 1762 1925
46 550 554 555 573 617 619 620 676 748 825 1014
47 543 549 552 563 572 582 586 590 620 676 739
```

Figure 4.12: Spikes stored as spike times in text a text file where each row is a different spike train with numbers representing each spike event time for that spike train.

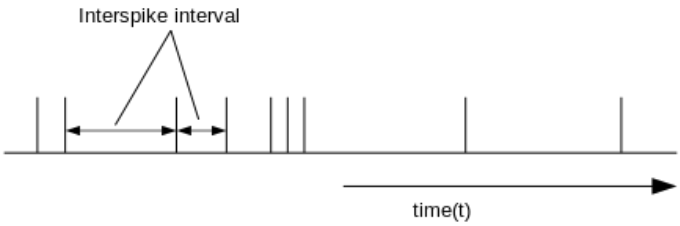

Figure 4.13: Illustration of interspike interval of a spike train.

4.4.3 First order statistics

In addition to the raster plot, statistical analysis helps to provide better insights into the dynamics of the neuronal population. Some of the most popular spike train statistics are the interspike interval histogram (ISIH) and the peri/post stimulus time histogram (PSTH) which provide a general overview of the dynamics of the population of the neuronal culture. The timestamps obtained from after spike detection were further processed with custom algorithms to perform first order statistical analysis such as firing rate, ISIH and PSTH.

4.4.3.1 InterSpike interval histogram

An interspike interval is the time interval between two consecutive spikes as illustrated in Figure 4.13. These distances are measured for all the consecutive spikes of all the spike trains from all the channels, and the distances are collated to get a histogram. The density estimation shows a specific kind of distribution which is similar to a γ distribution (Figure 4.14). The distribution reveals information about the firing dynamics of the neural population. Due to the refractory period of a neuron, neurons cannot repetitively fire instantly - there exists a resting period of 5-10 ms. Hence, the peak of the density estimation is expected to be around 10-100 ms. This helps to validate the spike detection algorithm in a broader sense. Since most of the firing happens within a window of 10-100 ms, as hypothesised by Donald Hebb [69], neurons firing within 40 ms of the last spike are more likely to have contributed to that firing, hence leading to strengthening of the synapses leading to long term potentiation. With that logic, it may be observed that most of the neuron responses are highly correlated, as most of the

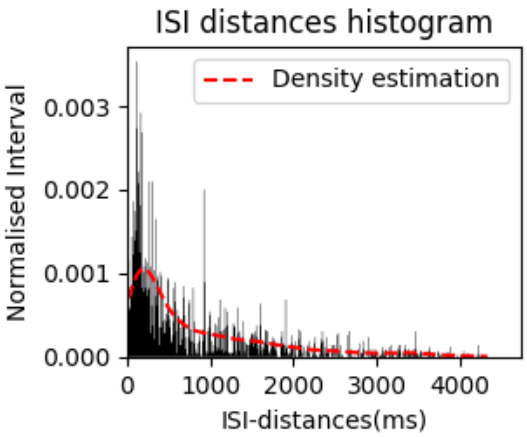

Figure 4.14: ISI Histogram with density estimation

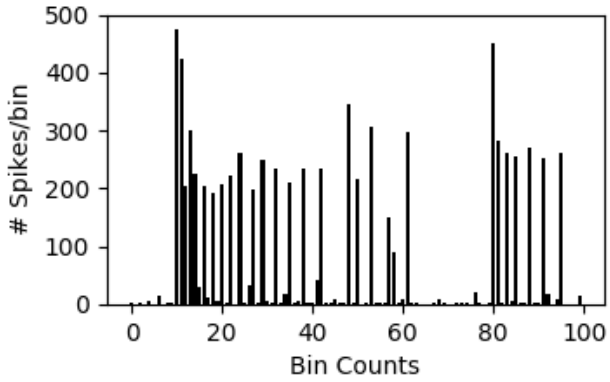

Figure 4.15: PSTH with bin size of 50 ms

subsequent spikes are within a 10-100ms window.

4.4.3.2 Peri/Post stimulus time histogram

PSTH is a histogram of neuron firing at a given time bin. A time bin is a small time interval in the time line. PSTH helps to monitor firing rate changes at different moments in time(Figure 4.15), before or after the onset of stimulation. During experiments involved with inducing a desired response with electrical stimuli, the PSTH shows how the firing rate is changing with stimulation and whether the changes are retained after the stimulation - which provides a bird's eye view of the network level dynamics.

4.4.4 Neural synchrony

Spike train synchrony estimation of neuronal cultures provides valuable insights into firing patterns of neurons in terms of degree of similarity or dissimilarity. These estimations have proven to be a useful tool in neuroscience since synchrony in neuronal networks is thought to be related to cognitive processes, sensory awareness, learning and neurological disorders. Many mathematical metrics have been developed to quantify spike train synchrony in terms of similarity or dissimilarity between spike trains [173–178]. The Victor-Pupura metric [173] is one of the most widely used metrics to measure spike train distances. This metric calculates the cost for transformation of one spike train to another with three basic operations; spike insertion, spike deletion and spike shifting. Another metric which measures the euclidean distance between two given spikes was proposed by van Rossum [174], while Schreiber et al [176] suggested utilising cross correlation of spike trains after filtering. All these methods require one cost parameter and are time-dependent. A parameter free and time-scale independent metric called Interspike Interval Distance (ISI-Distance) which is based on the relative length of ISIs was proposed in [177]. The ISI-distance quantifies spike train similarities in terms of firing rate profiles but fails to keep track of synchrony caused by timing of the spikes or coincident spikes. Hence, another metric was proposed [178] which inherits the parameter free and time-scale independent properties of the ISI-distance but gives special attention to the timing of the spikes to measure synchrony. These metrics are very useful when raster plots become difficult to interpret visually, or when greater insight into the overall dynamics among different groups of spike trains is needed.

4.4.5 System and software used

The analyses were performed using an Intel Xeon(R) CPU E5-2640 v3 @ 2.60GHz x 16 running Ubuntu 18.04.3 LTS. Computationally heavy tasks were run remotely on the research group's small cluster, an Intel(R) Xeon(R) Gold 6140 CPU @ 2.30GHz x 72, utilising all 72 cores in parallel. The majority of the spike analysis such as pre-processing, spike detection, spike sorting, burst analysis, connectivity visualisation etc were done with PYTHON version 3.x. HDF5 (Hierar-

chical Data Format) was used to store the raw voltage recordings. The HDF file system is a file format designed for the management of extremely large and complex data collections. Transfer entropy calculations and ROC analysis were done using MATLAB R2018b. Statistical analysis were done using PYTHON SciPy library and with SPSS. ImageJ was used for image processing and the open-source package Libre Draw was used to draw illustrations. LaTeXwith Texmaker editor was used for writing up all documents.

4.5 Conclusion

This chapter described the general methodology and analyses used for the thesis work. Many of these methods were utilised to achieve the results presented in subsequent chapters. Chapters focused on computational contributions (see Chapters 5,6) also have a dedicated methods section which are elaborated on the methodology for that particular chapter. Similarly, further specific details on the stimulation protocols are discussed in Chapter 7.

Chapter 5

Network Synchrony Analysis

In this chapter, mathematical metrics to quantify neuronal synchrony, which are based on the temporal interactions between groups of neurons, are discussed. The chapter discusses the main contribution of demonstrating methods to utilise synchrony metrics to evaluate synchrony changes in experimental data, such as HD-MEA recordings, which is the subject of this thesis. A thorough validation of the method utilising synthetic data is first presented (Section 5.3.1) followed by application onto real experimental data (Section 5.3.2). It is demonstrated that, despite the significant size of the datasets, the approaches are effective in identifying and quantifying interesting bursting or change in spike train behaviours which are not always obvious from the raster plot.

The materials presented in this chapter has been previously presented at the 2018 IEEE IJCNN conference and subsequently published in the IEEE proceedings.

5.1 Introduction

Understanding the mechanics of information processing in the brain is one of the most interesting and challenging problems in the field of neuroscience. At cellular level, neurons communicate via short pulses of current, known as 'action potentials' or 'spikes' [55, 179]. Earlier studies assumed that information is encoded in the rate of the spikes [57–59], a process also known as rate coding. However, it later became evident that rate coding cannot explain encoded information for complex behaviours, and timing of the spikes plays a key role in encoding information [60–62]. Hence, temporal analysis of the spike train is a valuable process that helps to provide greater insight into the neural code and allows for improved understanding of brain information processing.

With advances in High Density Multi Electrode Arrays (HD-MEAs), more and more multi-neuronal experimental datasets are available with multiple simultaneous spike trains, which are sequences of action potentials [180, 181]. Temporal analysis of spike trains between neurons is very useful to enable quantification of similarity or dissimilarity among two or more neurons, which corresponds to how they correlate with each other at finer timescale. This degree of estimation is also called spike train synchrony. A measure of similarity or dissimilarity and temporal correlation of spike trains provides great insights into neuronal response pattern to different stimulus and the assessment of neural populations in neural coding [182]. Neuronal synchrony is thought to be related to cognitive processes, learning, sensory awareness and neurological disorders [183, 184].

Many mathematical metrics have been developed to quantify spike train synchrony in terms of similarity or dissimilarity between spike trains characterised by spike train distances [173–178]. The Victor-Pupura metric [173] is one of the most widely used metrics to measure spike train distances. This metric calculates the cost for transformation of one spike train to another with three basic operations; spike insertion, spike deletion and spike shifting. Another metric which measures the euclidean distance between two given spikes was proposed by van Rossum [174], while Schreiber et al [176] suggested utilising cross correlation of spike trains after filtering. All these methods require one cost parameter and are time-dependent. A parameter free and time-scale independent metric called

Interspike Interval Distance (ISI-Distance) which is based on the relative length of ISIs was proposed in [177]. The ISI-distance quantifies spike train similarities in terms of firing rate profiles but fails to keep track of synchrony caused by timing of the spikes or coincident spikes. Hence, another metric was proposed [178] which inherits the parameter free and time-scale independent properties of the ISI-distance but gives special attention on the timing of the spikes to measure synchrony. These metrics are very useful when raster plots become difficult to interpret visually, or when greater insight into the overall dynamics among different groups of spike trains is needed.

Despite the established importance of spike train synchrony in the understanding of neural coding and overall firing relationships among different subsets of spike trains, spike train synchrony metrics have not been extensively explored for larger datasets with thousands of spike trains such as typically recorded from HD-MEA. These metrics are very useful to quantify spike train (dis)similarity when raster plots from large number of spike trains become difficult to intuitively infer this information or determine overall dynamics among different groups of spike trains.

This chapter applies Inter Spike Interval (ISI) and SPIKE-distance analysis proposed by [177, 178] on two different experimental HD-MEA datasets recorded using the 3Brain MEA acquisition system with 4096 electrodes to characterize and quantify bursting and oscillating behaviors and to demonstrate how such analysis is effective in identifying and quantifying various neuronal spiking patterns in large datasets.

5.2 Methods

5.2.1 Synchrony metrics

This section presents a short description of the metrics to quantify bivariate (dis)similarity profiles of two spike trains which can then be extended to multivariate profiles of multiple spike trains. Let S_1 and S_2 be two spike trains. The distance measure is normalised to limit the distance within the range from 0 to

1.

$$Distance : S_1, S_2 \rightarrow [0, 1] \tag{5.1}$$

5.2.1.1 ISI-distance

ISI-distance is based on the instantaneous interspike-interval of each spike train. This metric was derived by Kreuz et al. [177].

Consider two spikes in a spike train, namely a previous spike and a following spike. For a bivariate ISI-distance, for each spike train $n = \{x, y\}$ where x is the first spike train and y is the second spike train. At time t, let the time of the previous spike be $t_P^n(t)$,

$$t_P^n(t) = max(t_P^n | t_P^n \leq t), \tag{5.2}$$

and the time of the following spike be $t_F^n(t)$,

$$t_F^n(t) = min(t_F^n | t_F^n > t) \tag{5.3}$$

Figure 5.1 shows sample spike timings and ISI for each spike train. The interspike-interval is hence given by,

$$\nu_{ISI}^n(t) = t_F^n(t) - t_P^n(t) \tag{5.4}$$

Based on the ISI obtained, the ISI-distance profile $I(t)$ [177] can be calculated as the instantaneous ratio between ν_{ISI}^x and ν_{ISI}^y,

$$I(t) = \begin{cases} \frac{\nu_{\text{ISI}}^x(t)}{\nu_{\text{ISI}}^y(t)} - 1 & \text{if } \nu_{\text{ISI}}^x(t) \leq \nu_{\text{ISI}}^y(t) \\ -(\frac{\nu_{\text{ISI}}^y(t)}{\nu_{\text{ISI}}^x(t)} - 1) & \text{otherwise.} \end{cases} \tag{5.5}$$

With identical ISIs, the ISI-distance value becomes zero. With a faster initial spike train, the ISI-distance approaches -1 and with a slower initial spike train the ISI-distance approaches 1, as determined from equation (5.5). Hence, the similarity or synchrony is represented with a positive value.

The time averaged ISI-distance computation of any pair of spike trains from time T_0 to time T is,

$$D_I = \int_{T_0}^{T} I(t)dt \tag{5.6}$$

For multivariate spike trains, the ISI distance(D_I) is the average over all pairs of spike trains $< i, j >$ given by,

$$D_{Im} = \frac{2}{N(N-1)} \sum_{<i,j>} I^{i,j} dt, \tag{5.7}$$

where $I^{i,j}$ is a bivariate ISI-distance between spike train i and j and N is the total number of spike trains.

This term can be integrated over the desired period to obtain the average ISI-distance over that period.

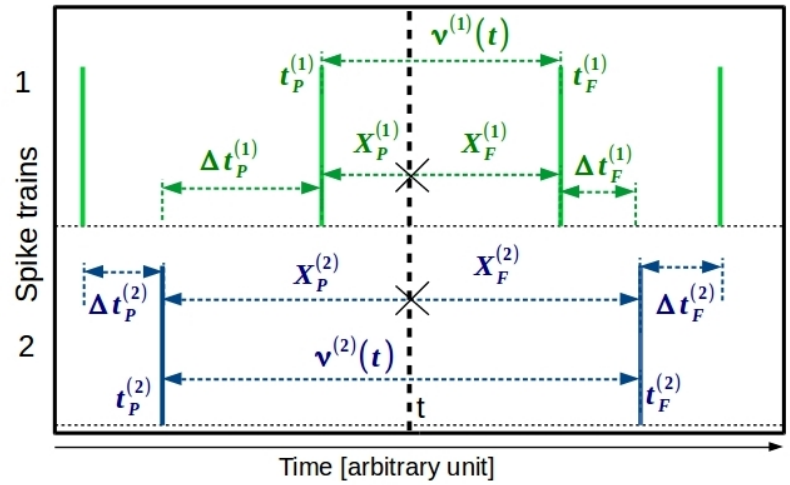

Figure 5.1: Illustration of bivariate ISI-distance and SPIKE-distance calculation with instantaneous time t. The figure shows how the distances are measured between two spike trains adapted from [185]

5.2.1.2 SPIKE-distance

The ISI-distance is well designed to quantify firing profiles but is not the best choice to capture the subtlety of synchrony caused by spike timing, specifically

the occurrence of coinciding spikes among spike trains [178]. This limitation was addressed in [178] with the inception of a new metric, *SPIKE-distance*, that inherits the parameter free, time-scale independence properties of ISI-distance with special focus on the timing of the spikes. It was further improved in [186]. SPIKE-distance essentially quantifies the dissimilarity profile $S(t)$.

The time difference between the previous and follower spikes is,

$$\Delta t_P(t) = t_P^x(t) - t_P^y(t), \tag{5.8}$$

$$\Delta t_F(t) = t_F^x(t) - t_F^y(t), \tag{5.9}$$

as shown in Figure 5.1. A SPIKE-distance profile computation, $S(t)$, relies on two preceding spikes, a spike from a first spike train $t_P^{(1)}(t)$ and a spike from a second spike train $t_P^{(2)}(t)$, and two following spikes, a spike from a first spike train $t_F^{(1)}(t)$ and a spike from a second spike train $t_F^{(2)}(t)$. For each spike, the distance to the nearest spike in the other spike train can be computed as,

$$\Delta t_{\mathrm{P}}^{(1)}(t) = \min_i(|t_{\mathrm{P}}^{(1)}(t) - t_i^{(2)}|), \tag{5.10}$$

and analogously for $\Delta t_{\mathrm{P}}^{(2)}(t)$, $\Delta t_{\mathrm{F}}^{(1)}(t)$ and $\Delta t_{\mathrm{F}}^{(2)}(t)$.

A local weighting factor, which is the time separation of the spikes from the current time t, is applied to each time difference from equation (5.8) and equation (5.9). These weighting factors are expressed as,

$$X_P^{(n)}(t) = t - t_P^{(n)}(t), \tag{5.11}$$

$$X_F^{(n)}(t) = t - t_F^{(n)}(t) \tag{5.12}$$

From Figure 5.1, it is evident that $\Delta t_P^{(1)}(t) + \Delta t_P^{(2)}(t) = \nu^{(1)}(t)$, which is the ISI distance for spike train 1, $S1$.

Hence, the weighted SPIKE-distance for the first spike train is,

$$S_1(t) = \frac{\Delta t_P^{(1)} X_F^{(1)}(t) + \Delta t_{\mathrm{F}}^{(1)} X_P^{(1)}(t)}{\nu^{(1)}(t)}, \tag{5.13}$$

and similarly $S_2(t)$ gives the expression for the second spike train.

These local spike distances are then weighted with the ISI distances and normalized to get the expression below,

$$S(t) = \frac{S_1(t)\nu^{(2)}(t) + S_2(t)\nu^{(1)}(t)}{2\left\langle \nu^{(n)}(t)\right\rangle_n^2} \tag{5.14}$$

In the spike profile obtained from equation (5.12), the value is bound between the limits $0 \leq S(t) \leq 1$. SPIKE-distance becomes 0 for identical spike trains and approaches 1 for dissimilar spike trains resulting in a positive value for more asynchronous spike trains.

For multiple spike trains i.e. $N \geq 2$, bivariate SPIKE-distances are averaged over all pairs i.e.,

$$S(t) = \frac{2}{N(N-1)} \sum_{<i,j>} S^{i,j}(t), \tag{5.15}$$

and averaged over a full period, T, of the spike train .

$$D_S = \int_{T0}^{T} S(t)dt \tag{5.16}$$

5.2.2 Spike detection

Conventional thresholding-based event detection on high density recording does not provide sufficient information to reliably detect true spikes; furthermore single unit identification and isolation is not possible for dense recordings [63]. The spikes are detected with the interpolation methods described in the Chapter 4.4.1.

5.3 Results

5.3.1 Synthetic data

Synthetic datasets are ideal for initial validation of the methods used. 40 spike trains of 4000 ms duration corresponding to 40 neurons were artificially generated [187]. The spike trains vary with time and synchrony, as is evident from the raster

plot in Figure 5.2. This dataset has highly synchronised neurons for the first 1500 ms followed by asynchronous firings and then a similar repetition.

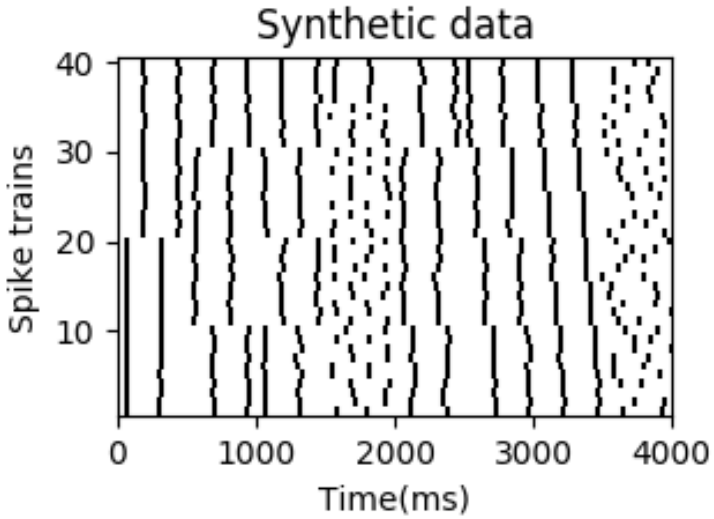

Figure 5.2: Raster plot of the synthetic data

The ISI-distance and SPIKE-distance metrics were used to analyse spike train synchrony of these spike trains. The Python based PySpike library was utilised for numerical calculations of ISI-distance and SPIKE-distance [187]. PySpike utilises cython implementation which improves computation performance in factors of 100-200 over just Python implementation. In addition, a Python multiprocessing package is utilised to run multiple calculations concurrently for faster processing.

The multivariate ISI-distance and SPIKE-distance were averaged over all pairs of spike trains, as given by equation (5.7) and equation (5.15) respectively.

5.3.1.1 Distance Profile

Figure 5.3 shows the multivariate, i.e. averaged over more than two spike train pairs, ISI-distance and SPIKE-distance profile of the first 10 spike trains from the group of 40 spike trains shown in Figure 5.2 over time. The first 10 spike trains are selected arbitrarily. Any group of spike trains that fires in synchrony could be selected but for this illustration, 10 spike trains are selected for more intuitive validation.

Considering spike trains from $1 - 10$ for the first set of spikes at around 50

ms, there is a perfect synchronous firing as a single group as evident from the raster plot in Figure 5.2. These periods of synchrony are reflected by very low SPIKE-distance values. The ISI-distance also remains low since ISI-distance lacks sensitivity for coincident events [186] as shown in Figure 5.3. However, this set of spike trains then fires highly synchronously, but not in perfect unison, as shown by relatively lower values of SPIKE-distance and the sudden rise and fall in ISI-distance until about 1500 ms in Figure 5.3. At around 1500 ms the spike trains fire more randomly without synchrony. This is successfully characterised by a sudden jump in SPIKE-distance value during the asynchronous firing period and a complementary drop in ISI-distance. Note that the approach provide numerical values assigned to the synchrony at each timestamp.

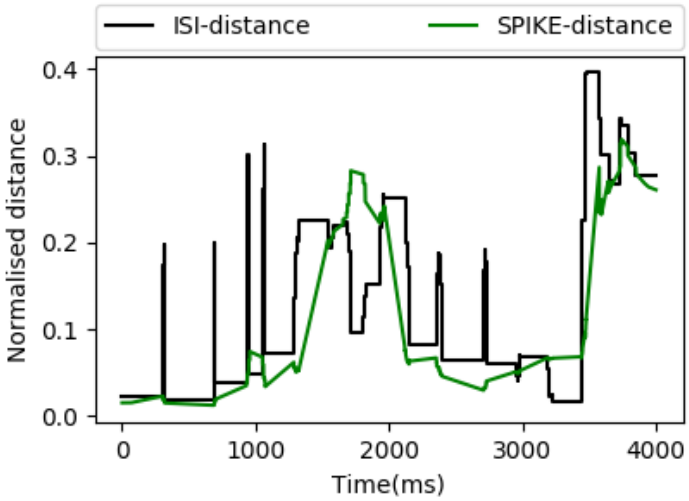

Figure 5.3: Multivariate ISI-distance and SPIKE-distance profile for the the first 10 spike trains.

The values calculated for all spike trains over the full period are shown in Table 5.1,

Apart from the average profile over time, another useful visualisation method is to show the pair wise distance between any two spike trains averaged over a certain period. This shows not just the average dynamics of the population but also synchrony between any two neurons or spike trains in a given period. Each spike train pair is represented as an element in an adjacency matrix with the size equal to the number of spike trains i.e. for N spike trains the matrix is of $N \times N$

Table 5.1:
MULTIVARIATE ISI-DISTANCE AND SPIKE-DISTANCE

Metric	Max Distance	Min Distance	Average Distance
ISI-distance	0.3493	0.01422	0.1705
SPIKE-distance	0.2976	0.1491	0.2076

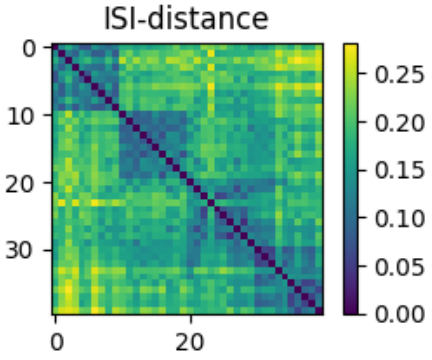

(a) Adjacency matrix showing averaged ISI-distance over the whole period

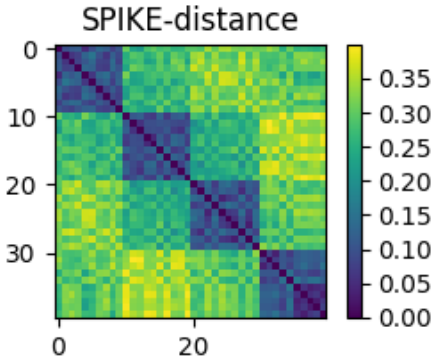

(b) Adjacency matrix showing averaged SPIKE-distance over the whole period

Figure 5.4: Temporally averaged metrics over the whole period[X and Y axis represent individual spike trains]

size. Figure 5.4 shows the pairwise distance metrics averaged through the whole period where temporally averaged distances indicates four distinct groups which are more visible with the SPIKE-distance. A smaller, more focused time window can reveal synchronous firing during that period hence providing better insights at any given moment in time or time period.

5.3.1.2 Interesting intervals

The time interval from $0 - 1000$ ms and $1500 - 2500$ ms are interesting regions since each reflects high and low synchrony respectively. The ISI-distance and SPIKE-distance metrics are validated by analysing the whole datasets at these intervals.

Figure 5.5 shows the change in pairwise synchrony between two different the time intervals from $0 - 1000$ ms and $1500 - 2500$ ms. Figure 5.5(b) clearly

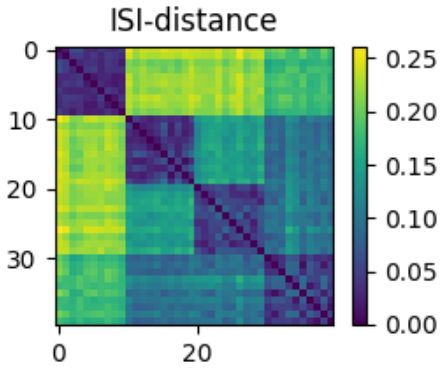

(a) ISI-distance matrix temporally averaged over $0 - 1000$ms

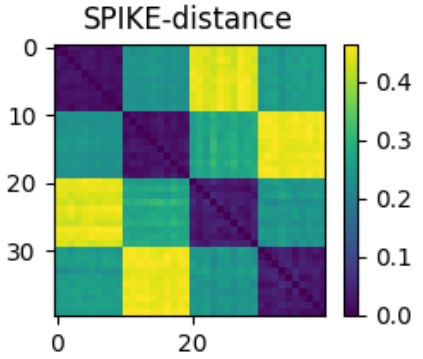

(b) SPIKE-distance matrix temporally averaged over $0 - 1000$ms

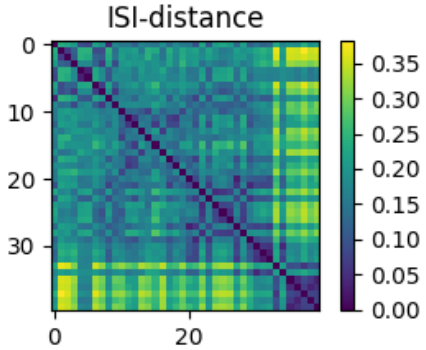

(c) ISI-distance matrix temporally averaged over $1500 - 2500$ms

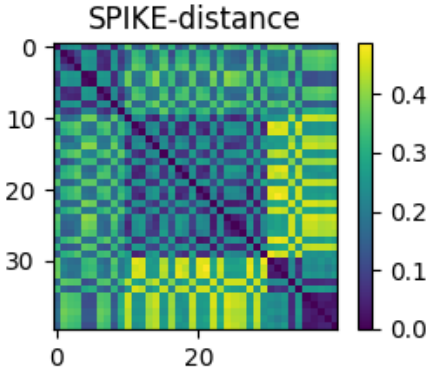

(d) SPIKE-distance matrix temporally averaged over $1500 - 2500$ms

Figure 5.5: ISI-distance and SPIKE-distance matrix at different intervals

shows four different clusters indicated with similar colour. During the interval of $1500 - 2500$ ms when the neurons are firing rather asynchronously, there is no visible clustering among pairs of neurons which is quantified with sparse distance matrices as visible in Figure 5.5(c)(d). The distance matrices in this interval show many tiny clusters which represent asynchronous firing.

Similarly, the same time interval is used to calculate ISI-distance shown in Figure 5.5(a)(c). The subtlety of synchrony caused by spike timing and occurrence of coincident spikes is demonstrated here. Comparing Figure 5.5(a) and Figure 5.5(b), it is clear that the SPIKE-distance metric represents the high synchrony among neurons more clearly than the ISI-distance metric. For the $1500 - 2500$

ms time window where neurons fire more randomly, the synchrony does not show any visible clusters indicating highly asynchronous firing patterns.

5.3.2 Experimental data

Extracellular neuronal recordings from dissociated rat hippocampal at 32 DIV were provided by Luca Berdondini, NETS3 lab at the Istituto Italiano di Technologia, and used as the experimental dataset. The recording was performed with a BioCam platform (3Brain GmbH) using BrainwaveX software at a sampling rate of 7702 Hz. The raw dataset consists of 5 seconds of spontaneous bursting firing patterns resulting in 38510 frames.

Spike train synchrony metrics, namely ISI-distance and SPIKE-distance, were utilised to quantify synchrony and characterize spontaneous bursting behavior of the experimental recording. The raw dataset was processed using the method developed by Muthamann et al. [63] for spike detection as mentioned in section 4.4.1. The details from the spike detection are summarised in Table 5.2. Upon successful detection, the time at which spikes occurred were registered and then processed to generate complete spike trains from all the recording channels. The raster plot in Figure 5.6(A) shows spontaneous firing activity from all 4096 channels organised in synchronous bursts. A corresponding plot of instantaneous mean firing rate with 50 ms time bin is also shown in Figure 5.7a. The ISI distribution in Figure 5.7b shows that most of the consecutive spikes take place in the first $100 - 200$ms.

Table 5.2:
SPIKE DETECTION DETAILS

Channels	Frames	Samplin Rate	Threshold	Spikes Detected
4096	38510	7702	600	15759

The raster plot itself provides good insights into how the population of neurons are firing over time. The general overview indicates pulsating behavior of the neuronal population at time periods. However, upon closer inspection into a smaller time window as shown in Figure 5.6(B)(C), the firing is more sparse in nature without clear intuitive or numerically quantified indications of the extent of

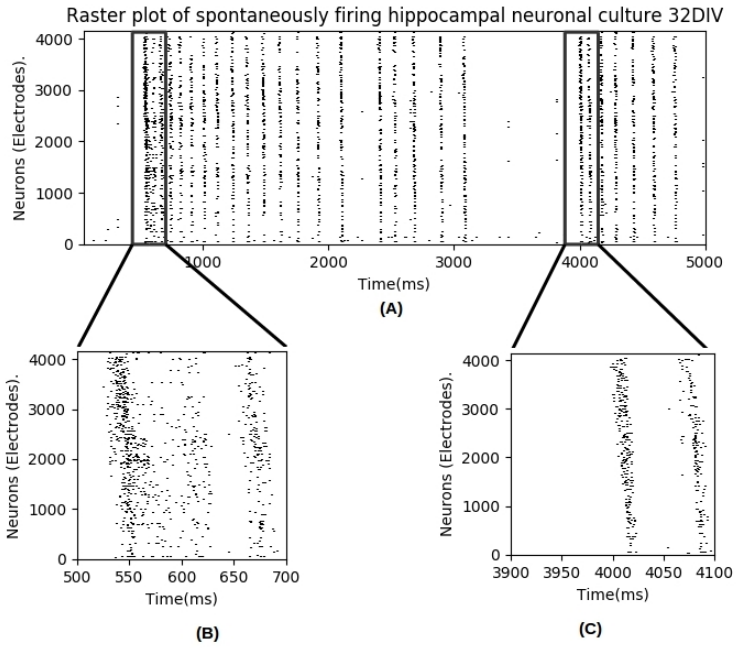

Figure 5.6: Spontaneous synchronous bursting of dissociated neuronal hippocampal culture at 32 DIV. (A) Raster plot of all 4096 electrodes/channels over 5 seconds period (B) Zoomed section from $500 - 700$ ms (C) Zoomed section from $3900 - 4100$ ms

synchronisation. Having a quantifiable metric to measure such synchrony among all the neurons at any given time can be very useful to characterize and compare synchronous behaviours of a neuronal culture.

In addition, Figure 5.8 shows bursting behaviour with spatial information where 4096 electrodes are presented in a $64X64$ matrix. This shows the actual spatial layout of the neuronal culture. The figure shows an inactive period at around 100 ms followed by bursting firing at around 550 ms; this is also visible to some extent from the corresponding raster plot in Figure 5.6(A) and Figure 5.7a.

A more detailed analysis to follow is sub divided into three main sections.(1) Firstly, a multivariate examination i.e. averaged over spike trains, reveals the overall dynamics of the whole population of neurons. (2) Bivariate distances investigate each pair of spike trains and quantifies the degree of synchrony between the two. (3) Finally, a different dataset, seemingly random, is utilised to demon-

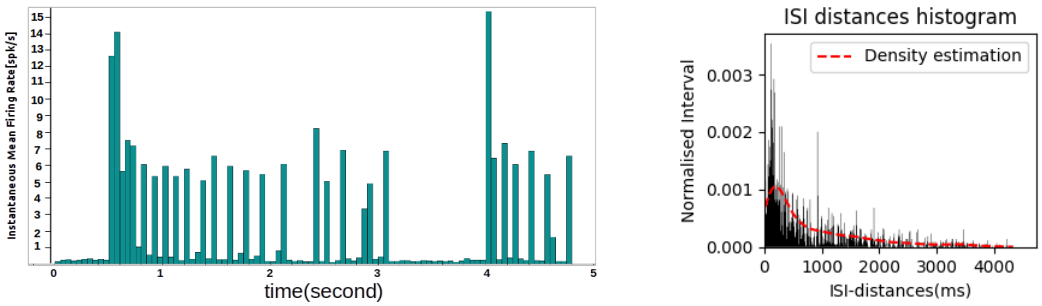

(a) Instantaneous mean firing rate (b) ISI distribution

Figure 5.7: Instantaneous mean firing rate and ISI distribution

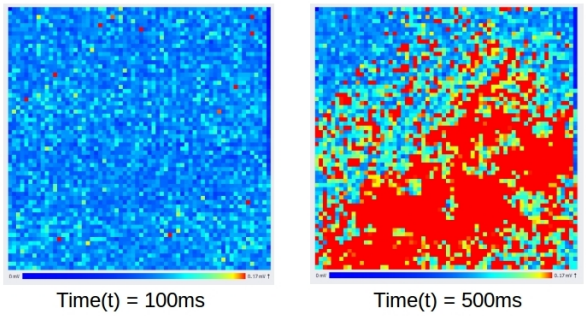

Figure 5.8: Voltage reading mapped as heatmap during data acquisition obtained from BrainWaveX software. Resting or inactive period at 100 ms followed with bursting firing at 550 ms.

strate how these metrics can reveal interesting information about a neuronal population from a seemingly random and visually unintuitive raster plot.

5.3.2.1 Multivariate distance profile

At each instance in time(t) the multivariate ISI-distance and SPIKE-distance are calculated to obtain a multivariate distance profile. Such measures provide an averaged distance value at each timestamp. Instantaneous measures are then temporally averaged over the whole time period to get average ISI-distance and SPIKE-distance measures as shown in Table 5.3.

Figure 5.9 shows the instantaneous ISI-distance and SPIKE-distance profile averaged over all the spike trains. A corresponding raster plot is also placed on top of the profiles for comparison. Clearly, the profiles give a much more

Table 5.3:
Multivariate ISI-distance and SPIKE-distance

Metric	Average Distance	Max Distance	Min Distance
ISI-distance	0.51587	0.66303	0.31061
SPIKE-distance	0.29381	0.31061	0.248148

informative assessment about the synchrony levels of the population compared to the raster plot. The maxima and minima points are circled in red for the ISI-distance and the SPIKE-distance respectively. The first 500 ms shows very little activity resulting in low values for ISI-distance where it reaches its minimum value. Similarly, SPIKE-distance shows an inverted parabola shape registering the change in synchrony from the small number of spiking events in this time interval. Right before the first set of synchronous bursting at 550 ms, the SPIKE-distance goes to its minimum point since there is no spiking activity. At 550 ms, there is a burst of spiking events shown by the sudden surge in values of ISI-distance and also of SPIKE-distance. The ISI-distance decays quickly because as Figure 5.6(B) shows there are lots of asynchronous firing upon closer observation. With a quantifiable metric that reports on these synchronous behaviours, one can make objective evaluation of the neuronal population dynamics.

The following 1500 ms period between $(500 - 2000$ ms) shows fluctuating profiles. The oscillating firing shows sudden bursts of firing followed by period of silence and repeat firing. The sample section highlighted in a red rectangle in Figure 5.9 shows the oscillating behavior of the neuronal culture. This fluctuation is present throughout the profiles to different degrees. Bursting firing and oscillating behavior is typical behavior for a rat hippocampal *in vitro* sample [188]. At around 4000 ms, similar behavior is observed after a long period of silence. The dynamics look similar to those around 550 ms indicating repetition of a similar pattern.

An examination of interesting intervals or time points preliminary indicated from raster plots reveals more localised spike train synchrony at any given moment in time. Here, the interesting intervals are areas of low activity, high activity and sparsely firing areas.

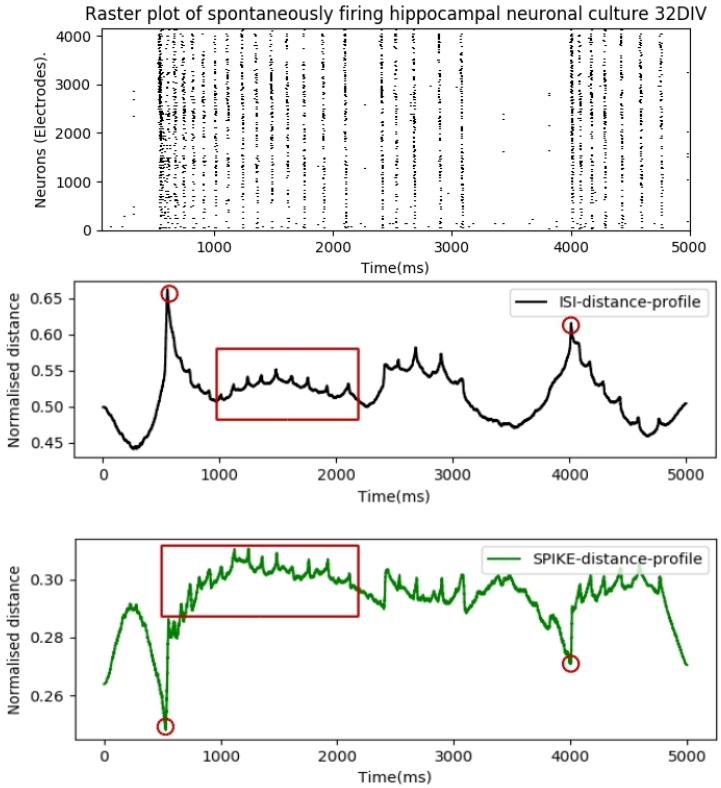

Figure 5.9: Instantaneous multivariate ISI-distance profile and SPIKE-distance profile

For the purpose of comparing distance metrics at different time periods, $t = \{100, 550, 1000, 2000, 3000, 4025\}$ ms are chosen arbitrarily. The multivariate ISI-distance and SPIKE-distance are calculated at each of these time points and listed in Table 5.4. The ISI-distance is lowest at 100 ms when there are very few spiking activities. At 550 ms, the averaged synchrony levels goes to a maximum with high ISI-distance value: complementary to this, the SPIKE-distance is at its minimum (disregarding the 100 ms when very little spikes are present).

5.3.2.2 Bivariate distance matrix

In addition to an averaged distance profile, synchrony among any two spike trains can also be analysed. For larger datasets, the bivariate distance matrix is difficult to analyse due to the large number of spike trains. However, a subset of the

Table 5.4: Distance metrics at different times

Time(ms)	ISI-distance	SPIKE-distance
100	0.47758	0.2775
550	0.65517	0.28083
1000	0.51323	0.30381
2000	0.51258	0.29895
3000	0.53267	0.29403
4025	0.59748	0.28937

dataset can be analysed to inspect the bivariate synchrony level at any given period of time.

Here, 10 such spike trains are arbitrarily extracted from channels $45 - 54$ from 4096 spike trains for bivariate analysis. Bivariate ISI-distance and SPIKE-distance from all the spike train pairs are calculated and are represented by a 10x10 heatmap matrix. Two time intervals, $540 - 560$ms and $2000 - 2500$ms are selected, which are the regions of high and low synchrony respectively.

In the $540 - 560$ ms interval, there are lots of coincident activity. Figure 5.10(b)(c) shows the pair wise synchrony among all the pairs of spike trains. A similar colour between two or more pairs represents the same level of synchrony. Figure 5.10 (b) shows a high level of synchrony with higher values of ISI-distance. However, visible clusters are not apparent from the matrix. There are lots of coincident events which the ISI-distance metric fails to capture. The SPIKE-distance is more suitable for identification of coincident spikes and Figure 5.10 (c) clearly shows one big cluster indicated in the dark blue area. This cluster indicates that there are 8 spike trains firing with high synchrony. The two yellow regions were not firing in this interval. Similarly for the next time interval ($2000 - 2500$ ms), many small clusters with different degree of synchrony are observed as shown in Figure 5.10(d)(e). Similar coloured groups are evidence of synchronous spike trains. The red highlighted area shows relatively higher degrees of synchrony. Also, it is evident that the last two spike trains are not active in this interval and hence show very low degree of synchrony.

Even with very large datasets one can examine such smaller subsets for deeper pairwise analysis of spike synchrony. However, the selection of the subset depends

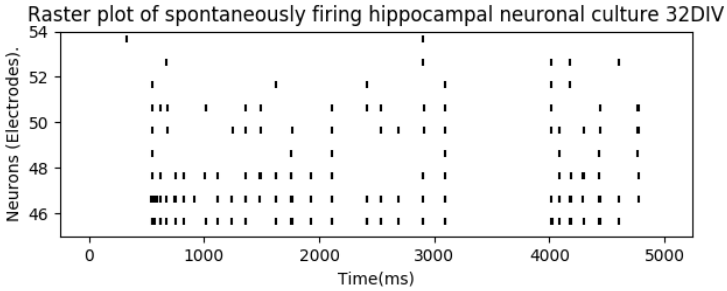

(a) Raster plot of 10 spike trains from channel $45 - 54$

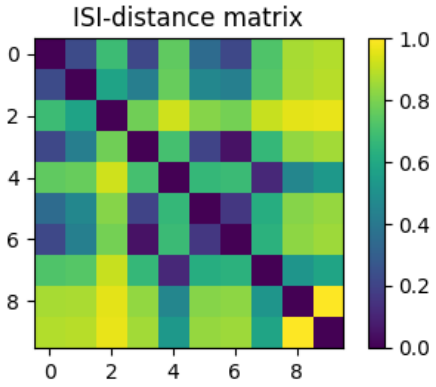

(b) ISI-distance matrix temporally averaged over $540 - 560$ms

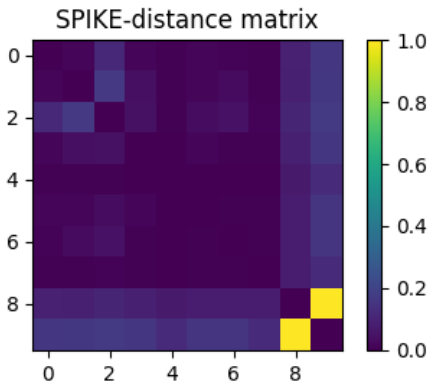

(c) SPIKE-distance matrix temporally averaged over $540 - 560$ms

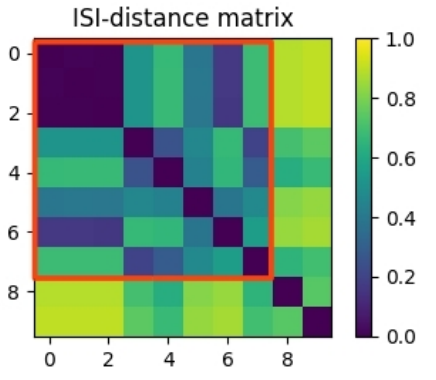

(d) ISI-distance matrix temporally averaged over $2000 - 2500$ms

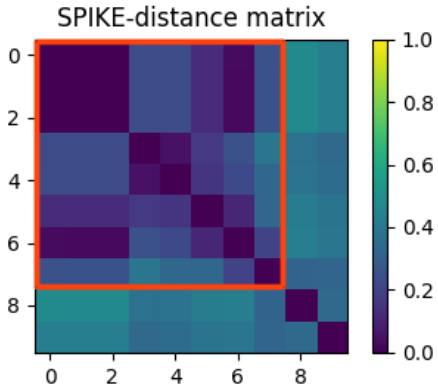

(e) SPIKE-distance matrix temporally averaged over $2000 - 2500$ms

Figure 5.10: ISI-distance and SPIKE-distance matrix at different intervals

on the nature of the experiment e.g. stimulus driven experiments.

5.3.2.3 Randomly firing neural population - Retina Dataset

Not all extracellular HD-MEA recording exhibit oscillatory bursting behavior. Some recordings are sparse, which makes it very difficult to get any clear information about the network dynamics visually from the raster plot.

Extending the analysis, this section briefly shows how quantifiable metrics make it easier to visualize network synchrony from seemingly random and sparse firing patterns. An extracellular recording from an acute retinal ganglion cells recorded from BioCam(3Brain GmbH) with BrainwaveX software obtained from 3Brain provided by the Institute of Neuroscience(ION), Newcastle University, is used here following the same spike detection methods described in section 5.2.2.

The raster plot of the retina dataset shown in Figure 5.11 shows instantaneous firing of 4096 channels over the period of 5000 ms. The raster plot itself appears to show random behaviour without any visible bursting patterns, as observed with hippocampal cultures. However, upon calculation of ISI-distance and SPIKE-distance more information on the the dynamics becomes apparent. This is evident from Figure 5.11(B)(C), where for a time period of 5000 ms, a clear pattern in synchrony is observable, indicating oscillating behavior similar to the hippocampal culture. Also, it is much more intuitive to visually track the network synchrony over time with distance metrics.

5.4 Summary and conclusion

Despite the importance of spike train synchrony in understanding of neural code being well established, the analysis metrics have not been explored for large high density datasets with thousands of electrodes. In this paper, the ISI-distance and SPIKE-distance metrics for spike train synchrony analysis have been applied to HD-MEA datasets making use of parallel processing and informative selection of the subset of the dataset to illustrate how these may be used to quantify and characterize bursting behaviors in large datasets. The metrics used were first validated with a smaller synthetic dataset that had deliberately incorporated varying degrees of synchrony. Both bivariate and multivariate analysis were performed. The analysis on the synthetic data showed a correct number of clusters. The

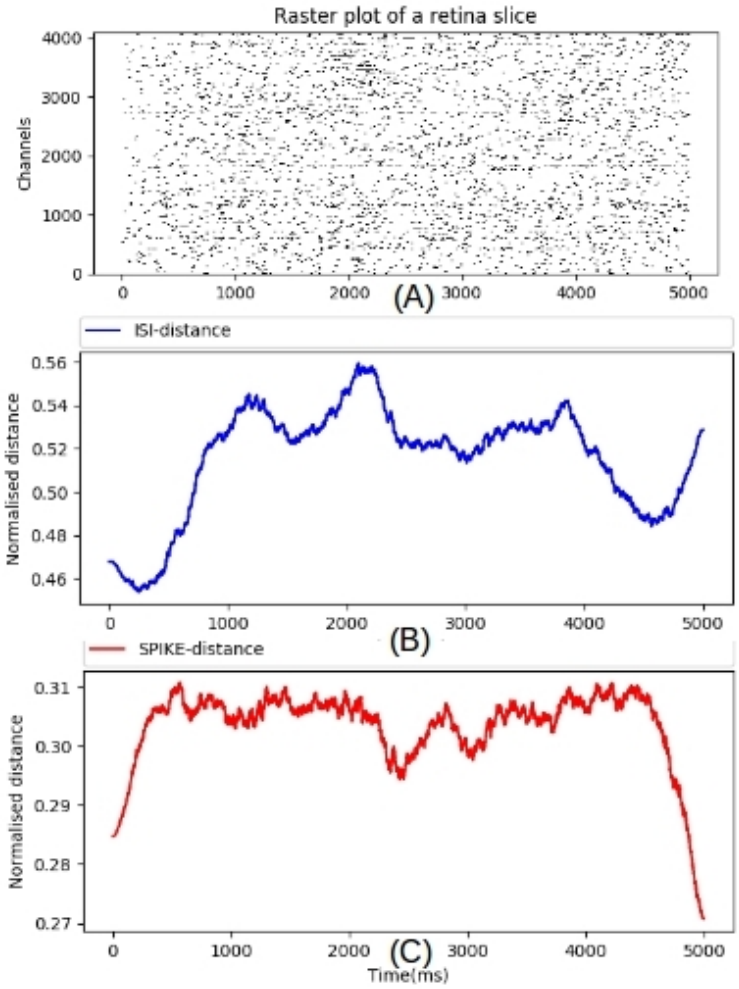

Figure 5.11: Instantaneous raster plot of a retinal ganglion cells with ISI-distance profile and SPIKE-distance profile subsequently.

bivariate distance matrix illustrated these clusters for a high synchrony period and showed much more smaller cluster during random firing as expected.

Secondly, for the hippocampal experimental dataset, ISI-distance and SPIKE-distance profile for the whole time period revealed synchrony levels among all channels over time. High and low synchrony periods were identified, and oscillating patterns with fluctuating synchrony levels revealed.

A bivariate distance matrix for such a large number of channels is not very insightful. Exploring a small subset of channels instead is useful when looking at pairwise synchrony. For demonstration purpose, a subset of spike trains from

channel $45-54$ were selected for bivariate analysis. The first interval of $540-560$ ms illustrated many coincident spikes which are recorded by the SPIKE-distance matrix as a big single cluster with high synchrony. In contrast, the ISI-distance metric fails to capture such coincident spikes resulting in less obvious clustering.

Finally HD-MEA data from a retinal ganglion cells was also utilized to show how information not observable from the raster plot may be obtained. Upon calculation of spike train synchrony, the dynamics in terms of averaged spike train synchrony are more discernible and what seemed like random firings in the raster plot are identified as fluctuating synchrony. The ability to utilise such metrics even on large scale experimental biological dataset such as HD-MEA recordings is invaluable in studying various neuronal properties.

Chapter 6

Information Theory Based Connectivity Analysis

6.1 Introduction

In this chapter, an information theory based approach to infer connectivity from neuronal recordings is presented. The chapter discusses two main contributions in connectivity inference from neuronal recordings. The first half of the chapter (Section 6.2) introduces the Transfer Entropy (TE) method for inferring connectivity. The method is validated with a simulated Izhikevich's network (Section 6.2.3.1) and is then applied to an experimental recording. Due to the lack of ground truth information, a new method of utilising firing density plot and superimposing it onto the connectivity map is introduced as an alternative to the ground truth information. The superimposition method shows a good fit between the density plot and the inferred connectivity (Section 6.2.3.3). The findings of this section have been published in the 2019 IJCNN conference proceedings [189].

The second half of the chapter (Section 6.3) tackles the issue of lack of ground truth for real neuronal cultures, by the addition of *surrogate* data. A new method of utilising the Inter-Spike Interval (ISI) distribution is presented. Surrogate data are generated as control data under some null hypothesis to measure the statistical significance of the connection inferred in the absence of ground truth information. The proposed method generates enhanced surrogate data due to variations

introduced during the sampling process. Section 6.3.3 demonstrates that the proposed method is able to successfully identify significant connections and also detect varying degrees of connection strength. Furthermore, ROC analysis shows a superior performance in comparison to an existing ISI shuffling method.

6.2 Transfer entropy based connectivity

6.2.1 Introduction

Connectivity characterisation of direct and indirect interactions in neuronal circuits is very useful in understanding neuronal dynamics, connectivity and neural information processing. The neuronal interactions are typically classified as physical, functional and effective connectivity [151]. Physical connections are synapses and gap junctions, correlated interactions between two neurons would represent a functional connectivity and a causal relationship between two neurons where firing of one neuron can be predicted based on the firings of another represents an effective connectivity [15].

The information flow in neuronal assemblies is typically distributed and inference from physical interconnections limits the understanding of information flow and the way information could flow. Hence, exploration of effective connectivity may reveal better insights into information flow and processing. With High Density (HD)-MEAs, it is now possible to record electrophysiological activities (action potentials or spikes) from thousands of tightly spaced electrodes at high temporal resolution. Electrophysiological recordings analysis in combination with graph theoretic approach and statistical physics have allowed for the inference of such functional and effective interconnections in neuronal cultures based on the correlated spiking behaviours [190, 191].

To infer a causal relationship between two neurons based on the spike timings, an information theory based model-free method called 'Transfer Entropy' has gained popularity in computational neuroscience [14–17]. Transfer entropy (TE) is an information theoretic based non-parametric measure of the flow of directed information between two random processes - proposed by Schreiber [160]. Transfer entropy is based on transitional probabilities of spiking events, is asym-

metric and incorporates both directionality and dynamic information. The TE method has outperformed many other popular methods such as cross-correlation (CC) [18], joint entropy [19], mutual information [14, 15] to identify connectivity from simulated networks. However, due to the lack of ground truth connectivity in real experimental living cultures, it is a challenging problem to differentiate true connections from spurious connections - even when inferred with a superior method such as TE. Delayed TE, which incorporates many previous time steps in the algorithm to take in account axonal delays present in real biological networks, proposed by Ito [15] has outperformed single delay TE approaches. Hence, the delayed TE approach was utilised to infer connectivity for this work.

In this section of this chapter, a method of utilising the spatial firing density plot of HD-MEAs (based on extracellular electrophysiological recordings) on the original spatial layout as an indicator of the physical connectivity, is presented as an alternative to the physical ground truth. It is demonstrated that by superimposing inferred connectivity based on a graph theoretic approach, one can test if the connectivity matches the density plot. The rationale for this approach is the fact that highly interconnected neurons tend to exhibit more firing behaviours due to more active interactions.

Firstly, a biologically realistic simulation of cortical network that incorporates biologically plausible axonal delays, synapses and dynamics, to test the algorithm's performance, was performed. The connectivity matrix based on the synaptic weights matrix provides an objective way to compare the performance of the TE method. Then, the method was applied to real experimental dataset of spontaneously firing hippocampal culture. The connectivity matrix computed was based on the delayed TE method and uses the superimposed firing density plot as a reference.

6.2.2 Materials and methods

6.2.2.1 Transfer Entropy

Transfer Entropy was introduced briefly in Chapter 3 (Section 3.5.2.2), where it was shown that the original expression for TE [160] between two random pro-

cesses, I and J (neurons in this scenario) is given as,

$$T_{J\to I} = \sum_{i_{t+1},i_t^{(k)},j_t^{(l)}} p(i_{t+1}, i_t^{(k)}, j_t^{(l)}) \log_2 \frac{p(i_{t+1}|i_t^{(k)}, j_t^{(l)})}{p(j_{t+1}|i_t^{(l)})} \tag{6.1}$$

$$p(i_{t+1}|i_t, j_t) = \frac{p(i_{t+1}, i_t, j_t)}{p(i_t, j_t)} \tag{6.2}$$

$$p(i_{t+1}|i_t) = \frac{p(i_{t+1}, i_t)}{p(i_t)} \tag{6.3}$$

where i_t and j_t represent the status of the neurons I and J at time t respectively, which could be 1 or 0 for spike or no spike. i_{t+1} is the the status of the neuron I at time, $t+1$. p is the probability of the status denoted in the parenthesis. The parameters k and l denotes the order of the TE; number of time bins to include from the past. The logarithm with base 2 is used so that the units are bits.

The conditional probabilities in equation 6.1 can be decomposed into joint and marginal probabilities as shown in equation 6.2 and equation 6.3.

Due to axonal delays and physical separation, the causal effect of one neuron may not be apparent in another neuron in the next time step, but might take multiple time steps. Considering this limitation with the traditional TE method, Ito et al [15] extended the single delayed TE method with multiple delays to account for these delayed causal interactions, which leads to a modified TE expression as.

$$T_{J\to I} = \sum_{i_{t+1},i_t^{(k)},j_{t+1-d}^{(l)}} p(i_{t+1}, i_t^{(k)}, j_{t+1-d}^{(l)}) \log_2 \frac{p(i_{t+1}|i_t^{(k)}, j_{t+1-d}^{(l)})}{p(j_{t+1}|i_t^{(l)})} \tag{6.4}$$

where d is the delay or number of previous time steps to include. The rest of the parameters remain as described in equation 6.1. The algorithm can be visualised as shown in Figure 6.1 using binned time series of neuron i and j. The time series of neuron i' is a back-shifted copy of neuron i by one time bin which is stacked on top of the other two time series. Each red pixel represents a spiking event and white pixel represents a silent event. For a given time window of T, for a delay of one time bin, the algorithm calculates the repetition of three different

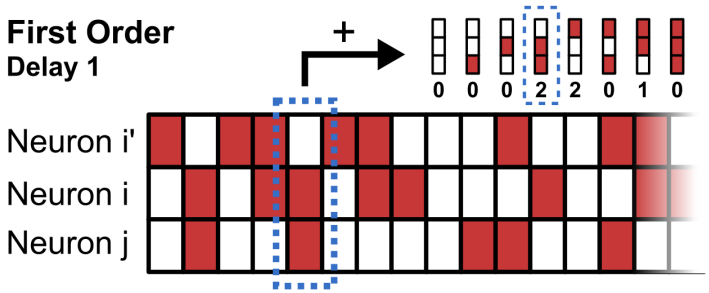

Figure 6.1: Illustration of first-order transfer entropy with a delay of 1 time bin.

patterns from the time series for neurons i', i, j. A time series represented by neuron i' takes into account the past events of neurons i. This delay can be easily extended with any desirable delay.

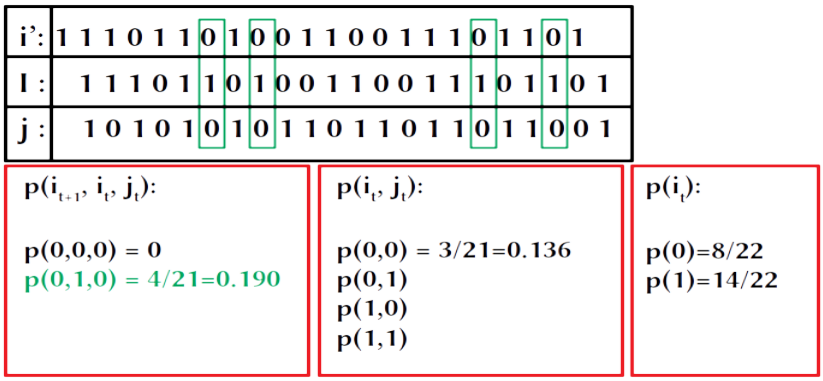

Figure 6.2: Illustration of computing the joint and marginal probabilities for TE. I,J and i' are neuron i,j and neuron i at time t-1 respectively. 0s are no spike events and 1s are the spiking events.

To further simplify the illustration of the algorithm, Figure 6.2 shows an example of how different probabilities can be computed. Once the conditional probabilities are expanded into joint and marginal probabilities, these joint and marginal probabilities can be computed as shown in the Figure 6.2 given a certain time window by counting the patterns for different combination and subsequently the probability of the occurrence within the given time window.

6.2.2.2 Simulation model

Before applying the TE method on experimental data, the method was validated with simulated data, because such simulated data has an empirical ground truth against which a comparison can be made to assess the accuracy of the inferred connectivity. The simulation model utilised to test the TE connectivity is based on Izhikevich's cortical network model [192] which incorporates biologically realistic synapses, delays and dynamics. Due to its biologically plausible properties, it is an appropriate model on which to test the TE algorithm before moving to experimental recordings.

The simulated model consists of N=1000 neurons, of which Ne=800 are regular excitatory spiking neurons and Ni=200 are inhibitory fast spiking neurons. Full details of the network can found in Appendix A from [192]. The network simulation configuration is adapted from Ito [15]. The simulation is run on MATLAB 2018b.

Spiking neurons Izhikevich's neuron model [193] is used to define the intrinsic neural dynamics which are represented by the following differential equations.

$$v' = 0.04v^2 + 5v + 140 - u + I \tag{6.5}$$

$$u' = a(bv - u) \tag{6.6}$$

with auxiliary after-spike resetting

$$if\, v \geq +30mV, then \begin{cases} v \leftarrow c \\ u \leftarrow u + d \end{cases} \tag{6.7}$$

Here, v and v' represent the membrane potential and time derivative of the membrane potential respectively, u is the recovery variable, u' is the time derivative of the recovery variable and I represents the total synaptic input into the neuron. Parameters a, b, c, d are adjustable parameters to adjust the firing behaviour of the neuron, which can exhibit regular spiking (RS), intrinsically bursting (IB) and fast spiking (FS).

RS cells were modelled with $(a, b, c, d) = (0.02, 0.2, -65, 8)$ and FS cells were modelled with $(a, b, c, d) = (0.1, 0.2, -65, 2)$.

After the membrane potential reaches its apex at +30 mV, the membrane voltage and the recovery variables are reset according to equation (6.7).

Spike-Timing-Dependent Plasticity The synaptic connections are based on the spike-timing-dependent plasticity (STDP) rule [84]. As per the STDP rule, if a spike from an excitatory presynaptic neuron arrives at the postsynaptic neuron and causes it to fire, then the synaptic weight is strengthened and the synaptic weight is weakened if postsynaptic firing precedes presynaptic firing. STDP has previously been described in Chapter 3 (Section 3.2.1)

Network Connectivity and Simulation In the simulated network, each neuron has delayed synapses to 100 random other neurons. Excitatory neurons can be connected to any other neurons while inhibitory are only connected to excitatory neurons. Synaptic connections from excitatory neurons have delays in the range from 1ms to 20ms whereas connections from inhibitory neurons have a fixed delay of 1ms. The excitatory synapse weights are in the range from 0 to 10mV and inhibitory synapse weights are set to -5mV. These parameters are model parameters for mammalian cortical network and were set in Izhikevich's network [192].

The simulation was run for 2 hours (simulation time) following Ito's methodology [15]. Spiking neurons were evaluated each millisecond. The spike raster plot shown in Figure 6.3 shows the spiking behaviour of the network evaluated over a 1000ms range. STDP was turned off after the first hour and spiking neurons were recorded for the last 30 minutes sampled, to allow the network to stabilise after synaptic weights were fixed. The synapse matrix generated after stopping the STDP was used to generate a connectivity matrix which served as the ground truth to compare with the connectivity inferred with TE method. 100 random neurons (80 from 800 excitatory; 20 from 200 inhibitory) were subsampled from the 1000 neurons for the connectivity analysis.

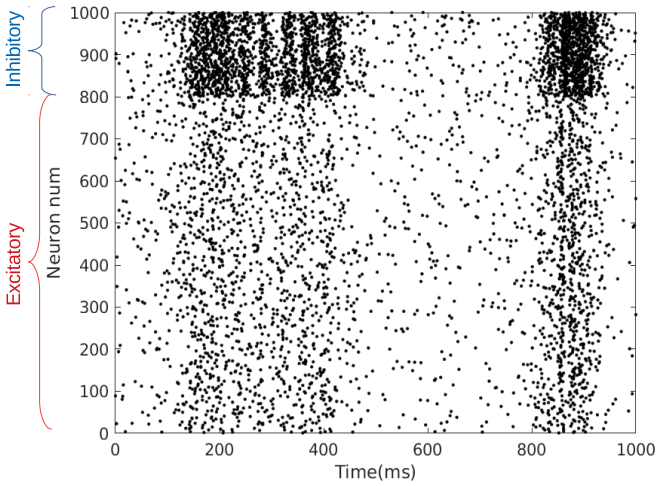

Figure 6.3: Raster plot showing rhythmic spiking activities of 1000 Izhikevich neurons with 800 excitatory neurons and 200 inhibitory neurons. The neurons are modelled with parameters as discussed in Section 6.2.2.2. As synaptic weights are evolved due to STDP rules, the rhythmic activities change from slower to faster rhythms.

6.2.2.3 Cell culture

In addition to the simulated data, a real experimental dataset of a neuronal culture was used with the TE method to estimate the connectivity.

Hippocampal tissue from E18 Sprague Dawley rat (BrainBits UK, now BrainBits USA) were dissociated to yield approximately 1.5 million viable cells. The neurons were plated on the CMOS based HD-MEA, BioChip HD-MEA Stimulo, from 3Brain AG which consists of 4096 recording channels (in a 64 x 64 grid; 21 x 21 μm^2, 81μm pitch) and 16 stimulating channels (in 4 x 4 grid; 21 x 21 μm^2, 1246μm pitch). BioChips were sterilized in 70% ethanol for 20 min and rinsed thoroughly with Sterilized Distilled Water (SDW) , then left to air dry under a laminar hood. The chips were then preconditioned with full culture medium, NbActive 4 BrainBits), which is composed of Neurobasal/B27 along with additional supplements - creatine, estrogen and cholesterol. The chips were incubated for 48 hours. After that, the medium was aspirated and the chips were again left to air dry under the laminar hood. BioChips were then pre-coated with a double

coating of laminin for 3 hrs followed by poly-D-lysine (both at 100µg/ml), and left overnight incubated at 37°C. After the cells were dissociated, the cell concentration was diluted to about 1000 cells/µl. 80,000 cells were seeded onto the MEA chips with a 80µl droplet. This was left to settle for 2 3 hours before adding 1.5ml of complete growth media. The culture was incubated at 37°C, 5% CO_2 and 65% humidity. Due to the fast evaporation rate, the chips placed inside the petridish were kept in a sterilized custom plastic box with a loose lid filled with 20 ml of SDW. This allows for the culture to settle down well without a drastic change in pH level due to evaporation. 25 µM glutamate was added to the medium for the first 4 days to promote cell survival after the seeding and was omitted after that. Half of the medium was changed every 4 days. After 2-3 weeks, the culture becomes mature enough to exhibit electrophysiological activities. The electrophysiological activities were recorded at day 25. The raw voltage traces were recorded at 17.85 kHz sampling frequency and spike events were detected using the methods as described by this author [39], adapted from [63].

6.2.3 Results and discussions

6.2.3.1 Validation with simulated data

Spike data from the network described in the above Section 6.2.2.2 were recorded every millisecond from the simulation model performed in MATLAB 2018b and exported as a *CSV(Comma Separated Values)* file. The average firing rate was stable over the whole duration of the simulated network as shown in Figure 6.4. Gamma oscillations (30Hz) were present as reported in [192]. Due to the STDP rule for synapse weight updates, synaptic weights tended to converge either to the maximum i.e. 10mV or the minimum i.e. 0mV over a longer period (typically after tens of minutes) of simulation.

The spike times extracted for the last 30 minutes of simulation were used to compute pair wise TE values for all the 100 subsampled neurons. TE values were computed for three different delays - 10, 20 and 30 time bins, which is the parameter d in equation 6.2. Peak values of the TE (TEPk) were considered to infer connectivity. Ito's method [15] was used to compute the delayed TE values.

To investigate the general trend of TEPk values inferred against the ground

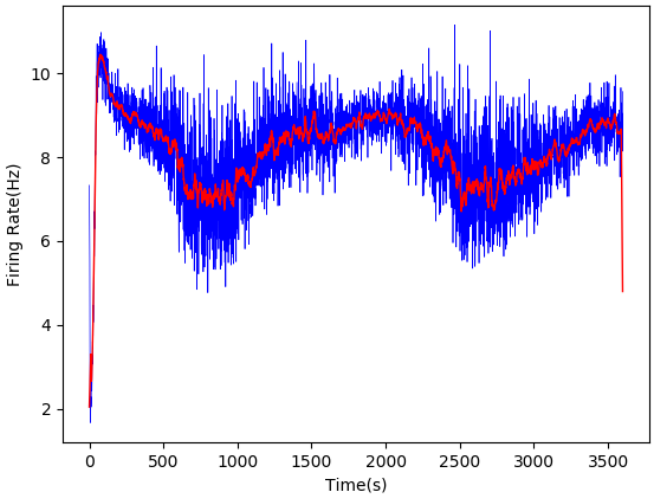

Figure 6.4: Firing rate for the first 1 hr of simulation activity. Red lines represent the mean firing rate averaged at 50 ms time bins.

truth synaptic weight, the TEPk values computed were plotted for each pair against the synaptic weights. Figure 6.5 shows the TEPk value and corresponding ground truth synaptic weight for each pair of neurons in a linear scale. As evident from Figure 6.5, the TEPk values increase with the synaptic weights in an exponential manner for the subsampled neurons. The log scale shows a linear relationship. Only the synaptic weights between 0mV and 10mV are included in the plot for better visualisation. Most of the connections converge either to the maximum or minimum - including those weights result in large clutter towards both ends.

A higher synaptic weight between two neurons represents a higher probability of effective connectivity which could potentially cause the post synaptic neuron to fire. TEPk values corresponding with synaptic weights from the same pair indicate that the inferred connectivity is actually the connection that is present in the simulation model. However, the plot only shows a general trend and not an empirical metric to measure the accuracy of the method. Receiver Operating Characteristic (ROC) analysis was performed to calculate the accuracy performance of the algorithm. Essentially, the problem becomes a classification problem to classify true connections from spurious connections. ROC analysis

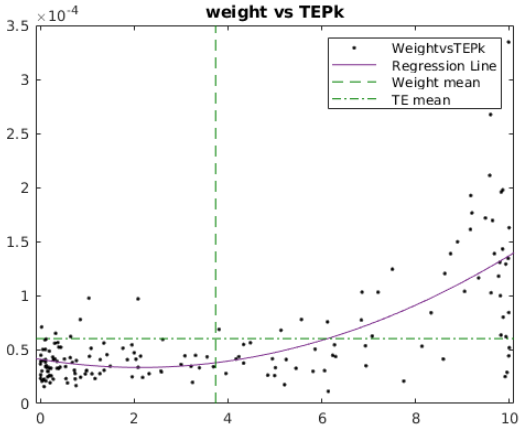

Figure 6.5: Relationship between inferred connectivity strength with the synaptic weights. X-axis represents the synaptic weights and Y-axis shows the TEPk values.

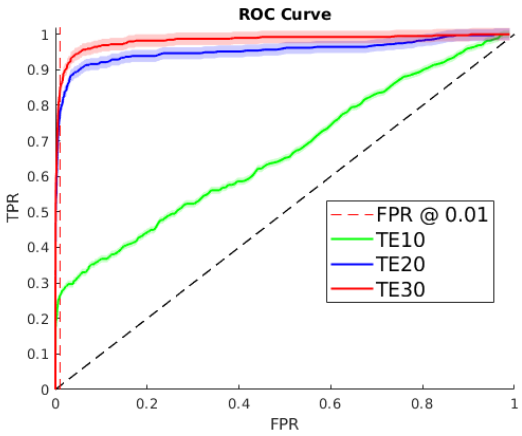

Figure 6.6: Performance comparison of effective connectivity estimation with the transfer entropy. TPR is plotted against FPR for 10,20 and 30 time bins delay.

provides an objective approach to quantify performance of a binary classifier algorithm [194–196].

After computation of TEPk, the task is to distinguish "True Positive(TP)" from "True Negative(TN)" and similarly also to identify "False Positives(FP)" and "False Negatives(FN)" . TP is the case when the algorithm identifies a connectivity between two neurons, which in fact exists in the model as well. TN is the case when the algorithm identifies no connection between two neurons, and in fact there is no connection in the model as well. FP is the case when the algorithm identifies a connection but in reality there is no connection in the model for a particular pair of neurons. Similarly, FN is a scenario when an algorithm identifies no connection between two neurons but there does exist a connection in the model. TP+FN actually reports total number of true connections identified by the algorithm and FP+TN reports the total true unconnected pairs.

ROC space analysis is done by plotting true positive rate(TPR) against false positive rate(FPR) . TPR and FPR are computed as,

$$TPR = \frac{TP}{TP + FN} \tag{6.8}$$

$$FPR = \frac{FP}{FP + TN} \tag{6.9}$$

To analyse the effect of the delay parameter,TEPk values for three different delays i.e. 10ms, 20ms and 30ms time bins were computed and corresponding TPR and FPR for each of these delays were plotted. In the model, the axonal delay is in the range from 1 to 20 ms. Figure 6.6 clearly shows a significant improvement in performance from 10 to 20 time bins delay which demonstrates that the delayed TE method is able to capture delayed interactions effectively. With a delay of 10 time bins, the algorithm misses a lot of delayed interactions resulting in poor performance whereas with delay of 20 time bins i.e. 20 ms, most of the delayed interactions are taken into account resulting in a much improved accuracy. A delay of 30 time bins improves the performance slightly compared to the 20 time bins, but not significantly. This is presumably due to the fact that the model has delays in the range of 1-20ms, which is mostly covered by TE delay of 20 ms.

To measure the performance, it is important to measure the TPR against FPR at a very low FPR rate. Accordingly, the TPR was measured at a constant FPR rate of 0.01 which is a very small percentage of FPR so that the performance is not compromised. For delays of 20 and 30 time bins, the TPR at FPR=0.01 was measured to be around 82±2% and 84±2% respectively, showing the effectiveness of the approach.

The delayed TE based method of inferring connectivity is hence accurate in the range of mid 80^{th} percentile, even for a biologically realistic model of a spiking neural network. The experiment on the simulated data thus established the reliability of the method for a realistic network with delays, STDP synapses and complex interactions. However, real experimental neuronal cultures are far more difficult to analyse, with complex interactions but without the ground truth against which the results can be empirically compared.

6.2.3.2 Experimental recordings and neuronal dynamics

Neural activities were recorded from a CMOS based HD-MEA (3Brain AG) from a spontaneously firing *in-vitro* hippocampal culture at day 25 when the culture is

mature so that synaptogenesis and other developmental stages are complete [8]. The activities were recorded for 10 minutes. The first 20 seconds were used to analyse the connectivity. Spikes were detected utilising the methods discussed in Chapter 4.4.1 and explained in [39], to generate a spike train for each channel. After the spikes were detected for each channel, spike times were extracted and plotted as a raster plot to visualize overall network dynamics.

A raster plot of the activities over the 20 second period is shown in Figure 6.7(A). The raster plot shows general firing behaviour of the whole network without any spatial information. Each dot represents a spiking activity for a channel at a particular time. Figure 6.7(B) shows the firing activities as colour mapped voltage changes in both spatial and temporal resolution, showing rich crescendo like spontaneous bursting of neural activities. The bursting firing repeats spontaneously without any stimulation for the whole 10 minutes recording.

In addition, the neuronal cultures from the recording chip were stained to fix the morphological and topological representation of the culture. The culture was stained with the MAP2 (Microtubule Associated Protein 2) antibody which stains the dendritic arborizations. Figure 6.7(C,D) shows fluorescence images of clusters of neurons and individual neurons respectively.

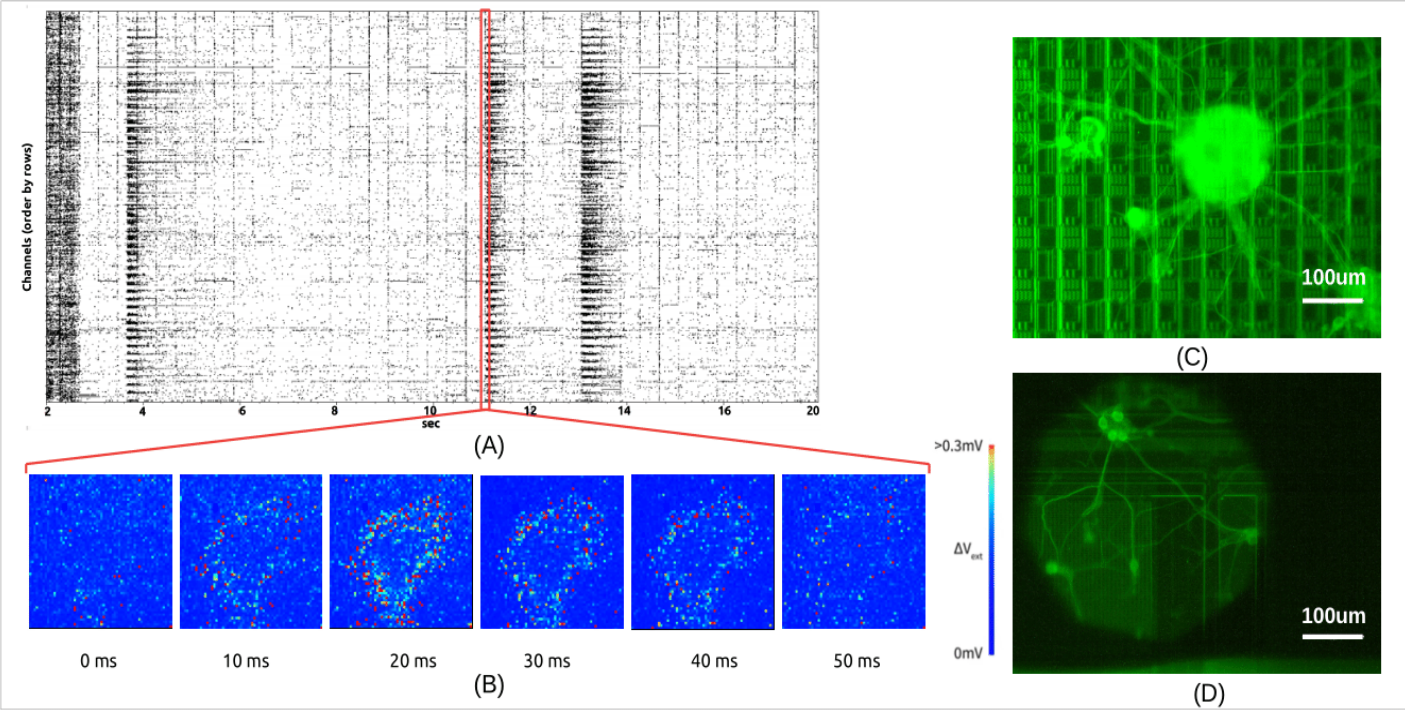

Figure 6.7: (A) Raster plot of the hippocampal culture of subsampled 20 seconds from a 10 minute long recording. The Y-axis is the number of channels i.e.4096 and X-axis is the time in seconds. (B) Spontaneous activity representation with a colour map where each pixel represents an electrode laid out in a 64 x 64 grid. (C,D) Fluorescence image of the neuron cluster and individual neurons on MEAs, respectively.

6.2.3.3 Connectivity inference

After the spike detection, delayed TE was applied for each pair of spike trains obtained from the neural recordings to infer the connectivity matrix based on TE values calculated with each pair. The delayed TE algorithm resulted in a final matrix of size 4096x4096 that encompassed all the pairs from 4096 electrodes. Most of the pairwise values were non-zero even if there were no apparent causal interactions. However, such non causal values were generally very low and filtered out at a later stage. For the experimental neuronal culture, the mean of the TE values was observed as 2.11x10e-5 with standard deviation of 8.67x10e-5 as shown in Table 6.1.

Table 6.1: TE values statistics

Min	Max	Mean	Std
1.08x10e-8	5.4x10e-3	2.11x10e-5	8.6x10e-5

The TE value obtained were generally quite low due to sparsity of the spiking data. However, even with the lower values, the causal links can be inferred since the larger values from such lower values indicate stronger causal interactions.

Every experimental model is different with network dynamics unique to that model so there are no fixed or expected TE values. Due to the presence of lots of false positive connections, it is important to filter out such false positive connectivity. Such false positives are prevalent due to synchronised bursting events, typical of hippocampal cultures, where most of the neurons firing together which may lead to show positive causal relation even though there are none.

The delayed TE algorithm with a delay of 30 time steps resulted in $44,864$ connections without filtering out false positive connections. Threshold filtering based on standard deviations from the mean value was applied to eliminate weaker connections which are most likely to represent a false positive connection. The algorithm only selected connections that fell in the region beyond 10 standard deviations from the mean value for thresholding to filter out potential false positives. The selection criteria covered most of the stronger connections while discarding weaker connections. After applying thresholding, $6,091$ connections as shown in Figure 6.8 was obtained. The distribution of connections for each

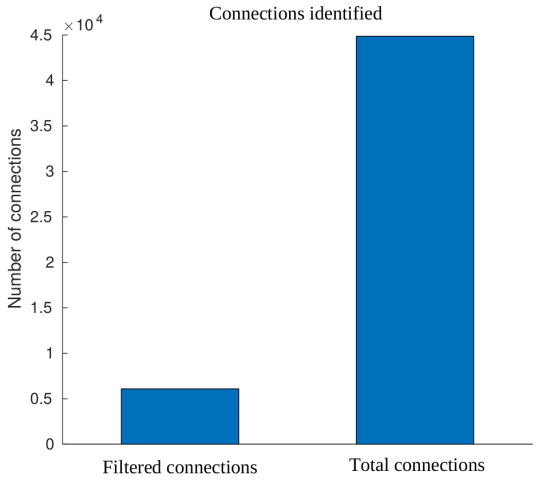

Figure 6.8: Total connections identified by delayed TE method and most prominent connections after filtering.

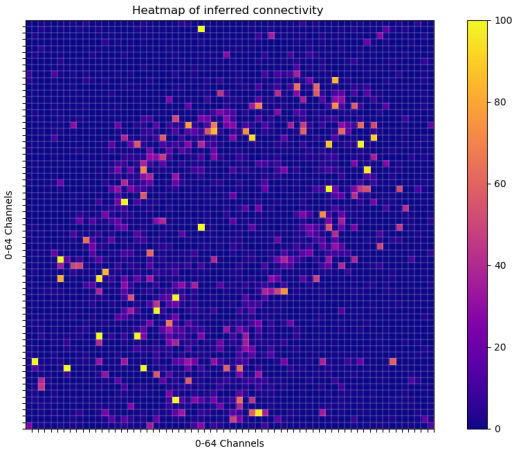

Figure 6.9: Number of connections identified for each channel

channel is shown in Figure 6.9, laid out in a 2D grid. The spatial 2D grid of 64 x 64 electrodes can be flattened out as 1,...,4096 electrodes where co-ordinate (0,0) = 1, (0,1) = 2, ... (1,0) = 65 and so on. Figure 6.9 shows a very close resemblance to the actual firing density plot shown in Figure 6.10(A) indicating accurate inference of connectivity.

For visualisation a graph theoretic approach [190, 197] was used to generate a connectivity map. Each channel was considered a node in the graph laid out in the 64 x 64 grid replicating the spatial layout of the actual recording MEAs. The TE values calculated for each pair represents an edge which was colour coded according to the strength of the connection. The TE values were normalised for a more prominent colour strength. The Python based NetworkX [198] library was utilised to generate graphs for this work.

The connections were laid out as a spatial layout of the channels to test if the inferred connectivity would actually match the spatial regions of the most active firing activities. Figure 6.10(A) shows the firing density over the period of 20 seconds laid out in a spatial grid that corresponds to the MEA layout on which neurons were grown. The reasoning for using firing density is that the likelihood of having more or stronger connections at the higher firing density region is also

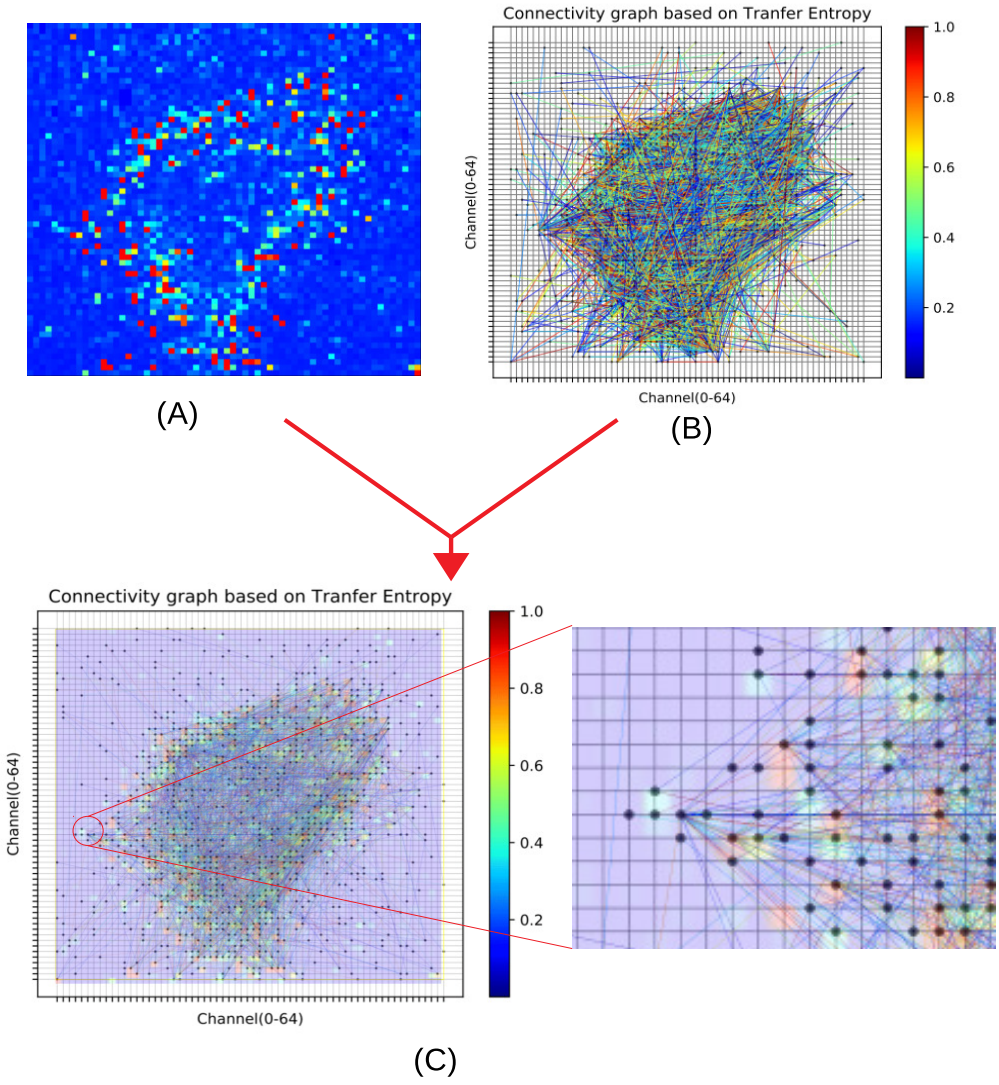

Figure 6.10: Estimated connectivity of the neuronal culture based on delayed TE method superimposed on the spatially laid out firing density. (A) Firing density laid out in a spatial configuration (B) Connectivity graph inferred after filtering the weaker connections. (C) Superimposed inferred connectivity onto the spatially laid out firing density. A zoomed in section is also shown where each square represents a channel that shows colour coded firing density and the matching connectivity inferred from these channels.

higher because a neurons firing depends mostly on the presynaptic inputs from other neurons. The firing density plot is taken as representative of structural layout of the network i.e. how neurons are organised on MEAs based on firing frequency. Figure 6.10(B), shows most of the connections concentrated in the middle of the MEAs spatial area, with few connections in the periphery.

Upon superimposition of the inferred connectivity on the firing density plot, it is noted that the inferred connectivity map fits very well on to the firing density plot, albeit with some exception of false positives and false negatives which are inevitable for such an estimation of connectivity. The superimposition is shown in Figure 6.10(C), and a zoomed in section alongside shows that most of the black dots which are channels with connections fall on the coloured squares which are the firing density plots for that particular channel. The connectivity inference was done separately without any structural prior or firing density information. Even without any prior information, the superimposition showed a reasonably good correspondence between firing density and connectivity. This demonstrates that the delayed TE method was in fact able to estimate the connectivity that matches the structural layout very well. Exploiting the firing density plot as a baseline proxy of connectivity can thus be very useful since the inference matches the firing plot. The connectivity can still be refined further based on the firing density plot and structural prior.

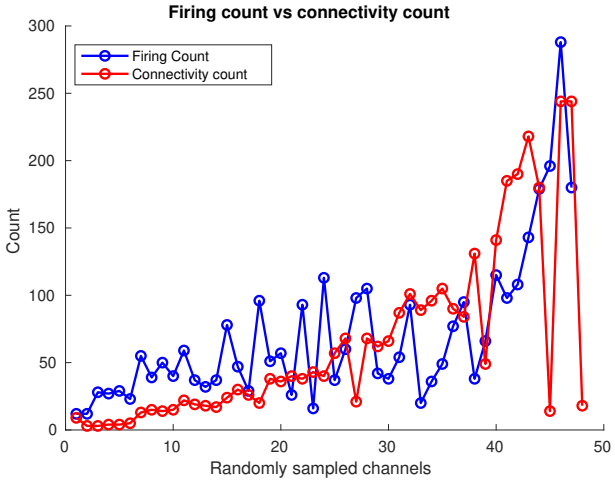

Figure 6.11: Relationship between firing count and connectivity count

Furthermore, 50 random channels were sampled from 4096 channels ranging from low to high connectivity to test the relationship between connectivity inference and the number of firing events. Figure 6.11 shows that number of firing count and connectivity count has a positively correlated relationship. The correlation coefficient was calculated to be 0.6692. The general trend of increment of connectivity of a recording channel with connectivity shows a linear relationship. This relationship helped us to exploit the information from the firing density plot and use it to build confidence on the connectivity estimation.

6.2.4 Summary on Superimposition Method

A superimposition method to estimate connectivity from live *in-vitro* experimental recordings to test if the estimated connectivity based on delayed TE corresponds to the firing density plot has been presented. The TE method has been proven to outperform other popular methods such as joint entropy, mutual information(MI) and cross-correlation(CC) on simulated data [14, 15]. Due to the presence of delayed interactions among neurons, a delayed TE method to estimate effective connectivity is a popular choice. Delayed TE incorporates additional delayed interactions, for a better estimation of the connectivity.

Firstly, the delayed TE method was validated with a simulation of a biologically plausible cortical network based on [192], with axonal delays, STDP synapses and realistic network dynamics. The simulation results showed an accuracy in the mid 80^{th} percentile in correctly identifying true connections. Also, previous results [15] have shown the delayed TE to have a superior performance in comparison to a more popular cross-correlation(CC) method. Hence, this method to estimate effective connectivity from an experimental living neuronal network was chosen.

Unlike simulated data where the ground truth connectivity is available against which the estimated connectivity can be compared, experimental data lacks this information making distinguishing true from spurious connections a difficult problem. To tackle this problem, a superimposition method was proposed where the estimated connectivity is superimposed onto the firing density plot to test if the estimated connectivity would correspond with the firing density plot and to give

confidence in using the derived connectivity for further analysis. Essentially the firing density plot was utilised as an alternative to ground truth. Figure 6.11 showed a positively correlated relationship between firing count and number of connectivity inferred. This information was exploited to establish a ground truth level prior with firing density. A neuron's firing depends on the presynaptic inputs and highly interconnected neuron tend to have more presynaptic inputs resulting in more frequent firing. Also, a firing density plot is laid out in a spatial manner which represents the structural layout as well to some degree. The method demonstrated that the connectivity estimated when superimposed onto the firing density plot shows a good fit.

For augmenting the connectivity estimation, structural information such as fluorescence images in conjunction with the firing density plot could be a possibility to better refine the connectivity inference objectively. In essence, such multi modality could help to better approximate ground truth connectivity. However, distinguishing true connections from spurious connections based on thresholding from a neuronal culture where the neurons are sparsely distributed without showing any clear apparent structure remains very difficult. Furthermore, to overcome the lack of ground truth information from an *in-vitro* neuronal cultures, statistical methods need to be utilised to infer statistical significance of the connectivity inferred.

6.2.5 Limitations in Connectivity Inference from Biological Networks

The TE method has outperformed many other popular methods such as cross-correlation(CC), joint entropy, mutual information [14, 15] to identify connectivity from simulated networks. So far, this method has been applied to HD-MEAs recordings from primary rat hippocmapal cultures and inferred connectivity based on the TE method [189] using a proposed superimposition method. However, due to the lack of ground truth connectivity information in real experimental living culture, it becomes a challenging problem to differentiate true connections from spurious connections - even when inferred with a superior method such as the Delayed TE [15], which incorporates many previous time steps in the algorithm.

Ideally, multiple trial measurements are conducted under the assumption of the same condition to compute statistical significance of the measurements and gain confidence in the inference. However, living dissociated neuronal cultures are non-stationary and always evolving with time which makes the multiple trial measurement unfeasible. As the culture matures and evolves it might respond differently from trial to trial; this problem is exaggerated in stimulation based experiments. Additionally, while computing TE values between two processes, statistical noises, biases and coincidental firings may imply a positive causal relationship even though there is none. To statistically determine the degree of potential causal relationship that should be large enough to have significance, the inferred value must be compared against the values which could be expected under some null hypothesis (hypothesis that there is no causal relationship),H_0. Upon exceeding the value, the alternative hypothesis that there exists a causal relationship, can then be accepted. Clearly, the accuracy of the testing depends on the quality of the control data generated under the null hypothesis.

The second half of this chapter will focus on the contribution on a new surrogate data generation method based on ISI distribution, for statistical testing of the connectivity inferred using TE method. Firstly, a simulation model of spiking neuron network is defined, followed with the TE computation presented earlier to validate the method. A series of thorough investigations on the ability of the proposed method to not only identify the significant connections but demonstrate the ability to capture connectivity strength as well which correspond with the actual synaptic weights, is presented. The method is then compared with ISI-shuffling method. Finally, how this method can also be used to set an objective threshold for filtering TE values, is demonstrated.

6.3 ISI Distribution Based Surrogate Data

6.3.1 Introduction

The surrogate data generation method is conceptually a simple method of generating control data to measure the statistical significance between parallel spike trains [166]. Control data provides trial set of possible data where the spike

timings are destroyed. The most interesting feature that potentially contributes towards causal interactions between spike trains is the timing of occurrence of the spikes or the temporal information of the firing patterns. Hence, surrogate data is generated such that the most relevant feature for causal interaction, which, in this case is the fine temporal information, is destroyed whilst retaining all the other statistical features such as firing rate, duration, time of the first spike, ISI statistics and number of spikes. Essentially, the data is generated under the null hypothesis that spike time has no effect on the causal interaction. The null hypothesis assumes that the spike times are not important,hence only that information is destroyed for surrogates. Upon rejection of the null hypothesis, the hypothesis that there must exist some causal relationship dependent on the timing of the spikes can then be accepted. The temporal information or the timing of the spikes is governed by the Inter Spike Interval (ISI) distance which is the temporal distance between two consecutive spikes. The remaining statistical features of the spike train such as the firing rate, number of spikes, time of the first spike and ISI statistics are retained.

Surprisingly, there are only a handful of methods that are applicable to discrete spike trains. Some popular methods that are commonly used are temporal jittering [167](i.e. independent randomization of the individual spike times within a defined interval), trial shuffling [168](i.e. trial data of one neuron is randomly assigned to other neurons thereby destroying potential spike relationship) and shuffling of inter-spike-interval(ISIs) [169](i.e. random combination of ISI values from a set of ISIs for each neuron). The existing methods either create poor surrogates due to weaknesses in retaining ISI information(trial shuffling, temporal jittering) or create an exact copy of the ISI distances shuffled randomly(ISI shuffling). The latter retains ISI distance statistics but fails to introduce variation for a rich set of surrogates. There exists a fine line between retaining the required statistics and introducing variation to simultaneously enhance the surrogate quality.

In contrast to the existing popular methods, which are direct manipulation of the spike train to generate surrogate data, a distribution based approach is proposed, where the distribution of the ISI interval from each spike train is empirically inferred. During surrogate data generation, spike times for the surrogate

spike trains are sampled from these distributions using the cumulative distribution such that the firing rate information is not changed. This is achieved by drawing the same number of samples as the number of spikes in the original spike train upon which the surrogates are based on. Since the samples are drawn from the ISI distribution, the sampled surrogate spike trains also share similar statistics of the original ISI distribution. Sampling from the original distribution is done such that it retains the firing rate statistics as well as the ISI statistics but introduces enhanced controlled variation in the surrogate data, which could potentially cover wider possibilities than the surrogate generated from direct shuffling of the ISIs. During the sampling process, it is demonstrated that the samples drawn follow a very close approximation to the original distribution while maintaining some degree of variation from the original spike train, though the variation is not too far off from the actual spike train distribution.

The proposed method accurately determine statistically significant connections from non-significant connections - validated with a realistic simulation model. In addition, the method was also able to detect the degree of strength of the connections. The method outperformed the ISI-shuffling method by achieving 93% accuracy at 0.01 false positive rate. Demonstration of a systematic way of setting the threshold for TE inferred from biological neuronal network and identification of connection strength, is also presented.

6.3.2 Methods

6.3.2.1 Transfer Entropy and Simulation Model

The same methods described for the transfer entropy and simulation model in Section 6.2.2.1 and Section 6.2.2.2 respectively are utilised for the TE computation and simulation model. The method and the simulation model is exactly the same as discussed previously.

6.3.2.2 Inverse Transform Sampling Under Null Hypothesis

Inverse transform sampling is used to sample randomly from the observed ISI distribution. A cumulative distribution function(CDF) given an ISI probability

distribution, is used to draw samples randomly and independently. The samples are drawn under some null hypothesis(H_0):

- H_0 : Temporal patterns of spiking events have no effect on pairwise TE values
- H_1: There must exist some temporal relationship in governing pairwise TE values

The inverse sampling transform can be expressed as:

Let X be a random variable described by CDF $F(x)$. The aim of the sampling is to generate values of X according to the given distribution. The inverse sampling algorithm can be explained as follows:

- Generate a random number in the interval $[0, 1]$ from a standard normal distribution; $U \tilde{} Unif[0, 1]$
- Compute the inverse of the CDF; $F_X^{-1}(x)$
- Compute $X = F_X^{-1}(u)$. The computed X has a distribution $F_X(x)$

These steps can also be simplified as: given a continuous uniform random variable U in $[0, 1]$ with the CDF F_X, the random variable $X = F_X^{-1}(u)$ has a distribution $F_X(x)$. For detailed proofs, please refer to [199]. Figure 6.12 shows a smoothed PDF and a CDF of ISIs of one spike train. Due to the smoothening of PDF for visual aesthetics, the lower bound extends to negative x-axis too, however, no negative ISIs are actually observed. As shown in Figure 6.12, for this particular PDF, most of the CDF values result in ISI values from 10ms to 300ms which matches the actual distribution of the ISI distances illustrated with blue dotted lines. This guarantees that the randomly sampled samples will end with a similar PDF of the values and hence preservation of the ISI statistics. During the sampling process, each sample is drawn independently from the next sample. After collating N number of samples for a target spike train with N number of spikes, new surrogate data is generated where the temporal information is destroyed whilst maintaining the ISI statistics, firing rate and time window.

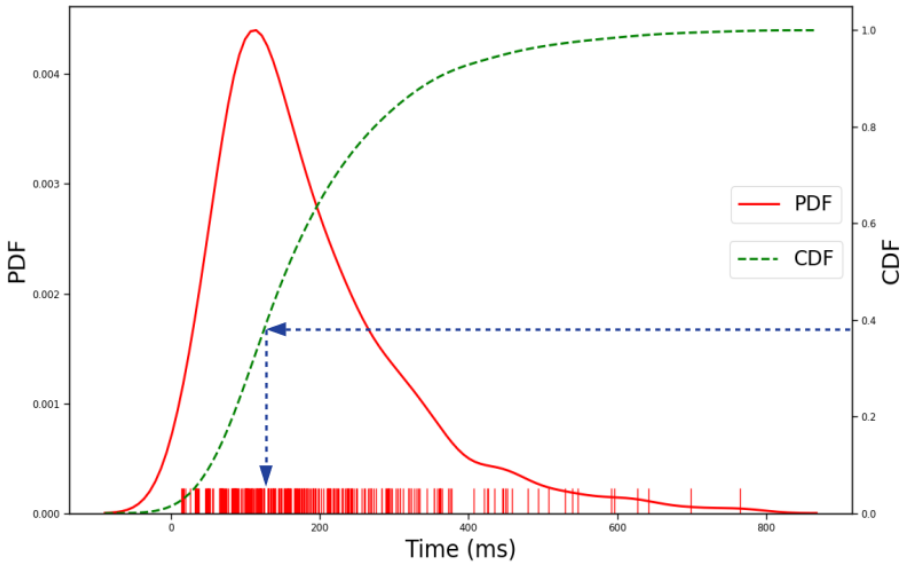

Figure 6.12: Smoothed Probability Density Function (PDF) and Cumulative Density Function (CDF) of ISI distances from a single spike train. Given a value of a CDF, corresponding ISI values can be mapped with a blue dotted line shown.

6.3.2.3 Surrogate Generation Algorithm

From the computation point of view, given a specific set of ISI distances, generating surrogates becomes a problem of finding combinations or rearranging ISI distances in the set to generate the unique set of new spike trains within a given time window. For a given time window, the sum of combinations of ISIs that could result in the exact same time window will result in a search space too big to search effectively for long spike trains duration. To simplify this process, an algorithm is developed as described in Algorithm 1. This guarantees that the spike count matches the target spike train, while meeting the duration criteria as well.

The number of samples that is drawn is the same number of spikes present in the original spike train. The samples drawn have to add upto the total duration such that the total samples count does not exceed the total time window. So each sample is added and stored as ISI sum to check if the samples exceed the total duration. The process loops until the sum of ISI exceeds the total duration of spike train which corresponds to step $1-5$ in Algorithm 1. Steps $1-5$ creates

Algorithm 1 Surrogate data generation algorithm

Require: ISI PDF of a target spike train
Require: # of spikes from each spike train, time of first spike, Duration, # of surrogates
Ensure: Sample one ISI sample at a time and append

```
while # of samples < # of target spikes do
    randomSample = InverseTransformSample()
    if (ISIsum < duration) then
        ISIsum ← ISIsum + randomSample
        SurrogateISIs.append(randomSample)
    else
        while True do
            maxCurrentISISample ← max(sampledISIs)
            if (maxCurrentISISample > newRandomSample) then
                SurrogateISIs.remove(maxCurrentISISample)
                SurrogateISIs.append(newRandomSample)
            else
                randomSample = InverseTransformSample()
            end if
            if (len(SurrogateISIs) > #Spikes then
                break
            end if
        end while
    end if
end while
```

one surrogate data; the steps are parallelised to generate the required number of surrogates. While the sum of the sampled ISI is less than the total duration, the process is continued until the total number of ISIs equals to the total spike count. Once the sum of the ISI exceeds the total duration, then a new sample is drawn. If the sample is less than the current ISI distance so far, then it is replaced with the recent new sample. This is to make sure to accommodate new samples within the given time duration. The whole process is repeated until the required number of ISI distances are sampled. Finally, the distributions are checked to see if they match with the original distribution. This enables the generation of 100 surrogates for 4096 spike trains in just under 2 minutes for 20 seconds of spike train with a 1 ms time bin. The computation time can fluctuate depending

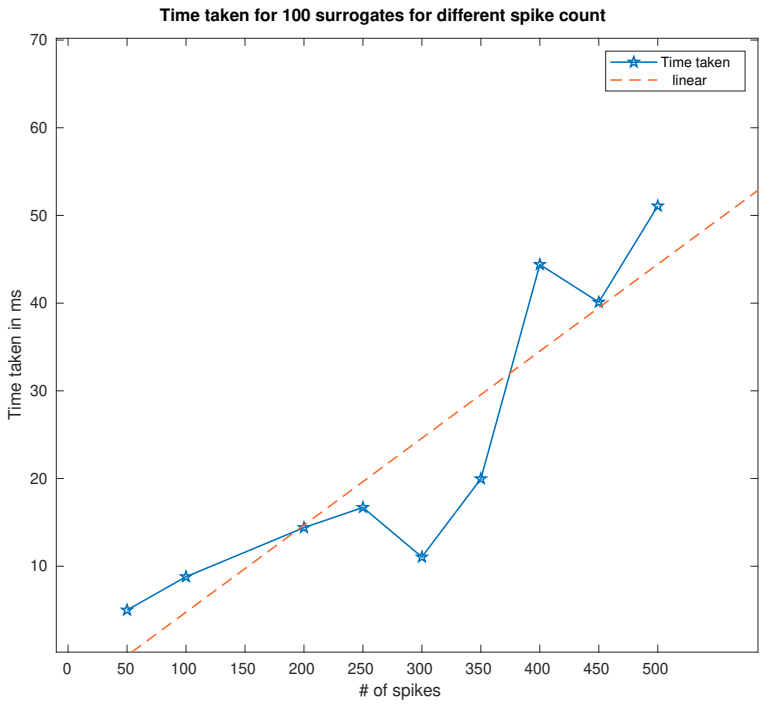

Figure 6.13: Computation time for generation of 100 surrogates based on different spike count spike trains.

on the number of spikes on each spike train and scales linearly with the number of spike times, as shown in Figure 6.13. The computation was performed on an Intel Xeon(R) CPU E5-2640 v3 @ 2.60GHz with 16 cores running Ubuntu 18.04.3 LTS with Python 3.5. The algorithm utilised multiprocessing making use of the available 16 cores.

6.3.2.4 Workflow

The concept of surrogate data generation itself is straightforward, however, there are many stages in the workflow pipeline from target spike train to computing significance of the pairwise TE values computed. The complete methodology opted for the presented surrogate based method is succinctly illustrated in Figure 6.14. Based on the functionality of different stages, the workflow can be categorised as below:

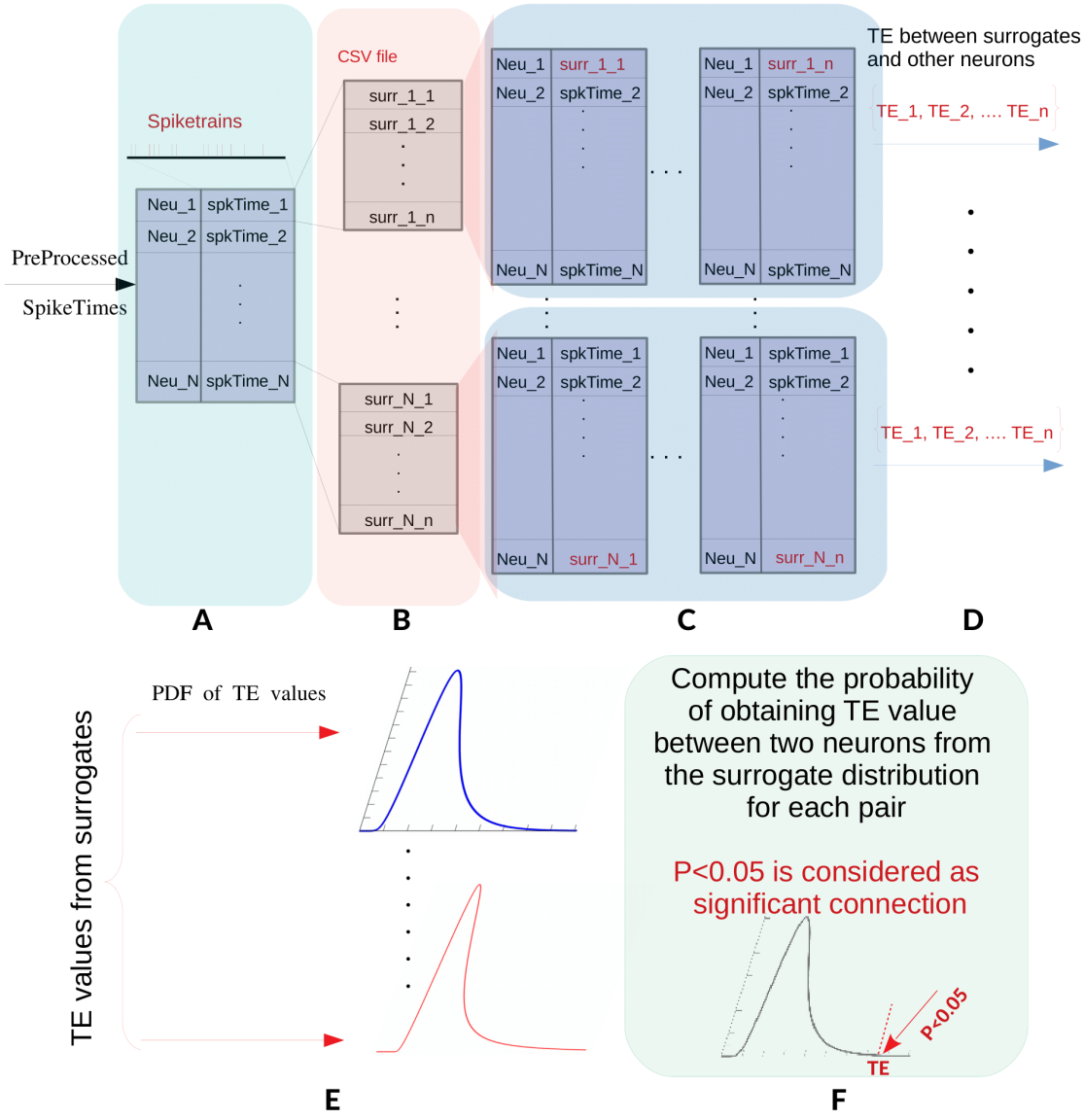

Figure 6.14: Workflow illustrating different stages of surrogate data generation to identifying significant connections based on surrogate data

Pre-process: The workflow starts with a pre-processed spike train from an experiment. The spike trains are stored as a simple spike times *CSV* file where each line corresponds with a neuron in an ascending order such as [Neuron1,Neuron2.....

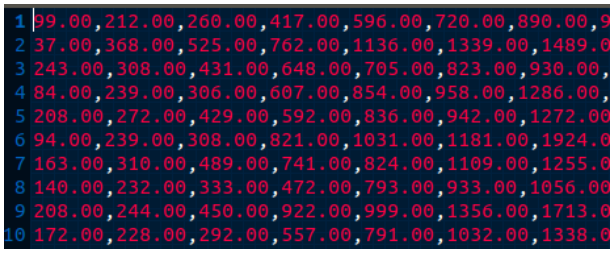

Figure 6.15: Screenshot of spiketrains arranged in a CSV file

NeuronN] as shown in the first part of Figure 6.14(A). The actual CSV file is arranged as shown in Figure 6.15 where line $1-10$ corresponds to neurons and numbers in each line is the actual spike times in ms. The goal is to generate n number of surrogates from each Neuron or each line of the CSV file.

Surrogate Generation: The custom script automatically scans through all N spike trains(Figure 6.14(B)) and generates n surrogates(Figure 6.14(C)) into a corresponding folder, with all the surrogates generated as per Algorithm 1.

Replace Target Spike Trains: The next stage is to replace the original spike train with its surrogates whilst keeping the other spike trains as in the original CSV file. As shown in Figure 6.14(C), for one target spike train with n surrogates; the final set of data has n new spike train $CSVs$, where each surrogate data replaces the target spike train. The goal is to use these replaced surrogates to compute pairwise TE values with all other spike trains. Since these surrogates are sampled under the null hypothesis, the temporal correlations are reflected in the pairwise TE values.

Compute Pairwise TE: After generating a new set of spike train $CSVs$ with surrogates, the pairwise TE between surrogates and other spike trains are computed using the methods described in Section 6.2.2.1. The pairwise TEs are then collated into a list(Figure 6.14(D)). For n surrogates, a list size of n pairwise TE values is generated. The original target spike train also has a pairwise TE against which the rest of the pairwise TE are compared statistically. The process is repeated for each target spike train. For N number of spike trains, N number of pairwise TE lists are generated.

PDF inference: The distribution of the pairwise TE values from the surrogates can be inferred empirically (Figure 6.14(E)) as a PDF . Given this distribution, the probability of the original pairwise TE between the target neuron's (spike train) and the other neurons' (spike trains) was computed. Due to non normality of the distribution, a non parametric test, Wilcoxon Signed test is performed to compute statistical significance,$p - value$. The empirical cumulative distribution function(ecdf) was utilised from the Python Statsmodel library to compute probability(p) of the occurrence of the original TE value(Figure 6.14(F)) given the PDF of the surrogate TEs. A probability of observation of the original target TE value from the surrogate distribution less than 0.05 is considered as a significant connection. The rational is that, if the target spike train has a causal relationship with another spike train, then the surrogate TEs sampled under null hypothesis should be significantly different from the original TE. If the target falls within the distribution of the surrogate TEs then the target TE is not significantly different from the surrogate TEs. This implies that there isn't any specific significant difference if the temporal information is destroyed in the target spike train which indicates no causal interaction and such connections can be discarded. The degree of the probability can be used to infer degree of strength in the connectivity as well.

6.3.3 Results

The method is validated with simulated data based on Izhikevich's network of 100 subsampled neurons from 1000 neurons of 60 seconds recording as in Section 6.2.2.2.

6.3.3.1 Validation of ISI matching

It is crucial that the ISI distribution of the sampled surrogates retains all the statistical features whilst destroying the spike timing information. Since the method proposed doesnt use shuffling of the ISIs, the sampled surrogates haves to follow a similar ISI distribution to the original spike train to have reliable surrogates. A raster plot of one original spike train and its 100 surrogates is shown in Figure 6.16, for 60 seconds of the recording from the Izhikevich network.

Note that the surrogate spike trains appear similarly spread out throughout the total duration of the original spike train but the temporal patterns are destroyed with random spike times as the surrogate spike train raster look different to the original spike train.

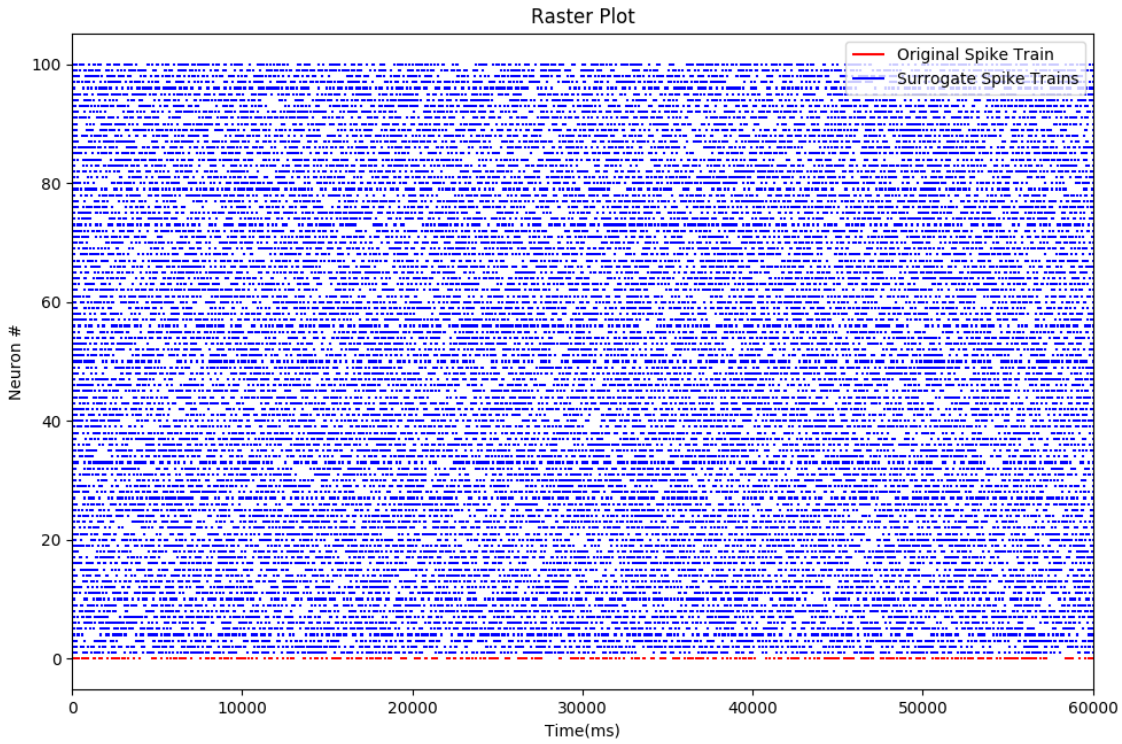

Figure 6.16: 100 Surrogate data generated from target original spike train

To demonstrate that the surrogates also follow a similar distribution, the distribution of the original ISI is plotted overlaid with 10 randomly selected surrogate ISIs from the 100 surrogates generated as shown in Figure 6.17. The figure clearly shows a very similar distribution of the surrogates and the original target spike train(black line) with some variations which help to enrich the quality of the surrogates. The surrogates generated are very close to the original but not exactly the same, and no two surrogates are exactly the same either. Each spike train has a distinct ISI distribution which ensures that the surrogate data generated are unique to that particular distribution. Figure 6.18 shows that the ISI distribution of the surrogate spike trains are distinct. Only five spike trains are selected for clarity; the figure shows that each spike train is different from other

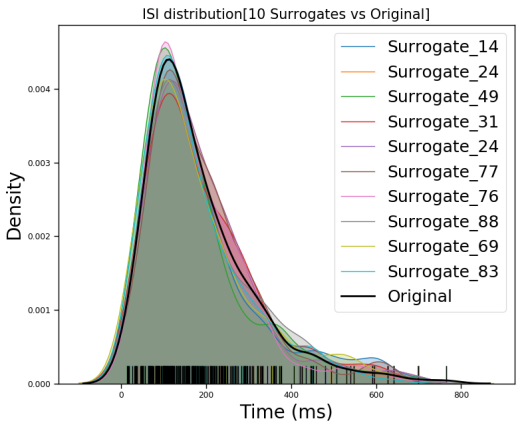

Figure 6.17: Original ISI distribution(black line) and the ISI distribution of 10 randomly selected surrogate spike trains.

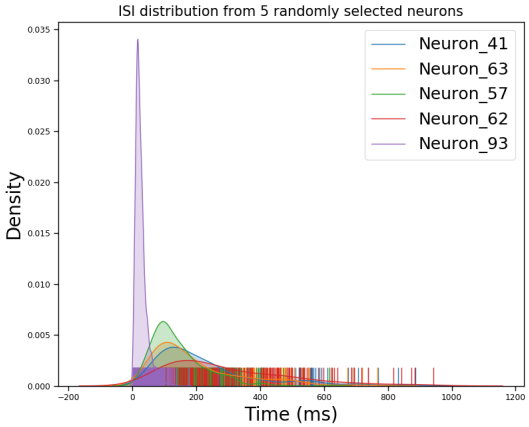

Figure 6.18: ISI distribution of five randomly selected surrogate spike trains from simulation recordings. The number is limited to five for clarity.

spike trains.

Descriptive statistics of the original and a number of the surrogate spike trains are also shown in Table 6.2, showing a very close similarity to the original spike train which also corresponds with Figure 6.17. The ISI distances are non-normally distributed which is clearly evident from Figure 6.17. The original ISI distribution is positively skewed as reported in Table 6.2, with a positive kurtosis. The extreme values at the right tail of the distribution are considered as outliers and discarded after filtering the ISI distances. Considering possible axonal delays and transmission delays, cutting off the ISI distance after 1000 ms would cover most of the information based on the distribution.

6.3.3.2 Identification of Significant Connections

After validating the surrogate data generated from the ISI distribution, generating new sets of spike trains for TE computation and computing all the TE values from such sets of spike trains, a list of TE values for each surrogate from the different original neurons (spike trains) is obtained. The next step is to test if the TE values that are computed show any statistical significance and how they correspond to the model synaptic weights.

Table 6.2: Descriptive ISI statistics of the surrogate and the original spike train

SpikeTrain	NoOfObs	Mean	Variance	Skewness	Kurtosis
Original	313	185.4855	16132.2699	1.5460	2.8916
Surrogate14	313	190.1277	19678.4387	1.5188	1.9797
Surrogate24	313	189.4313	15930.7332	1.5403	2.8784
Surrogate49	313	175.0673	16719.8957	1.5586	2.5429
Surrogate31	313	191.0447	16840.2159	1.2439	1.4084
Surrogate24	313	189.4313	15930.7332	1.5403	2.8784
Surrogate77	313	189.3386	15316.8204	1.4123	2.3219
Surrogate76	313	178.7380	14007.6811	1.5488	2.9157
Surrogate88	313	189.5974	16899.6643	1.3083	1.6207
Surrogate69	313	183.9067	19049.8590	1.4587	2.0795
Surrogate83	313	175.7339	15297.8357	1.4226	2.3554

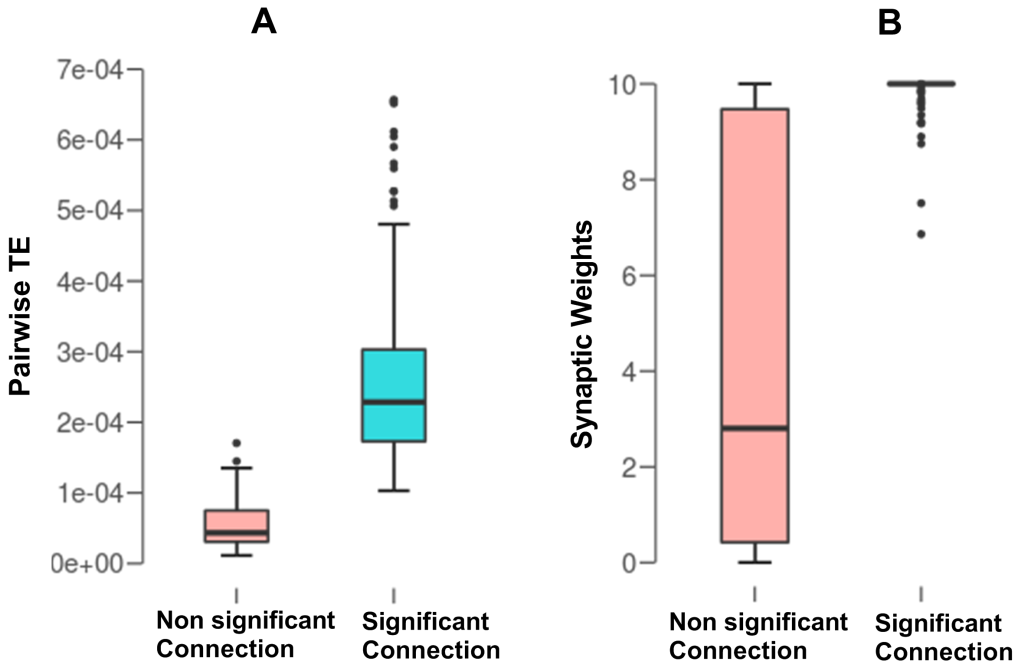

Figure 6.19: Significant and non-significant connections identified based on p values based on pairwise TE (A) and corresponding model synaptic weights as described in Section 6.2.2.2 (B)

For all pairwise connections, the significance of the inferred connection is computed against the TE distribution of the surrogate TE values. If the probability

of observing the actual TE values is less than 0.05, the connection is considered significant. From all the TE connections, the significant and non significant connections were plotted in Figure 6.19(A) as a box plot. Corresponding synaptic weights for significant and non significant connections are also plotted in Figure 6.19(B). The significant connections identified by the surrogate method show a clear separation from non-significant TE values. The significant TE values have a median value of approx. 0.00025 and range from 0.0001 to 0.0007. The corresponding synaptic weights show that most of the identified significant connections in fact have the highest synaptic weights with some outlier weights from $6-9$ that were also classified as significant. Similarly, non significant TE connections had TE values from $0-0.00015$ with a median of 0.0005 with a narrow range. The significant and non significant pairwise TE values have a clear distinction in their range of TE values. Corresponding synaptic weights for identified non significant connections had weights values ranging from $0-10$ with wide spread in values. The median value however is observed to be 3 which is a much lower synaptic value and is considered a non significant value in the model as well. In the simulation model, most of the significant connections converge to the value of 10 . A synaptic weight of 10 suggest a definite significant connection and the connection gets weaker with a decreasing value.

The connections identification based on the surrogate method has found significant connections which in fact have a very strong synaptic weight in the model. This correspondence between the identified connection from the surrogate method with the actual synaptic weights demonstrates the ability of the method to accurately infer strong connections from the weak ones. In the next section, the degree of the strength of the connections is also analysed.

6.3.3.3 Detection of Connection Strength

In addition to the identification, the proposed surrogate method is also able to detect the subtlety of the strength of the connections. In this case, model weights are used to validate the method, however, for biological recordings the method can still be applied to set ranges for different degrees of connection strength and facilitates with a threshold reference point which will be discussed in Section

6.3.3.4. Any connections with a p value less than 0.05 are considered as significant connections. To evaluate how the significant connections' TE values correspond with the weights, the p values are sub divided into groups i.e.$\{< 0.05, < 0.04, < 0.03, < 0.02, < 0.01\}$.

Figure 6.20 shows the distribution of TE values for different p values and the corresponding synaptic weights in the model. As the p values progress from < 0.05 to < 0.01, the corresponding synaptic weights distribution were found to become more concentrated towards synaptic weight value of 10 as shown in the second column of Figure 6.20. The distribution of the TE values also gets narrower. Furthermore, the mean value of the TE distribution, represented by peak of the distribution, gets larger with decreasing p values as shown in Figure 6.20 in the first column. This is an indication that as the significance of the TE values increases, there is increased probability that the corresponding weights also get stronger. Due to this correlated effect between the TE connections which are identified as significant with surrogate data and the corresponding model synaptic weights, this relationship can be also utilised to infer connectivity strength based on the statistical significance of the connection.

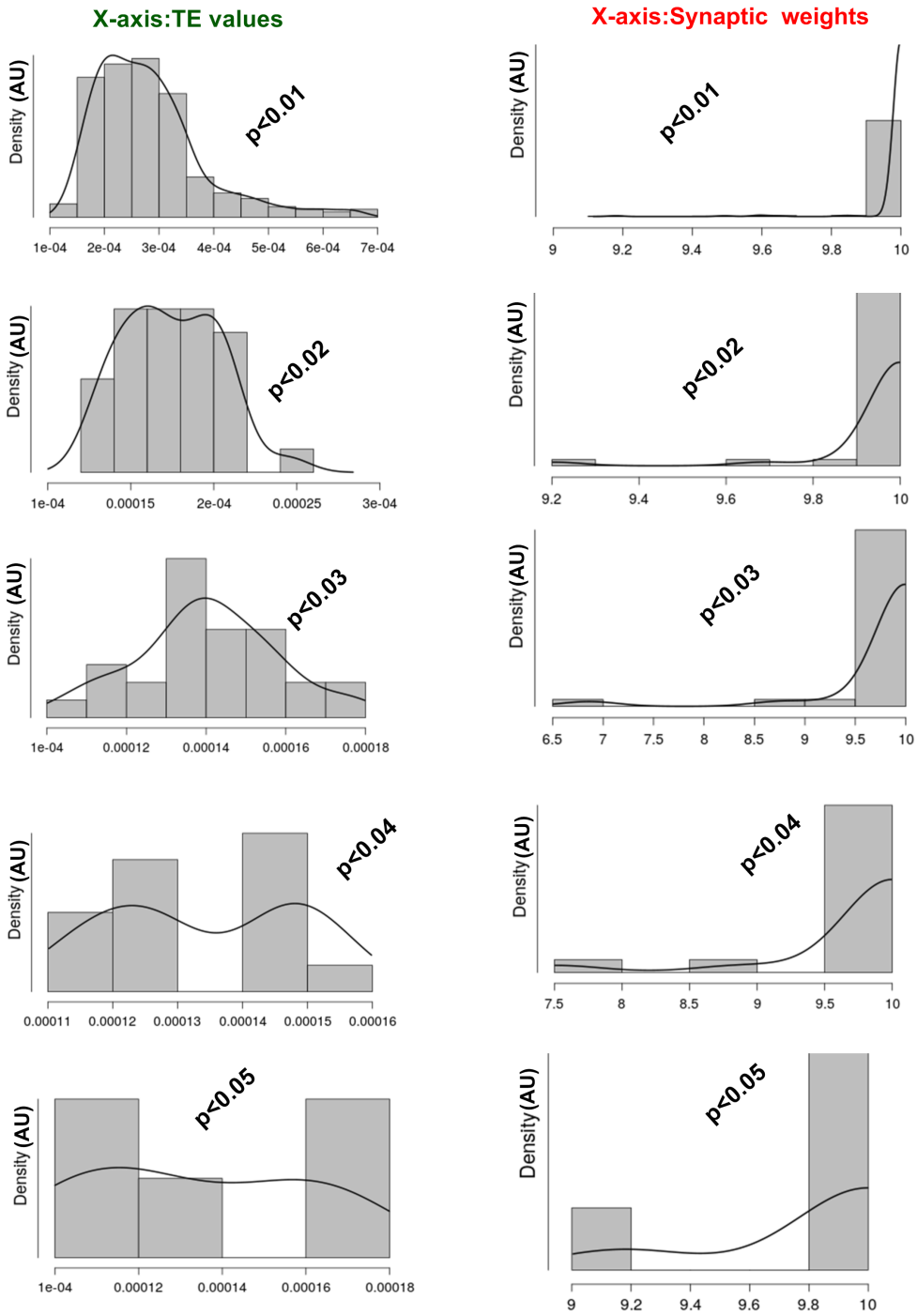

Figure 6.20: Distribution of p values and corresponding model synaptic weights distribution.

This can be further broken down into different p values and corresponding synaptic weights as boxplots, as shown in Figure 6.21. A boxplot of different p values reveals a clear trend of increasing pairwise TE values with decreasing p values from 0.05 to 0.01(Figure 6.21(A)).The p values of less than 0.04 and 0.05 have a very similar median but this changes after 0.03. For non-significant connections, pairwise TE values are the lowest which suggest the connection is too weak to have an effect on the post synaptic connection. Figure 6.21(A) shows that pairwise TE values for different p values clearly have a different distribution and the non-significant connections clearly fall into a different, much lower, range of TE values. $p < 0.01$ has the largest median TE value and subsequently the value decreases as the p value increases to 0.05. Figure 6.21(B) shows corresponding boxplots of the synaptic weights. Since most of the values are already close to the synaptic weight of 10, it is easy to see the trend from the box plots. However, the correlated activity of the weights in terms of distribution is shown in Figure 6.20.

6.3.3.4 ROC analysis

To measure the accuracy of the surrogate method, an ROC diagnostic test is conducted and compared against the ISI shuffling method, which is the closest comparable method to the proposed method. ROC analysis compares the accuracy of a system to compute TPR against FPR, which is also called *Sensitivity* and *(1 - specificity)* respectively. The TPR values were evaluated at different FPR rates. To keep the false positives to minimum, the accuracy of the system was evaluated at FPR rate of 0.01.

Based on the ROC analysis, the proposed ISI distribution surrogate method was able to achieve accuracy of 93% evaluated at 0.01 FPR rate. The ISI shuffling method was only able to achieve an accuracy of about 80% evaluated at FPR of 0.01 as shown in Figure 6.22. The proposed method also has a larger AUC(Area Under the Curve) in comparison to the ISI shuffling method as shown by the red and blue curves in Figure 6.22. This is a significant improvement in the performance and the fact that the proposed method is able to capture the subtleties of the degree of the strength of the connections, makes it a superior method to test

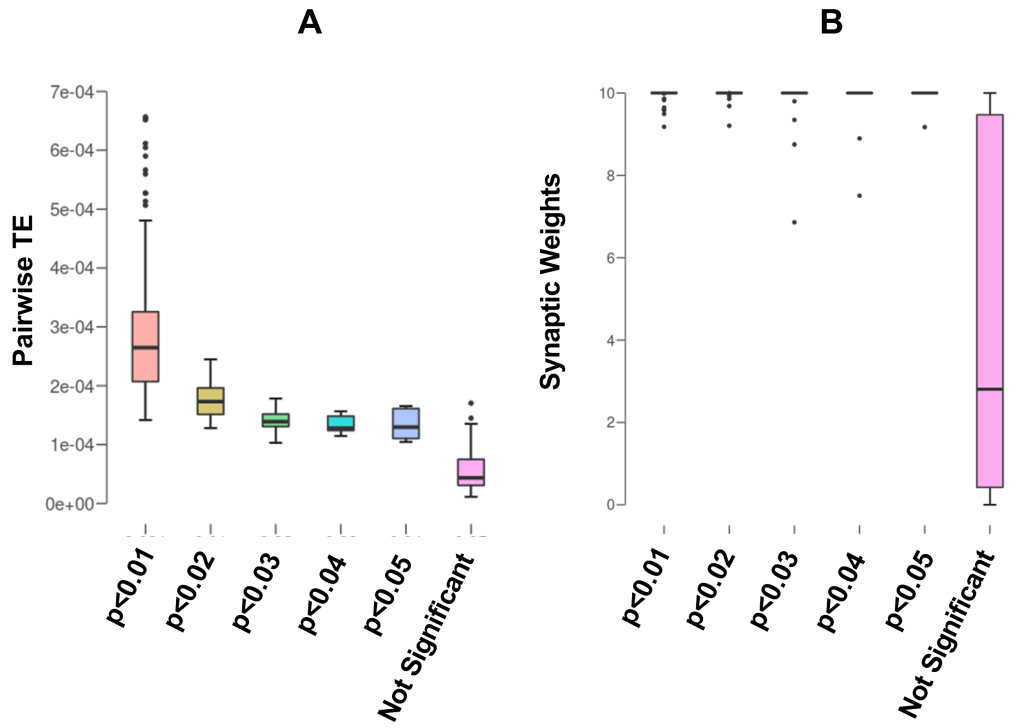

Figure 6.21: TE values detects connection strengths. (A) Pairwise TE values for different p values and non significant connections. (B) Synaptic weights for the pairwise connections

the significance of the inferred pairwise TE connections.

Additionally, TPR and FPR values can be used to objectively set a threshold value for TE values for biological networks where ground truth information is not available. This can be applied as a system method of evaluating threshold. Figure 6.23 shows TPR value and corresponding FPR. Red circles shows TPR evaluated at FPR of 0.01. Corresponding TE values can be set as the thresholding values. The values above this threshold can be objectively considered as significant connection in the actual network.

6.3.3.5 Discussion

To tackle the limitations of lack of ground truth information and unfeasibility of having multiple trials as discussed in Section 6.2.5, a novel surrogate data

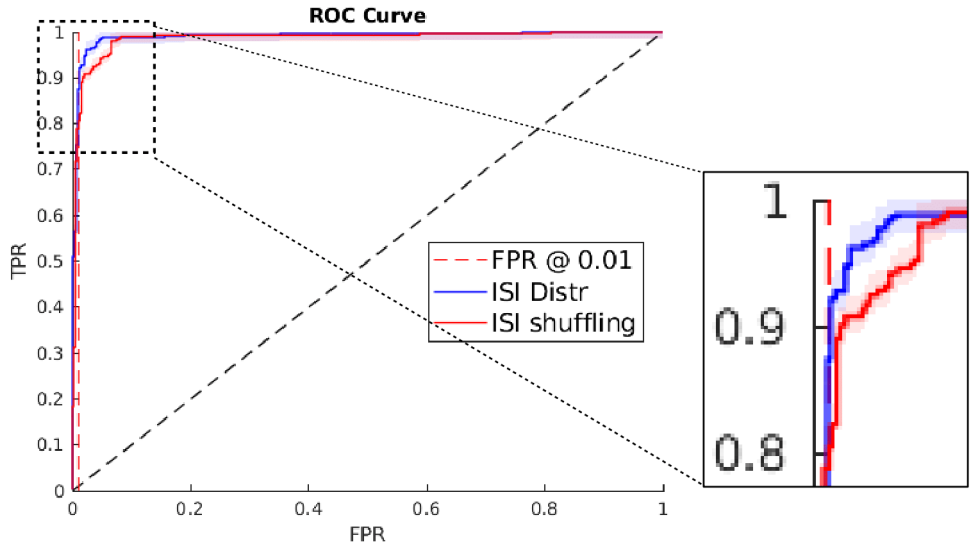

Figure 6.22: Performance comparison of ISI shuffling and ISI distribution surrogate methods to identify true connections from false. TPR is plotted against FPR and the performance is evaluated at a very low FPR rate of 0.01. The red vertical dotted line marks the 0.01 FPR. Zoomed in inset on the right for clarity.

generation method was proposed utilising the ISI distribution of the target spike train. The method has been validated with a realistic biological cortical network based on Izhikevich's model [192]. The method utilised surrogate data generation method to infer connections based on TE methods, and showed correlated correspondence with the model synaptic weights when compared. Throughout the process of surrogate and TE computation, no information about the model weights or parameters were used - only output spike trains. Similarly, in a real experimental scenario, only spike train data is available. The same steps could be applied to infer connections and make statistical comparisons on which connections to keep and which to filter out, even in the absence of knowledge of actual synaptic weights. The method is applied to experimental recordings in the upcoming chapter.

Some popular methods that are commonly used are temporal jittering [167] i.e. independent randomization of the individual spike times within a defined interval, trial shuffling [168] i.e. trial data of one neuron are randomly assigned

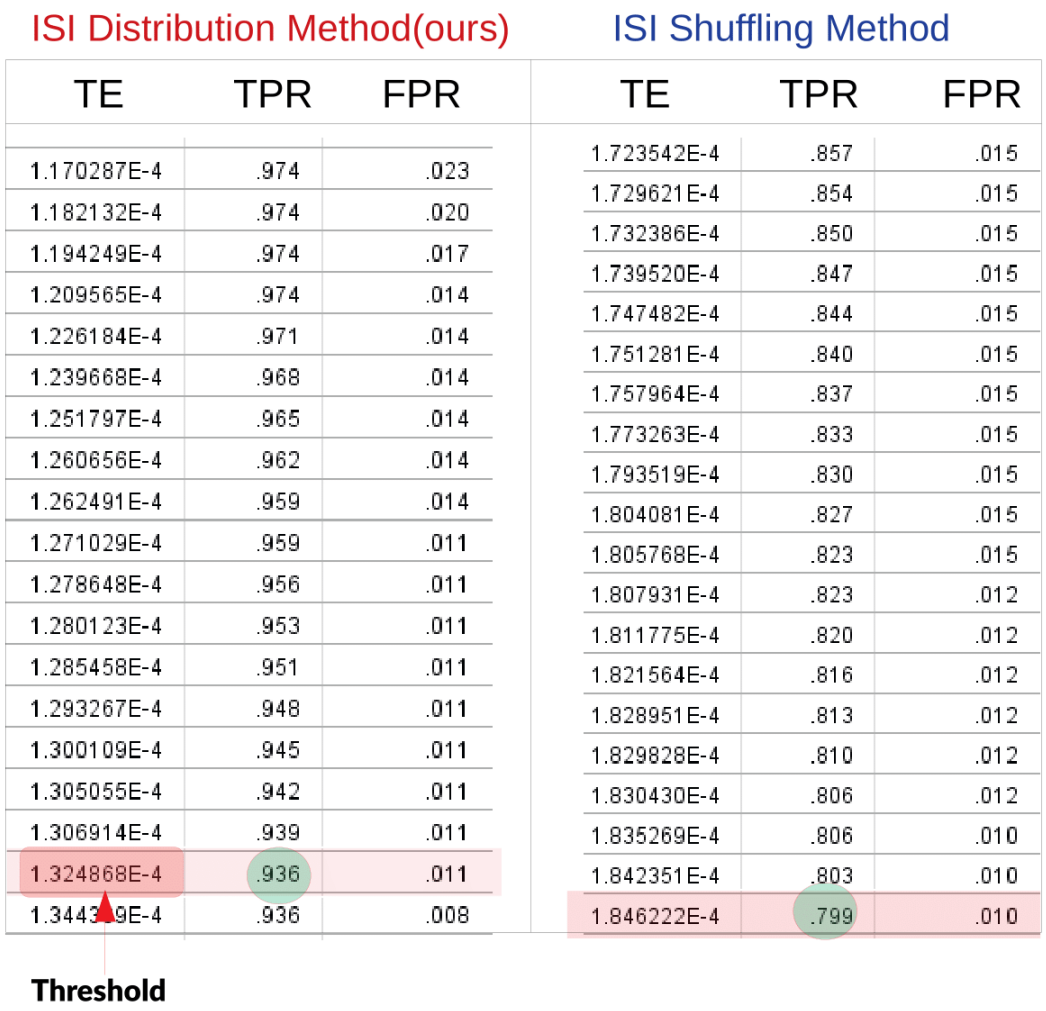

TE	TPR	FPR
1.170287E-4	.974	.023
1.182132E-4	.974	.020
1.194249E-4	.974	.017
1.209565E-4	.974	.014
1.226184E-4	.971	.014
1.239668E-4	.968	.014
1.251797E-4	.965	.014
1.260656E-4	.962	.014
1.262491E-4	.959	.014
1.271029E-4	.959	.011
1.278648E-4	.956	.011
1.280123E-4	.953	.011
1.285458E-4	.951	.011
1.293267E-4	.948	.011
1.300109E-4	.945	.011
1.305055E-4	.942	.011
1.306914E-4	.939	.011
1.324868E-4	.936	.011
1.344[illegible]9E-4	.936	.008

TE	TPR	FPR
1.723542E-4	.857	.015
1.729621E-4	.854	.015
1.732386E-4	.850	.015
1.739520E-4	.847	.015
1.747482E-4	.844	.015
1.751281E-4	.840	.015
1.757964E-4	.837	.015
1.773263E-4	.833	.015
1.793519E-4	.830	.015
1.804081E-4	.827	.015
1.805768E-4	.823	.015
1.807931E-4	.823	.012
1.811775E-4	.820	.012
1.821564E-4	.816	.012
1.828951E-4	.813	.012
1.829828E-4	.810	.012
1.830430E-4	.806	.012
1.835269E-4	.806	.010
1.842351E-4	.803	.010
1.846222E-4	.799	.010

Figure 6.23: TPR evaluated at 0.01 FPR rate.

to other neurons thereby destroying potential spike relationship, and shuffling of inter-spike-interval(ISIs) [169] i.e. random combination of ISI values from a set of ISIs for each neuron). The existing methods temporal jittering [167], trial shuffling [168] and shuffling of inter-spike-interval (ISIs) either create poor surrogates due to weakness in retaining ISI information (trial shuffling, temporal jittering) or create an exact copy of the ISI distances shuffled randomly (ISI shuffling). The latter retains ISI distance statistics, but fails to introduce variation

for a rich set of surrogates.

A novel surrogate method based on an ISI distribution has been presented. Unlike ISI shuffling, which is a randomised shuffling of ISI distances in a list, the new surrogate method makes use of sampling from an ISI distribution such that the surrogates follow a similar distribution as the original ISI, while introducing just enough variations. This feature helps to generate enhanced surrogates. The method was tested against simulation data from a biologically realistic spiking neuronal network based on Izhikevich's network. Comparing the ISI distribution of the surrogates demonstrated that the surrogates closely follow the distribution of the original ISI but are not exactly the same. The method was tested firstly for *identification of the connections* then for *detection of connection strength* and finally the accuracy of the system was measured with an ROC analysis. The connections identified by the use of the surrogate method correlated with the synaptic weights in the model network. The significant connections identified shows very strong synaptic weights in the model, which indicates the ability to identify the connections(Figure 6.19). In addition, the detected connections were further analysed to evaluate the relationship between the degree of significance and their corresponding synaptic weights in the model. For larger significance, the distribution of the weights was focused more towards the strongest possible synaptic weight and the distribution was wider and spread out for lower significant weight (Figure 6.21,6.20). This relationship can be exploited to infer the connectivity strength based on the TE values or significance. Furthermore, an ROC analysis clearly showed a superior performance of 93% evaluated at 0.01 FPR, in comparison to 80% for the ISI shuffling method. An objective approach for setting up thresholding values for the TE is also identified by selecting a desired TPR and FPR. This systematic way of using the surrogate data can be exploited for simulated data as well as real biological networks because no underlying connection information is utilised to infer connectivity and the surrogate method utilises statistical testing to identify significant from spurious connections. Due to the surrogate data and relying on statistical approaches, one can gain much more confidence in the connectivity inference from a single trial biological network.

6.4 Summary

This chapter discussed two main contributions related to connectivity inference from neuronal recordings. The first contribution discussed the superimposition method, which enables greater confidence for identified connections. The second half of the chapter extended the work to tackle the limitations of lack of ground truth information in real cultures by proposing a novel surrogate data generation method exploiting the ISI distribution. The proposed method showed superior performance in comparison to the ISI shuffling method and also demonstrated the ability to extract connectivity strength.

The systematic connectivity inference and surrogate methods developed in this chapter can be an important contribution to study complex biological network during plasticity. In the upcoming chapter, these methods will be tested during controlled stimulation and induction of plasticity in neuronal cultures coupled with HD-MEAs. The surrogate method will be utilised to infer connectivity development during plasticity.

Chapter 7

Induced Network Response: Low Level Learning

7.1 Introduction

In this chapter, the effects of repeated stimulation on long term network responses, germane to neural plasticity, and connectivity development during plasticity (evoked responses) are presented.

Three different neuronal dynamic responses were observed and are discussed - (i) potentiated ,(ii) depressed and (iii) regularised (Section 7.4). Protocols for successful induction of network wide potentiation are presented and the adaptation of the network response to a particular stimulation is validated (Section 7.4.2.2). Furthermore, the network connectivity analysis which was developed and discussed in Chapter 6, was utilised to infer network connectivity development during LTP induction. The connectivity method was able to highlight the development of new network connections during the potentiated stage after stimulation (Section 7.5).

7.2 Development of spontaneous activity in neuronal cultures

In addition to neuronal culture methodology described in Chapter 4(section 4.2), further spontaneous firing activity characterisation and development of spontaneous activity is presented in this section. Due to the sensitive nature of neuronal cultures on Biochips (as previously discussed), handling and recording were kept to a minimum for the first two weeks after seeding cells on MEAs to avoid cell deaths and detachments. Hence, recordings before day 12 were not performed and the cultures were only disturbed for mandatory media change. Electrophysiological activities were recorded on day 12 for the first time for comparison purpose and only after day 18 for experiments and regular recordings.

It is typical for a rat hippocampal cultures to exhibit spontaneous synchronised burst of activities without external stimuli [3]. As cultures mature, they exhibit rich synchronised bursting activity [200]. Random and uncorrelated firing patterns become less frequent, and the activity patterns are dominated by a network wide bursting patterns during development. This development of synchronous bursting behaviour implies that wider connections are also explored, possibly as a consequence of the rapid chemical synaptogenesis during the second week in culture [201].

Figure 7.1 shows two raster plots of a hippocampal culture, recorded at 12 DIV and 18 DIV. The recordings were performed for 5 minutes. The raster plots make it easier to observe the electrophysiological activity of the whole network represented by a dot for each spike. As anticipated, significant random firing appears on both plots, and the subsequent recordings. However, the firings became more synchronised with spontaneous bursts of events as the culture matured - indicated by the presence of highly synchronous bursting patterns at 18 DIV recording as shown by red vertical rectangles in Figure 7.1 (DIV18) in comparison to DIV12. Due to the highly interconnected network, synchronous behaviour became more evident as the cultures matured. Some of the channels were saturated (indicated in Figure 7.1) which could be due to blocking of channels due to cellular debris caused by dead cell structures. Such channels showed continuous firing which is not plausible in reality due to the required refractory period necessary for neu-

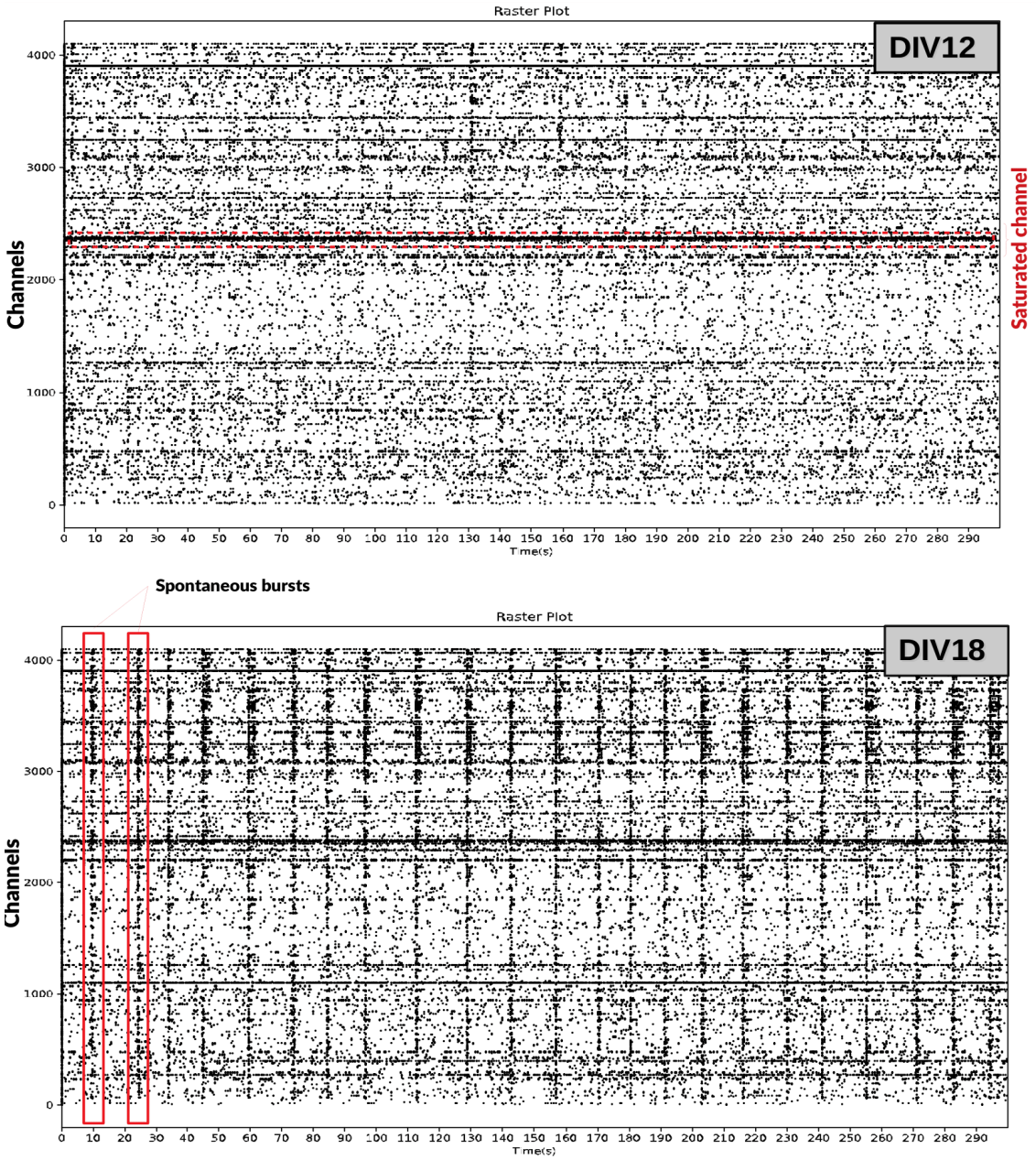

Figure 7.1: Electrophysiological activity of a dissociated hippocampal network recorded at DIV12 and DIV18 during the development phase. Continuously firing saturated channels are highlighted with a dotted red horizontal rectangle. Bursting patterns are indicated by a red vertical rectangles.

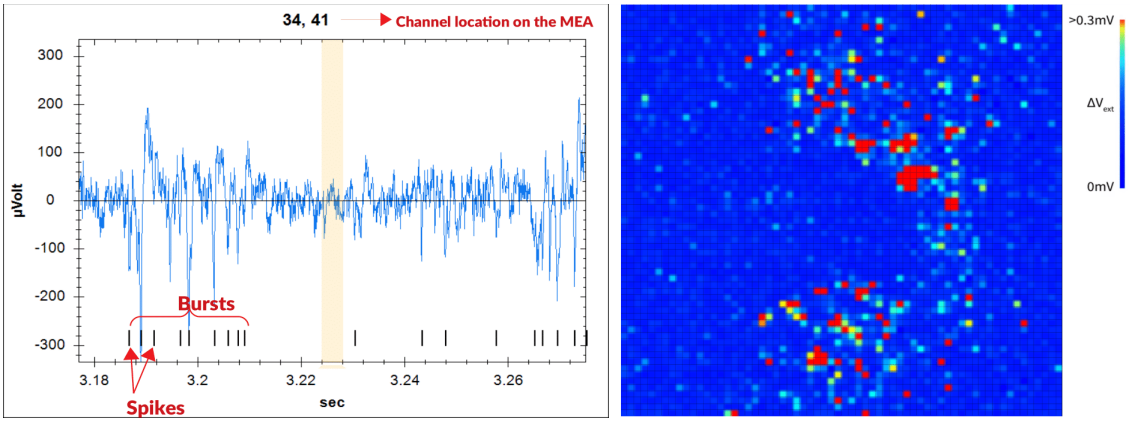

Figure 7.2: (A)Raw voltage fluctuations recorded from a single channel. Each vertical line underneath the waveform indicates a detected activity as a spiking event. (B)Snapshot of a real time activity laid out in MEA layout where each pixel is an electrode.

rons to recover before firing again. The presence of such channels is inevitable in live cultures and were filtered out in further analysis. Single channel electrophysiological activity can also be observed as a series of voltage fluctuations shown in Figure 7.2(A). Each vertical line underneath the waveform indicates a spiking event as shown in Figure 7.2(A) and the firing pattern resembles the general firing pattern of the network wide bursting firing (Figure 7.1) where a bursting firing is followed by a quiescence period. Figure 7.2(B) on the other hand shows a snapshot of network-wide activity in real time for the culture, represented with a colour map, where each pixel represents an electrode laid out in a 64 x 64 grid mimicking the actual MEA layout.

Furthermore, Peristimulus time histogram (PSTH) analysis (Figure 7.3 (A,B)) clearly shows an emergence of firing patterns characterised as highly synchronised bursting patterns from day 12 to day 18. The PSTH bin size was set to 1000ms, and shows the firing rate measured at every second of the 5 minute recording. Figure 7.3(A) at day 12 does show synchronous patterns as oscillating firing behaviour with some instances of highly synchronous patterns observed at around 130 seconds and 160 seconds (note the ms scale on the plot), but the general firing was still rather random without discernible network wide bursts. Also, the

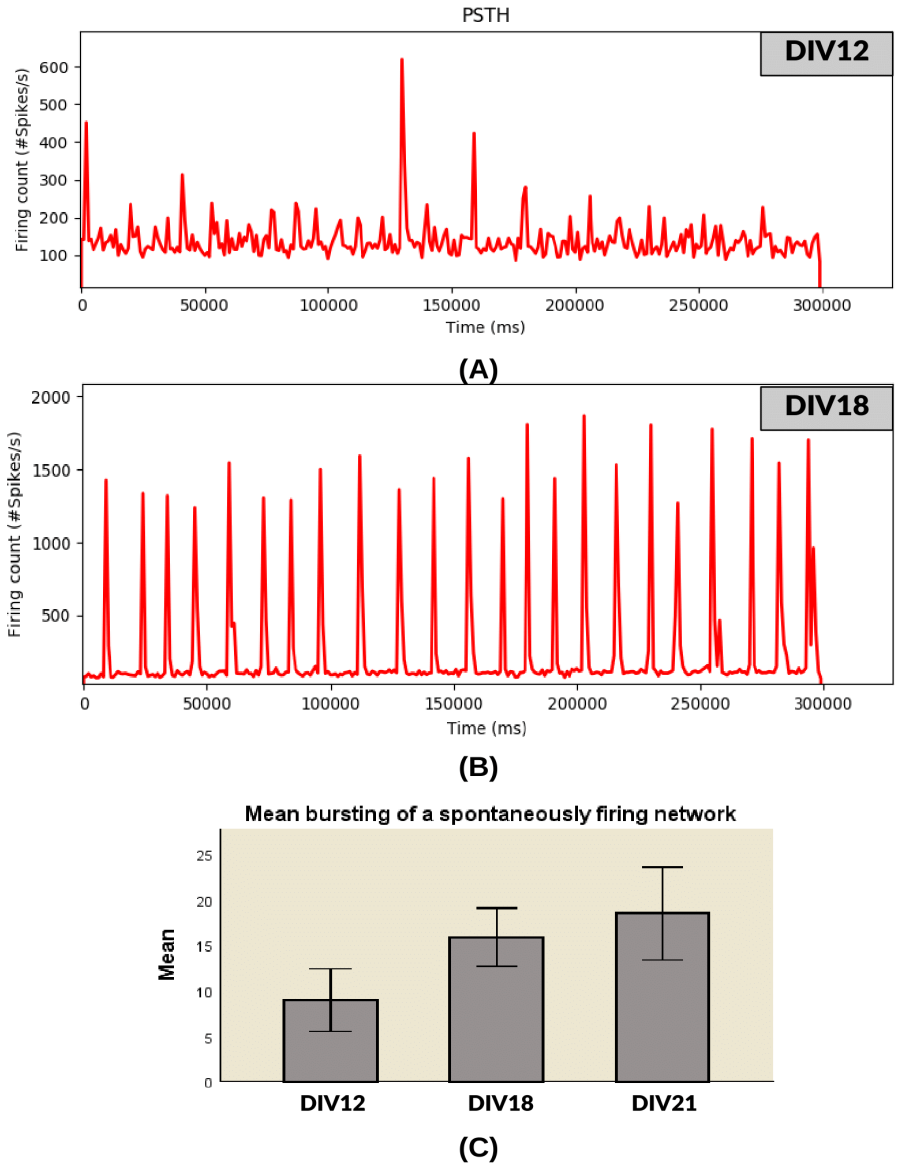

Figure 7.3: Activity characterisation of a spontaneously firing rat hippocampal network. (A) PSTH plot at day12(DIV12). (B)PSTH plot at day 18(DIV18) (C) Mean bursting of a spontaneously firing network measured at day 12,18 and 21. [*95% confidence interval*]

firing rate was much lower than at DIV18. This indicates a culture which is yet to mature. When the culture reached day 18, the culture started to mature indicated by clearly visible highly synchronous firing patterns, where the firing

rate was almost double that observed at day 12 (Figure 7.3(B)). The network was bursting regularly followed by a period of quiescence. This behaviour was prevalent all throughout the period of the culture up to week 4. After DIV32, the culture began to degrade and eventually died few days after. Hence, the experiments were performed between day 21 to day 32.

To further characterise the spontaneous activity of the network, the mean bursting rate was computed for the same culture over three stages that correspond to (a) an early stage(DIV12); (b) maturing stage(DIV18); and (c), matured stage(DIV21), as shown in Figure 7.3(C). Not surprisingly, the development of bursting activity followed the pattern as anticipated from the PSTH plots (Figure 7.3(A,B)). There was a clear increment in the bursting activity from day 10 to day 18. Even though, the bursting activity increases with maturity, at around day 21 the bursting activity plateaued as reported in the previous studies [8, 200, 202]. From week 3-4, the bursting profiles become increasingly narrow hence shorter burst - this change is attributed to the development of GABAergic neurotransmission(inhibitory) which was observed to occur after a delay of 1-2 weeks as compared to the glutamatergic (excitatory) system [114].

7.3 Criteria for selection of cultures for stimulation studies

One of the major challenges with dissociated neuronal cultures when studying induced plasticity is the variability among different batches of neuronal cultures. No two cultures are the same, and due to self-organisation and subsequent synaptogenesis, neuronal cultures achieve different stable homeostasis while continuing to grow functionally. Regardless of such dynamical nature of the neuronal cultures, it is important that the cultures that are undertaken for plasticity studies should have common baseline electrophysiological properties that are able to evoke responses to external stimuli. A systematic selection criteria is presented for selecting those cultures as candidates considered for a better investigation of induced network plasticity.

To demonstrate that the cultures were in fact responsive towards external

stimuli - which is critical to induce any plastic behaviour the spontaneous activity of each network was measured for 5 minutes at the beginning of the experiment at DIV21 as Mean Firing Rate(MFR_{pre}) and right after the first set of test stimuli, the spontaneous activity was measured again (MFR_{post}) for 5 minutes. MFR rate is a direct representation of network activity. Both pre- and post-stimulation spontaneous responses of 20 cultures were plotted as shown in Figure 7.4, where x-axis corresponds to MFR_{pre} and y-axis to MFR_{post}. A linear regression line is also plotted as a solid blue line (Figure 7.4). The mean squared error from this regression provides a quantitative measure of MFR change after introduction of external stimulation. Cultures above the regression line represent increased evoked responses after stimulation, cultures along the regression line represent evoked responses that were not too far off from pre stimulation spontaneous responses and cultures that fall below the regression line represent decreased evoked responses.

The selection criteria for cultures can be categorised as :

7.3.1 Spontaneous mean firing rate

For a systematic selection of neuronal culture, firstly, the spontaneous firing rate was considered. Those with MFR less than 300 spikes/sec were discarded as such networks, on biochips with 4096 electrodes, had very little activity to start with in order to be considered as a reliable experimental model for plasticity induction. Such low firing rate cultures were also found to have significant cell deaths within first few days of seeding hippocampal neurons even though the culture in general survived and continued to mature. Such low firing cultures showed a sporadic distribution of neurons as clusters with limited interconnections within small group of clusters. The cause for such early deaths could be initial growth conditions, state of dissociated tissue, poor coating or poor handling in general. Even though each culture were handled very carefully, there were a few cultures which showed a significant cell death early on. Hence, such cultures were discarded from experiments, as shown in oval region as sub-threshold in Figure 7.4.

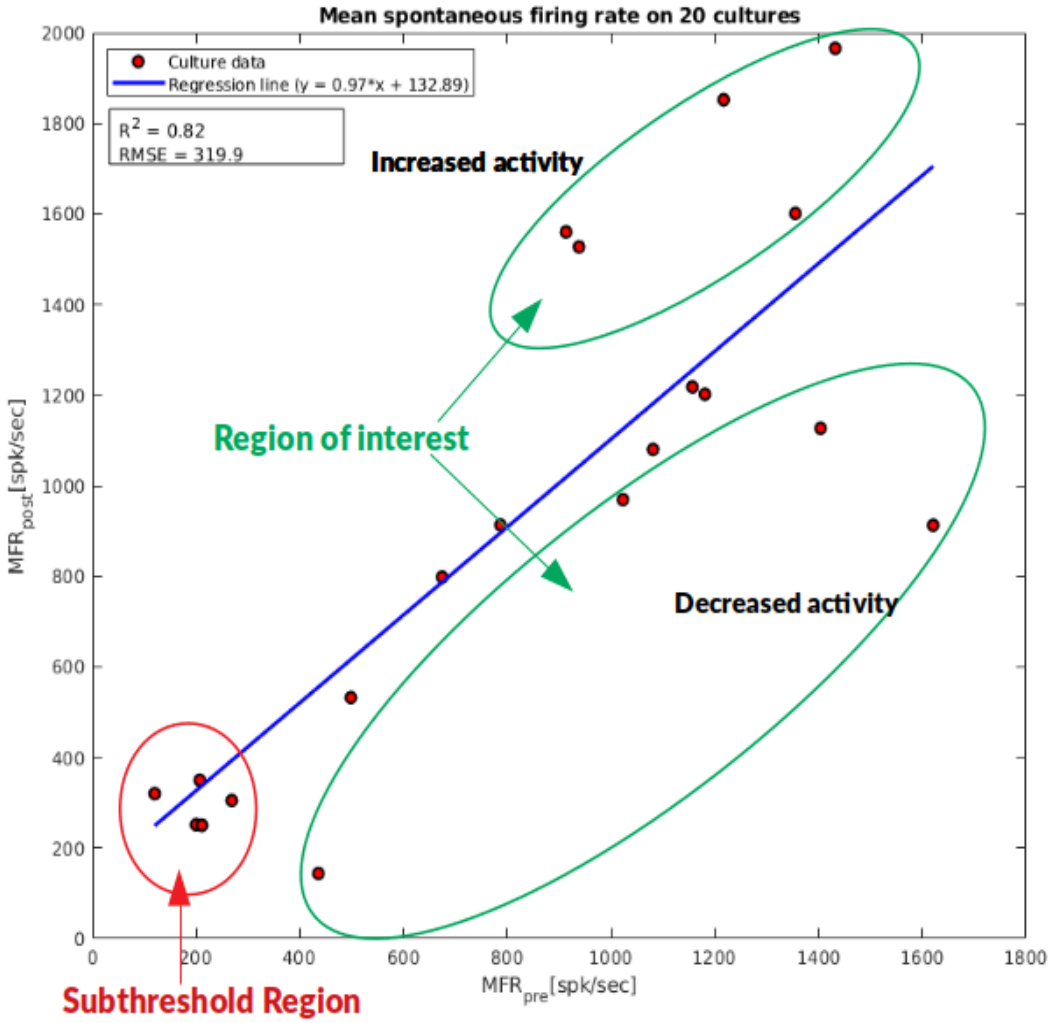

Figure 7.4: Mean spontaneous firing rates on 20 neuronal cultures. Spontaneous activity of each culture before and after stimulation indicated as red dots with a linear fit line. A red circle indicates a sub-threshold region where the firing activity is not strong enough to take as a reliable culture for experiments. Green regions indicates the region of interest. Both positive and negative evoked responses are considered for experiments.

7.3.2 Stability and responsiveness

Stability and responsiveness of neuronal cultures are paramount [9] when selecting the culture for plasticity studies. All cultures were monitored for 2-3 days after DIV18 regularly, before the test stimulation, to check if the spontaneous

network responses would vary drastically even without any external stimulation. An unstable network where the firing activity fluctuates drastically even without any external stimulation makes it difficult to assess induced changes in the presence of an external stimulation. This could lead to misleading biases in the dataset. To mitigate this bias, only the cultures that showed stable activity after DIV18 up to DIV21 were selected. By DIV21, neuronal cultures mature with stable bursting and firing dynamics. From these sets of cultures, to measure network responsiveness to external stimuli, test stimulation of low frequency (1Hz) biphasic stimulation with 500μA phase and duration of 100μs was applied repeatedly at every 20 seconds for 5 minutes as described in Chapter 4.3.1. This test stimulation is not part of the repeated experimental stimulation and only used to test the responsiveness of the culture. The scatter plots that are very close to the linear fit line (Figure 7.4), represent cultures that evoked very little responses measured as the firing activity before and after the test stimulation since there is very little difference between MFR_{pre} and MFR_{post}. Since the responsiveness feature was not evident from such cultures, indicated as scatter plots that lies very close to the regression line (Figure 7.4), they were not considered for further studies. To assure that the stimulation was applied to the region in close proximity to where neurons are distributed on the chip, all cultures were tested with stimulation from all 16 stimulating electrodes.

Regions shown in green oval (Figure 7.4 - top green oval), represent cultures that evoked either increased activity or decreased activity (Figure 7.4 - bottom green oval). Both increased and decreased activity are evoked MFR responses to the test stimulation and shows network wide potentiation and depression respectively immediately after the first set of test stimuli. Different variation of responses were observed by changing the stimulation site. The site that evoked the most prominent and long lasting responses were selected for further repeated stimulation.

7.3.3 Root Mean Squared Error (RMSE) thresholding

In order to provide a thresholding mechanism to objectively select cultures that exhibit evoked network responses, root mean squared error of the scatter plot of

mean firing rate before and after test stimuli (Figure 7.4) was calculated as well as the root squared error for each culture as a linear error distance of each scatter point to the predicted regression line as below,

$$RMSE = \sqrt{\frac{1}{n}\Sigma_{i=1}^{n}\left(\frac{y - predicted}{\sigma_i}\right)^2} \tag{7.1}$$

$$RootSquaredError(RSE) = \sqrt{(y - predicted)^2} \tag{7.2}$$

where n =number of data points, y = actual data point, $predicted$ = regression best fit line and σ =standard deviation

RSE computes individual error and RMSE is the mean of the errors. In this context, larger errors indicate larger change in the corresponding evoked responses as the data points deviate further from the regression line. To select only the cultures with larger evoked responses, the cultures with RSE larger than RMSE were selected. Due to squaring of the errors, negative errors from decreased activity were also incorporated. As mentioned earlier, both increased and decreased evoked responses are considered for this work.

In this section, a systematic approach to select the best cultures for plasticity studies based on different criteria: mean firing rate, stability and responsiveness and objective thresholding based on RMSE , has been described. It was crucial that all experimental cultures were subjected to all of these selection criteria before proceeding with further experiments.

Terminologies: To facilitate clarity throughout the rest of the sections, a comprehensive list of terminologies used and what they represent is shown in Table 7.1.

7.4 Results: Network response to stimulation

To demonstrate the effect of repeated stimulation on firing dynamics, network connectivity and achievement of evoked homeostasis of healthy neuronal cultures that implies a new stable state (learned state), the post stimulation responses of cultures were categorised as (i) potentiated (ii) depressed and (iii) regularised.

Table 7.1: Terminologies and what they represent

Term	Meaning
preStim/spont	Mean firing rate of spontaneous activity before repeated stimulation
postStim	Mean firing rate immediately after repeated stimulation
postStim_1hr	Mean firing rate 1 hour after repeated stimulation
postStim_2hr	Mean firing rate 2 hours after repeated stimulation
postStim_3hr	Mean firing rate 3 hours after repeated stimulation
pre-repeated stim	Immediate evoked response to single set of test stimulation before repeated stimulation (not to be confused with PreStim and PostStim MFR)
post-repeated stim	Immediate evoked response to single set of test stimulation one day after repeated stimulation

Based on these categorised responses, the stimulation protocols were applied as discussed in Chapter 4.3 with parameters shown for each culture from Table 7.2; the table shows 10 different cultures selected for experiments with corresponding stimulation parameters. The stimulation frequency, repetition and location of stimulation electrode were manually selected based on the initial post stimulation responses observed at various configuration.

Two different variations of stimulation parameters are used based on frequency and repetition:

Frequency : Generally, stimulation frequencies of over 10Hz resulted in over-saturation of electrodes and stimulation of less than 1 Hz didn't elicit any network evoked network responses - although higher repetition of such frequency for a prolonged period was able to. A 10 repetition of 1Hz stimulus results in 10 pulses that lasts for 10 seconds. Stimulation frequencies of 2Hz and 5Hz were selected as they represented the lower and upper limits at which evoked network responses were observed. Frequencies of 5Hz to 10Hz was able to evoke responses but these were not consistent and showed saturation of electrodes. Due to wide range of stimulation frequencies that could potentially be explored even within the range of 2-5Hz, the studies here only takes in account two frequencies of 2Hz and 5Hz.

Stimulation repetition : To maintain a consistent methodology, repetition of either 10 or 20 stimulation pulses with a gap of every 10 or 20 seconds were applied to all cultures for 5 minutes of recording. The time gap of 10 or 20 seconds between each set of stimulation allowed for the network to regain regular firing dynamics whilst still maintaining the effect of evoked responses without allowing the network to revert back the pre-stimulation dynamics. For 5Hz frequency case, a burst of 20 stimulation pulses was applied with a temporal gap of 20 seconds to avoid over saturation. When 10 second gap was implemented for the same case, the culture quickly saturated due to too strong stimulation. In case of 10 repetition of stimulation pulses, either 10 or 20 seconds gap were able to have an effect without causing saturation. The target is to apply stimulation such that the network is constantly encouraged to form new connections and modify already existing connections without falling into the trap of saturation or be damaged.

Table 7.2: Overview of cultures used

Overview of cultures used					
Culture	**DIV**	**Stimulation frequency**	**Repetition**	**Stimulation Electrode**	**Network Effect**
Chip1	21	2 Hz	10 pulses every 20 secs	2,4 and 4,4	Regularising
Chip2	25	5 Hz	10 pulses every 10 secs	1,4 and 3,2	Long term potentiation
Chip3	21	2 Hz	10 pulses every 20 secs	1,4 and 3,1	Short term depression
Chip4	23	5 Hz	20 pulses every 20 secs	1,4 and 4,1	Long term potentiation
Chip5	26	5 Hz	10 pulses every 20 secs	1,2 and 3,2	Long term potentiation
Chip6	26	2 Hz	10 pulses every 20 secs	3,1 and 4,4	Short term depression
Chip7 (control)	19	No stim	–	–	–
Chip8	23	5 Hz	10 pulses every 10 secs	1,4 and 3,2	Long term potentiation
Chip9	25	5 Hz	10 pulses every 20 secs	3,1 and 4,4	Long term potentiation
Chip10	26	5 Hz	20 pulses every 20 secs	3,1 and 4,4	Regularising

7.4.1 Single channel stimulation

Single channel stimulation was explored where the stimulation site with the most responses was selected. Recordings for both single channel stimulation and later

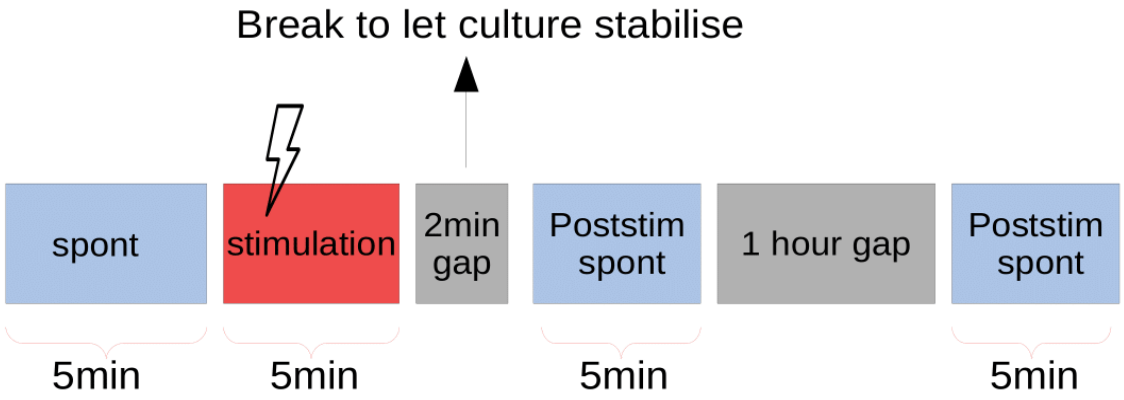

Figure 7.5: Stimulation time line for each day of stimulation. Spontaneous activities are first recorded followed by 5 minutes of repeated firing. The culture is then left to to settle for 2 minutes followed by interval spontaneous recordings again.

spontaneous spiking were performed, each for 5 minutes. The evoked responses were measured 2 minutes after the stimulation completed (to allow the network to stabilise) and spontaneous recording one hour after such stimulation . The next day, spontaneous activities were recorded again to enable a comparison with the earlier day's spontaneous activity. The timeline can be better understood from the illustration shown in Figure 7.5, which summarises how the recordings are performed for each day. The recordings start firstly with spontaneous activity (no external input), followed by repeated stimulation and spontaneous after 2 minutes and 1 hour. The process repeats for the next day. Hence, spontaneous activity of the next day reveals if the evoked responses due to stimulation still persisted.

Figure 7.6 presents an example of a culture at 23 DIV that was stimulated with 2Hz biphasic pulses with a repetition of 10 pulses every 20 seconds for 5 minutes. Immediately after the stimulation, the post stimulation activity was found to show a significant increase in activity, however, the effect was short lived. In agreement to what previous studies have mentioned [9, 46], single site stimulation yielded no significant long lasting responses. Measurement of the the evoked responses commenced after 2 minutes of stimulation (to allow the

network to stabilise first). Such measurements then commenced with a recording of the spontaneous firing, and were repeated after 1 hour (Figure 7.5). The next day, spontaneous activities were recorded again to compare with the earlier day's spontaneous activity. This was repeated over three days to observe any long lasting changes.

Figure 7.6(A) shows a correlation heat map where the numbers on each square shows Spearmans correlation coefficient. Post-stimulation activity was highly correlated with a Spearman's coefficient of 0.993, as shown in the correlation heatmap in Figure 7.6(A). The correlation dropped significantly one hour after stimulation to 0.509 as shown in Figure 7.6(A). This rather short term potentiation represented by correlation was further confirmed from PSTH profiles as evoked responses as shown in Figure 7.6(B), before and after repeated stimulation.

The plot in Figure 7.6(B) shows PSTH profiles evoked immediately after the application of a single set of stimulus; the effect of stimulation can be visualised by each profile over 1000 ms after stimulation. It is important to note that the evoked responses discussed in this plot are not the same as MFR measured before and after stimulation. Evoked responses focuses only on the responses in the presence of just one set of stimulus, before and after repeatedly stimulating. Such evoked responses indicate adaptation of network response to a particular stimulation after repeated stimulation.

A similar evoked PSTH profiles indicate that the culture responds in a similar way to the same stimulation. On the first day before repeatedly stimulating the culture, the evoked responses were recorded as a PSTH profile immediately after the onset of the test stimulus - shown in the red trace in the plot (Figure 7.6(B)). The culture was then subjected to repeated regular stimulation for 5 minutes, and the next day evoked responses were measured again with a single set of test stimulus - shown in the blue trace in the plot (Figure 7.6(B)). Both evoked profiles on two different days show very similar trend without any significant changes (either increase or decrease) as a result of the stimulation, over two days. This response profile after the stimulation shows no significant changes over the next day period. The correlation heatmap in Figure 7.6(A) suggests a short term potentiation, which dropped rapidly after 1 hour as indicated by a rapidly falling

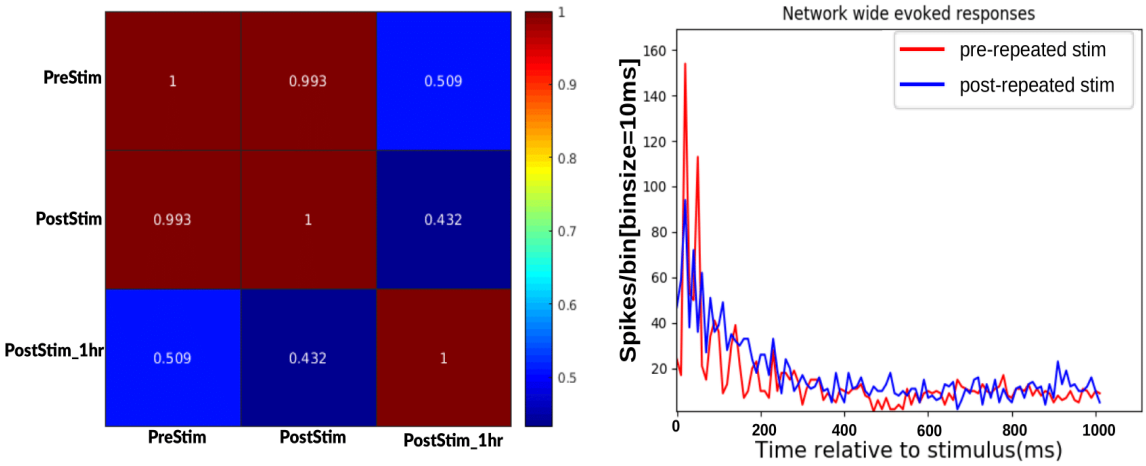

Figure 7.6: Short term evoked responses with single channel stimulation (A) Correlation matrix of pre and post stimulation network activity. (B) Network wide evoked responses after the onset of single set of stimulation to measure evoked responses.

correlation index after an hour. Further MFR comparison tests confirm this.

Table 7.3: Test of Normality (Shapiro-Wilk)

			W	p
preStim	-	postStim	0.057	$< .001$
postStim	-	postStim_1hr	0.043	$< .001$
preStim	-	postStim_1hr	0.075	$< .001$

Note. Significant results suggests a deviation from normality

Table 7.4: Wilcoxon signed rank test

			W	p
preStim	-	postStim	11760	$< .001$
postStim	-	postStim_1hr	102026	$< .001$
preStim	-	postStim_1hr	60601	0.355

To statistically measure the significance of evoked responses after stimulation, a paired hypothesis test was performed. The Shapiro-Wilk normality test suggested that the MFR at different time points were non-normally distributed($p<0.001$),

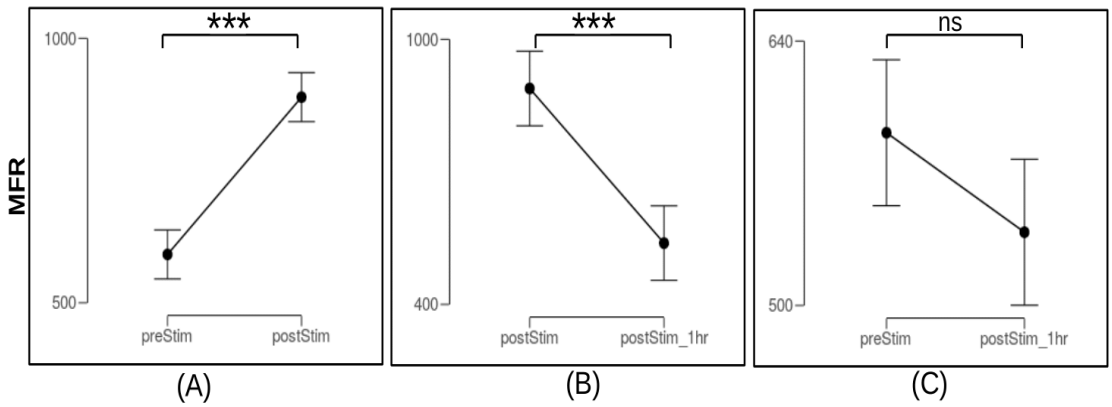

Figure 7.7: Significance between pre and post stimulation MFR. (A) A significant network wide potentiation immediately after stimulation. (B) Significant drop in potentiated activity just 1 hour after stimulation (C) The MFR difference at pre stimulation stage and after 1 hour of stimulation are insignificant. [Y-axis scales are different, but shows absolute MFR values]

as shown in Table 7.3. Due to non-normality nature of the data, a non-parametric paired Wilcoxon signed-rank testing was adopted. The statistical test suggested that there was a significant increment in MFR after the stimulation (Table 7.4 Wilcoxon signed-rank:$p<0.001$), however, this effect decreased significantly after just one hour(Table 7.4: Wilcoxon signed:$p<0.001$). There was no significant change between the initial pre-stimulation dynamics and the dynamics after one hour of stimulation, suggesting that the culture had reverted back close to the initial stage before stimulation (Table 7.4: Wilcoxon signed-rank:$p>0.005$)).

A comparative MFR at different stages after the stimulation is shown in Figure 7.7. As suggested by the statistical testing, a significant increment in MFR can be seen between pre-stimulation state (preStim) and post-stimulation (postStim) (Figure 7.7(A)) which suggests the achievement of network wide potentiation. This change significantly decreased when measured after one hour (Figure 7.7(B)). When the pre-stimulation state was compared with post-stimulation after one hour(postStim_1hr), it was found to be not significantly different, indicating return to the original state of firing dynamics. This suggests inability of single channel stimulation to exhibit long term potentiation . Furthermore, the MFR measured over three days of stimulation showed short term potentiation which

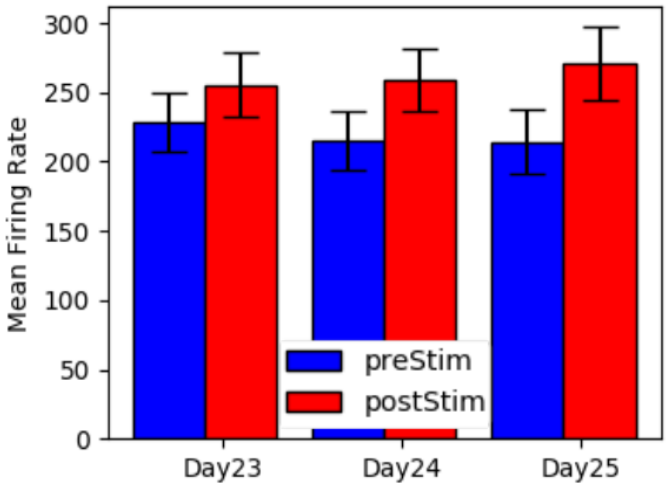

Figure 7.8: Mean firing rate before and after stimulation over three days of repeated stimulation (5minutes each day)

can only be observed immediately after the stimulation. The firing dynamics returned back to the initial state after each day of repeated stimulation as shown in Figure 7.8 which shows a short term increment in MFR after each stimulation, however, the effect is reverted back the following day. Hence, multi channel approaches were explored see if long term responses can push effective connectivity to a new stable state.

7.4.2 Multi-site Stimulation

As demonstrated in earlier sections, single channel stimulation was not enough to reliably induce evoked responses that underlie synaptic plasticity behaviour. Multi-site stimulation has been previously shown to induce potentiation at population level [9, 103] - though for low density glass based MEAs. A systematic methodology to study induced responses on embryonic hippocampal cultures coupled with CMOS based HD-MEAs with thousands of simultaneously recording and stimulating electrodes as presented in this work has not hitherto been conducted. Due to the high density and culture sensitive nature of the MEA, the

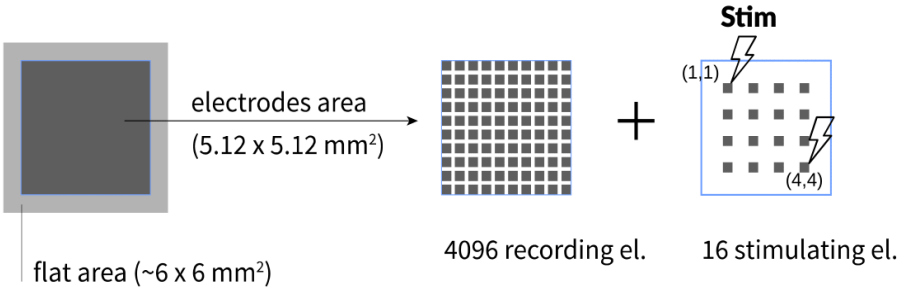

Figure 7.9: Illustration of stimulating electrodes interleaved onto recording electrodes.

stimulation sites and parameters were chosen for each culture by manually stimulating all stimulation sites based on the cellular distribution from visual inspection and selecting those that showed the strongest evoked responses.

For this work, depending on the distribution of neurons on the MEAs, the stimulation site was selected such that they were at least one stimulation electrode apart to avoid overlapping signals from closely spaced electrodes.If neurons are homogeneously distributed then the stimulating electrodes could be further apart and if neurons are clustered in a particular region then the stimulating electrodes have to be selected such that electrodes are also in the same region to ensure effective stimulation for inducing responses. Figure 7.9 illustrates the position of stimulating electrodes interlaced with the recording electrodes. Position(1,1) is the position of stimulating electrode starting from the top left corner and the location co-ordinates move from top left to bottom right (Figure 7.9). With biphasic stimulation as described in the Materials and Methods section (Chapter 4.3.1), two series of pulses of current were injected from the selected stimulating electrodes in sequence, one after the other without any delay.

An example culture at 23 DIV is discussed henceforth to demonstrate and validate long lasting evoked responses. The culture was stimulated with a biphasic stimulation at 5Hz with repetition of 20 pulses every 20 seconds from stimulation site (1, 4) and (4, 1) as shown in the illustration (Figure 7.11), where biphasic stimulation pulses were applied with a set gap of 20 seconds after both channels supplied 20 pulses. Similar to Section 7.4.1, the culture was stimulated and recorded for the next 3 hours - 5 minutes at every hour.

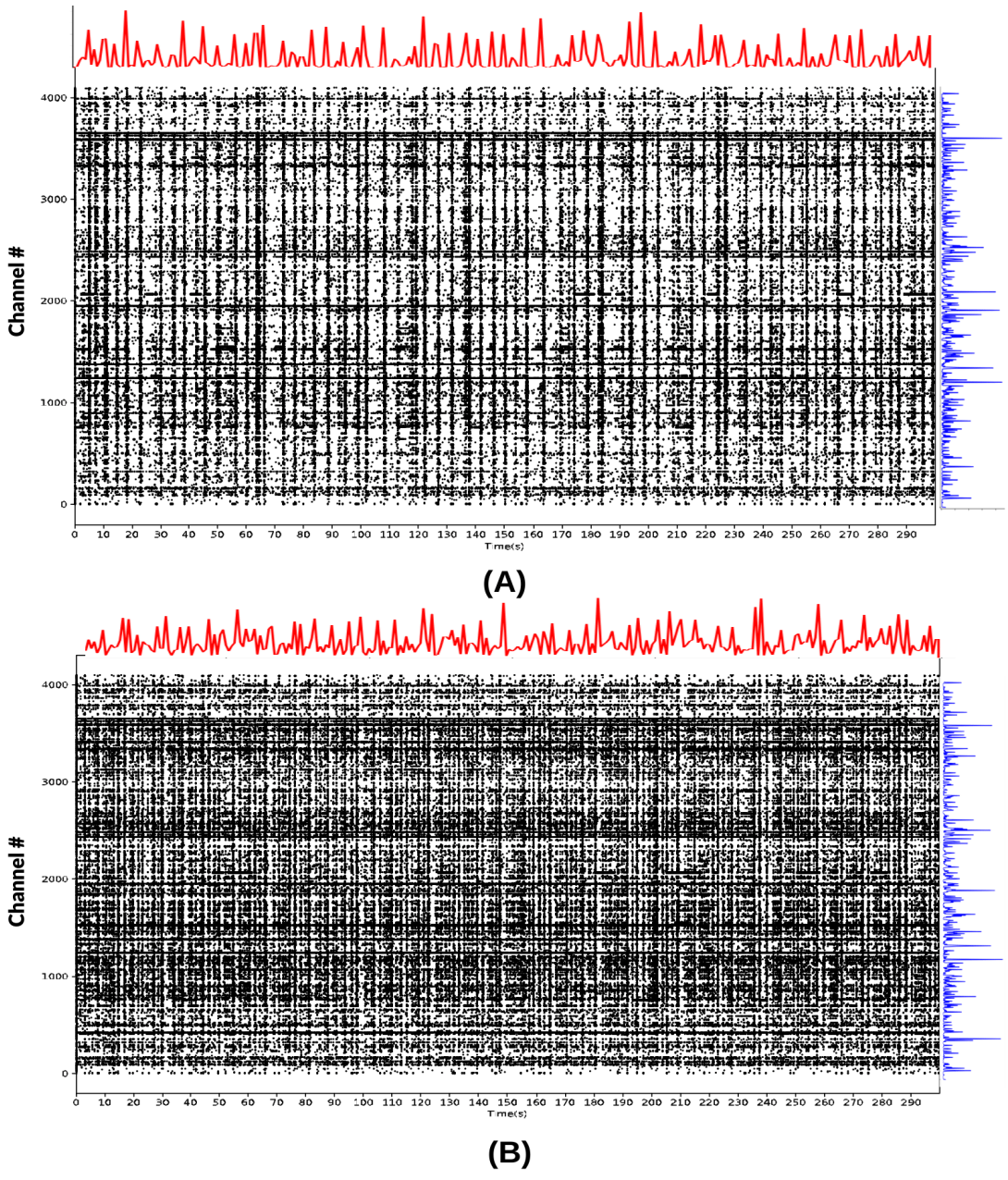

Figure 7.10: Raster plot with firing profile.The top red plot shows network firing rate over 5 minutes and the blue plot on the right indicates each electrodes firing over the 5 minute duration (A) Pre stimulation spontaneous firing represented by a network wide raster plot for 5 minutes. (B) Immediate post-stimulation network wide firing for 5 minutes.

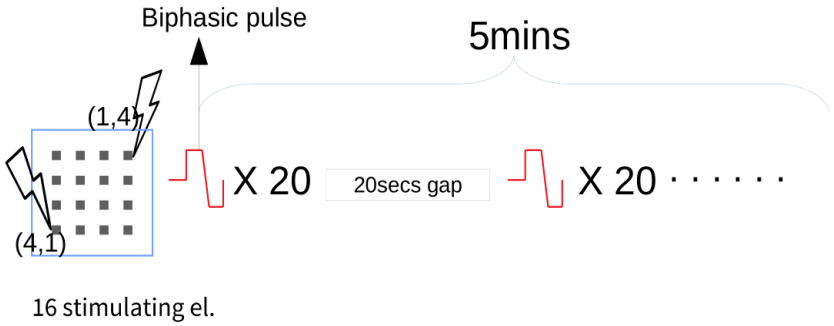

Figure 7.11: Illustration of stimulating electrodes interlaced onto recording electrodes.

Table 7.5: Test of Normality (Shapiro-Wilk)

			W	p
preStim	-	postStim	0.383	$< .001$
preStim	-	postStim_1hr	0.114	$< .001$
preStim	-	postStim_2hr	0.128	$< .001$
preStim	-	postStim_3hr	0.064	$< .001$

Note. Significant results suggests a deviation from normality

Figure 7.10 shows two raster plots before and after the stimulation pulses were applied for 5 minutes, respectively. The red plots on the top of each raster plot indicate the network firing rate trend over 5 minutes for all the electrodes combined and the blue vertical plots on the right hand side show firing activity from each of the 4096 electrodes. A visual comparison of the two red traces in Figure 7.10, suggest that the network wide firing dynamics have changed. However, using raster plots alone is difficult to objectively tell if changes have indeed taken place, as they do not convey the complete information of the responsiveness and long lasting nature of the responses. Therefore, the hourly comparisons and statistical significance of the increment are discussed in the next section for greater clarity and objective assessment.

7.4.2.1 Hour-to-hour recording of cultures

Recordings were performed at various time points to allow for a detailed overview of network dynamics before and after stimulation. First of all, network responses

were analysed at every hour for three hours after the stimulation was applied. Figure 7.12 shows hour by hour MFR(Mean Firing Rate) and MBR(Mean Bursting Rate) data, before and after the stimulation, recorded for 5 minutes every hour for three consecutive hours over three days. Stimulation was started at DIV23, at which point (third week) the culture was fully mature, with a good balance of excitatory and inhibitory synapses [111, 112].

Normality tests suggest a non normal distribution as shown in Table 7.5. A non-parametric test, paired Wilcoxon signed-rank, was hence adopted for statistical testing. After the first set of stimulation, the culture evoked potentiated responses characterised by a significant increment ($p<0.01$) in MFR and MBR. This response was consistent over each day of stimulation and is indicated by significance in Figure 7.12. The incremental trend was not always evident at the hourly recording performed after the stimulation. In fact, both firing rate and bursting rate dropped after the first hour of stimulation which was also consistent with other cultures (postStim - postStim 1hr plot in Figure 7.12). The potentiated dynamics, however, were retained beyond the first hour of stimulation and the MFR and the MBR showed potentiated dynamics in comparison to the initial rate, but not drastically changed at the end of hour 3. The actual cause for this unexplained initial drop after the first hour not was clear and is yet to be investigated in detail. The probable cause could be over-handling of the chips. Hourly recordings do allow for much better inspection of dynamics but taking the chips out of the incubator and recording does add a lot of stress on the cultures as the incubation environment cannot be maintained during the recording. Due to the complex circuitry of the 3Brain Chips, incubating BioCam recording device under cell culture environment (65% humidity) is not recommended.

Furthermore, correlation analysis performed over each time point revealed a decreasing correlation index pattern after the onset of stimulation consistent over all cultures. Due to non-normality of the data, pairwise Spearman's correlation was performed for all recordings at different time points. The pairwise correlation matrix is presented as a heatmap in Figure 7.13, which shows corresponding correlations for MFR and MBR over three days, with respect to Figure 7.12, where each pixel is colour coded for Spearman's correlation index(ρ). The rows and columns are indexed from 1-5 as *1 - preStim, 2 - postStim, 3 - postStim_1hr, 4*

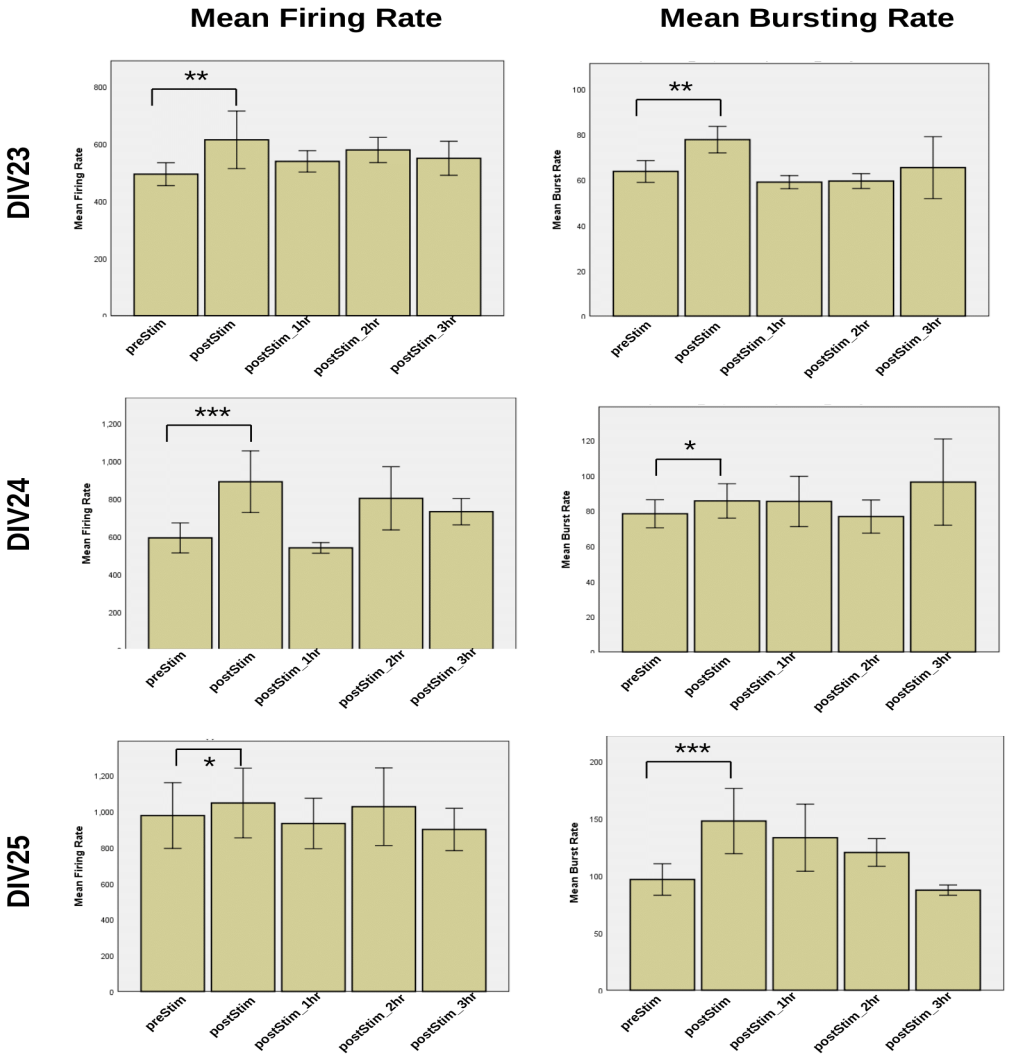

Figure 7.12: Mean firing rate and mean bursting rate dynamics after stimulation recorded over three days at five different time points Spontaneous firing before stimulation(preStim), immediately after stimulation (postStim), 1 hour after stimulation (postStim_1hr), 2 hours after stimulation (postStim_2hr) and 3 hours after stimulation (postStim_3hr) . It is seen that stimulation was able to evoke subsequent network wide potentiation, as seen in both the MFR and MBR plots, although the hourly record tended to fluctuate. [*p<0.05, **p<0.01, ***p<0.001]

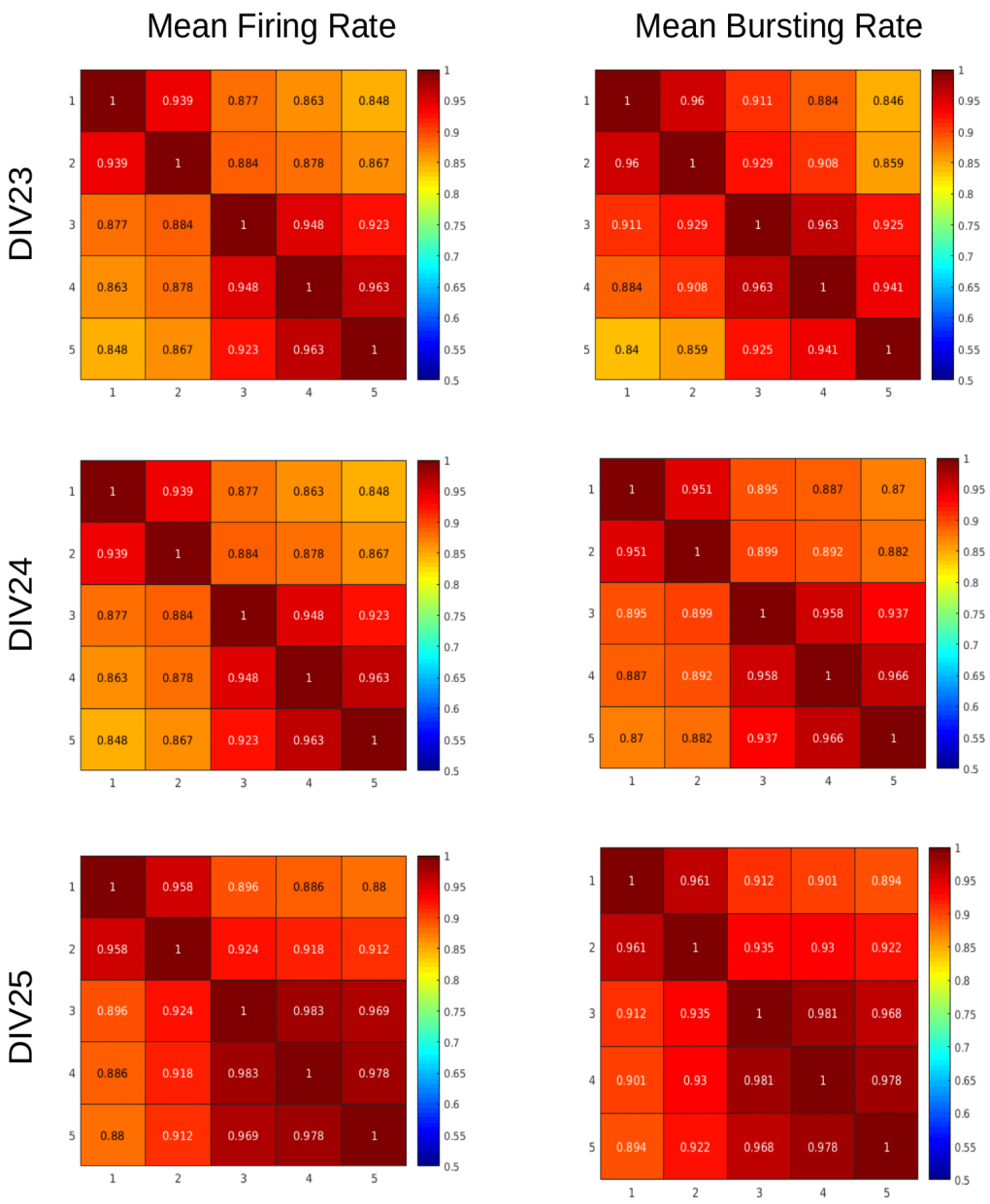

Figure 7.13: Correlation between pre and post stimulation dynamics. A corresponding correlation heatmap of Figure 7.12 where each pixel represent a Spearman's correlation index(ρ).[*Indexing: 1 - preStim, 2 - postStim, 3 - postStim_1hr, 4 - postStim_2hr, 5 - postStim_3hr*]

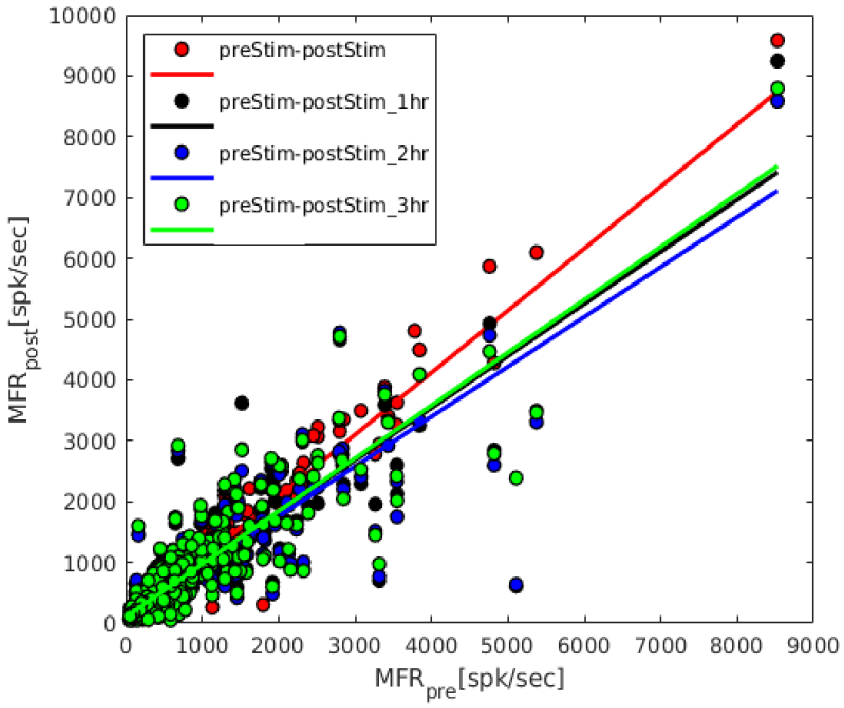

Figure 7.14: Scatter plot of pre- and post-stimulation network wide MFR plots at three different time points after the stimulation. Each dot in the scatter plot corresponds to an electrode firing before and after stimulation. Linear regression lines for each time point shows network response trend after the stimulation

- *postStim_2hr, 5 - postStim_3hr* . Both MFR and MBR showed a high positive correlation which got weaker with time, however, the correlation doesn't fall drastically and maintains a correlation index of more than 80% in all cases, even after 3 hours. A comparison to a short term potentiation correlation index discussed in Figure 7.6(A) shows that the correlation index dropped to 0.5, 1 hour after stimulation.

As expected, the culture showed a trend where the culture demonstrated a stronger response initially indicated by a high correlation coefficient, and with time settled back to some homeostasis as indicated with decreasing correlation coefficients, whilst maintaining more than 80% correlation index. This decreasing correlation can be supplemented with manifested change in MFR for clarity, with a comparative response trend over three hours of post stimulation stage as

shown in Figure 7.12. The general trend line based on the MFR rate is shown in Figure 7.14 for different time points, represented as different colours with each corresponding linear fit line in the same colour. Each plot represents an active electrode that showed firing activity during recording. Figure 7.14 shows that the evoked responses immediately after the stimulation is much stronger than responses after 1/2/3 hours of stimulation, as indicated by the top red linear fit line. The responses measured for the next three hours fluctuate but remain in close proximity to each other as shown by green, black and blue lines clustered close to each other in Figure 7.14.

7.4.2.2 Induced potentiation after stimulation

So far, evoked network responses after repeated stimulation were measured and analysed every hour for three hours, over three days. Correlation analysis and statistical testing showed that there was in fact a significant change after the onset of stimulation in both MFR and MBR. In addition, it is critically important to also measure the responsiveness of the culture to the same stimulus, which over an extended time period (>hours), to assess whether network wide activity has both increased and also adapted response to the stimulation. To clarify further, how the network responds to the same stimulation after being repeatedly stimulated, shows the adaptation of the network to that stimulation. During post stimulation recordings so far, the responses were measured at specific time points after the stimulation i.e. from a few minutes to 1 - 3 hours over three days. In order to demonstrate successful induction of some level of plasticity behaviour, the same single instance of stimulus should be able to induce a different response, measured on different days, after the repeated stimulation. During repeated stimulation, connections are either formed or changed and new neural pathways are established, due to the adaptable nature of the brain to external stimulation - in a way, the network is re-learning or re-organising its connections in response to the stimulation, hence demonstrating neural plasticity behaviour.

Accordingly, network responses to the first set of stimulation only were measured over 4 days subsequent to the stimulation. The steps can be better understood from the illustration (Figure 7.15). On the first day, the response to

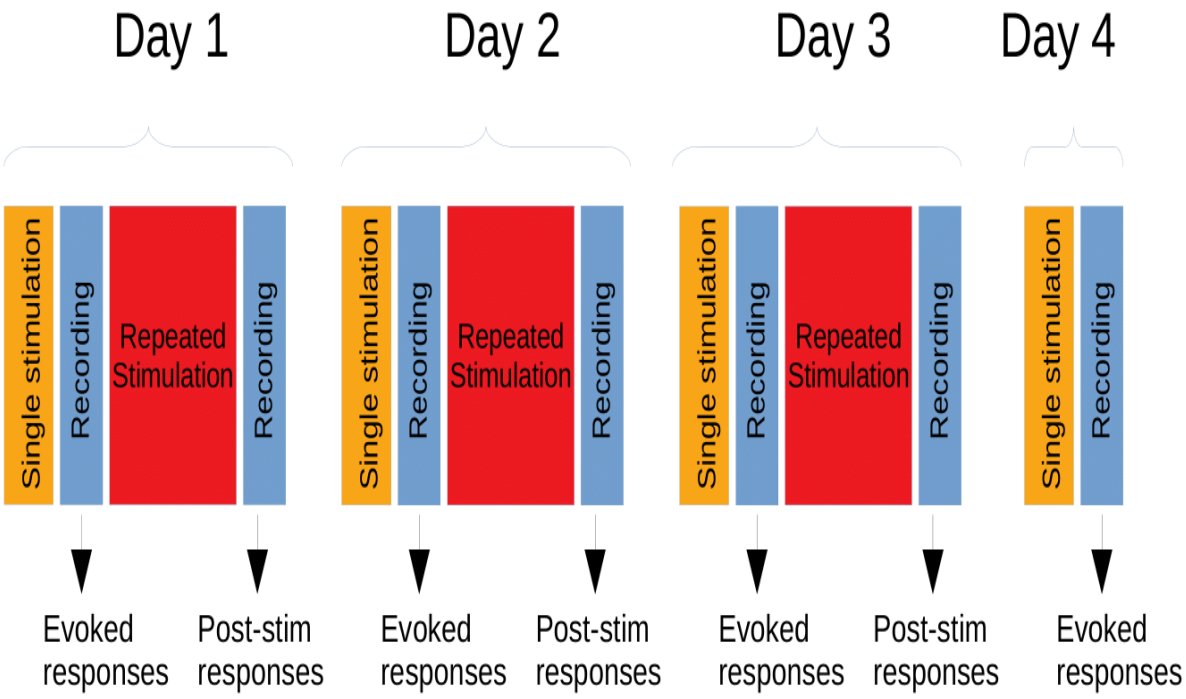

Figure 7.15: Evoked and post stimulation response measurement with repeated stimulation timeline shown over 4 days.

the first set of stimuli was recorded as evoked responses due to single stimulation (Figure 7.15). After that, repeated stimulation was applied to induce plasticity. The next day, the original stimulus was applied again to record the response and subsequently repeated stimulation was applied. This was repeated over four days. On the last day, only the test stimulus was applied and the experiment was concluded without further repeated stimulation. Hence, the actual repeated stimulation was performed over three days but the evoked response was also measured on the day 4 as shown in Figure 7.15.

If a network had indeed adapted to new stimulation, the responses would be different to the same stimulation as the network *"learns"* to modulate its responses. Figure 7.16 shows four different network responses after stimulating the culture for three days. The time point zero on the x-axis is the time of onset of stimulation. Pre stim (day1) is the first day of stimulation, where the culture had never been subjected to any external stimulation. The initial evoked response

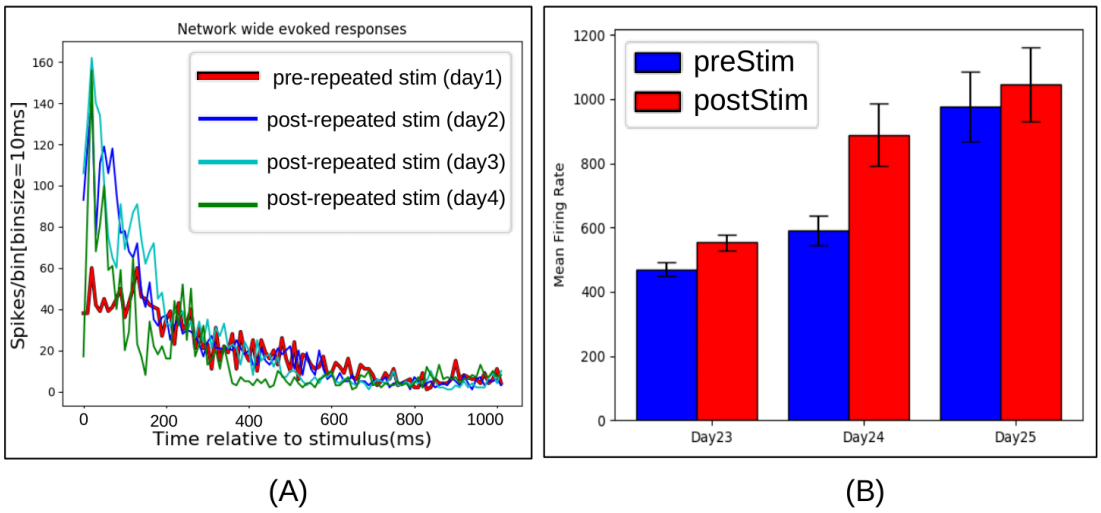

Figure 7.16: Network dynamics after repeated stimulation to induce long term evoked responses. (A) Evoked responses to only one set of stimulation over four days of repeated stimulation. (B) MFR increment over three days after repeated stimulation for 5 minutes on each day.

to the same stimuli is clearly quite different from the other post stimulation days. On a first look, the responses after the first set of stimuli shown in the red trace (Figure 7.16(A)) has a much weaker and wider response to the stimulation peaking at around 60 spikes/bin(binsize=10ms) and stretches up to 200ms after the stimulation. The response gradually decreases with time as the network comes back to the initial state of spontaneous firing.

After the first day of stimulation, the culture was presented with the same single stimulation (24 hours later). The stimulation was applied to the same location under the same conditions. 24 hours is a long enough time to allow the network to revert back to an equilibrium state. This ensures that the subsequent network responses were not subjected to any other factors such as state of excitation or short term potentiation due to insufficient relaxation time. The responses after day1 clearly show that the network has in fact changed and consistently showed stronger responses, peaking at up to 2.6 times the initial response ie. 160 spikes/bin, as evident from the sharper initial peaks of the post stimulation traces, as shown in Figure 7.16(A). After subsequent days of stimulation, the traces for day 2,3,4 after stimulation continues to evolve suggested by the fluctu-

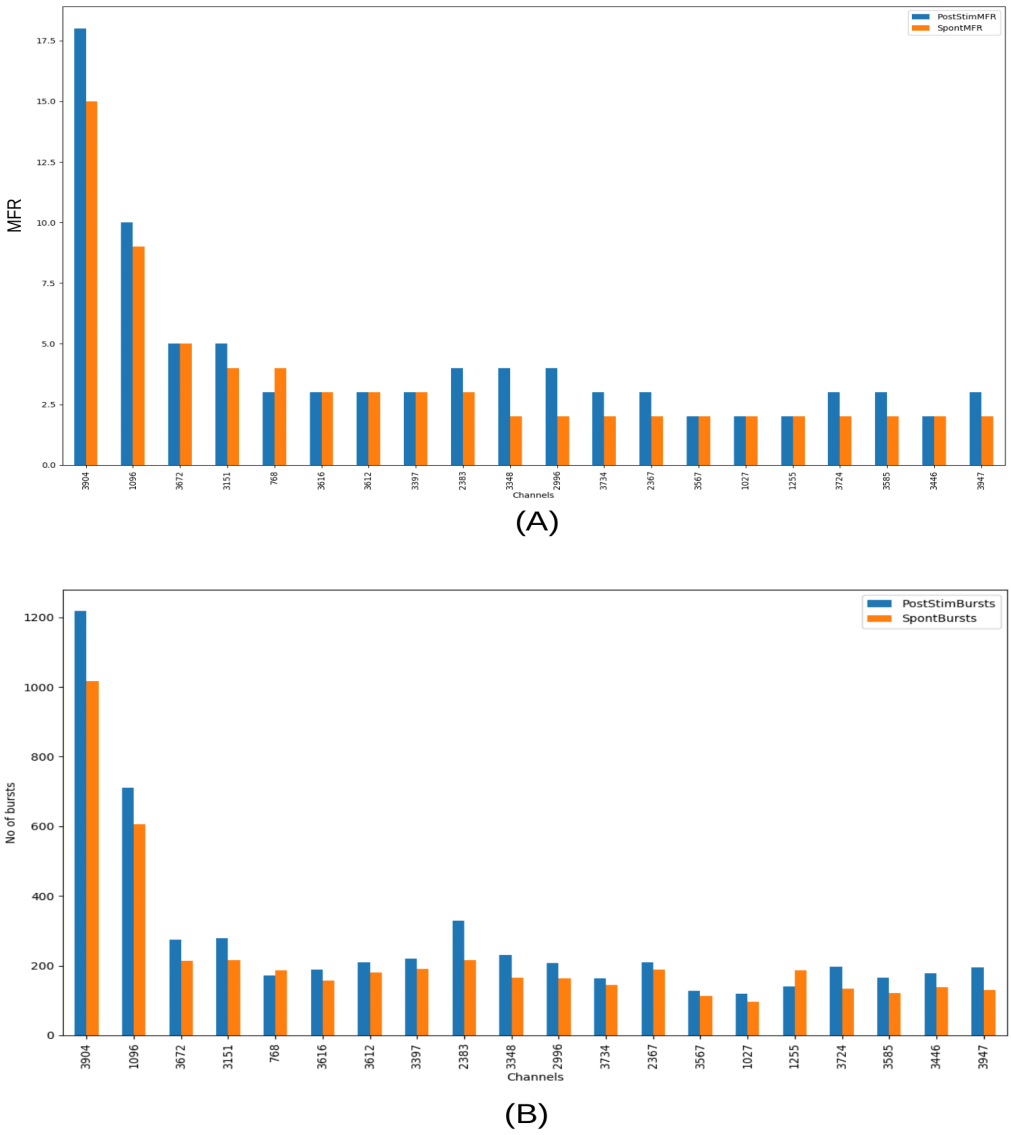

Figure 7.17: MFR and burst count for 20 randomly selected channel before and after stimulation. (A) MFR comparison before and after stimulation (B) Number of bursts from each channel before and immediately after stimulation

ating response profile for these days whilst maintaining a much larger response profile, evident from higher and broader peaks, in comparison to day1 (Figure 7.16(A)). The response profile within 400ms after the onset of stimulation is gen-

erally considered to monitor and compare evoked responses [9, 126]. To confirm the fact that an induced responses has been achieved and sustained after the stimulation, Figure 7.16(B) shows the MFR responses after stimulation on each day and also a significant increment in MFR after each day of stimulation. Furthermore, Figure 7.17 shows the MFR and number of bursting activities from 20 randomly selected channels within the vicinity of the stimulation site. Both MFR and bursting activities show an increment in activity from almost all selected channels. This helps to illustrate that the mean activities are not heavily skewed by a small number of channels, but are well distributed across channels. A clear pattern of long term potentiation can be identified with the responses to stimulation and the overall network response.

7.4.2.3 Induced depression after stimulation

In contrast to long term potentiation, 3 out of 10 cultures, exhibited depressed behaviour in response to repeated stimulation. Predicting which culture would result in potentiation or depression based on initial dynamics was a difficult task because the spontaneous dynamics across all cultures initially appeared similar in terms of dynamics of periodic bursting.

Even though some cultures evoked a network wide depression response, long term depression lasting many days was not observed. Networks eventually returned back to their earlier stage after 3-4 days, though the depression was very prominent for a few hours after stimulation. Figure 7.18 shows analysis from one of the cultures with decreased firing rate after the onset of stimulation. Based on firing rate traces of the spontaneous and post stimulation stages at different intervals for 5 minutes, as shown in Figure 7.18(A), the firing rate drops significantly post stimulation over the course of three hours. However, the evoked response trace measured over four days tells a different story. The red trace in Figure 7.18(B) sets a baseline response recorded at first day after stimulation. After stimulating the network, the response decreases rapidly shortly after stimulation, and reaches a plateau at a low level thereafter, as shown in the blue trace. This inhibition however, slowly recovers over the course of next two days and settles back to the initial condition as shown by cyan and green traces, which get closer

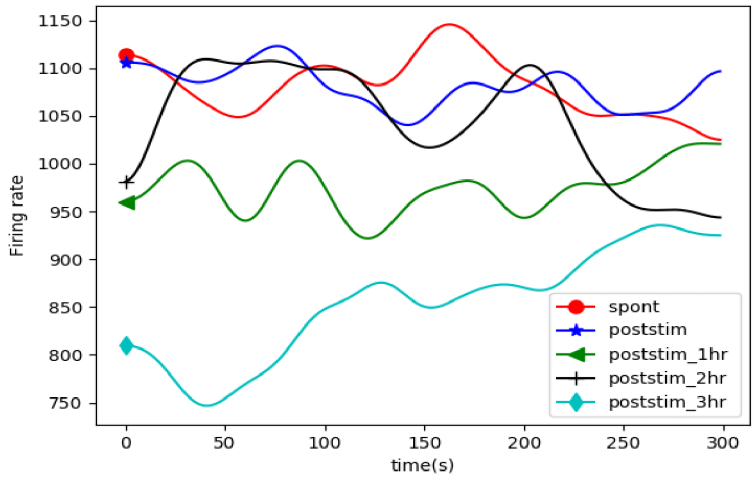

(A)

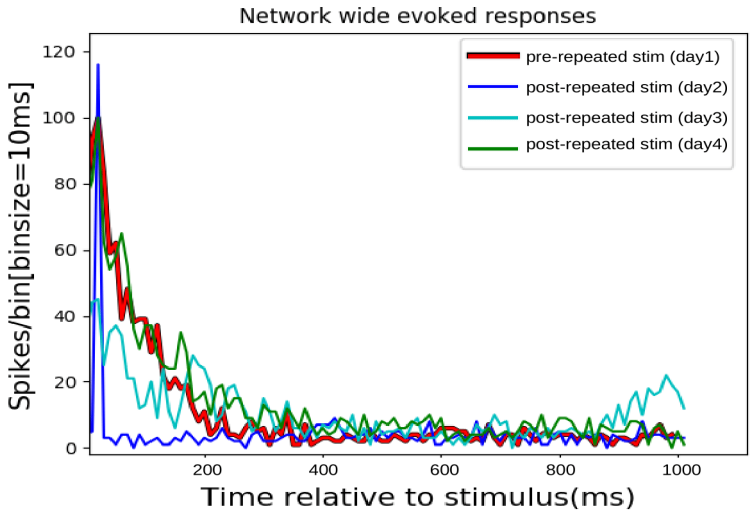

(B)

Figure 7.18: Evoked depression after stimulation. (A) Network wide response as firing rate to stimulation measured for 5 minutes after stimulation(B) Evoked response profile after the onset of single set of stimulus .

to the red trace in Figure 7.18(B). Further studies on depression behaviour is needed to draw a more reliable conclusion on this behaviour.

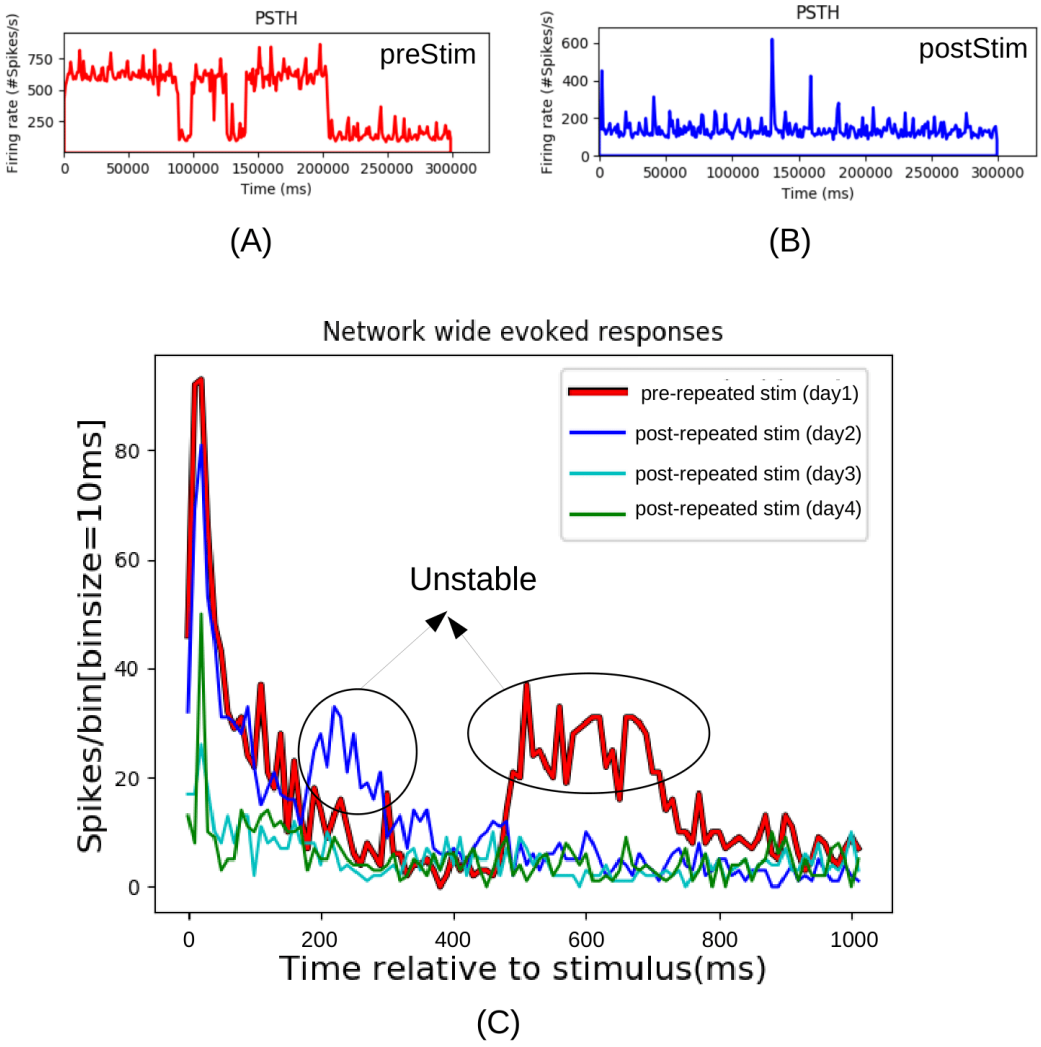

Figure 7.19: Regularisation of unstable network dynamics (A) Highly fluctuating firing rate profile before stimulation(B) Regularised firing profile into periodic bursting after stimulation (C) Network response traces after stimulation over four days which shows mitigation of unstable firing

7.4.2.4 Stimulation effect on unstable network activity

During the course of stimulation and recording, an interesting behaviour was ob- served with neuronal cultures which exhibited fluctuating firing dynamics, as opposed to regular burst firing. This was observed in two cultures.

The stimulation was conducted as normal and it was noted that the post stimulation firing dynamics were regularised into regular intervals of bursting patterns. Figure 7.19(A) illustrates an examples of unstable firing dynamics, where the firing patterns increase and decrease quite drastically, but quickly settled down into regular bursting patterns after the first set of stimulation as shown in Figure 7.19(B). The stimulation was then continued for the next three days to monitor the changes and make further analysis on whether the regularisation was by chance or if the initial unstable firing pattern was by chance and would have eventually stabilised even without stimulation.

Similar to the previous protocol, over the course of next four days, evoked network responses to stimuli (5Hz, 20 repetitions, 20seconds gap) were traced as spike counts per bin after the onset of stimuli for 1 second (Figure 7.19(C)). The first trace (shown in red) clearly shows a surge in firing at around 500ms after the stimulation, exhibiting unstable random firing. The next day's response trace (blue trace) shows reduced random bursts, and reduced temporal width of such bursts - however, the random burst was still apparent as indicated in highlighted black circle and oval (Figure 7.19(C). Subsequent days revealed that the responses were regularised and no random bursts were apparent as shown via the cyan and green line traces (Figure 7.19(C)). Also, it is clear that, the responses are depressed, as seen from the decreasing traces from day1-4 during stimulation. Even though the finding was interesting, only two samples were able to show such behaviour and further extensive work is required to draw a definitive conclusion.

7.5 Transfer entropy based connectivity inference

During repeated stimulation of neuronal cultures coupled with MEAs, long term potentiation, short term potentiation, short term depression and even stabilising effects were observed. Long potentiation experiments showed long lasting evoked responses for a particular stimulation, with evoked network wide responses observed even after 24 hours post stimulation, which were strengthened by further

repeated stimulation. Studies have shown that different emergent connectivity topologies induce different response states [116, 203]. The controlled emergence of neural connectivity, that allows quantification of neural pathways and neural interconnections is of great interest to the neuroscientific community This section utilises novel techniques developed to quantify and visualise the emergence and development of network connectivity during induced evoked responses.

The Information Theoretic Transfer entropy method, which was adapted for HD- MEA recordings (as described in Chapter 6.2), was applied to infer functional connectivity of such evoked responses during the emergence of plasticity behaviour, established by achievement of long term potentiation. Inferred connections were statistically validated and subsequently false positive connections were filtered by utilising a novel ISI distribution based surrogate method (described in Chapter 6.3), developed as part of this work.

7.5.0.1 Filtering based on novel ISI distribution surrogate method

Spike times from the neuronal recordings were used to compute delayed TE. The TE approach has gained popularity in computational neuroscience and shown better performance in comparison to popular cross-correlation, mutual information and joint entropy, being validated on synthetic data [14–16, 159]. However, for HD-MEAs with thousands of electrodes, the number of spurious and statistically insignificant connections identified can be overwhelming, since the number of possible connections increases exponentially with an increasing number of channels. In this work, MEAs have 4096 electrodes which is a significant number of channels in comparison to most reports in the literature which pre-dominantly utilise 64 or 256 channel MEAs, especially for plasticity studies. Figure 7.20(A,B) shows colour coded connectivity based on the normalised connection strength superimposed onto the MEA's 64×64 grid. Figure 7.20(A) shows an overwhelming number of inferred connections which makes it extremely difficult to see any structural or functional layout. This is why, especially when dealing with real recordings, it is critical to apply filtering to separate spurious from statistically significant connections. Figure 7.20(B) shows the post-filtered out connections after testing the statistical significance of inferred connections with the aid of

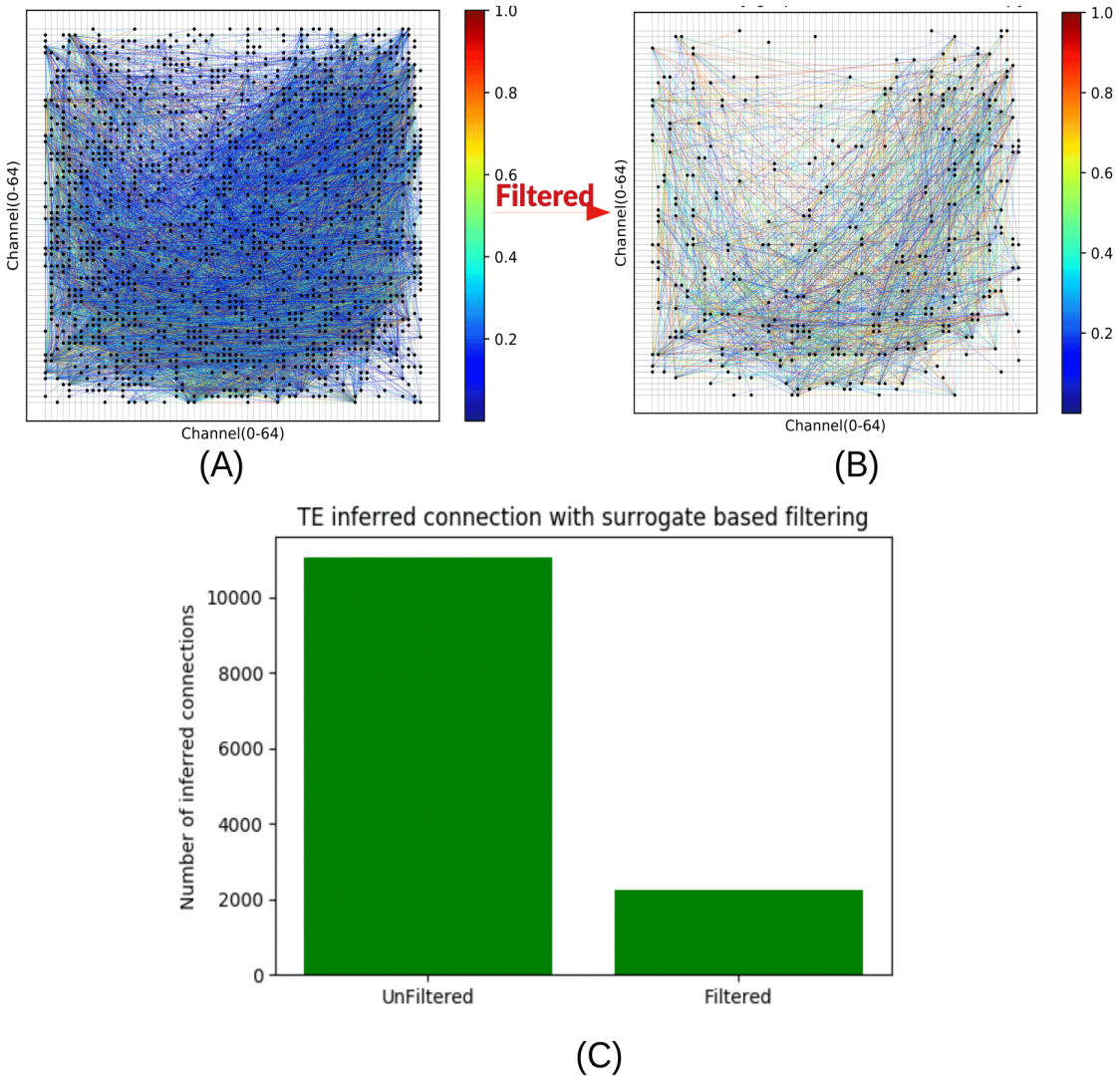

Figure 7.20: Network connectivity inference and subsequent filtering of insignificant connections. (A) Dense connectivity inferred from TE computation. (B) Connectivity map after filtering of insignificant connections identified with the aid of surrogates. (C) Number of functional connections before and after filtering. *[Heatmap colour bar in (A,B) represents normalised strength of connections based on TE values]*

the surrogate data approach discussed in Chapter 6.3. Figure 7.20(C) shows the number of functional connections before and after filtering, demonstrating a significant change.

Due to the dynamical nature of neuronal cultures, getting multiple trials is not viable as it is extremely challenging to have two cultures with statistically similar dynamics, let alone have enough trials for statistical comparison. Hence, surrogate methods are often used to obtain enough trials in such scenarios. A novel, more effective methodology designed for surrogate method was described in detail in Chapter 6.3. The method was validated with biologically realistic synthetic data based on Izhikevich's model.

Following the same methodology, 100 surrogate spike trains were generated for each spike train from the 4096 channel recordings. The algorithm described in Chapter 6.3.2.3, Algorithm I was used to generate surrogates. In order to demonstrate that the surrogates were similar to the original spike train and did not deviate from the original spike train, ISI distributions of 10 randomly sampled surrogates against the original surrogate are plotted in Figure 7.21(A). The ISI distributions were similar, though not exactly the same. This is a desired property which results in variations in the samples resulting in a much richer set of surrogates. If the distributions are very different, it indicates that the generated surrogates fail to retain ISI features leading to failure of the requirement that all except spike time features are destroyed for subsequent hypothesis testing. Furthermore, to demonstrate that ISI distributions of different spike trains are indeed different, a separate ISI distribution comparison is made. Figure 7.21(B) shows ISI distributions of five randomly selected channels. The ISI distributions are all different. Since, the surrogates generated are based on the ISI distribution of a particular target or original spike train, different ISIs will have surrogates that corresponds to their target spike train's ISI distribution. This ensures that surrogates generated for different channels are also different and relevant. An example of generated surrogate spikes can be visualised in a comparative raster plot of surrogates (in blue vertical dashes) and original (in red vertical dashes) spike trains in Figure 7.22. Even though the surrogates are very different from the original spike train, only the spike times are changed whilst following very similar ISI distribution of the original spike train.

Finally, TE for original recordings were computed and subsequent TE for each surrogate data was also computed. The statistical test described in Chapter 6.3 was performed to compute p-values. Connections that have p-values less

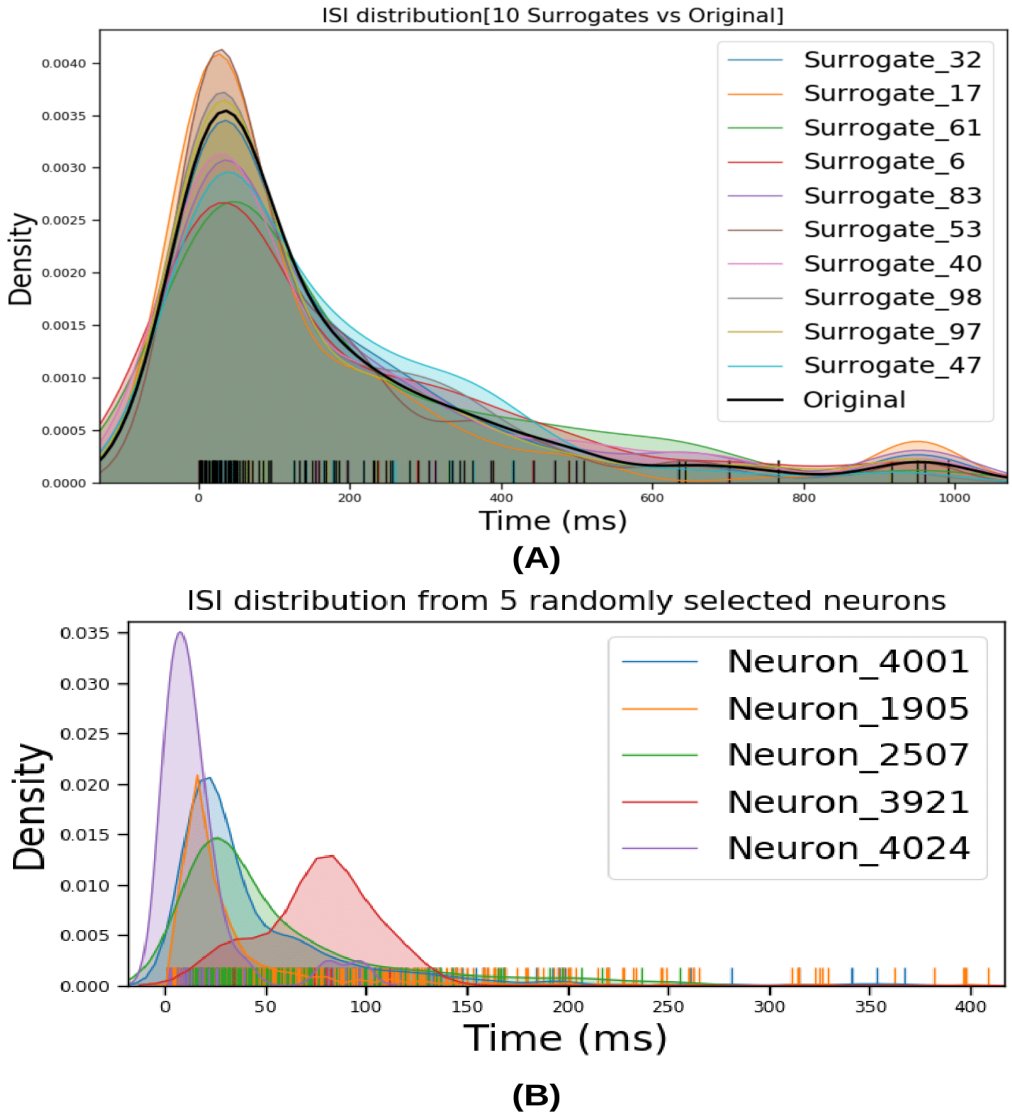

Figure 7.21: ISI distribution of surrogate spike trains and real spike trains from neuronal recordings (A)ISI distribution of 10 randomly selected surrogates vs original spike train. (B) 5 randomly selected neuronal spike trains and their corresponding ISI distribution.

than 0.05 were considered significant connections. Anything more was flagged as insignificant or spurious and discarded.

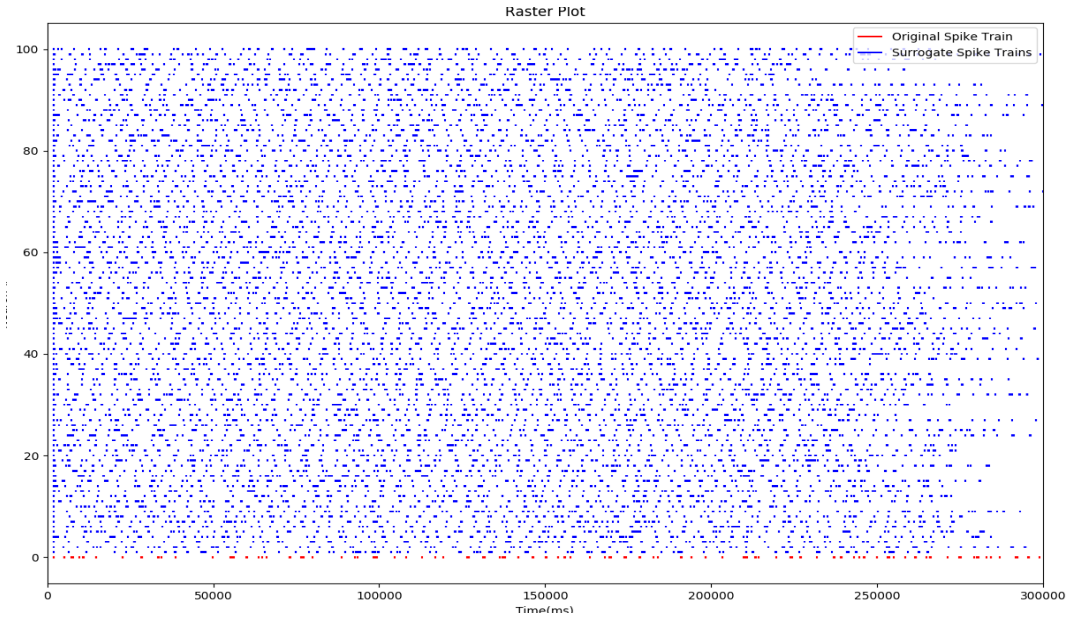

Figure 7.22: Raster plot of original spike train and its 100 surrogates

7.5.0.2 Connectivity development during plasticity

In Section 7.4, modulation of emerging neuronal dynamics by electrical stimulation was discussed. The question of whether the underlying functional connectivity is modified or not during long term plasticity, indicated by long term potentiation, is discussed in this section. Connectivity maps were mainly analysed for two conditions, (i) control - no stimulation and (ii) stimulated - long term potentiated networks.

It has been established that without external input in dissociated neuronal cultures, they maintain stable firing patterns, as well as stable connectivity [204,205] - though a slight drift in the observed activity patterns is present [204]. To ensure stability of network connectivity inferred for a stable spontaneously firing cultures that have not been subjected to any external stimulation, four connectivity maps from the same culture were plotted for each days over four days of spontaneously firing culture. This particular culture is Chip7 as mentioned in Table 7.2 as the control chip, meaning no stimulation was applied to this culture. Only spontaneous activity was recorded for 5 minutes every day for 4 days. Figure 7.23 shows the functional network connectivity, as discussed in Section 7.5.0.1, where

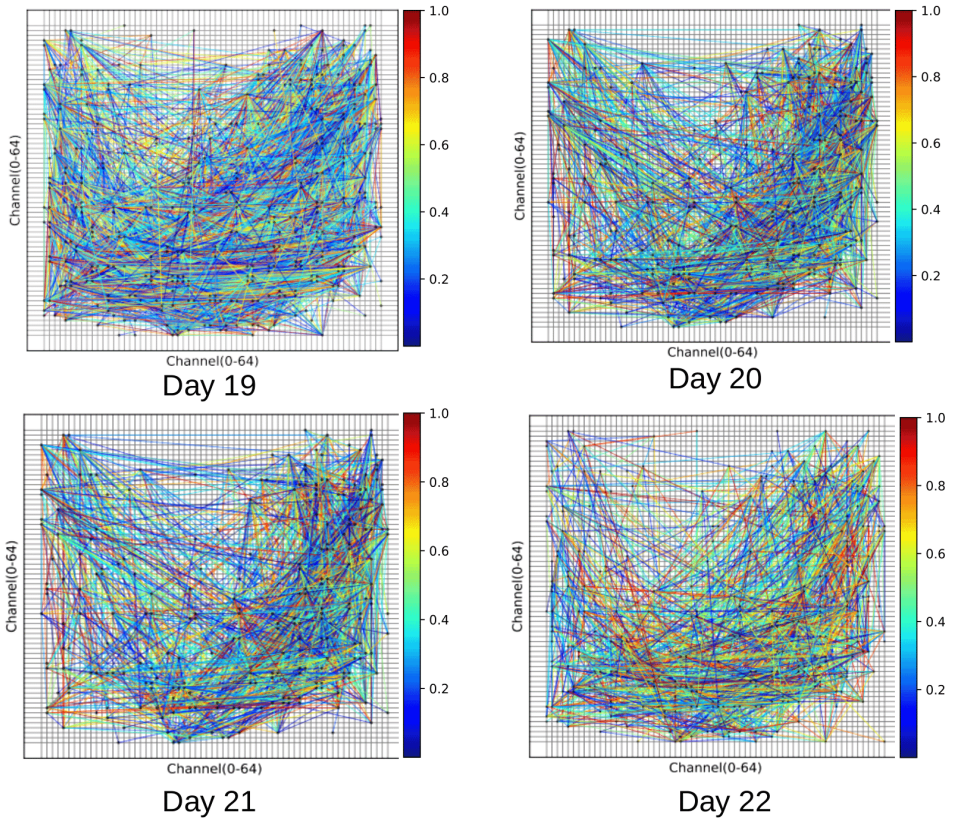

Figure 7.23: Connectivity maps of a spontaneously firing culture over 4 days without any external stimulation

each electrode is laid out in 64×64 grid, mimicking the original electrode layout. Each colour coded line is a significant connection with colours representing a heatmapped indication of normalised connection strength. Even though the inferred connections drift from one day to the next, the overall connectivity pattern is largely conserved and the pattern looks stable as previously studied [204–206]. The culture is still maturing at this stage and stronger connections become more prominent as the culture reaches day 21. This helps to establish that the connectivity inference corresponds to the stability of the network.

In comparison, connectivity was inferred for networks during induction of long term plasticity over many days, which was previously established in Section 7.4.2.2. Figure 7.24 shows the development of functional connectivity identified with the TE method. The connectivity was inferred from a spontaneously firing

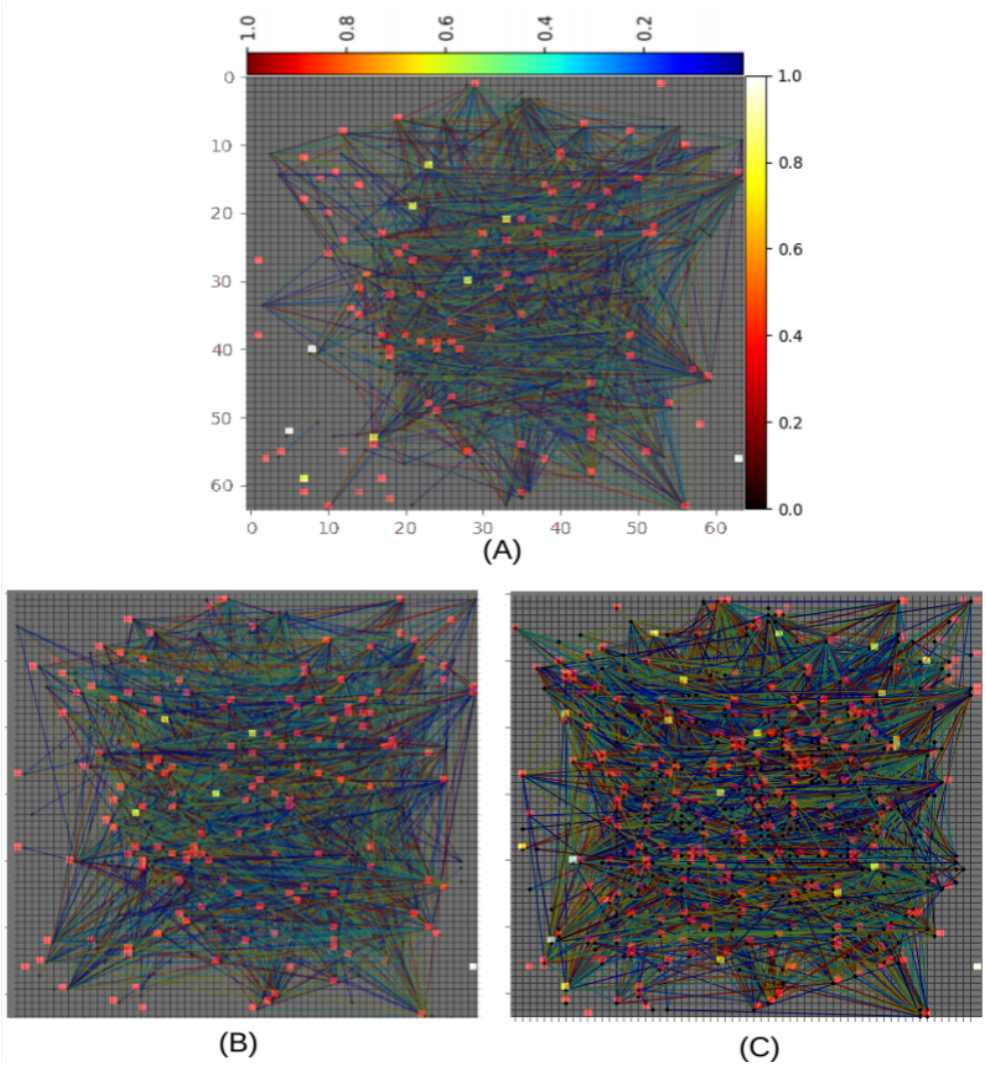

Figure 7.24: Development of functional connectivity during long term potentiation. A firing density plot is superimposed onto a connectivity map for better reference, where the most active connections are represented by red and yellow pixels. Connections are represented with coloured lines linking two channels. Horizontal colourbar represents normalised strength of connection and vertical colourbar represents normalised firing density.(A) Connectivity map during the start of controlled repeated stimulation - DIV23 (B) A day after 5 minutes of stimulation where the connections get denser with new connections clearly visible at the bottom left - DIV24 (C) Connectivity development after 3 days (5mins on each day) of repeated stimulation - DIV25

network before repeated stimulation on each day. The baseline activities were mostly focused on the middle of the chip with a rather even distribution of firing activities, with firing density indicated by pixels corresponding to the vertical colourbar (Figure 7.24(A), DIV23). Superimposition of the firing density plot showed that not all highly firing channels necessarily have a connection, and not all low firing channels necessarily do not have connections. Since TE incorporates the causal effect between two spike trains, two spike trains may be highly active but there may be no functional causal effect, which is as observed from Figure 7.24. However, the probability that highly firing neurons would have more connections remains, as discussed in Chapter 6.2.3.3.

By visually analysing the connectivity growth alongside the firing density from DIV23-25, as shown in Figure 7.24(A-C), it can be inferred that as the potentiated response growth was observed over different days, a similar growth in density of the connections was also observed. After the first day of stimulation which resulted in long term potentiation, there were lots of new connections observed on DIV24 (the bottom left of Figure 7.24(B)) even though the area was fairly active before the stimulation, as can be seen with density plots on the bottom left of Figure 7.24(A) at DIV23. The connections at DIV25 (Figure 7.24(C)) get even denser as further stimulation which successfully resulted in a long term evoked responses, whilst maintaining the general area of the activity patterns. The physiological explanation of development of connections could potentially be explained by STDP rule, which states that many action potentials occurring during repeated stimulation fall in the time window of STDP, leading to strengthening of synaptic efficacy and hence helps to establish a connection [77, 78, 82].

The increments in firing density and corresponding number of connections were also analysed. Figure 7.25 shows the normalised increment rate for the firing rate and inferred connections. With a small increment in network wide firing rate, there was a much larger increment in new connections, observed at day24 after the stimulation. It appears that the number of new connections starts to increase rapidly and slows down as the network adapts its responses to a particular stimulation, even though the network wide firing keeps increasing.

By utilising the TE based connectivity inference method, alongside the novel

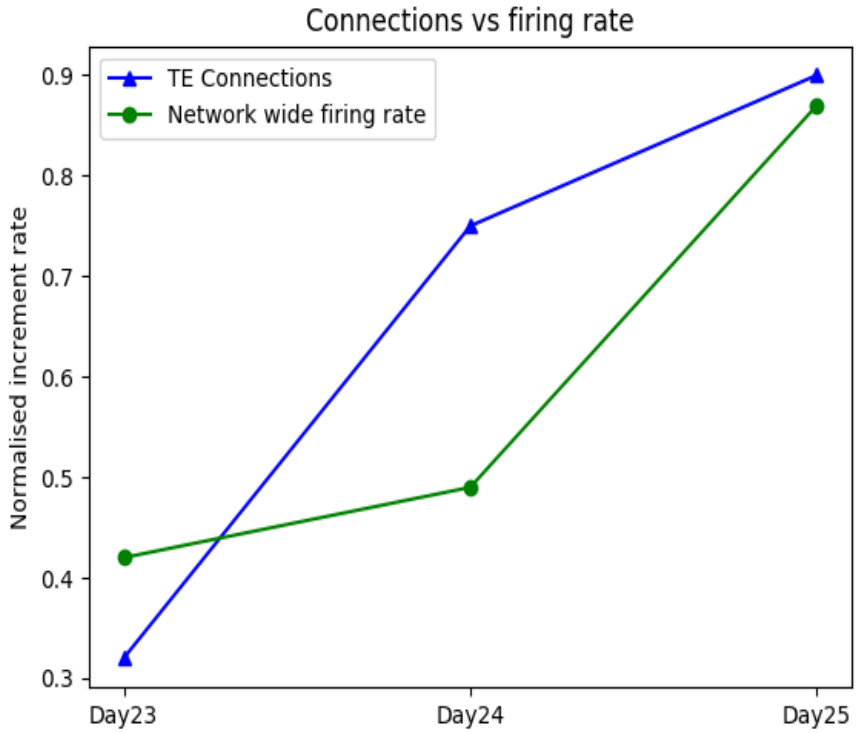

Figure 7.25: Increment rate of firing density and network wide connections over 3 days of long term potentiation

ISI distribution based surrogate method, it was possible to monitor and visualise the connectivity growth during long term potentiation induced by repeated stimulation. Due to the fact that these data arise from real experimental recordings, ground truth information cannot be obtained. However, the surrogate method helps to mitigate the uncertainty with statistical testing to filter out only the relevant connections. The addition of structural information from fluorescence images could possibly supplement the surrogate method as well [126, 207], but is beyond the scope of this thesis.

7.6 Discussion and conclusions

This chapter mainly focused on the induced evoked responses in the presence of controlled repeated stimulation. A systematic selection criteria was determined and followed, so as to select only those cultures that were both responsive to external stimuli and simultaneously stable. These are important aspects to avoid unwanted biases in the dataset.

After manual optimisation of stimulation protocols, two main types of stimulation were selected based on frequency(2Hz and 5Hz) and number of stimulation sites(single site, multi-site). Single site stimulation resulted in no significant sustained network response change. The post stimulation evoked responses to the same stimulation were also not different from pre stimulation responses, indicating that the culture had not actually responded to the stimulation. However, 5Hz multi-site stimulation (from two separate sites) was able to successfully induce long lasting network potentiation (LTP) which was consistently stable over the next day. The response curve also showed that the network responses to the same stimulation were indeed changed after the stimulation. Both the response trace and the overall network potentiation were evidence that the stimulation had induced network responses as a consequence of that particular stimulation - *"induced plasticity"*. Similar potentiation effects were also observed in other cultures. During optimisation, it was found that the stimulation site and the initial response during selection play a key role in determining possible responses to stimulation. The stimulation site was critical because where the stimulation was applied greatly affected which part of the culture was affected. Neuronal cultures have mixture of excitatory and inhibitory neurons and both respond differently to external inputs.

Induced depression effect was also observed. The cultures that initially demonstrated induced depression exhibited the depression effect throughout the stimulation stage, regardless of stimulation. Unlike LTP, the depression effect was short lived. The network depressed significantly after the stimulation, but recovered after a few days. The response curve confirmed this observed pattern . The cellular distribution of excitatory and inhibitory neurons during the initial seeding may be the probable cause that dictates potentiated response or depressed

response. However, due to an insufficient number of culture samples displaying this effect, no substantial further analysis was performed.

Additionally, an interesting behaviour of stabilising/regularising effect of stimulation on the cultures that exhibited unstable network dynamics was also observed, whereby firing patterns were stabilised with repeated stimulation. However, it is problematic to infer cause and effect in this context - i.e. just from the dynamics of the firing pattern. There could potentially be no effect from the stimulation, and the culture could already be stabilising on its own - though the cause for such unstable firing was not clear. The response curve after stimulation, however, showed that the network response before and after stimulation of such unstable cultures were indeed different, where the response changed from multi-peaks unstable to gradually decreasing single peak stable responses. Although this is not sufficient evidence, the result is indicative of some effect of the stimulation in terms of network stabilisation, as shown by the gradual decrease in unstable evoked response (Figure 7.19(C)).

The ISI distribution based surrogate method developed as part of this thesis and discussed in Chapter 6 was applied to neuronal recordings to analyse network connectivity development during plasticity behaviour. The fact that without any external input, a culture maintains stable firing activity [204, 205], inferred connections were tested firstly to monitor if inferred connections from a control culture without any external input over 4 days would show consistent connectivity patterns. The connectivity over 4 days of the control culture was found to be very similar which indicates that the TE computation and the surrogate based filtering were consistent over same culture recorded over many days without any external stimulation. Furthermore, the network analysis of LTP induction after stimulation also showed a good correspondence with the firing density. New connections were observed after the network achieved *"learned"* state, due to repeated stimulation. The connections kept getting denser with subsequent strengthening of LTP. The relationship between the increase in connections and firing density, was clearly not linear. The number of connections grew much rapidly in comparison to the firing density increment, which later slowed down as the LTP got stronger.

To summarise, a systematic method of assessing neuronal cultures for induction of evoked responses persisting for days has been achieved. The network

dynamics during the stimulation process were analysed and response traces confirmed adaptation of stimulation to a different response, which at a low level can be referred to as “learning”. In addition, a connectivity analysis was performed and a novel ISI distribution based surrogate method, developed as part of this work, has been applied to real recordings of hippocampal cultures during induced network responses.

Chapter 8

Summary and conclusions

The aim of this thesis has been to utilise state-of-the-art CMOS based MEAs to study neuronal dynamics, focused on induced plasticity behaviour and to develop novel methods for network connectivity analysis. This necessitated the development of multidisciplinary expertise across bioscience, computing and electronics. The establishment of successful growth and maintenance of dissociated neuronal cultures on CMOS based MEAs was achieved, with cultures remaining healthy for a prolonged period of time (up to 4 weeks). These cultures then enabled successful electrophysiological recordings on a 3Brain MEA system. A systematic selection of neuronal cultures for plasticity studies was found to be paramount and determined the evoked responses.

High density MEAs produce huge datasets even for short recordings, necessitating developments of analytics techniques to gain an understanding of the neuronal dynamics. Computational tools and techniques to facilitate the analysis of neuronal dynamics and functional connectivity during induced long term responses were developed and validated. The investigations in this thesis mainly covered experimental contributions and algorithmic/computational tool development for electrophysiological recordings. In this chapter, a summary of the key contributions of this thesis are provided followed by a description of potential future directions.

8.1 Summary of key contributions

The main contributions of this thesis can be summarised into two categories:

Computational contribution

There are three main computational contributions presented in this thesis.

1. Two mathematical metrics, ISI-distance and SPIKE-distance, to quantify neuronal synchrony, which are based on the temporal interactions between groups of neurons, were adapted for large HD-MEA recordings. These were demonstrated to be effective in identifying and quantifying synchronous patterns. This contribution was also accepted and presented in the 2018 IEEE IJCNN conference and subsequently published in the IEEE proceedings. (Chapter 5)

2. Transfer entropy(TE), an information theory based approach, to infer functional connectivity was applied to HD-MEA neuronal recordings. To supplement TE inference, a novel firing density superimposition method was proposed as an alternative to ground truth information for better confidence in the inference. The method showed a good fit between the firing density plot and the inferred connectivity for real experimental recordings. This contribution was also accepted and presented in the 2019 IEEE IJCNN conference and subsequently published in the IEEE proceedings (Chapter 6.2)

3. A novel ISI distribution based surrogate method to compensate for the lack of ground truth information by generating surrogate data was developed. The proposed method generates enhanced surrogate data due to variations in- troduced during the sampling process. The method was validated with a realistic Izhikevichs network of 1000 neurons and ROC analysis showed a superior performance in comparison to an existing ISI shuffling method. (Chapter 6.3)

Experimental contribution

There are three main experimental contributions presented in this thesis.

1. Development and optimisation of cell culture methods for sensitive CMOS based MEAs so as to successfully grow and maintain dissociated neuronal cultures for prolonged periods (up to 4 weeks). It is extremely difficult to grow high quality cell cultures on CMOS based MEAs, which unlike glass substrates, have surfaces less conducive to healthy cell growth. In Chapter 4.2, a method for optimising MEA chip preparation was presented, along with general cell culture methods. Humidity and evaporation was found to be crucial to avoid early cell death during incubation. To mitigate this issue, a custom made humidity chamber was designed for each chip to allow enough humidity and reduce rapid evaporation.

2. Establishment of neuronal cultures for plasticity studies and design of criteria to select potential cultures for plasticity based on responsiveness, stability and firing rate. A systematic selection criteria were utilised based on (i) firing rate, (ii) firing stability and (iii) responsiveness to stimulation to ensure that the neuronal cultures met standards for evoked responses to stimulation. Such selection criteria determine different network responses to repeated stimulation. (Chapter 7.2, 7.3 and 7.4)

3. Stimulation protocol selection to induce wide range of evoked network responses. Multi-site and single-site stimulation were explored where only multi-site stimulation was found to evoke long lasting responses. Furthermore, 2Hz and 5Hz frequencies were explored. Multi-site 5Hz stimulation was able to induce LTP responses sustained over many days. (Chapter 7.5)

4. Network connectivity development during plasticity based on TE method supplemented with proposed surrogate method. The developed superimposition and ISI distribution based surrogate methods were applied to the LTP responses recorded over many days. The developed methods were able to identify and track statistically significant network connections developed over the period of 3 days. (Chapter 7.6)

Further discussion on the contributions are presented.

8.2 Neuronal synchrony analysis

During the early stage of establishing cell culture methods for stable cell growth, neural synchrony metrics were adapted and applied to identify synchronous patterns from spontaneously firing neuronal cultures from 3Brain HD-MEAs (Chapter 5). Neural synchrony quantifies temporal correlation between spike trains and can provide great insights into neuronal response pattern to different stimulus and the assessment of neural populations in neural coding [182]. The ISI-distance and SPIKE-distance metrics for spike train synchrony analysis have been applied to HD-MEA datasets. Theses exploit parallel processing and informative selection of a subset of the dataset to quantify and characterize bursting behaviours in large datasets. The metrics used were first validated with a smaller synthetic dataset that had deliberately incorporated varying degrees of synchrony. Both bivariate and multivariate analysis were performed. The method was also shown to be applicable to larger HD-MEA experimental dataset. The ability to utilise such metrics especially on large scale experimental biological datasets such as those generated from HD-MEA recordings is invaluable in studying various neuronal properties that underlie many neurological disorders.

8.3 Transfer entropy connectivity estimation

To infer functional connectivity, an information theory based transfer entropy approach was utilised in Chapter 6. Firstly, the method was thoroughly validated with a biologically realistic simulated network with the STDP learning rule, synaptic delays and a mixture of excitatory and inhibitory neurons. The TE connectivity inference method was then applied to experimental HD-MEA recordings of spontaneously firing hippocampal cultures. Unlike simulated data where the ground truth connectivity is available against which the estimated connectivity can be compared, experimental data lacks this information, making distinguishing true from spurious connections a difficult problem. To tackle this problem, a superimposition method was developed, where the estimated connectivity is superimposed onto the firing density plot to test if the estimated connectivity corresponds with the firing density plot and to give confidence in us-

ing the derived connectivity for further analysis (Chapter 6.2.3.2). The method demonstrated that this approach, i.e. the estimations of connectivity when superimposed onto the firing density plots show a good fit. However, the method itself doesn't provide any statistical significance testing of inferred connections.

Ideally, multiple trial measurements are conducted under the assumption of the same condition to compute statistical significance of the measurements and gain confidence in the inference. However, living dissociated neuronal cultures are non-stationary and always evolving with time which makes the multiple trial measurement unfeasible. As the culture matures and evolves it might respond differently from trial to trial; this problem is exaggerated in stimulation based experiments. To overcome this problem, a novel surrogate method based on the ISI distribution was proposed to generate multiple trials (Chapter 6.3.2). In contrast to existing methods [167–169], which are direct manipulation of the spike train to generate surrogate data, the proposed distribution based approach adopted sampling from the ISI distribution of each spike train such that the ISI and firing rate information are not destroyed, but only temporal information in the spike train is destroyed. The sampling process enables the achievement of surrogates with the ISI distributions as close approximation to the original ,but not exact copies. This introduces enhanced controlled variation in the surrogate data, hence a richer set of surrogates. The proposed method was validated with simulated data and was able to accurately determine statistically significant connections from non-significant connections. In addition, the method was also able to detect the strength of the inferred connections based on $p - value$. The method was compared with the closest method, ISI shuffling, which showed an improved accuracy of 93% at 0.01 false positive rate from 80% for the ISI shuffling method. To strengthen the connectivity inference, incorporating structural information from fluorescence imaging [126, 207] may help refine network connectivity.

8.4 Controlled repeated stimulation to induce long term plasticity

In Chapter 7, the declared goal of inducing plasticity on neuronal cultures growing on MEAs, by integrating methodologies and computational tools developed in the preceding chapters was delivered. In particular, contributions in the experimental aspect of the project were presented. Building on the cell culture, electrophysiology and computational tools discussed thus far, stimulation experiments were performed and recordings analysed. Systematic selection criteria were utilised based on (i) firing rate, (ii) firing stability and(iii) responsiveness to stimulation (Chapter 7.4) to ensure that the neuronal cultures met the standard to evoke responses to stimulation. Such selection criteria determine different network responses to repeated stimulation.

Two different stimulation frequencies were applied, 2Hz and 5Hz. Manual optimisation of stimulation revealed that stimulation at frequencies greater than 5Hz for multi-site stimulation resulted in saturation of electrodes; while stimulation under 2 Hz led to no discernible evoked responses. It was demonstrated that single site stimulation was not able to evoke long lasting responses (Chapter 7.5.1). Multi-site stimulation with 5Hz pulses was able to induce LTP, which was sustained consistently over many days (Chapter 7.5.2). LTP responses became stronger with repeated stimulation. The response curve also showed that the network responses to the same stimulation was indeed changed after the stimulation. Both the response trace and the overall network potentiation were in agreement that the stimulation had induced network responses adapted for that particular stimulation - "*induced plasticity*". However, during optimisation, it was found that the stimulation site and initial response during selection play a key role in determining possible responses to stimulation. Such a systematically detailed method of selecting cultures and inducing LTP for CMOS based HD-MEAs has not conducted before and is potentially an effective experimental model to study many neurophysiological disorders.

In addition to LTP, induced depression effect was also observed (Chapter 7.5.2.3). It was found that the cultures that initially demonstrated induced depression exhibited depression responses throughout, regardless of stimulation.

The induced depression effect, however, was short lived and didn't show evoked response son subsequent days. During stimulation, the network depressed significantly after the stimulation, but recovered after a few days and the stimulation had limited effect compared to LTP. Hence, LTD effect was not observed with those cultures. The cellular distribution of excitatory and inhibitory neurons during the initial seeding may be a probable cause that dictates potentiated response or depressed response, but substantially more culture samples are needed to further study this effect, with extensive biological analysis.

Additionally, an interesting stabilising/regularising effect of stimulation on the cultures that exhibited unstable network dynamics was also observed (Chapter 7.5.2.4) in two cultures. It is therefore problematic and scientifically unsound to infer from the dynamics of just two samples. There could potentially be no effect of the stimulation, and the culture could already be stabilising on its own - though the cause for such unstable firing was not clear. The response curve, however, showed that the network response before and after stimulation of such an unstable culture were indeed different where the response changed from unstable multi-peaks to gradually decreasing single peak stable responses.

The work presented herein has demonstrated that multi-site stimulation (2 channel) was able to induce LTP; however, the initial conditions of the culture determine the type of responses evoked with repeated stimulation. For reliable LTP induction, cultures that exhibit potentiated responsiveness with test stimulus are the best candidates. However, substantially more culture samples would be needed to establish a set of parameters that could reliably lead to controlled, programmable plasticity. Further experimentation is required to better understand how depression evoked responses are caused and if the cell composition of excitatory and inhibitory actually plays a role in determining the type of evoked responses.

Furthermore, connectivity analyses based on transfer entropy was applied to neuronal culture recordings during induced plasticity (Chapter 7.6) . The algorithm proposed and developed as part of this thesis work (Chapter 6) was applied to real experimental recordings of spontaneously firing cultures over 4 days and also during evolvement of connectivity during induced plasticity. Neuronal cultures without any external input maintain a stable firing activity [204, 205]. The

developed ISI distribution based surrogate method showed very similar connectivity on spontaneously firing cultures over 4 days of recording(control culture without stimulation). When applied to LTP recordings over 3 days, the network analysis of LTP induction after stimulation also showed a good correspondence with the firing density. New connections were observed after the network achieved a newly learned state, due to repeated stimulation. The connections kept getting denser with subsequent strengthening of LTP. The increment in connections and firing density were not however found to have a clear linear relationship. Connections grew much more rapidly in comparison to the firing density increment, which later showed slower increment as the LTP got stronger. The TE method and the proposed surrogate method can be a vital addition in the area of computational neuroscience and could facilitate robust statistical analysis from dynamical systems such as neuronal cultures.

8.5 Future work

The work presented in this thesis demonstrated a significant body of work in induced plasticity behavior and development of novel computational tools. However, this is a rapidly developing field and major challenges remain. Two main directions - 3D neuronal cultures and closed-loop systems, are identified to extend and explore this research.

8.5.1 3D neuronal cultures

The work presented so far established computational tools and experimentation for studies focused on neural plasticity and connectivity development based on 2D planar substrates. Such 2D *in-vitro* models utilised in this work are currently the gold standard models to investigate various neurophysiological mechanisms. However, they offer a limited representation of the true 3D *in-vivo* like environment in terms of cell morphology, cell-to-cell interaction and neurite growth [208]. The logical next step is to extend the approaches in this thesis to 3D multi layered architectures, where the cell growth is not limited to planar 2D surface but exhibits growth in the z-direction.

An increasing number of studies have shown that cells grown on a planar 2D substrate do not have the same cell morphology [209], proliferation rates [210], gene expression [211] in comparison to 3D culture. Also, 3D culture of neuronal cells have shown longer neurites growth and cell longevity [212, 213] with much more rounded and bulbous shape of the somata [214]. In addition, 3D neuronal culture may be more suited for electrophysiological studies. Studies have shown that Ca^{++} dynamics are over exaggerated in 2D neuronal culture environments as compared to the 3D environment [215, 216]. Calcium is an important signaling molecule that regulates a variety of functions such as synthesis and release of neurotransmitters, neuron excitability and also long term effects such as memory [217].

Some preliminary works have been attempted towards 3D neuronal cultures as summarised below.

8.5.1.1 3D structures based on glass microbeads scaffold

Two main approaches have been utilised in attempts to engineer 3D neuronal culture that mimics cell density and connectivity similar to the *in-vivo* - polymer gels and solid porous matrices. The cell viability in 3D neuronal cultures depends on the cell density. Using polymer gels and solid porous matrices, the cell density was observed to be around 3750 cells/mm^3($500 - 600$µm thick cultures) [218] which is much lower than the in-vivo situation. For example, the cell density measured in the mouse brain cortex is about 91,000 cells/mm^3.

In contrast to these methods, Pautot et.al [219] successfully demonstrated growth of dissociated neurons on moveable spherical glass beads of nominal diameter of 40 ± 2 µm allowing for mechanical manipulation to form multiple layers, with the possibility of seeding different types of neurons on each layer (Figure 8.1). The glass beads self assemble into uniform hexagonal arrays. Each bead is large enough to provide an adhesion surface for neurons to grow upon. By altering the size of the glass beads, it is possible to obtain cell densities of up to 75,000 cells/mm^3 [220] which is close to the real *in-vivo* cell density.

This method along with further works by Frega et al [3] who demonstrated successful coupling of such colloid scaffolds with glass based MEAs by stacking

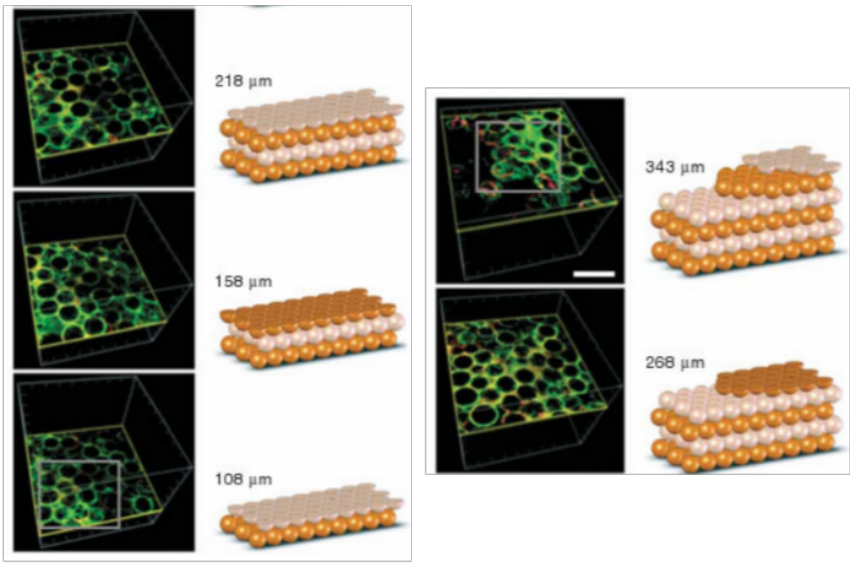

Figure 8.1: Self assembled 3D neuronal network with glass micro beads. Three week old culture of 3D neuronal network assembly fixed and stained with the neuron-specific antibody to alpha tubulin (green) and the glial-specific antibody to GFAP (red). Five layers, a $450 \times 450 \times 388$ µm volume of the assembly, were imaged by confocal microscopy. The images extracted from the z-stack for the green and red channels (left) are shown with schematic representations of the corresponding layer position (right). From Pautot et al [219]

layers of glass beads in a constrained structure onto MEA surface has opened up new ways to perform electrophysiological studies in a 3D neuronal culture.

Reported blow are some preliminary studies on 3D structures utilising glass beads, performed as part of this research.

8.5.1.2 Neuronal culture on glass microbeads

Glass microbeads of nominal diameter of 40 ± 2 µm (Distrilab-Duke Scientific, The Netherlands) were sterilized in 70% ethanol in a conical vial for 2 hrs whilst gently shaking every 30 mins. The beads were rinsed with sterilized water for 3-4 rinses. The vial was further sterilized in a UV chamber for 20 mins and again rinsed with sterilized water for 2 rinses. Microbeads were coated with adhesion factors, laminin and poly-D-lysine(PDL) at 50µg/ml and incubated overnight at 37°C. 95% of the coating factor was aspirated the next day and rinsed once with

sterilized water. Again, 95% of water was aspirated and the vial was filled with NbActive 4 growth media. Using a coarse pipette, 200 µl of treated microbeads were distributed onto a multi well plate with membrane insert with pore diameter of 0.4µm where glass beads self-assembled into a uniform layer. Figure 8.2(A) shows an illustration of the process. Each membrane well was filled with 0.5ml of complete growth media and left in the incubator until the neurons were ready for seeding.

Due to their smaller diameter, which helps to form a layered network with fewer glass beads, 96 well plates were used for this part of the experiment. The well plate was coated with laminin and PDL at 50µg/µl and left overnight at 37°C in the incubator.

After the cell dissociation, a cell density of about 1000 cells/µl was obtained and about 150 µl of the suspension was distributed on the surface of the microbeads, resulting in about 150,000 cells. The process can be visualized with the illustration presented in Figure 8.2(B). Meanwhile, 30,000 cells i.e. 30µl of the suspension was also seeded on to the well plate to form a bottom layer of neurons. After 6-8 hours, the suspension with glass beads, with neurons attached, was transferred from the transwell into 96 well plates with about 50µl at each succession as shown in Figure 8.2(C). This duration allows glass beads to self assemble into a uniform layer as shown in Figure 8.3. Finally, 300 µl of growth media was carefully added and incubated at 37°C in the incubator.

Brightfield images from different regions representing different density of glass beads were captured to demonstrate neuronal growth. The reason for showing low beads density regions is to show neuronal growth along side beads. When there are multiple layers of glass beads, it becomes extremely difficult to visualize neuronal growth with just bright field images. Confocal fluorescence image characterization helps to characterize cell growth when it is visually difficult to characterise and is discussed later in Section 8.5.1.3

The top three images of Figure 8.4 show neuronal growth at day 7. Glass beads and neurite projections are indicated by arrows. Neurons survive for up to 4 weeks. The bottom three images in Figure 8.4 show neurons growing at day 28. By this point, neurons are mature and also form clusters of neurons to improve survival. The top right and bottom right images has multi layered glass beads

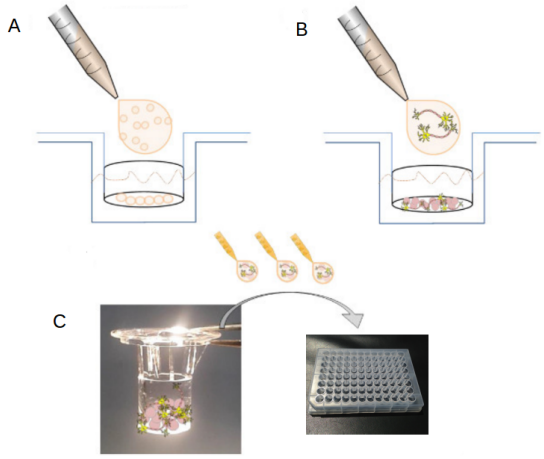

Figure 8.2: Illustration of steps to create a multilayered 3D structure with stacked micro glass beads (A) Glass beads self assembling on transwell membrane insert. (B) Neurons seeded on the assembled glass beads (C) Transfer of glass micro beads with neurons attached into 96 well plate with succession with a minute interval [221]

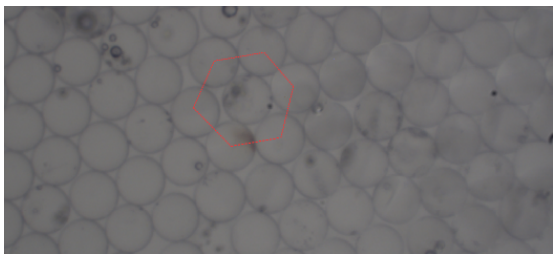

Figure 8.3: Micro glass beads self assembling into a uniform hexgonal topology. Hexagonal topology outlined with dotted red lines

indicated by arrows.

8.5.1.3 Fluorescence Image Characterization

Neurons growing on glass micro beads stacked scaffolds were fixed and stained with neuron specific anti-βIII tubulin antibody. The fluorescence images were acquired using a Leica confocal microscope. Neurite extensions are marked with a red colour while the blue colour shows DAPI stained nuclei as shown in Figure 8.5. In the same figure, the black circular voids shown in yellow rectangles and circle(indicated with arrows) are the glass beads which are not stained resulting

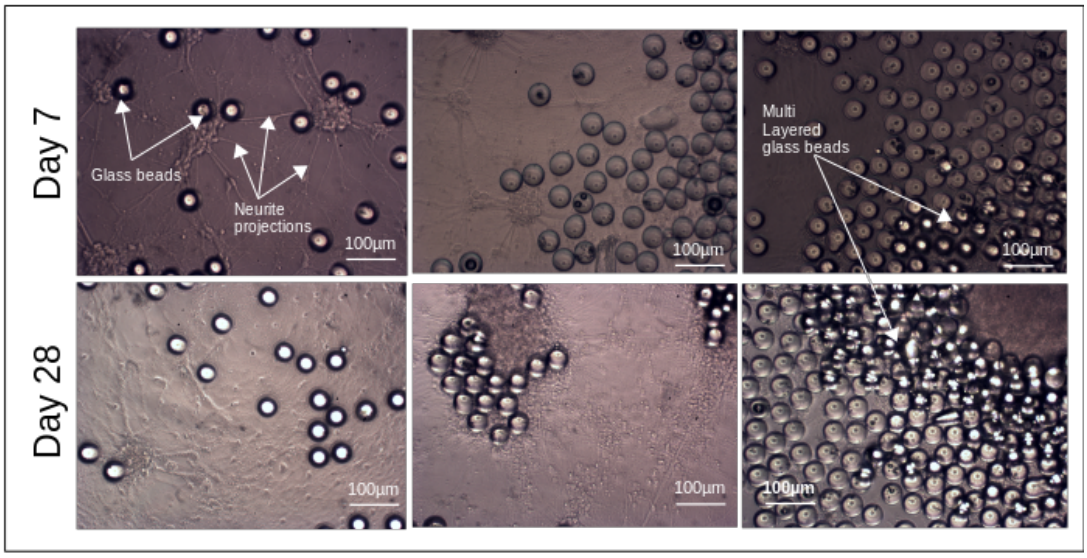

Figure 8.4: Neuronal growth on and along micro glass beads. The arrows show glass beads, neurite projections and regions of multi layered stacked beads. Glass beads density increases from left to right.

in black circular voids. Looking into yellow rectangles, it is clear that the neurons, indicated by blue dots, are growing around the glass beads. For example, a yellow circle in Figure 8.5 shows a neuron growing directly on top of the bead indicated with a DAPI stained blue dot. For a better characterization of 3D scaffolds, z-stack images of the culture are needed which can be merged offline to produce a 3D image.

So far only 3D growth on well plates was achieved. Methodology optimisation and viability tests can be seen as future work to move towards a 3D culture that can be coupled with sensitive CMOS based HD-MEAs to study plasticity and make comparisons with 2D culture plasticity.

8.5.2 Closed-loop system - Neurorobotic systems

The STDP rule states that if two synaptically connected neurons fire within tens of milliseconds of each other, the connectivity strength of the synapse gets potentiated or depressed, depending on the order with which the spiking event happens [78, 82]. The brain is a feedback system exhibiting a learning process,

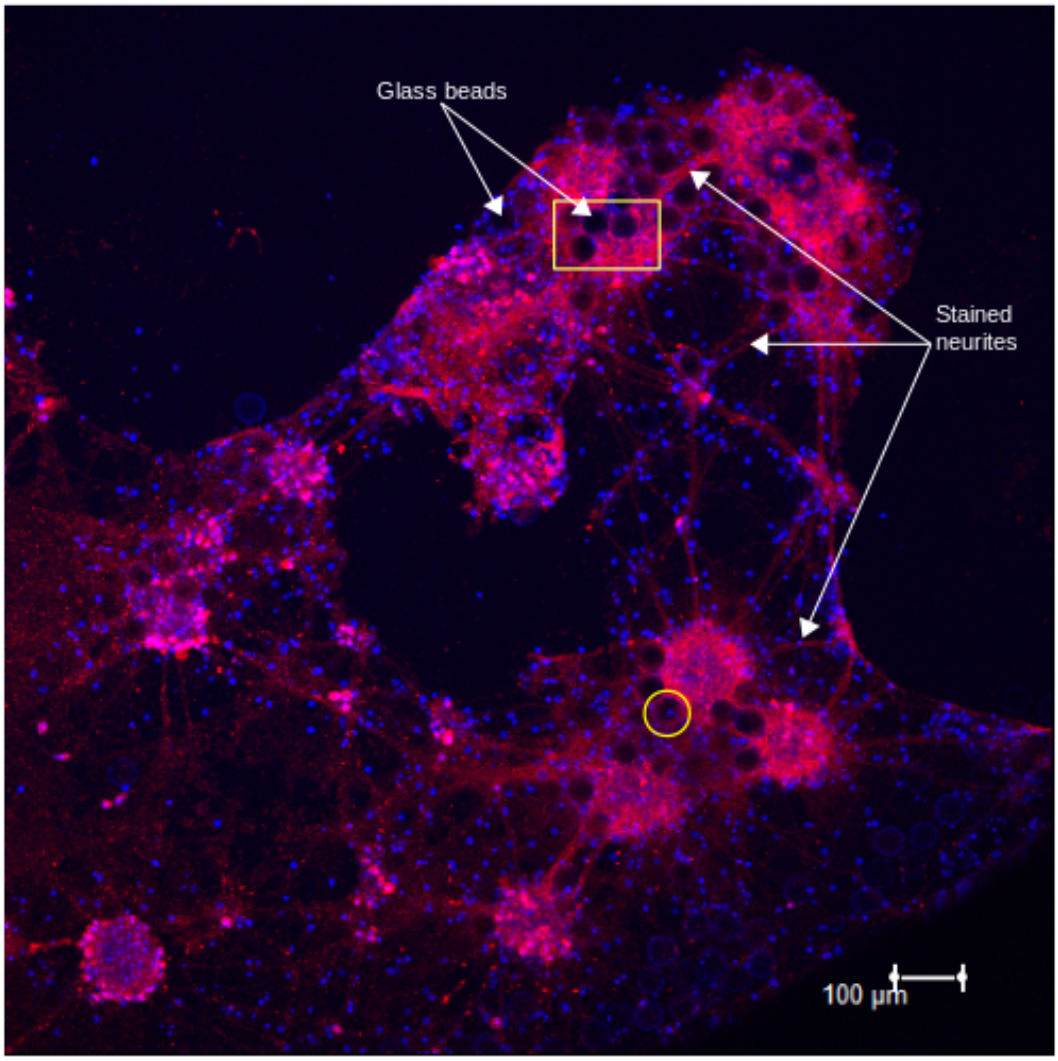

Figure 8.5: Fluorescence images of a neuronal culture on a monolayered glass beads stained with anti-βIII tubulin and DAPI stained nuclei. Glass beads and neurites are shown with arrows. A yellow circle shows neuron growing on the glass beads as indicated with a DAPI stained nuceli (blue dot) on the glass bead.

essentially strengthening or weakening connections. The ability to create a closed loop circuit between input stimulation and output neural recording would allow for precise control over stimulation at time t based on the output at time $t-1$. The cultures could be subjected to true learning where cultures learn or adapt to input stimulation based on the output signals.

To date, plasticity studies in closed-loop experiments investigate whether such models may be taught to learn a particular task without the need for a separate rewarding entity [7, 146, 222–224]. The stimulation is modulated based on the output to force the culture to produce a specific patterns. Potter's group [146] utilised such a neuronal culture to control the movement of an "animat"(i.e. artificial animal). The training was done by delivering a stabilisation pattern every time the animat approached the intended location, and conversely delivering stimulating signals to provoke a change in the animat's behaviour. The movement of such an animat is controlled by a biological neuronal culture - hence the name neurorobotic system.

The ability to take into account the output signals to modulate the responses to input signals in a. feedback loop is a close approximation of in-vivo like learning in a closed-loop system. Combining a 3D culture with a closed-loop system could establish ground breaking experimental models to study, not just learning and memory, but also various neurological diseases.

Furthermore, such experimental model could potentially be utilised to study the pharmacological effects of drugs in learning and memory, the understanding of which is crucial in the study of memory related neurological disorders such as Dementia and Alzheimer's.

All recordings are stored as HDF5 data format which is a hierarchical data format with embedded metadata in a single individual file. All data are stored in Computational Neuroscience and Cognitive Robotics (CNCR) group's data server within Nottingham Trent University and can be made available with Prof Martin McGinnity's permission

References

[1] Shimon Marom and Goded Shahaf. Development, learning and memory in large random networks of cortical neurons: Lessons beyond anatomy. *Quarterly Reviews of Biophysics*, 35(1):63–87, 2002. 1, 33

[2] Chadwick M Hales, John D Rolston, and Steve M Potter. How to Culture, Record and Stimulate Neuronal Networks on Micro-electrode Arrays (MEAs). *Journal of Visualized Experiments*, (39):39, 2010. 1, 37

[3] Monica Frega, Mariateresa Tedesco, Paolo Massobrio, Mattia Pesce, and Sergio Martinoia. Network dynamics of 3D engineered neuronal cultures: A new experimental model for in-vitro electrophysiology. *Scientific Reports*, 4, 2014. 1, 35, 37, 144, 196

[4] Eisaku Maeda, Yoichiro Kuroda, Hugh P. C. Robinson, and Akio Kawana. Modification of parallel activity elicited by propagating bursts in developing networks of rat cortical neurones. *European Journal of Neuroscience*, 10(2):488–496, 1998. 2, 35, 38, 39, 42

[5] Yasuhiko Jimbo, Hugh P.C. Robinson, and Akio Kawana. Strengthening of synchronized activity by tetanic stimulation in cortical cultures: Application of planar electrode arrays. *IEEE Transactions on Biomedical Engineering*, 45(11):1297–1304, 1998. 2, 39, 42, 43

[6] Takashi Tateno and Yasuhiko Jimbo. Activity-dependent enhancement in the reliability of correlated spike timings in cultured cortical neurons. *Biological Cybernetics*, 80(1):45–55, 1999. 2, 39

[7] Goded Shahaf and Shimon Marom. Learning in Networks of Cortical Neurons. *The Journal of Neuroscience*, 21(22):8782–8788, 2001. 2, 15, 35, 39, 45, 202

[8] Daniel A Wagenaar, Jerome Pine, and Steve M Potter. An extremely rich repertoire of bursting patterns during the development of cortical cultures. *BMC Neuroscience*, 7, 2006. 2, 33, 35, 36, 39, 40, 43, 113, 148

[9] Michela Chiappalone, Paolo Massobrio, and Sergio Martinoia. Network plasticity in cortical assemblies. *European Journal of Neuroscience*, 28(1):221–237, 2008. 2, 39, 41, 42, 43, 44, 150, 156, 160, 172

[10] Joost Le Feber, Jan Stegenga, and Wim L C Rutten. The effect of slow electrical stimuli to achieve learning in cultured networks of rat cortical neurons. *PLoS ONE*, 5(1), 2010. 2, 39, 41, 44, 46

[11] Thierry Nieus, Valeria D'Andrea, Hayder Amin, Stefano Di Marco, Houman Safaai, Alessandro Maccione, Luca Berdondini, and Stefano Panzeri. State-dependent representation of stimulus-evoked activity in high-density recordings of neural cultures. *Scientific Reports*, 8(1):5578, 2018. 2, 37, 39, 69

[12] P.S. Churchland and T.J. Sejnoswki. *The Computational Brain*. MIT Press, 1992. 2, 46

[13] O Sporns, G Tononi, and R Ktter. The Human Connectome:A Structural Description of the Human Brain. *PLoS Comput Biol*, (4):e42, 2005. 2, 46, 47

[14] Matteo Garofalo, Thierry Nieus, Paolo Massobrio, and Sergio Martinoia. Evaluation of the performance of information theory-based methods and cross-correlation to estimate the functional connectivity in cortical networks. *PLoS ONE*, 4(8), 2009. 2, 50, 51, 102, 103, 119, 120, 176

[15] Shinya Ito, Michael E Hansen, Randy Heiland, Andrew Lumsdaine, Alan M Litke, and John M Beggs. Extending transfer entropy improves identification of effective connectivity in a spiking cortical network model. *PLoS ONE*, 6(11), 2011. 2, 48, 51, 52, 102, 103, 104, 106, 107, 109, 119, 120, 176

[16] Olav Stetter, Demian Battaglia, Jordi Soriano, and Theo Geisel. Model-Free Reconstruction of Excitatory Neuronal Connectivity from Calcium Imaging Signals. *PLoS Computational Biology*, 8(8):1002653, 2012. 2, 51, 102, 176

[17] Terry Bossomaier, Lionel Barnett, Michael Harré, and Joseph T Lizier. *An Introduction to Transfer Entropy*. 2016. 2, 51, 102

[18] E Salinas and T.J. Sejnowski. Correlated neuronal activity and the flow of neural information. *Nat. Rev. Neurosci*, (2):539–550, 2001. 2, 49, 103

[19] Jinghua Xu, Zeng rong Liu, [Ren Liu], and Qing fei Yang. Information transmission in human cerebral cortex. *Physica D: Nonlinear Phenomena*, 106(3):363 – 374, 1997. 2, 103

[20] Eric Kandel, James H.Schwartz, Thomas M. Jessell, Steven A.Siegelbaum, and A.J. Hudspeth. *Principles of Neural Science*. McGraw Hill Medical, 5th edition, 2000. 8, 28

[21] Patrick R. Hof, Grahame Kidd, Javier DeFelipe, Jean de Vellis, Miguel A. Gama Sosa, Gregory A. Elder, and Bruce D. Trapp. Chapter 3 - cellular components of nervous tissue. In Larry R Squire, Darwin Berg, Floyd E Bloom, Sascha du Lac, Anirvan Ghosh, and Nicholas C. Spitzer, editors, *Fundamental Neuroscience (Fourth Edition)*, pages 41 – 59. Academic Press, San Diego, fourth edition edition, 2013. 8

[22] Kenya Song. Anatomy and physiology, 2019. [Online; accessed 25-September-2019]. 8

[23] Dominique Debanne, Emilie Campanac, Andrzej Bialowas, Edmond Carlier, and Gisle Alcaraz. Axon physiology. *Physiological Reviews*, 91(2):555–602, 2011. 9

[24] Kristjan R Jessen and Rhona Mirsky. Glial cells in the enteric nervous system contain glial fibrillary acidic protein. *Nature*, 286:736–737, 1980. 9

[25] A L Hodgkin and B Katz. The Effect of Sodium Ions on the Electrical Activity of the Giant Axon o f the Squid. *J. Physiol. (I949)*, 8:1–41, 1949. 9

[26] Eric Kandel, James H.Schwartz, Thomas M. Jessell, Steven A.Siegelbaum, and A.J. Hudspeth. *Principles of Neural Science*. McGraw Hill Medical, 5th edition, 2000. 10

[27] Ariel Y. Deutch. Chapter 6 - neurotransmitters. In Larry R. Squire, Darwin Berg, Floyd E. Bloom, Sascha du Lac, Anirvan Ghosh, and Nicholas C. Spitzer, editors, *Fundamental Neuroscience (Fourth Edition)*, pages 117 – 138. Academic Press, San Diego, fourth edition edition, 2013. 11

[28] Eric Kandel, James H.Schwartz, Thomas M. Jessell, Steven A.Siegelbaum, and A.J. Hudspeth. *Principles of Neural Science*. McGraw Hill Medical, 5th edition, 2000. 11

[29] Rose G. Harrison, M. J. Greenman, Franklin P. Mall, and C. M. Jackson. Observations of the living developing nerve fiber. *The Anatomical Record*, 1(5):116–128, 1907. 11

[30] Ross Granville Harrison. The outgrowth of the nerve fiber as a mode of protoplasmic movement. *Journal of Experimental Zoology*, 9(4):787–846, 1910. 11

[31] Larry J Millet and Martha U Gillette. Over a century of neuron culture: From the hanging drop to microfluidic devices. *Yale Journal of Biology and Medicine*, 85(4):501–521, 2012. 12

[32] Dandan Sun, Douglas B. Kintner, and Brooks B. Pond. Chapter 25 - the role of cation-chloride transporters in brain ischemia. In F. Javier Alvarez-Leefmans and Eric Delpire, editors, *Physiology and Pathology of Chloride Transporters and Channels in the Nervous System*, pages 501 – 517. Academic Press, San Diego, 2010. 12

[33] Martha U Gillete. SCN Electrophysiology In Vitro: Rhythmic Activity and Endogenous Clock Properties. In DC Klein, RY Moore, and SM Reppert, editors, *Suprachiasmatic Nucleus: The Mind's Clock*, pages 125–143. Oxford University Press, New York,NY, 1991. 12

[34] Enrico Ferrea, Alessandro Maccione, Lucian Medrihan, Thierry Nieus, Diego Ghezzi, Pietro Baldelli, Fabio Benfenati, and Luca Berdondini.

Large-scale, high-resolution electrophysiological imaging of field potentials in brain slices with microelectronic multielectrode arrays. *Frontiers in Neural Circuits*, 6:80, 2012. 13

[35] Wei Gong, Jure Sencar, Douglas J Bakkum, David Jackel, Marie Engelene J Obien, Milos Radivojevic, and Andreas R Hierlemann. Multiple Single-Unit Long-Term Tracking on Organotypic Hippocampal Slices Using High-Density Microelectrode Arrays. *Frontiers of Neuroscience*, 10(537), 2016. 13

[36] 3BrainAG. Rat Hippocampal Slice Recording. https://www.youtube.com/watch?v=e_O6U7p8QhY, 2017. [Online; accessed 19-July-2018]. 13

[37] E.R Peterson and Murray. M.R. Myelin sheath formation in cultures of avaian spinal ganglia. *Am J Anat*, 93(4):319–355, 1955. 14

[38] A Kreigstein and M Dichter. Morphological Classification of Rat Cortical Neurons in Cell Culture. *The Journal of Neuroscience*, 3(8):1634–1647, 1983. 14

[39] Nikesh Lama, Alan Hargreaves, Bob Stevens, and T M Mcginnity. Spike Train Synchrony Analysis of Neuronal Cultures. In *2018 International Joint Conference on Neural Networks (IJCNN)*, pages 1–8. IEEE, 2018. 14, 35, 109, 113

[40] S.I Morefield, E.W Keefer, K.D Chapman, and G.W Gross. Drug evaluations using neuronal networks cultured on microelectrode arrays. *Biosensors and Bioelectronics*, 15(7-8):383–396, 2000. 15, 35

[41] Daniel A Wagenaar. Controlling Bursting in Cortical Cultures with Closed-Loop Multi-Electrode Stimulation. *Journal of Neuroscience*, 25(3):680–688, 2005. 15, 37, 38, 40

[42] S. Martinoia, L. Bonzano, M. Chiappalone, and M. Tedesco. Electrophysiological activity modulation by chemical stimulation in networks of cortical neurons coupled to microelectrode arrays: A biosensor for neuropharmacological applications. *Sensors and Actuators B: Chemical*, 108(1):589 – 596,

2005. Proceedings of the Tenth International Meeting on Chemical Sensors. 15, 37

[43] Alberto Mazzoni, Frédéric D Broccard, Elizabeth Garcia-Perez, Paolo Bonifazi, Maria Elisabetta Ruaro, and Vincent Torre. On the dynamics of the spontaneous activity in neuronal networks. *PLoS ONE*, 2(5):439, 2007. 15

[44] Atsushi Sugie, Marchetti Giovanni, and Tavosanis Gaia. Structural aspects of plasticity in the nervous system of Drosophila. *Neural Development*, 13(14), 2008. 15, 37

[45] Massimo Scanziani and Michael Häusser. Electrophysiology in the age of light. *Nature*, 461(7266):930–939, 2009. 15

[46] Alexey Pimashkin, Arseniy Gladkov, Ekaterina Agrba, Irina Mukhina, and Victor Kazantsev. Selectivity of stimulus induced responses in cultured hippocampal networks on microelectrode arrays. *Cognitive Neurodynamics*, 10(4):287–299, 2016. 15, 37, 39, 44, 156

[47] Y. Zhao, S. Inayat, D. A. Dikin, J. H. Singer, R. S. Ruoff, and J. B. Troy. Patch clamp technique: Review of the current state of the art and potential contributions from nanoengineering. *Proceedings of the Institution of Mechanical Engineers, Part N: Journal of Nanoengineering and Nanosystems*, 222(1):1–11, 2008. 15

[48] Claire Wood, Christine Williams, and Gareth J. Waldron. Patch clamping by numbers. *Drug Discovery Today*, 9(10):434 – 441, 2004. 15

[49] Darrell A. Henze, Zsolt Borhegyi, Jozsef Csicsvari, Akira Mamiya, Kenneth D. Harris, and Gyrgy Buzski. Intracellular features predicted by extracellular recordings in the hippocampus in vivo. *Journal of Neurophysiology*, 84(1):390–400, 2000. 16

[50] Timothy J. Blanche, Martin A. Spacek, Jamille F. Hetke, and Nicholas V. Swindale. Polytrodes: High-density silicon electrode arrays for large-scale multiunit recording. *Journal of Neurophysiology*, 93(5):2987–3000, 2005. 18

[51] C.A. Thomas, P.A. Springer, G.E. Loeb, Y. Berwald-Netter, and L.M. Okun. A Miniature Electrode Array to Monitor the Bioelectric Activity of Cultured Cells. *Experimental Cell Research*, 74(972):61–66, 1972. 17

[52] Jerome Pine. Recording action potentials from cultured neurons with extracellular microcircuit electrodes. *Journal of Neuroscience Methods*, 2(1):19–31, 1980. 17, 35

[53] Peter Fromherz, A Offenhäusser, T Vetter, and J Weis. A neuron-silicon junction: a Retzius cell of the leech on an insulated-gate field-effect transistor. 252:1290–1293, 1991. 18, 35

[54] Kilian Imfeld, Simon Neukom, Alessandro Maccione, Yannick Bornat, Sergio Martinoia, Pierre André Farine, Milena Koudelka-Hep, and Luca Berdondini. Large-scale, high-resolution data acquisition system for extracellular recording of electrophysiological activity. *IEEE Transactions on Biomedical Engineering*, 55(8):2064–2073, 2008. 19

[55] P Dayan and L F Abbott. *Theoretical Neuroscience: Computational and Mathematical Modelling of Neural Systems*. The MIT Press, USA, 2001. 21, 81

[56] Antnio R.C. Paiva, Il Park, and Jos C. Prncipe. Chapter 8 - inner products for representation and learning in the spike train domain. In Karim G. Oweiss, editor, *Statistical Signal Processing for Neuroscience and Neurotechnology*, pages 265 – 309. Academic Press, Oxford, 2010. 21

[57] E D Adrian. The impulses produced by sensory nerve endings: Part I. *The Journal of Physiology*, 61(1):49–72, 1926. 21, 71, 81

[58] E D Adrian and Y Zotterman. The impulses produced by sensory nerve endings: Part III. *The Journal of Physiology*, 61(1):465–483, 1926. 21, 71, 81

[59] Michael N Shadlen and William T Newsome. Noise, neural codes and cortical organization. *Current Opinion in Neurobiology*, 4(4):569–579, 1994. 21, 71, 81

[60] Simon Thorpe, Arnaud Delorme, and Rufin Van Rullen. Spike-based strategies for rapid processing. *Neural Networks*, 14(6-7):715–725, 2001. 21, 71, 81

[61] Richard B Stein, E.Roderich Gossen, and Kelvin. E Jones. Neuronal variablility:noise of part of the signal? *Nature Reviews Neuroscience*, 6:389–397, 389. 21, 71, 81

[62] Adam L Jacobs, Gene Fridman, Robert M Douglas, Nazia M Alam, Peter E Latham, Glen T Prusky, and Sheila Nirenberg. Ruling out and ruling in neural codes. *Proceedings of the National Academy of Sciences*, 106(14):5936–5941, 2009. 21, 71, 81

[63] Jens-Oliver Muthmann, Hayder Amin, Evelyne Sernagor, Alessandro Maccione, Dagmara Panas, Luca Berdondini, Upinder S Bhalla, and Matthias H Hennig. Spike Detection for Large Neural Populations Using High Density Multielectrode Arrays. *Frontiers in Neuroinformatics*, 9:1–21, 2015. 23, 72, 73, 74, 86, 91, 109

[64] Felix Franke, David Jäckel, Jelena Dragas, Jan Müller, Milos Radivojevic, Douglas Bakkum, and Andreas Hierlemann. High-density microelectrode array recordings and real-time spike sorting for closed-loop experiments: an emerging technology to study neural plasticity. *Frontiers in neural circuits*, 6(December):105, 2012. 23, 46, 72

[65] Cyrille Rossant, Shabnam N. Kadir, Dan F.M. Goodman, John Schulman, Maximilian L.D. Hunter, Aman B. Saleem, Andres Grosmark, Mariano Belluscio, George H. Denfield, Alexander S. Ecker, Andreas S. Tolias, Samuel Solomon, György Buzski, Matteo Carandini, and Kenneth D. Harris. Spike sorting for large, dense electrode arrays. *Nature Neuroscience*, 19(4):634–641, 2016. 23, 72

[66] S.R. Cajal. Degeneracio n y regeneracio n de los nervios. *Estudios sobre la degeneracio n y regeneracio n del sistema nervioso*, 1, 1913. 27

[67] Karunesh Ganguly and Mu ming Poo. Activity-dependent neural plasticity from bench to bedside. *Neuron*, 80(3):729–741, 2013. 27

[68] S.R. Quartz and T.J. Sejnowski. The Neural Basis of Cognitive Development: A Constructivist Manifesto. *Bhav Brain Sci.*, 20:537–56, 1997. 27

[69] D.O Hebb. *organization of Behavior: A Neuropsychological Theory*. Wiley Inc., 1949. 27, 76

[70] T V P Bliss and T Lomo. Longlasting potentiation of synaptic transmission in the dentate area of the unanaesthetized rabbit following stimulation of the perforant path. *The Journal of Physiology*, 232(2):357–374, 1973. 28, 36

[71] G V Goddard, McIntyre D C, and Leech C K. A permanent change in brain function resulting from daily electrical stimulation. *Experimental Neurology*, 25:295–330, 1969. 28

[72] Gunther S Stent. A Physiological Mechanism for Hebb's Postulate of Learning. In *Proceedings of the National Academy of Sciences*, volume 70, pages 997–1001, 1973. 28

[73] T. J. Sejnowski. Statistical constraints on synaptic plasticity. *Journal of Theoretical Biology*, 69(2):385–389, 1977. 28

[74] H. Z. Shouval. Models of synaptic plasticity. *Scholarpedia*, 2(7):1605, 2007. revision #144654. 28

[75] Masao Ito and Masanobu Kano. Long-lasting depression of parallel fiber-Purkinje cell transmission induced by conjunctive stimulation of parallel fibers and climbing fibers in the cerebellar cortex. *Neuroscience Letters*, 33(3):253 – 258, 1982. 28, 36

[76] J. Sjstrm and W. Gerstner. Spike-timing dependent plasticity. *Scholarpedia*, 5(2):1362, 2010. revision #184913. 29

[77] H Markram and B Sakmann. Action potentials propagating back into dendrites triggers changes in efficacy. *Soc.Neurosci.Abs.*, (21), 1995. 29, 183

[78] H Markram, J Lubke, M Frotscher, and B Sakmann. Regulation of synaptic efficacy by coincidence of postsynaptic APs and EPSPs. *Science*, 213(275), 1997. 29, 183, 200

[79] W.B. Levy and O. Steward. Temporal contiguity requirements for long-term associative potentiation/depression in the hippocampus. *Neuroscience*, 8(4):791 – 797, 1983. 29

[80] Curtis C Bell, Victor Z Han, Yoshiko Sugawara, and Kirsty Grant. Synaptic plasticity in a cerebellum-like structure depends on temporal order. *Nature*, 387(March):278–281, 1997. 29

[81] Li I Zhang, Huizhong W Tao, Christine E Holt, William A Harris, and Mu-ming Poo. A critical window for cooperation and competition among developing retinotectal synapses. *Nature*, 395:37–44, 1998. 29, 30

[82] Guo-Qiang Bi and Mu-Ming Poo. Synaptic Modifications in Cultured Hippocampal Neurons: Dependence on Spike Timing, Synaptic Strength, and Postsynaptic Cell Type. *The Journal of Neuroscience*, 18(24):10464–10472, 1998. 29, 183, 200

[83] W. Gerstner, R. Kempter, J. L. Van Hemmen, and H. Wagner. A neuronal learning rule for sub-millisecond temporal coding. *Nature*, 383(6595):76–78, 1996. 30

[84] S Song, K D Miller, and L F Abbott. Competitive Hebbian learning through spike-timing-dependent synaptic plasticity. *Nature neuroscience*, 3(9):919–926, 2000. 30, 107

[85] Jean-Pierre Eckmann, Ofer Feinerman, Leor Gruendlinger, Elisha Moses, Jordi Soriano, and Tsvi Tlusty. The Physics of Living Neural Networks. 60, 2010. 31

[86] Jordi Soriano, M. Rodriguez Martinez, Tsvi Tlusty, and Elisha Moses. Development of input connections in neural cultures. *Proceedings of the National Academy of Sciences*, 105(37):13758–13763, 2008. 31

[87] P G Nelson. Nerve and Muscle Cells in Culture. *Physiological Reviews*, 55(1):1–61, 1975. 31

[88] Marc A. Dichter. Rat cortical neurons in cell culture: Culture methods, cell morphology, electrophysiology, and synapse formation. *Brain Research*, 149(2):279–293, 1978. 31, 33

[89] Daniel Mazia, Gerald Schatten, and Winfield Sale. Adhesion of Cells to Surfaces Coated with PolyLysiine. *Application to Electron Microscopy*, 66:198–200, 1975. 31

[90] Matt Carter and Jennifer Shieh. Chapter 14 - cell culture techniques. In Matt Carter and Jennifer Shieh, editors, *Guide to Research Techniques in Neuroscience (Second Edition)*, pages 295 – 310. Academic Press, San Diego, second edition edition, 2015. 32

[91] T Morrow, M R Song, and A Ghosh. Sequential specification of neurons and glia by developmentally regulated extracellular factors. *Development*, 128(18):3585–94, 2001. 33

[92] Nitzan Herzog. *Rapid solution exchange to entire neuronal cultures grown on multi electrode arrays*. PhD thesis, 2017. 33

[93] D. L. Benson, F. H. Watkins, O. Steward, and G. Banker. Characterization of GABAergic neurons in hippocampal cell cultures. *Journal of Neurocytology*, 23(5):279–295, 1994. 33

[94] Elaine A Neale, Wolfgang H Oertel, Linda M Bowers, and Virginia K Weise. Glutamate Decarboxylase Immunoreactivity and y-[3H] aminobutyric acid accumulation within the same neurons in dissociated cell cultures of cerebral cortex1. *The Journal of Neuroscience*, 3(2):376–382, 1983. 33

[95] Paolo Bonifazi, Maria Elisabetta Ruaro, and Vincent Torre. Statistical properties of information processing in neuronal networks. *European Journal of Neuroscience*, 22(11):2953–2964, 2005. 33

[96] M. A. Corner, J. Van Pelt, P. S. Wolters, R. E. Baker, and R. H. Nuytinck. Physiological effects of sustained blockade of excitatory synaptic transmission on spontaneously active developing neuronal networks - An inquiry into the reciprocal linkage between intrinsic biorhythms and neuroplasticity in early ontogeny. *Neuroscience and Biobehavioral Reviews*, 26(2):127–185, 2002. 33

[97] AR Kriegstein and MA Dichter. Morphological classification of rat cortical neurons in cell culture. *Journal of Neuroscience*, 3(8):1634–1647, 1983. 33

[98] Ronen Segev, Morris Benveniste, Yoash Shapira, and Eshel Ben-Jacob. Formation of electrically active clusterized neural networks. *Phys. Rev. Lett.*, 90:168101, Apr 2003. 33

[99] A A Gladkov, N Y Belenkov, ; A S Pimashkin, and Neurotechnology Department. Functional Connectivity of Neural Network in Dissociated Hippocampal Culture Grown on Microelectrode Array Connectivity of Neural Network in Dissociated Hippocampal Culture Grown on Microelectrode Array. 9(2), 2017. 33, 34

[100] Daniele Poli, Vito P Pastore, and Paolo Massobrio. Functional connectivity in in vitro neuronal assemblies. *Frontiers in Neural Circuits*, 9(9), 2015. 33, 34

[101] F. van Huizen, H.J. Romijn, and A.M.M.C. Habets. Synaptogenesis in rat cerebral cortex cultures is affected during chronic blockade of spontaneous bioelectric activity by tetrodotoxin. *Developmental Brain Research*, 19(1):67 – 80, 1985. 33

[102] Kazuyo Muramoto, Masumi Ichikawa, Masahiro Kawahara, Kazuo Kobayashi, and Yoichiro Kuroda. Frequency of synchronous oscillations of neuronal activity increases during development and is correlated to the number of synapses in cultured cortical neuron networks. *Neuroscience Letters*, 163(2):163 – 165, 1993. 33

[103] Hayder Amin, Alessandro Maccione, Federica Marinaro, Stefano Zordan, Thierry Nieus, and Luca Berdondini. Electrical responses and spontaneous activity of human iPS-derived neuronal networks characterized for 3-month culture with 4096-electrode arrays. *Frontiers in Neuroscience*, 10(MAR), 2016. 34, 160

[104] Steve M Potter and Thomas B DeMarse. A new approach to neural cell culture for long-term studies. *Journal of Neuroscience Methods*, 110(1-2):17–24, sep 2001. 34, 35

[105] D H Hubel. Thungsten microelectrode for recording from single units. *Science*, 125(3247):549–550, 1957. 34

[106] Gyorgy Buzsaki, Costas A Anastassiou, and Christof Koch. The origin of extracellular fields and currents EEG, ECoG, LFP and spikes Electric current contributions from all active cellular processes within a volume of brain tissue superimpose at a given location in the extracellular medium and generate a potent. *Nature Reviews Neuroscience*, 13(6):407–420, 2016. 35

[107] Eisaku Maeda, HP Robinson, and A Kawana. The mechanisms of generation and propagation of synchronized bursting in developing networks of cortical neurons. *Journal of Neuroscience*, 15(10):6834–6845, 1995. 35, 38, 39

[108] John M Beggs and Dietmar Plenz. Neuronal Avalances in Neocortical Circuits. *The Journal of Neuroscience*, 23(35):11167 – 11177, 2003. 35

[109] Y Jimbo, T Tateno, and H. P.C. Robinson. Simultaneous induction of pathway-specific potentiation and depression in networks of cortical neurons. *Biophysical Journal*, 76(2):670–678, 1999. 35, 43

[110] Heiko J. Luhmann, Anne Sinning, Jenq-Wei Yang, Vicente Reyes-Puerta, Maik C. Stttgen, Sergei Kirischuk, and Werner Kilb. Spontaneous neuronal activity in developing neocortical networks: From single cells to large-scale interactions. *Frontiers in Neural Circuits*, 10:40, 2016. 35

[111] Thoralf Opitz, Ana D. De Lima, and Thomas Voigt. Spontaneous development of synchronous oscillatory activity during maturation of cortical networks in vitro. *Journal of Neurophysiology*, 88(5):2196–2206, 2002. 35, 164

[112] Hiroyuki Kamioka, Eisaku Maeda, Yasuhiko Jimbo, Hugh P.C. Robinson, and Akio Kawana. Spontaneous periodic synchronized bursting during formation of mature patterns of connections in cortical cultures. *Neuroscience Letters*, 206(2-3):109–112, mar 1996. 35, 164

[113] Li Zheng and Morgan Sheng. Some assembly required: the development of neuronal synapses. *Nature Reviews Molecular Cell Biology*, 4(11):833–841, 2003. 35

[114] Catherine Croft Swanwick, Namita R Murthy, Zakaria Mtchedlishvili, Werner Sieghart, and Jaideep Kapur. Development of γ-aminobutyric acidergic synapses in cultured hippocampal neurons. *Journal of Comparative Neurology*, 495(5):497–510, 2006. 35, 148

[115] Jyothsna Suresh, Mihailo Radojicic, Lorenzo L. Pesce, Anita Bhansali, Janice Wang, Andrew K. Tryba, Jeremy D. Marks, and Wim Van Drongelen. Network burst activity in hippocampal neuronal cultures: The role of synaptic and intrinsic currents. *Journal of Neurophysiology*, 115(6):3073–3089, 2016. 35

[116] V Pasquale, P Massobrio, L L Bologna, M Chiappalone, and S. Martinoia. Self-organization and neuronal avalanches in networks of dissociated cortical neurons. *Neuroscience*, 153(4):1354–1369, 2008. 36, 37, 176

[117] Xiao-Jing Wang. Neurophysiological and computational principles of cortical rhythms in cognition. *Physiological Reviews*, 90(3):1195–1268, 2010. 36

[118] John E. Lisman. Bursts as a unit of neural information: making unreliable synapses reliable. *Trends in Neurosciences*, 20(1):38 – 43, 1997. 36

[119] Tiago Branco and Kevin Staras. The probability of neurotransmitter release: variability and feedback control at single synapses. *Nature Reviews Neurosciences*, 10(5):373 – 383, 2009. 36

[120] J. Gerard G. Borst. The low synaptic release probability in vivo. *Trends in Neurosciences*, 33(6):259 – 266, 2010. 36

[121] Alex M. Thomson. Activity-dependent properties of synaptic transmission at two classes of connections made by rat neocortical pyramidal axons in vitro. *The Journal of Physiology*, 502(1):131–147, 1997. 36

[122] Rdiger Khrahe and Fabrizio Gabbiani. Burst firing in sensory systems. *Nature Reviews Neurosciences*, 5(1):13 – 23, 2004. 36

[123] M J Thomas, A M Watabe, T D Makhinson, and T J O'Dell. Postsynaptic complex spike bursting enables the induction of ltp by theta frequency synaptic stimulation. *J.Neurosci*, 18:7118–7126, 1998. 36

[124] Fenella G Pike, Rhiannon M Meredith, Andrew W A Olding, and Paulsen. Postsynaptic bursting is essential for hebbian induction of associative long-term potentiation at excitatory synapses in rat hippocampus. *J.Physiol*, 518(Pt2):571–576, 1999. 36

[125] B Birtoli and D Ulrich. Firing mode-dependent synaptic plasticity in rat neocortical pyramidal neurons. *J.Neurosci*, 24(21):4935–4940, 2004. 36

[126] Paolo Massobrio, Jacopo Tessadori, Michela Chiappalone, and Mirella Ghirardi. In vitro studies of neuronal networks and synaptic plasticity in invertebrates and in mammals using multielectrode arrays. *Neural Plasticity*, 2015, 2015. 37, 38, 39, 40, 41, 172, 184, 192

[127] Hai Hai, Joseph Shappir, and Micha E Spira. In-cell recordings by extracellular microelectrodes. *Nature Methods*, 7(200), 2010. 37

[128] Craig H. Bailey and Eric R. Kandel. Chapter 10 synaptic remodeling, synaptic growth and the storage of long-term memory in aplysia. In Wayne S. Sossin, Jean-Claude Lacaille, Vincent F. Castellucci, and Sylvie Belleville, editors, *Essence of Memory*, volume 169 of *Progress in Brain Research*, pages 179 – 198. Elsevier, 2008. 37

[129] Carlo Natale Giuseppe Giachello, Pier Giorgio Montarolo, and Mirella Ghirardi. Synaptic functions of invertebrate varicosities: What molecular mechanisms lie beneath. *Neural Plasticity*, 2012:14, 2012. 37

[130] Paolo Massobrio, Mariateresa Tedesco, Carlo Giachello, Mirella Ghirardi, Ferdinando Fiumara, and Sergio Martinoia. Helix neuronal ensembles with controlled cell type composition and placement develop functional polysynaptic circuits on micro-electrode arrays. *Neuroscience Letters*, 467(2):121 – 126, 2009. 37

[131] R. Alexander Kaul, Naweed I. Syed, and Peter Fromherz. Neuron-semiconductor chip with chemical synapse between identified neurons. *Phys. Rev. Lett.*, 92:038102, Jan 2004. 37

[132] CJ Coates and AG Bulloch. Synaptic plasticity in the molluscan peripheral nervous system: physiology and role for peptides. *Journal of Neuroscience*, 5(10):2677–2684, 1985. 37

[133] A. G. M. Bulloch and R. L. Ridgway. Neuronal plasticity in the adult invertebrate nervous system. *Journal of Neurobiology*, 20(5):295–311, 1989. 37

[134] Gregory J Brewer, Michael D Boehler, Alessandro N Ide, and Bruce C Wheeler. Chronic electrical stimulation of cultured hippocampal networks increases spontaneous spike rates. *Journal of Neuroscience Methods*, 184(1):104–109, 2009. 37, 39

[135] P. Massobrio, P. L. Baljon, A. Maccione, M. Chiappalone, and S. Martinoia. Activity modulation elicited by electrical stimulation in networks of dissociated cortical neurons. In *2007 29th Annual International Conference of the IEEE Engineering in Medicine and Biology Society*, pages 3008–3011, Aug 2007. 37

[136] Guenter W. Gross, Barry Rhoades, and Russell Jordan. Neuronal networks for biochemical sensing. *Sensors and Actuators B: Chemical*, 6(1):1 – 8, 1992. 37

[137] P Laplace. *Essai Philosophique sur les Probabilits*. Paris: Gauthier-Villar, 1825. 38

[138] A Aldo Faisal, Luc P.J. Selen, and Daniel M Wolpert. Noise in the nervous system. *Nature Reviews Neuroscience*, 9(4):292–303, 2008. 38

[139] Maria Elisabetta Ruaro, Paolo Bonifazi, and Vincent Torre. Toward the Neurocomputer : Image Processing and Pattern Recognition With Neuronal Cultures. *IEEE Transactions on Biomedical Engineering*, 52(March):371–383, 2005. 39

[140] Carrie P Marder and Dean V Buonomano. Timing and balance of inhibition enhance the effect of long-term potentiation on cell firing. *Journal of Neuroscience*, 24(40):8873–8884, 2004. 40

[141] Ole Paulsen and Terrence J Sejnowski. Natural patterns of activity and long-term synaptic plasticity. *Current Opinion in Neurobiology*, 10(2):172–180, 2000. 42

[142] Zenas C Chao, Douglas J Bakkum, and Steve M Potter. Region-specific network plasticity in simulated and living cortical networks: comparison of the center of activity trajectory (CAT) with other statistics. *Journal of neural engineering*, 4(3):294–308, 2007. 43

[143] Patric K Stanton and Terrence J Sejnowski. Associative long-term depression in the hippocampus induced by hebbian covariance. *Nature*, 339(6221):1245–218, 1989. 43

[144] Yan You Huang, Christopher Pittenger, and Eric R Kandel. A form of long-lasting, learning-related synaptic plasticity in the hippocampus induced by heterosynaptic low-frequency pairing. *Proceedings of the National Academy of Sciences of the United States of America*, 101(3):859–864, 2004. 43

[145] Pimashkin Alexey, Gladkov Arseniy, Mukhina Irina, and Kazantsev Victor. Adaptive enhancement of learning protocol in hippocampal cultured networks grown on multielectrode arrays. *Frontiers in Neural Circuits*, (APR 2013), 2013. 46

[146] Zenas C Chao, Douglas J Bakkum, and Steve M Potter. Shaping embodied neural networks for adaptive goal-directed behavior. *PLoS Computational Biology*, 4(3):1000042, 2008. 46, 202

[147] A Novellino, P. D'Angelo, L Cozzi, M Chiappalone, V Sanguineti, and S Martinoia. Connecting neurons to a mobile robot: An in vitro bidirectional neural interface. *Computational Intelligence and Neuroscience*, 2007:13, 2007. 46

[148] Kevin Warwick, Dimitris Xydas, Slawomir Nasuto, Victor M Becerra, and Mark W Hammond. Controlling a Mobile Robot with a Biological Brain. *Defence Science Journal*, 60(1):5–14, 2010. 46

[149] Jacopo Tessadori, Marta Bisio, Sergio Martinoia, and Michela Chiappalone. Modular neuronal assemblies embodied in a closed-loop environment: To-

ward future integration of brains and machines. *Frontiers in Neural Circuits*, (DEC), 2012. 46

[150] W Gerstner, WM Kistler, R Naud, and L Paninski. *Neuronal dynamics:From single neurons to networks and models of cognition* . Cambridge University Press, 2014. 47

[151] Karl J. Friston. Functional and Effective Connectivity: A Review. *Brain Connectivity*, 1(1):13–36, 2011. 47, 102

[152] C.K. Knox. Detection of neuronal interactions using correlation analysis. *Trends Neurosci*, (4):222–225, 1981. 49

[153] C. Babiloni, V. Pizzella, C. D. Gratta, A. Ferretti, and G. L. Romani. Fundamentals of electroencefalography, magnetoencefalography, and functional magnetic resonance imaging. *Int. Rev. Neurobiol*, (86):67–80, 2009. 49

[154] I.C. Shannon. A Mathematical Theory of Communication. *Bell System Technical Journal*, (27):379–423, 1948. 50

[155] F Rieke, D Warland, R de Ruyter van Steveninck, and W Bialek. *Spikes:Exploring the Neural Code*. MIT Press, Cambridge,MA, 1997. 50

[156] K.P. Burnham and D.R. Anderson. *Model Selection and Multimodel Inference: A Practical Information-Theoretic Approach*. Springer Science, New York, second edition edition, 2002. 50

[157] E.T. Jaynes. Information theory and statistical mechanics. *Phys.Rev.*, 106(4):620, 1957. 50

[158] M.A. Nielsen. *Quantum Computation and Quantum Information*. Cambridge University Press, Cambridge, 2010. 50

[159] Vito Paolo Pastore, Daniele Poli, Aleksandar Godjoski, Sergio Martinoia, and Paolo Massobrio. ToolConnect: A Functional Connectivity Toolbox for In vitro Networks. *Frontiers in Neuroinformatics*, 10, 2016. 50, 176

[160] Thomas Schreiber. Measuring information transfer. *Physical Review Letters*, 85(2):461–464, 2000. 51, 102, 103

[161] Max Lungarella, Teresa Pegors, Daniel Bulwinkle, and Olaf Sporns. Giorgio A. Ascoli Erik De Schutter David N. Kennedy. *Neuroinformatics*, 3:243–262, 2005. 51

[162] P Bonifazi, M Goldin, M. A. Picardo, I. Jorquera, A. Cattani, G. Biancon, A. Represa, Y. Ben-Ari, and R. Cossart. Gabaergic hub neurons orchestrate synchrony in developing hippocampal networks. *Science*, (11). 52

[163] Naoya Takahashi, Takuya Sasaki, Wataru Matsumoto, Norio Matsuki, and Yuji Ikegaya. Circuit topology for synchronizing neurons in spontaneously active networks. *Proceedings of the National Academy of Sciences of the United States of America*, 107(22):10244–10249, 2010. 52

[164] Daniel A Butts, Chong Weng, Jianzhong Jin, Chun I. Yeh, Nicholas A Lesica, Jose Manuel Alonso, and Garrett B Stanley. Temporal precision in the neural code and the timescales of natural vision. *Nature*, 449(7158):92–95, 2007. 52

[165] Masanori Shimono and John M Beggs. Functional clusters, hubs, and communities in the cortical microconnectome. *Cerebral Cortex*, 25(10):3743–3757, 2015. 52

[166] S. Grun. Data-Driven Significance Estimation for Precise Spike Correlation. *Journal of Neurophysiology*, 101(3):1126–1140, 2009. 53, 121

[167] A Amarasingham, M.T. Harrison, N.G. Hatsopoulos, and S Geman. Conditional modeling and the jitter method of spike resampling. *J Neurophysiol*, 107(2):517 – 531, 2011. 53, 122, 139, 140, 192

[168] George L. Gerstein and Donald H. Perkel. Mutual temporal relationships among neuronal spike trains: Statistical techniques for display and analysis. *Biophysical Journal*, 12(5):453 – 473, 1972. 53, 122, 139, 140, 192

[169] Michal Rivlin-Etzion, Ya'acov Ritov, Gali Heimer, Hagai Bergman, and Izhar Bar-Gad. Local shuffling of spike trains boosts the accuracy of spike train spectral analysis. *Journal of Neurophysiology*, 95(5):3245–3256, 2006. 53, 122, 140, 192

[170] Yang Dan and Mu ming Poo. Spike timing-dependent plasticity of neural circuits. *Neuron*, 44(1):23 – 30, 2004. 54

[171] G. J. Brewer, J. R. Torricelli, E. K. Evege, and P. J. Price. Optimized survival of hippocampal neurons in b27-supplemented neurobasal, a new serum-free medium combination. *Journal of Neuroscience Research*, 35(5):567–576, 1993. 58

[172] E. Cotterill and S. J. Eglen. Burst detection methods. In *In Vitro Neuronal Networks From Culturing Methods to Neuro-Technological Applications*, pages 1–27. 2018. 71

[173] JD Victor and KP Purpura. Nature and Precision of Temporal Coding in Visual Cortex: a metrix-space analysis. *Journal of Neurophysiology*, 76(76):1310–1326, 2007. 78, 81

[174] M C van Rossum. A novel spike distance. *Neural computation*, 13(4):751–763, 2001. 78, 81

[175] R Quian Quiroga, T Kreuz, and P Grassberger. Event synchronization: A simple and fast method to measure synchronicity and time delay patterns. *Physical Review E - Statistical Physics, Plasmas, Fluids, and Related Interdisciplinary Topics*, 66(4):9, 2002. 78, 81

[176] S Schreiber, J.M. Fellous, D Whitmer, P Tiesinga, and T.J. Sejnowski. A new correlation-based measure of spike timing reliability. *Neurocomputing*, 52-54:925–931, 2003. 78, 81

[177] Thomas Kreuz, Julie S Haas, Alice Morelli, Henry D I Abarbanel, and Antonio Politi. Measuring spike train synchrony. *Journal of Neuroscience Methods*, 165(1):151–161, 2007. 78, 81, 82, 83

[178] Thomas Kreuz, Daniel Chicharro, Martin Greschner, and Ralph G Andrzejak. Time-resolved and time-scale adaptive measures of spike train synchrony. *Journal of Neuroscience Methods*, 195(1):92–106, 2011. 78, 81, 82, 85

[179] Fred Rieke, David Warland, Rob de Ruyter Steveninck, and William Bialek. *Spikes:Exploring the Neural Code*. The MIT Press, Cambridge, Massachusetts, 1999. 81

[180] A M Litke, N Bezayiff, E J Chichilnisky, W Cunningham, W Dabrowski, A A Grillo, M Grivich, P Grybos, P Hottowy, S Kachiguine, R S Kalmar, K Mathieson, D Petrusca, M Rahman, and A Sher. What Does the Eye Tell the Brain?: Development of a System for the Large-Scale Recording of Retinal Output Activity. *IEEE TRANSACTIONS ON NUCLEAR SCIENCE*, 51(4), 2004. 81

[181] Jason S. Prentice, Jan Homann, Kristina D. Simmons, Gašper Tkačik, Vijay Balasubramanian, and Philip C. Nelson. Fast, scalable, bayesian spike identification for Multi-Electrode arrays. *PLoS ONE*, 2011. 81

[182] W. Martin Usrey and R. Clay Reid. Synchronous Activity in the Visual System. *Annual Review of Physiology*, 61(1):435–456, 1999. 81, 191

[183] A.K. Engel, P Fries, and W Singer. Dynamic predictions:oscillations and synchrony in top-down processing. *Nat.Rev.Neurosci*, 10:704–716, 2002. 81

[184] Lawrence M Ward. Synchronous neural oscillations and cognitive processes, 2003. 81

[185] Mario Mulansky, Nebojsa Bozanic, Andreea Sburlea, and Thomas Kreuz. A guide to time-resolved and parameter-free measures of spike train synchrony. *Proceedings of 1st International Conference on Event-Based Control, Communication and Signal Processing, EBCCSP 2015*, 2015. 84

[186] Thomas Kreuz, Daniel Chicharro, Conor Houghton, Ralph G Andrzejak, and Florian Mormann. Monitoring spike train synchrony. *Journal of Neurophysiology*, 109(5):1457–1472, 2013. 85, 88

[187] Mario Mulansky and Thomas Kreuz. PySpike - A Python library for analyzing spike train synchrony. *SoftwareX*, 2016. 86, 87

[188] Yaron Penn, Menahem Segal, and Elisha Moses. Network synchronization in hippocampal neurons. *Proceedings of the National Academy of Sciences*, 113(12):3341–3346, 2016. 94

[189] N. Lama, A. Hargreaves, B. Stevens, and T. M. McGinnity. Transfer entropy based connectivity estimation of spontaneously firing hippocampal cultures on multi electrode arrays. In *2019 International Joint Conference on Neural Networks (IJCNN)*, pages 1–8, July 2019. 101, 120

[190] Olaf Sporns. Graph Theory Methods for the Analysis of Neural Connectivity Patterns. In *Neuroscience Databases. A Practical Guide*, pages 171–185. 2003. 102, 116

[191] Alessandro Maccione, Matteo Garofalo, Thierry Nieus, Mariateresa Tedesco, Luca Berdondini, and Sergio Martinoia. Multiscale functional connectivity estimation on low-density neuronal cultures recorded by high-density CMOS Micro Electrode Arrays. *Journal of Neuroscience Methods*, 207(2):161–171, 2012. 102

[192] Eugene M Izhikevich. Polychronization: Computation with Spikes. *Neural Computation*, 18(2):245–282, 2006. 106, 107, 109, 119, 139

[193] Eugene M Izhikevich. Simple Model of Spiking Neurons. *IEEE Transactions on Neural Networks*, 14(6):1569–1572, 2003. 106

[194] The Meaning and Use of the Area Under a Receiver Operating Characteristic(ROC) curve. *Radiology*, 143(1):29–36, 1982. 111

[195] Tom Fawcett. An introduction to ROC analysis. *Pattern Recognition Letters*, 27:861–874, 2006. 111

[196] David M W Powers. Evaluation: From Precision, Recall and F-Factor to ROC, Informedness, Markedness & Correlation. *Journal of Machine Learning Technologies*, 2(1):37–63, 2011. 111

[197] Mikail Rubinov and Olaf Sporns. Complex network measures of brain connectivity: Uses and interpretations. *NeuroImage*, 52(3):1059–1069, 2010. 116

[198] Hagberg Aric, dan Schult, and Pieter Swart. *NetworkX*, 2018 (accessed July 27, 2018). 116

[199] Luc BDevroye. *Non-Uniform Random Variate Generation*. New York:Springer-Verlag, 1986. 124

[200] Michela Chiappalone, Marco Bove, Alessandro Vato, Mariateresa Tedesco, and Sergio Martinoia. Dissociated cortical networks show spontaneously correlated activity patterns during in vitro development. *Brain Research*, 1093(1):41–53, 2006. 144, 148

[201] Yan Chiang Lin, Zu Han Huang, I. Sam Jan, Chia Chun Yeh, Han Jay Wu, Yun Chia Chou, and Yen Chung Chang. Development of excitatory synapses in cultured neurons dissociated from the cortices of rat embryos and rat pups at birth. 67(4):484–493, 2002. 144

[202] J. van Pelt, P. S. Wolters, M. A. Corner, W. L. C. Rutten, and G. J. A. Ramakers. Long-term characterization of firing dynamics of spontaneous bursts in cultured neural networks. *IEEE Transactions on Biomedical Engineering*, 51(11):2051–2062, 2004. 148

[203] Paolo Massobrio, V Pasquale, and S Martinoia. Self-organized criticality in cortical assemblies occurs in concurrent scale-free and small-world networks. *Sci Rep*, 5, 2015. 176

[204] J Stegenga, Joost Le Feber, E Marani, and WL Rutten. Analysis of Cultured Neuronal Networks Using Intraburst Firing Characteristics. *IEEE Trans Biomed Eng.*, 55(4):1382–90, 2008. 180, 181, 186, 194

[205] Joost Le Feber, WL Rutten, J Stegenga, PS Wolters, GJA Ramakers, and J van Pelt. Conditional Firing Probabilities in Cultured Neuronal Networks: A Stable Underlying Structure in Widely Varying Spontaneous Activity Patterns. *J Neural Eng*, 4(2):54–67, 2007. 180, 181, 186, 194

[206] Joost Le Feber, Wybren Postma, Eddy de Weerd, Marcel Weusthof, and Wim L.C. Rutten. Barbed channels enhance unidirectional connectivity between neuronal networks cultured on multi electrode arrays. *Frontiers in Neuroscience*, 9(NOV):1–10, 2015. 181

[207] Simona Ullo, Thierry R Nieus, Diego Sona, Alessandro Maccione, Luca Berdondini, and Vittorio Murino. Functional Connectivity Estimation

Over Large Networks at Cellular Resolution Based on Electrophysiological Recordings and Structural Prior. *Front Neuoanat*, 8(137), 2014. 184, 192

[208] Eleonora Carletti, Antonella Motta, and Claudio Migliaresi. *Scaffolds for Tissue Engineering and 3D Cell Culture*, pages 17–39. Humana Press, Totowa, NJ, 2011. 195

[209] E. Cukierman, R. Pankov, D. R. Stevens, and K. M. Yamada. Taking cell-matrix adhesions to the third dimension. *Science*, 294(5547):1708–1712, 2001. 196

[210] Stephanie M Willerth, Kelly J Arendas, David I Gottlieb, and Shelly Elese Sakiyama-Elbert. Optimization of fibrin scaffolds for differentiation of murine embryonic stem cells into neural lineage cells. *Biomaterials*, 27(36):5990–6003, 2006. 196

[211] Hui Liu, Jian Lin, and Krishnendu Roy. Effect of 3D scaffold and dynamic culture condition on the global gene expression profile of mouse embryonic stem cells. *Biomaterials*, 27(36):5978–5989, 2006. 196

[212] S E Blackshaw, Scott Arkison, Claire Cameron, and J a Davies. Promotion of regeneration and axon growth following injury in an invertebrate nervous system by the use of three-dimensional collagen gels. *Proceedings. Biological sciences / The Royal Society*, 264(1382):657–661, 1997. 196

[213] B. Pardo and P. Honegger. Differentiation of rat striatal embryonic stem cells in vitro: Monolayer culture vs. three-dimensional coculture with differentiated brain cells. *Journal of Neuroscience Research*, 59(4):504–512, 2000. 196

[214] A P Balgude, X Yu, A Szymanski, and R V Bellamkonda. Agarose gel stiffness determines rate of DRG neurite extension in 3D cultures. *Biomaterials*, 22(10):1077–1084, 2001. 196

[215] Anu Desai, William S Kisaalita, Charles Keith, and Z. Z. Wu. Human neuroblastoma (SH-SY5Y) cell culture and differentiation in 3-D collagen hy-

drogels for cell-based biosensing. *Biosensors and Bioelectronics*, 21(8):1483–1492, 2006. 196

[216] Tao Xu, Cassie A Gregory, Peter Molnar, Xiaofeng Cui, Sahil Jalota, Sarit B Bhaduri, and Thomas Boland. Viability and electrophysiology of neural cell structures generated by the inkjet printing method. *Biomaterials*, 27(19):3580–3588, 2006. 196

[217] Pietro Gareri, Rosario Mattace, Felice Nava, and Giovambattista De Sarro. Role of calcium in brain aging. *General Pharmacology*, 26(8):1651–1657, 1995. 196

[218] D Kacy Cullen, John A Wolf, Varadraj N Vernekar, Jelena Vukasinovic, and Michelle C. LaPlaca. Neural Tissue Engineering and Biohybridized Microsystems for Neurobiological Investigation In Vitro (Part 1). *Critical Reviews in Biomedical Engineering*, 39(3):201–240, 2011. 196

[219] Sophie Pautot, Claire Wyart, and Ehud Y Isacoff. Colloid-guided assembly of oriented 3D neuronal networks. *Nature Methods*, 5(8):735–740, 2008. 196, 197

[220] Monica Frega, Mariateresa Tedesco, A Constestabile, M Nanni, L Bonzano, G Maura, and M Chiappalone. Cortical cultures coupled to micro-electrode arrays: a novel approach to perform in vitro excitotoxicity testing. *Neurotoxicology and Teratology*, 34(1). 196

[221] Mariateresa Tedesco, Monica Frega, Sergio Martinoia, Mattia Pesce, and Paolo Massobrio. Interfacing 3D Engineered Neuronal Cultures to Micro-Electrode Arrays: An Innovative In Vitro Experimental Model Video Link. *J. Vis. Exp*, 53080(10410):1–10, 2015. 199

[222] Jan Mller, Douglas Bakkum, and Andreas Hierlemann. Sub-millisecond closed-loop feedback stimulation between arbitrary sets of individual neurons. *Frontiers in Neural Circuits*, 6:121, 2013. 202

[223] Jacopo Tessadori, Marta Bisio, Sergio Martinoia, and Michela Chiappalone. Modular neuronal assemblies embodied in a closed-loop environment: To-

ward future integration of brains and machines. *Frontiers in Neural Circuits*, 6:99, 2012. 202

[224] Marta Bisio, Alexey Pimashkin, Stefano Buccelli, Jacopo Tessadori, Marianna Semprini, Timoth Levi, Ilaria Colombi, Arseniy Gladkov, Irina Mukhina, Alberto Averna, Victor Kazantsev, Valentina Pasquale, and Michela Chiappalone. *Closed-Loop Systems and In Vitro Neuronal Cultures: Overview and Applications*, volume 22. 2019. 202